PREDICATION OF BEAD GEOMETRY IN GAS METAL ARC WELDING BY STATISTICAL REGRESSION ANALYSIS

By

Rahul Ram Chandrasekaran

A thesis
presented to the University of Waterloo
in fulfillment of the
thesis requirement for the degree of
Master of Applied Science
in
Mechanical and Mechatronics Engineering

Waterloo, Ontario, Canada, 2019

Author's Declaration

This thesis consists of material all of which I authored or co-authored: see Statement of Contributions included in the thesis. This is a true copy of the thesis, including any required final revisions, as accepted by my examiners.

I understand that my thesis may be made electronically available to the public.

Statement of Contribution

Sections of Chapter 3 and 4 in this thesis contain contents and materials from journal paper "**Multi-variable statistical models for predicting the bead geometry in Gas Metal Arc Welding"** which I co-authored with Michael Benoit, Jeffery Barret and Adrian Gerlich, and expected to be submitted to Journal for Material Processing Technology for further review. In this contribution, I was responsible for the planning, conducting experiments, experimental analysis, and writing of the paper. Michael Benoit and Jeffery Barret performed the programming in R and supported statistical analysis, and Adrian Gerlich supervised the work and edited the writing.

Abstract

Manufactures in fabrication industry have long depended on Gas Metal Arc welding as one of the most reliable and economical techniques for joining parts. The need for reducing costs and addressing a skills shortage on the shop floor, often limits productivity in the manufacturing industry involving welding. Developing a welding procedure for instance, involves a lot of time and cost, and currently there is a gap in welding industry where few available methodologies can predict even the basic features of weld geometry based on input parameters. To provide a methodology for prediction, the aim of this thesis focusses on developing a statistical model for the weld inputs and outputs in the Gas Metal Arc Welding process to predict the various geometries of the weld bead. To study the effect of welding process parameters—such as wire feed speed, voltage, travel speed and gas type—on the resultant bead geometry such as bead width, penetration, reinforcement height, reinforcement area and penetration area a factorial design of experiment was used. Low carbon electrode (ER 70S-6) of two different diameters was used, and a total of 242 welds were made with 121 for each wire diameter. Two cross sections were cut from each weld bead and the geometries were measured, and a linear regression analysis was performed to develop a statistical model for each of the bead geometry based on experimental data. Analysis of variance (ANOVA) indicated the significant squared and interaction variables for each of the bead geometry with 95% confidence interval. The trends of geometry for each diameter varied with gas type. Residual analysis revealed that all assumptions inherent in the regression analysis were satisfied. Finally the statistical models were validated in bead on plate, fillet and V-groove joint positions. A total of 8 fillet tests and 5 groove tests were performed for both the wire types and it was found that predicted values were in good agreement with the measured values for bead on plate and fillet conditions, whereas welds with a V-groove joint geometry

had a significantly under-predicted penetration area due to increased heat transfer and faster cooling down of weld with a higher equivalent sample thickness.

Acknowledgement

I would like to thank and express my heartfelt gratitude to my supervisor, Dr. Adrian P. Gerlich for giving me this exciting opportunity to work on this project and also for his undoubted support throughout this research program. His guidance and feedback from our weekly discussion has supported me immensely for the last two years, and helped me grow academically and professionally. I owe him for making my academic experience at University of Waterloo enjoyable and memorable.

I would also like to express thanks to my present and past colleagues in CAMJ, Rafael Ribeiro, Nazmul Huda, James Choi, Rangarajan, Paulo Dangelo, Abdelbaset Midawi, Luqman Shah, Emanuel dos Santos and other members for helping me, and sharing their knowledge and discussions in welding and research. Special thanks to Rafael for encouraging me to write my first conference paper and would also like to thank Michael Benoit and Jeff Barrett with whom I had privilege in working and writing a journal paper. I would also like to acknowledge Dr. Charles Kwan for providing me with a Teaching Assistantship.

Finally, I thank my always supportive family and friends, especially my parents, for their abundant emotional and practical support.

Table of Contents

Lists of Figures

List of Tables

Chapter 1. Introduction

1.1 History of Welding

Ever since the industrial revolution, the manufacturing industry has been undergoing rapid changes and continues transforming the way that products are manufactured and produced today. Modern manufacturing is driven by automation with advancement in technologies such as robotics, artificial intelligence, and smart manufacturing, making the manufacturing of complex design streamlined with increased efficiency and higher output.

The welding and fabrication industry is an integral part of the manufacturing process, and has also undergone huge changes over the years. The earliest history of welding can be traced back to bronze age where welders produced weldments by applying pressure to join heated metals together. This technique was later expanded in late 1800's with use of acetylene and oxygen gas to produce a hot flame capable of heating the metal to the melting point and enabling them to join [1]. This technique prevailed until the early 19^{th} century, as a leading predecessor to the first electric arc welding process, i.e. Shielded Metal Arc Welding (SMAW), where a carbon coated electrode is used. The need for better techniques for joining emerged in the aircraft industry during World War II for joining aluminium and magnesium to produce parts faster, easier and with better metallurgical characteristics. This led to new methods where electric current was used replacing oxygen-fuel torches to heat up the metal by producing an electric arc with an electrode shielded by inert gas [2]. Some of the earliest arc welding systems and procedures developed include Submerged Arc Welding (SAW) where an arc is submerged by a layer of flux, and Tungsten Inert Gas (TIG) welding which has a tungsten electrode producing an electric arc covered with a shielding gas without any filler metal involved [1]. The successor to this was Gas Metal Arc/ Metal Inert Gas Welding

(GMAW/MIG) which uses a consumable electrode as a filler metal to produce an electric arc. The latest research and developments in the field of welding aim to address the demand for better welding technology for joining complex materials and shapes, and has led to the discovery of laser and electron beam welding to melt and join the metals. Other methods such as friction welding have subsequently emerged for joining materials like aluminium and copper which are more sensitive to heat or difficult to heat locally.

Nowadays, the welding industry has evolved with better welding equipment and the development of integrated/solid-state circuit technology. The control circuits are embedded into the latest equipment and coupled with mechanization and numerical control, offering increased arc and puddle control along with the availability to use a wide range of consumables, and provides broader choice for a particular application along with higher weld quality. These advances represent leading edge technology, and resulted in significant changes in the field of welding and fabrication industry, making it the essential technique for joining in manufacturing process. The modern application of welding reaches all metal fabrication industry sectors from structural, automotive, aerospace, rail, naval, energy, electronics, pipelines, offshore structures, pressure vessels, and heavy industrial machinery. For example, Figure 1 shows a pipeline being constructed in Alberta, Canada where multiple pipes are welded together to create a pipeline system for transporting natural gas thousands of kilometers [44], highlighting the importance of welding process in today's world. A recent study conducted in 2016 by Allied Market Research [3] has found that arc welding processes account for the highest share of industrial use in terms of both volume and revenue generation due to its low cost and flexibility for different materials and joint designs. These processes include Gas Metal Arc Welding (GMAW), Shielded Metal Arc Welding (SMAW), Flux Cored Arc Welding (FCAW), and Gas Tungsten Arc Welding (GTAW), and Submerged Arc Welding (SAW) as the most popular procedures utilized in the fabrication industries.

Figure 1 Typical pipeline being joined together for transporting oil [44]

1.2 Motivation

Arc welding is one of the most widely used welding processes for joining not only due to the high flexibility, but also higher deposition efficiency, weld quality, and low cost compared to other processes. Even though arc welding has been used in joining process for various applications for almost half a century, there is still a lack of information or reliable data for welders to predict the outcome of the weld bead geometry for a specific parameter selected. To this date, there still remains a considerable challenge if one aims to predict even basic features of the weld pool, such as the dimensions of the weld geometry. In many cases welding engineers need to design a joint with a fixed geometry and would like to predict whether a weld bead will cover a prescribed width or penetrate a required depth. In most cases this is simply achieved in the field by experience, typically based on welding procedures for joint designs with comparable geometry, or by performing several trials, which is both costly and time consuming.

To overcome this lack of available information for predicting the characteristics of weld bead geometry, the aim of this study is to develop a statistical model of how the

geometry of the bead varies with different combinations of parameters and gas types during GMAW. This statistical model for welding bead measurements correlates welding parameters to their outputs, such as width, depth of penetration, reinforcement height, penetration area, reinforcement area, dilution ratio, deposition rate and efficiency, average current, heat input and other measurements, that can be used by welders and engineers to answer simple questions like whether the fusion zone area would be sufficient for joining two pieces using the selected parameters.

Developing this information requires performing a number of welds using different wire sizes and materials. The collected data obtained from these experiments would represent a wealth of information, and would be highly useful to a variety of users from welders, welding engineers, students, and researchers. This information would help to make better choices about welding parameters, and to gain a better understanding of how the welding process will affect their resulting outputs.

From a research point of view, developing this information would require the application of statistical models, an understanding how the significant parameters control the geometry of the bead, and the most important parameters along with their interaction effects. From application standpoint of view, the information generated would enable one to predict the basic geometry of the bead, calculate and predict the number of number of passes required for filling a groove, and other important features such as estimating the cost for welding process based on the input parameter selected by the user. This information can be further developed into a large database for different processes, which would be tremendously useful to a wide range of people in the welding field, and significantly reduce the amount of time and effort in developing welding procedures.

1.3 Objective

The primary objective of this research is to study the effect of welding parameters and to provide a method for predicting the output bead geometry during GMAW. To-date, few experimental studies have captured the role of welding parameters and shielding gas type in GMAW, or the effect of changing inputs and their interaction effects on the corresponding bead geometry. For example, the gas type is known to have an influence weld bead shape and penetration, and wire feed speed is also known to directly influence penetration, but the overall effect when both parameters are simultaneously changed has not been studied. To obtain the primary goal stated above, following sequence of experimental work and analysis were performed as part of this thesis:

1. Design and execute a comprehensive experimental study to evaluate the effects of different welding parameters such as wire feed speed, voltage, travel speed and gas type on weld bead geometry in gas metal arc welding using ER 70S-6 welding wire of two different diameters.
2. Develop statistical model through regression analysis, to establish the degree to which welding parameters and their interaction effects control the various weld bead dimensions, such as width, penetration, reinforcement height, reinforcement area and penetration area.

1.4 Past Work

Some methods have been explored to develop tools for predicting weld bead geometry based on statistical models from experimental data. Some of the methods which have been used in prior efforts to model arc welding processes include: factorial design of experiment (DoE) technique for predicting geometry in SAW [29]; predicting the output of optimized weldments in SAW based on Taugichi's L25 orthogonal array [30]; welding bead

geometry prediction for obtaining an optimal bead geometry based on input parameters in GTAW using on Taugichi's orthogonal array technique [31]; and response surface optimization using a four factor, five level central composite rotatable design matrix for predicting weld bead geometry based on input parameters in SAW [32]. Another popular method for developing a predictive process model has involved the use of neural networks, and examples of these have been developed for SMAW using back-propagation method for estimating the weld bead width and penetration geometric parameters [33], and prediction of weld bead geometry in the pulsed GMAW process using the back-propagation algorithm [34]. These methods are useful in providing tools which can be applied by welding engineers to design joints, or implemented in automated systems to progress towards closed loop control of welding process in SAW, GTAW and GMAW.

There are also some slide-rule based tools and apps provided by several welding equipment manufacturers such as Lincoln Electric™, Miller Electric™, Fronius ™ which provide some basic information such as current/Wire Feed and Voltage range for specific range of transfer modes along with information about which materials and process to suit for a given welding application. Figure 2 shows a basic weld scale tool provided by Miller Electric to determine the current range and is based on basic input parameters which are recommend for different sized electrodes [35]. The welding app from Lincoln Electric shown in Figure 3 is available on Google Play [4] for Android devices, with a similar app from Miller Electric's [5] and Fronius shown in Figure 3 [6]. Each of these provide users with the ability to quickly calculate values based on the inputs, however detailed output features such as predicted weld bead size are not given.

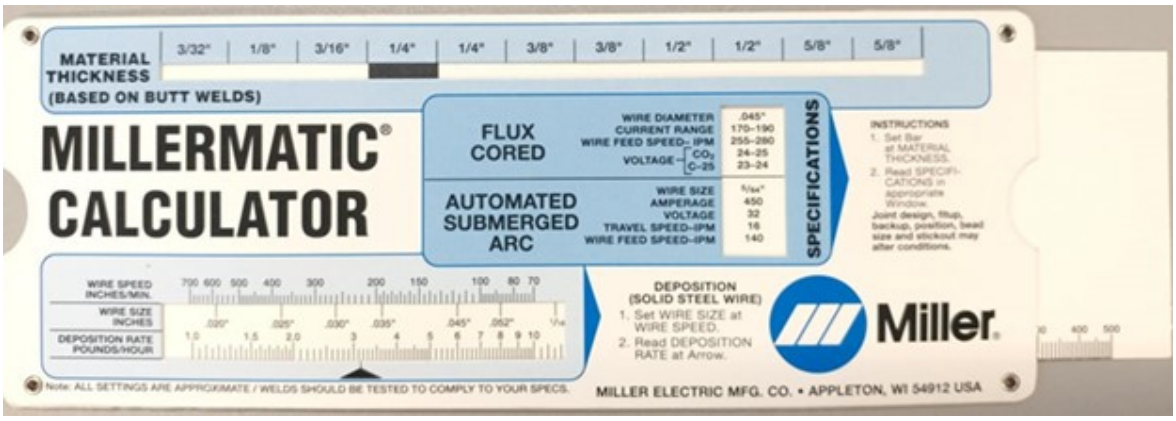

Figure 2 Millermatic Calculator, Miller Electric™ [35]

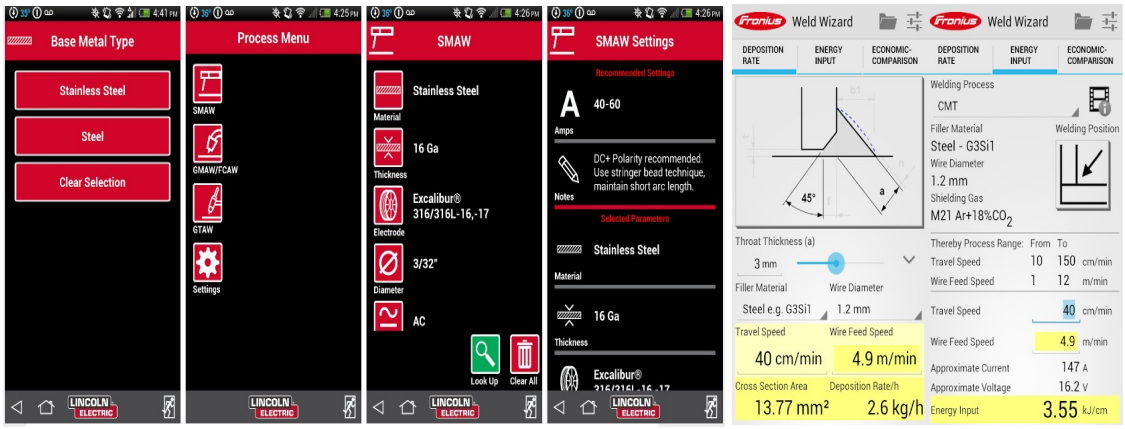

Figure 3 Screen shots from the Lincoln Electric "Weld Parameter Guide app" and Fronius " Weld Wizard App" [4, 6].

There is still much room for improvement and additional features in these welding apps. These apps primarily provide some guidelines about the basic recommended settings for welding, similar to the manufacturer information datasheet for each wire electrode. It does not provide examples of the output that will be obtained, any details about the size of the weld and so on. The statistical data developed from this study will provide a resource with a far richer supply of information regarding the welding outputs. This will provide a major advantage over other current available data since there will be a wide range of welding conditions and greater details offered.

1.5 Thesis Organization

The introduction chapter has briefly discussed about the currently available methodology for selecting the parameter for welding and predicting the outcome of the weld bead geometry in GMAW, however these available methods cannot be applied to wide range of parameters and different wire types. This thesis discusses the development of welding data for predicting the bead geometry in GMAW, and the chapters included focus on the following:

Chapter 2 presents the background with theories and principle around the GMAW process, the effect of different process variable on arc and output characteristics, transfer modes associated with the parameter, fluid flow and other mechanism occurring inside the weld pool and statistical methods followed for analyzing the data.

Chapter 3 discusses the experimental set-up and procedure, materials and consumables used, experimental design used to perform the study, the welding parameters chosen for the design and methodology for measuring the post-weld geometry of weld bead.

Chapter 4 mainly discusses the experimental results for different wires and wire diameters along with statistical analysis, parameters and their interaction effects, model verification and other key results obtained from this study.

Finally, *Chapter 5* outlines the conclusions obtained in this study based on the experimental results and statistical analysis performed, along with future work to be performed related to this study.

Chapter 2. Background

This chapter provides a background behind the Gas Metal Arc Welding (GMAW) process and important welding process variables, how they affect the welding and bead characteristics overall, along with an explanation of heat and fluid flow mechanisms happening inside the weld pool during the welding process. A precursor to background about design of experiments and statistical analysis is provided in later sections of this study.

2.1 Gas Metal Arc Welding (GMAW)

2.1.1 Working principles of GMAW

GMAW is one of the most commonly used process for joining metal. The basis behind heat generation in this process is Joule's law of heating, where an applied electric current produces heat due to resistance across an electric arc, which heats the filler metal and base metal to form a weld pool. This molten metal is protected from oxidation from the surrounding atmosphere by a cover of inert shielding gas.

In the GMAW process, a wire is fed continuously from spool, during which an electric arc is established between the base metal and this wire. The schematic in Figure 4 shows the schematic of the GMAW process. The heat of the electric arc melts part of the base metal and filler metal (wire). As a result, the melted metal transfers from the wire to the weld pool on the plate, which on cooling forms a weld bead as shown in Figure 5. In addition, the weld torch is surrounded and covered by a shielding gas so as to protect the melted weld pool from outside surrounding thus preventing porosity.

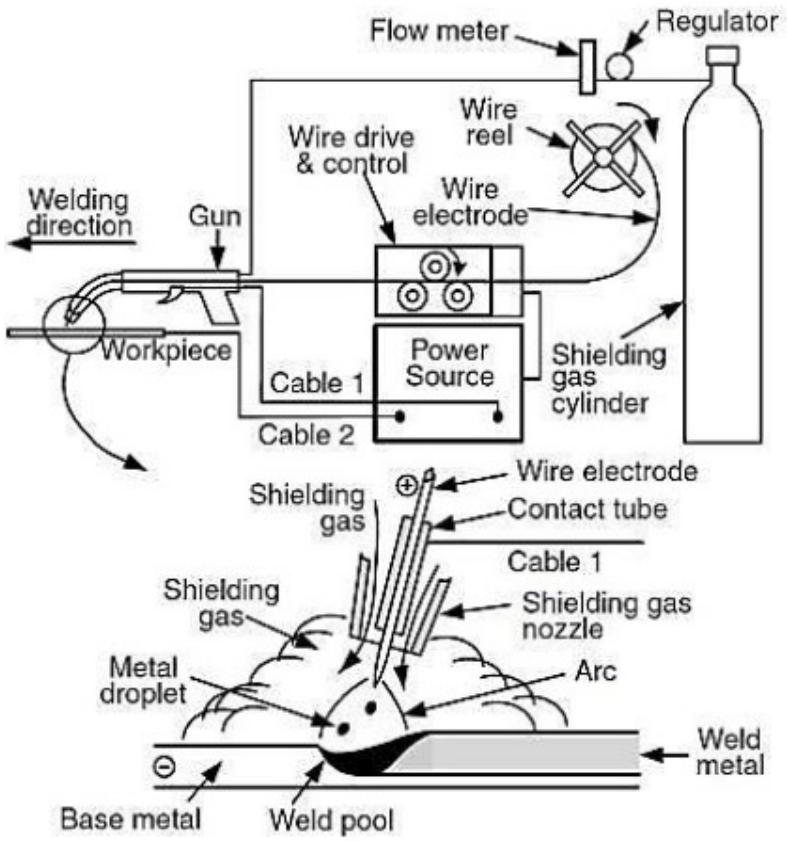

Figure 4 Gas Metal Arc Welding (GMAW) process [16]

Figure 5 Weld bead made by Gas Metal Arc Welding

2.1.2 GMAW Process Variables

In GMAW, the selected welding parameters control the geometry of the bead, metal droplet transfer mode, stability of the arc, bead quality, and overall weld properties. A number of past studies have identified the significant parameters controlling the geometry of

bead [18, 19, 29, 32, and 33]. The prior studies have found that the penetration and reinforcement height of the weld increases with increases in wire feed speed, but width remains unaffected, while increasing voltage will increase the arc length and produces a wider bead [26]. Wire feed speed, which is related to welding current determines the amount of metal deposited affecting the reinforcement height and penetration of weld, and is most directly correlated to the arc current [18]. The process parameters which are critical to the arc characteristics also determine the resulting bead geometry such as width, depth, reinforcement height, and area. Some of these weld parameters have a greater influence than other on specific weld bead geometry and the effects of this parameter are explained as follows.

2.1.3 Wire feed Speed

Wire feed speed is the amount of filler metal fed into the weld pool, and is usually expressed in $\frac{m}{min}$ or $\frac{in}{min}$. In constant voltage (CV) welding process wire feed rate is directly related to the current passing through the arc, where the internal circuitry of the welding equipment selects appropriate current in CV mode to melt the wire depending on the selected wire feed speed.

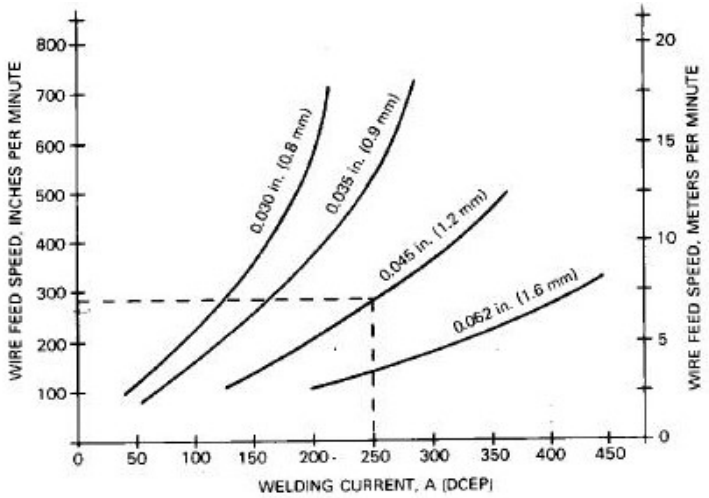

Figure 6 Relationship between Welding current and wire feed speed for different carbon electrode diameters [17]

The Figure 6 shows the relationship between welding current and wire feed speed for different carbon steel electrode diameters. In general, with increases in current, the effect of the electromagnetic Lorentz force increases, resulting in deeper penetration of weld. The schematic in Figure 7 shows the effect of current on weld penetration, where it can be seen that weld penetration increases progressively with increase in current. There is also significant difference in current with electrode type used in welding. In general, tubular/cored wires promote higher current density and have deeper penetration compared to solid wires.

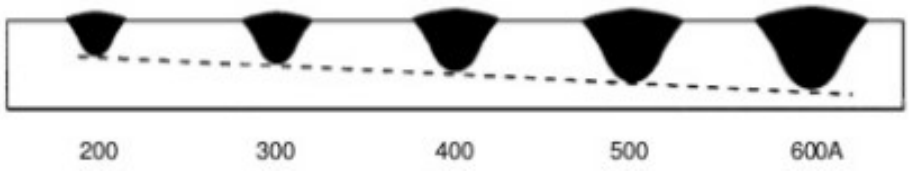

Figure 7 Effect of penetration on Bead penetration [18]

2.1.4 Arc Voltage

Voltage directly influences the arc length and size of arc cone, playing an important role in maintaining the arc between torch and work sample. The arc voltage is not linearly distributed along the arc, it is composed of three distinct regions, namely: anode, cathode and arc column regions, as shown in Figure 8 [22]. The anode and cathode voltage are extremely small regions; while the arc column is region where transfer of droplet and electrons occurs, and is formed by ionized plasma of shielding gas and vaporized metal, playing an important role in maintaining the arc [21, 23].

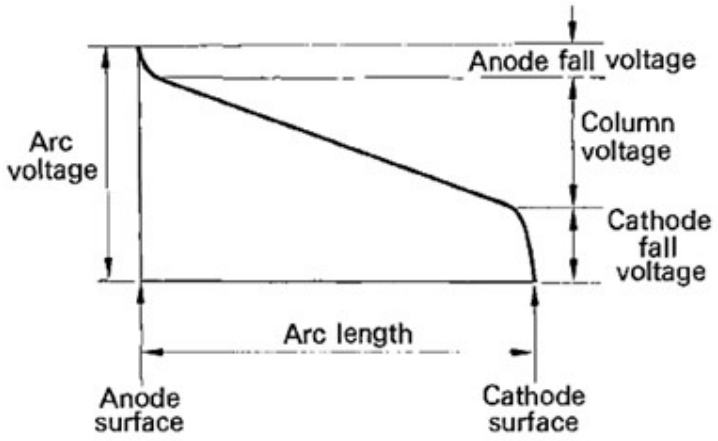

Figure 8 Voltage distribution inside an electric arc [22]

Depending on arc length determined by the voltage, the size of plasma column varies, thereby affecting the size of arc cone. Usually at lower voltage the voltage across arc column region is low, giving a smaller arc length and arc cone, and vice versa at higher voltage. Figure 9 schematically illustrates the relationship between arc cone size with arc voltage.

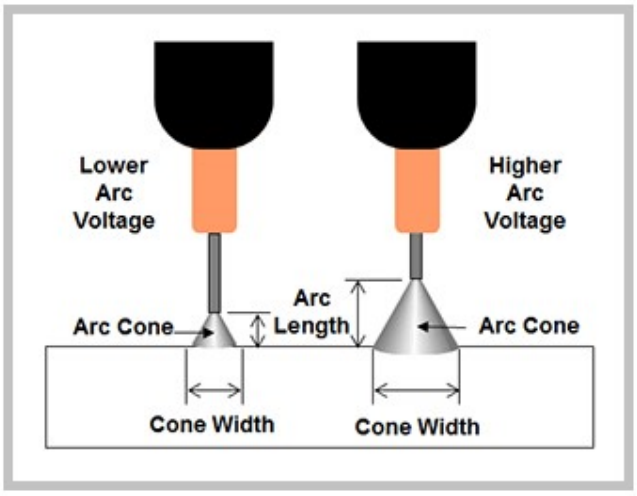

Figure 9 Effect of Voltage on Size of Arc cone and Arc length [19]

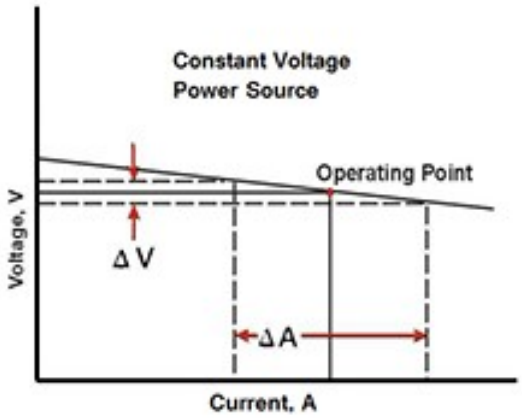

Figure 10 V-I Characteristics of welding equipment (CV mode) [19]

Figure 10 depicts the V-I characters of welding equipment in CV mode. It can be seen from this figure that for a small variation in the voltage, there is a relatively larger variation in the current. Though the name CV suggests that voltage is constant, there is always a variation in voltage due to the relative resistance and inductance of the welding equipment. The power source i.e. welding equipment provides the required current to melt the wire feed rate at the specified pre-set voltage level. And during the welding process depending on the arc length, this voltage is slightly varied to produce a constant stable arc. Also the applied current during welding in CV mode varies greatly depending on specifics of V-I characteristics curve of the welding equipment used, as each equipment has unique and different V-I characteristics from each other one.

2.1.5 Travel Speed

Travel speed is the velocity at which the welding torch moves over the work piece during the welding process, and it is usually specified in units of $\frac{m}{min}$ or $\frac{in}{min}$. The travel speed of torch greatly affects both the width and penetration of the weld bead. When the torch travels faster, the amount of filler metal deposited per unit area and the heat input per applied per unit area will decrease, while at slower speed the amount of metal deposited and heat input is high which results in higher penetration and increased weld width. Figure 11 shows

three different welds of length 80mm, made at a constant wire feed speed 400 $\frac{in}{min}$ (10.16$\frac{m}{min}$), and voltage of 26V, but with three different travel speeds, being 16, 24, and 32 $\frac{in}{min}$ (0.41, 0.61 and 0.81$\frac{m}{min}$) respectively.

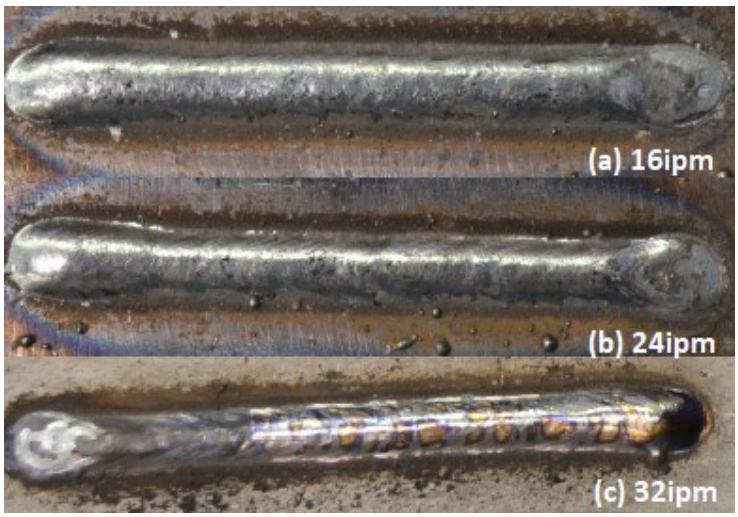

Figure 11 Effect of Travel speed on bead geometry (Bead length: 80mm)

2.1.6 Shielding Gas

Type of shielding gas used plays an important role in geometry of weld bead. Some of the most commonly used gases in GMAW are Ar, CO_2, He, O_2. Often the gasses are blended with each other to provide better arc stability and more effective shielding. Table 2-1 shows the properties of commonly used shielding gas [20, 50].

Table 2-1 Properties of Gas [50]

Gas	Ionization potential (eV)	Thermal Conductivity at 300K ($\frac{W}{mK}$)	Thermal Conductivity at 600K ($\frac{W}{mK}$)
Argon (Ar)	15.7	0.018	0.030
Carbon di-oxide (CO_2)	14.4	0.017	0.042
Helium (He)	24.5	0.155	0.252
Oxygen (O_2)	13.2	0.027	0.048

Differences in ionization potential explain the relative ease with which a gas can be ionized. Arc initiation is easier with gases having lower ionization potential as they require less energy to be ionized compared to higher ionization potential ones. Another important factor is the thermal conductivity of a gas. Gasses with higher thermal conductivity have higher arc temperature, which can transfer more energy to the workpiece, resulting in greater penetration compared to gas with lower thermal conductivity [16, 19]. Another influential factor in determining the output character of a bead is the gas flow rate. Lower gas flow rates may produce an unstable arc resulting in spatter and defects in weld, and above a certain limiting point, the rate of gas flow does not significantly affect the bead geometry [27, 28].

2.1.7 Polarity

Polarity specifies the way electric current flows through circuit during the welding process. The direction of current can be changed depending on terminals of electrode, with three possible polarities namely DCEN, DCEP, and AC each having unique characteristics.

In Direct Current Electrode Negative (DCEN) mode, the electrode is connected to the negative terminal of the power supply, and the sample is connected to positive terminal. The electrons flow from electrode to sample, while current flows in opposite direction. In DCEN mode, a higher energy is required electrons to release an electron from the electrode due to the work function of the material, and hence less energy is released onto work sample resulting in shallow weld penetration [16]. In Direct Current Electrode Positive (DCEP) mode the electrode is connected to positive terminal and the workpiece is connected to the negative terminal of the power supply. The current flows from electrode to sample, and a large amount of energy is released onto work sample, leading to a higher penetration (deeper welds). In AC mode, the direction of current and electrons are alternating, and this gives an

intermediate penetration a compromise between DCEP and DCEN modes. The Figure 12 below shows different polarity modes during arc welding.

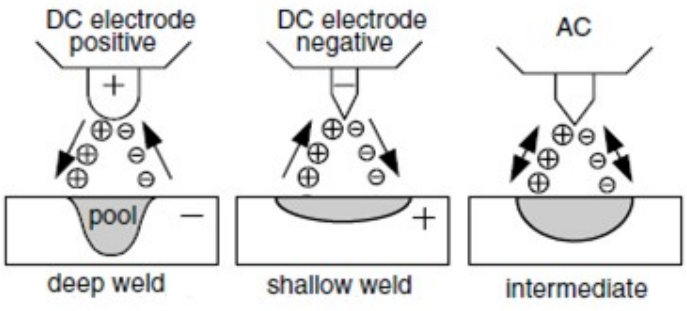

Figure 12 Polarities in Welding modified from [16]

2.1.8 Electrodes

The electrode used in welding process plays an important role in the structural integrity, quality and appearance of the weld joint. Electrodes used in welding are both consumable and non-consumable depending on the specific welding process. Welding using a non-consumable electrode may require an additional filler metal for deposition to fill a gap between two pieces, whereas with a consumable electrode, the electrode acts as filler metal and is deposited during the process. An example for this being Gas Metal Arc Welding (GMAW), while the former is Gas Tungsten Arc Welding (GTAW).

In the case of GMAW, the consumable electrode used in the process is further categorised as plain solid wire, or cored (tubular) electrodes. The in contrast to simple solid wires, cored electrodes have powder metal and flux inside a crimped or seam welded fine tube. Solid wires are the most heavily used in welding because they are inexpensive compared to cored ones, but there are some advantages to cored electrodes over solid ones such as, facilitating better maintenance of arc, protecting the molten pool from oxygen in atmosphere, and providing a means of introducing metal alloys into the weld. In addition,

cored wires also offer higher deposition rate, higher current density, and better resistance to lack of penetration due to a wider penetration profile [7].

These electrodes are classified by the American Welding Society (AWS) which publishes the electrode classification index for different welding process based on electrode type, metallurgical composition of electrode filler metal, mechanical properties and usability characteristics of the electrode [13]. For example, carbon steel electrodes and rods used for GMAW are classified in the clause AWS A5.18/A5.18M:2005 which specifies different carbon electrodes along with the specification and properties which they should conform to [14].

2.1.9 Transfer Modes

Transfer mode refers to mechanism by which the metal droplets are transferred from arc plasma to weld pool. There are three different modes of transfer in GMAW namely Short-circuiting Globular and Spray transfer. The type of transfer mode occurring depends on both arc voltage and current, with voltage being the predominant factor controlling short circuiting, and current controlling the transfer from globular to spray transfer. Figure 13 shows the range of voltage and current across which different transfer mode occurs.

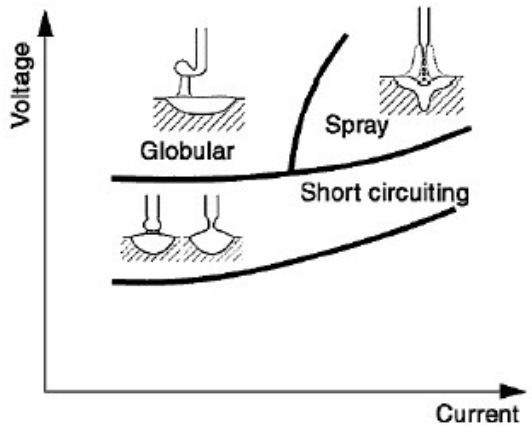

Figure 13 Metal droplet transfer modes in GMAW [18]

Short-circuit transfer occurs at a lower voltage and current range when the arc energy available at the torch is less than the rate at which wire is fed, causing the arc to extinguish. After the arc extinguishes current raises and the arc starts again and the cycle continues [21]. Globular transfer mode occurs at higher voltage and lower current region. In globular transfer mode, wire melted to form a droplet, and grows into a size close to or larger than the electrode diameter. After growing into a sufficient size they fall down into weld pool under the influence of gravity as discrete droplets with diameters larger than the diameter of the wire. Spray transfer mode occurs at high voltage and current range. At higher current, small discrete metal droplets (less than the wire diameter) travel across arc gap at higher frequency and speed than in globular mode under the influence of electromagnetic force, resulting in spray transfer [16, 18].

2.1.10 Fluid Flow theory

A weld pool is created when metal droplets from arc plasma are deposited onto the base metal. Depending on current and voltage, a pressure is exerted by arc on weld pool and there are number of driving forces acting inside weld pool such as buoyancy force, electromagnetic force (Lorentz force), shear stress induced by surface tension and shear stress due to arc plasma jet [36-40]. These driving forces inside weld pool can highly influence the geometry of weld bead. Figure 14 below shows the effect of each driving forces inside weld pool, which will be discussed in the following sections.

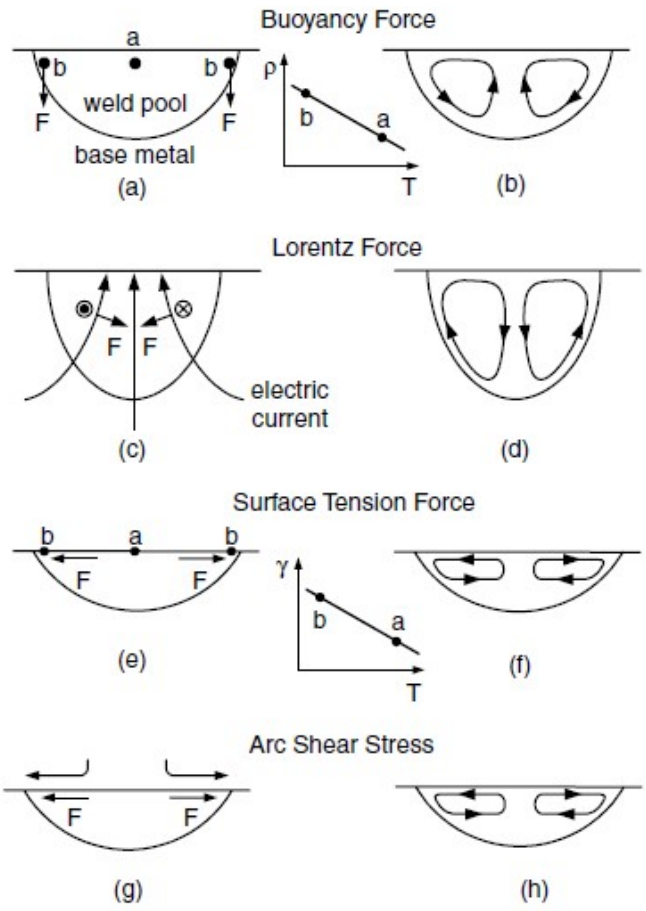

Figure 14 Driving force for weld pool convection (a,b) buoyancy force; (c,d) Lorentz Force; (e,f) shear stress by surface tension gradient; (g,h) shear stress by arc plasma [16]

2.1.10.1 Buoyancy Force

Figure 14 (a, b) shows buoyancy force acting inside the weld pool. This force is caused due to difference in density inside weld pool, as the density of liquid metal decrease with increasing temperature [16]. The cooling rate is faster at point *b* on weld pool which is close to boundary compared to point *a* at the center. This faster cooling at the boundary forms a high density liquid at the edges, which leads to the molten flow to the central bottom of pool shown in Figure 14 a, while high temperature liquid with low density liquid at centre point *a* is pushed up due to buoyancy force created by the high density liquid metal [42]. The flow induced by buoyancy force is centrally outward and its magnitude is given by the equation [43],

$$F_b = \beta \rho g (T - T_0) \qquad \textit{Equation (1)}$$

here ρ is the density of liquid metal, g is the gravity acceleration, β is the thermal expansion coefficient, T is the temperature of the liquid metal, and T_0 is the reference temperature.

2.1.10.2 Lorentz Force

A current currying conductor produces a small magnetic field around it, and by Flemings Left hand rule, a force is induced perpendicular to the direction of magnetic field. This force is known as electromagnetic force, or Lorentz force, and its magnitude is given as,

$$\vec{F} = \vec{J} * \vec{B} \qquad \textit{Equation (2)}$$

Where $\vec{J}$ current density is vector and $\vec{B}$ is magnetic flux vector. This Lorentz force exerts a downward pressure on the weld pool and the liquid metal rises along the pool boundary and flows in circular inward direction as in Figure 14 d [40, 41].

2.1.10.3 Shear Stress due to surface tension

In general, the surface tension of a liquid metal decreases with increasing temperature. As stated before in 2.1.10.1, the temperature at the boundary of the weld pool is less compared the center where the arc is focused, and so the cooler liquid metal at point *b* has higher surface tension and pulls the warmer liquid metal at point *a* towards it as indicated on Figure 14 e. This results in metal from center being pulled to edge and returned back down to due to difference in density, causing a circular inward motion in weld pool as shown in Figure 14 f [16, 40]. This surface tension force is also commonly known as Marangoni Force and its magnitude is given as [43],

$$F_s = \frac{d\gamma}{dT} \Delta T \qquad \textit{Equation (3)}$$

Here $d\gamma$ is change in surface tension of liquid metal and dT is the difference in temperature from one point to another on the weld pool surface.

2.1.10.4 Shear Stress induced by arc plasma jet

The arc plasma moving at high speed across the pool surface exerts an outward shear stress on surface of pool as shown in Figure 14 g, causing liquid metal at the center of the pool surface to flow toward the edge of weld pool, causing a circular outward motion of liquid metal as shown in Figure 14 h [16]. This force is also known as arc pressure exerted by moving arc plasma.

Eisazadeh et *al*. [43] conducted a study on driving forces in weld pool and found that arc pressure (plasma jet) and buoyancy forces are often negligible compared to Lorentz and Marangoni force at currents greater than 100A, and at currents of less than 100A, buoyancy Lorentz and Marangoni forces are the three dominant forces controlling flow pattern. The Figure 15 below shows the comparative effect of each of these forces inside weld pool,

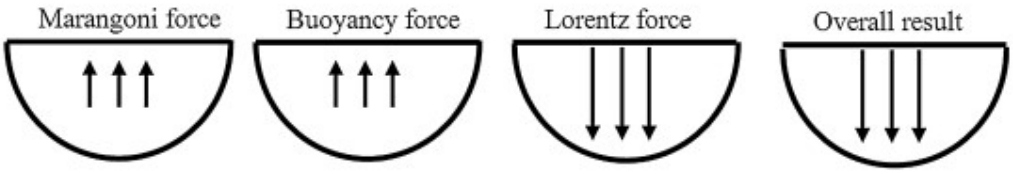

Figure 15 Schematic diagram of direction of forces acting inside weld pool [43]

2.2 Statistical Analysis

2.2.1 Design of Experiments (DoE) design

The Design of Experiments (DoE) technique of optimization is performed to identify the choice of experiments to be performed in an efficient methodology. DoE allows experimenter to plan, conduct, analyze and interpret controlled tests to evaluate independent factors based on the dependent factors that control the experiment [15]. Independent factors in an experiment are variables which are uncontrollable, while dependent factors are variables which can be controlled in an experiment by pre-setting the variables which affects

them. Based on number of independent factors selected for the study and range of their variability, the experimental design allows for experimenter to optimize the number of test to be performed depending on the scope of the experiment, time, cost and range of other factors [8].

There are number of DoE techniques available for optimization depending on the statement of problem, choice of factors, level, range of variables, and selection of response variable [11]. Techniques such as Box-Behnken, Definitive screening, Plackett-Burman design and fractional-factorial design provide methods to optimize down the number of significant independent variables in an experiment by screening all the potential independent variables set by the experimenter. Once the final number of independent factor is set, designs such as Block design, Factorial design, or Taguchi method can be employed to optimize the number of runs to be performed [10].

2.2.1.1 Full-Factorial Design

A full-factorial design is a commonly used method in experimental design for studying response of every possible combination of independent factors and their levels. Depending on number of factors selected (n) and number of levels (k) for each factors in the design, the number of experimental runs (i.e. Sample size N) to be performed in this design is $N=k^n$. The 2^n and 3^n factorial designs are the most commonly used, and Figure 16 shows a 3^3 factorial design with 27 runs which is used in further in this study. The factors in a three factorial design are noted down as low, intermediate and high also represented by -1, 0, and +1.

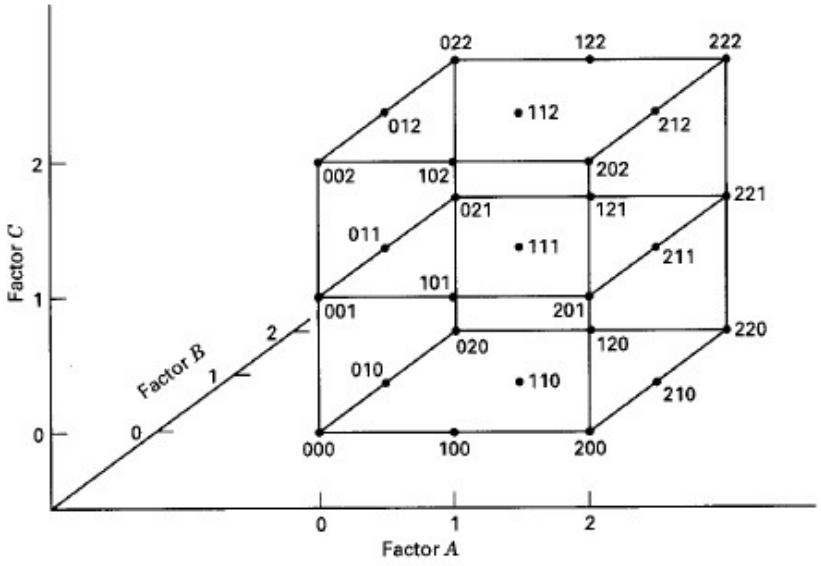

Figure 16 A 3^3 factorial design with data points [10]

The full-factorial design makes efficient use of data and do not confound the effects of parameter (i.e. possible to evaluate main and interaction effects clearly) [15], so it is a better choice for an experimenter concerned about curvature in the response function [9] [12]. On the other hand, the main limitation of this design is the sample size grows with number of parameters and levels. The Table 2-2 below shows a comparison of number of trial runs for a two and three level design with varying factors:

Table 2-2 Number of experimental runs in full factorial design with different factors

Number of Factors (n)	Number of runs (N)	
	k=2	k=3
2	4	9
3	8	27
4	16	81
5	32	243

2.2.2 Regression Analysis

Regression analysis is a statistical method of measuring the relationship between two or more variables in terms of original unit of data. The intent of the analysis is to identify the effect of independent variable on dependent variable. Here the variable evaluated on based one other variable known as the dependent variable, while the other variable is called as independent variable. The type of regression analysis performed on data set can be categorized into linear and non-linear. Linear relationships are a straight line trend, while non-linear relationship represents curved trend lines whose equations are parabolic.

A regression relationship is basically derived based on lines of regression which are drawn by the method of least squares [8]. The method based on the sum of least squares tries to fit a regression line such in a way that error/residual is minimum/zero, in order to give a best estimate of one variable for known value of another variable, i.e. for a given a set of data points in k+1 dimension (example for k=1, in 2D points as (x_1, y_1), (x_2, y_2)... (x_n, y_n)), we try to find the line (y=mx+c) whose slope is (m) and intercept is (c) such that the sum of the total distances between each individual point and the line measured perpendicular to the line direction is minimum.

In a multiple-linear regression, the number of independent variable (x) related to dependent variable (y) may be more than two. Consider a multiple linear regression coded for a k independent variable x_1,x_2...x_k and one response variable y for an n observation, this can be represented as,

$$y_i = \beta_0 + \beta_1 x_{i1} + \cdots + \beta_k x_{ik} + \in_i, i = 1,2,3 \ldots., n$$

$$\in_{\boldsymbol{i}} = \boldsymbol{y_i} - (\boldsymbol{\beta_0} + \boldsymbol{\beta_1 x_{i1}} + \cdots + \boldsymbol{\beta_k x_{ik}}), \boldsymbol{i} = \boldsymbol{1,2,3 \ldots., n} \qquad \textit{Equation (4)}$$

Here, $\in_i$ is the error term associated, while β_0, β_1.. β_k are regression coefficients which describes the change in response in (y) with change in corresponding variable x. In method of

least squares, the value of β is varied so as to find one which gives least residual for a specific point (x_n,y_n). The least square function is written as:

$$L = \sum_{i=0}^{n} \in_i^2$$

$$\boldsymbol{L = \sum_{i=0}^{n}(y_i - \beta_0 - \sum_{j=1}^{k}\beta_j x_{ij})^2} \qquad \textit{Equation (5)}$$

This function L should be minimized by adjusting the values of $\beta_0, \beta_1 .. \beta_k$. The equation (2) is differentiate partially *w.r.t* to β_0, β_k and set to zero (minimum function) to derive the least squares coefficient estimates $\widehat{\beta_0}, \widehat{\beta_1} \ldots, \widehat{\beta_k}$. Applying the above conditions to equation (2),

$$\boldsymbol{\frac{\partial L}{\partial \beta_0} = -2 \sum_{i=0}^{n}(y_i - \widehat{\beta_0} - \sum_{j=1}^{k}\widehat{\beta_j} x_{ij}) = 0} \qquad \textit{Equation (6)}$$

$$\boldsymbol{\frac{\partial L}{\partial \beta_j} = -2 \sum_{i=0}^{n}(y_i - \widehat{\beta_0} - \sum_{j=1}^{k}\widehat{\beta_j} x_{ij})\, x_{ij} = 0 \quad , j = 1, 2, 3, \ldots k} \qquad \textit{Equation (7)}$$

The final simplified equation obtained from equation (3) & (4) is given below, [9]

$$n\widehat{\beta_0} + \widehat{\beta_1} \sum_{i=0}^{n} x_{i1} + +\widehat{\beta_2} \sum_{i=0}^{n} x_{i2} + \cdots + +\widehat{\beta_k} \sum_{i=0}^{n} x_{ik} = \sum_{i=0}^{n} y_i$$

$$\begin{array}{lllll}
\widehat{\beta_0}\sum_{i=0}^{n} x_{i1} + \widehat{\beta_1}\sum_{i=0}^{n} x_{i1}^2 & + \widehat{\beta_2}\sum_{i=0}^{n} x_{i1}x_{i2} + \cdots + \widehat{\beta_k}\sum_{i=0}^{n} x_{i1}x_{ik} & = \sum_{i=0}^{n} x_{i1}y_i \\
\cdot & \cdot & \cdot & \cdot & \cdot \\
\cdot & \cdot & \cdot & \cdot & \cdot \\
\widehat{\beta_0}\sum_{i=0}^{n} x_{ik} + \widehat{\beta_1}\sum_{i=0}^{n} x_{ik}x_{i1} + \widehat{\beta_2}\sum_{i=0}^{n} x_{ik}x_{i2} + \cdots + \widehat{\beta_k}\sum_{i=0}^{n} x_{ik}^2 & & & = \sum_{i=0}^{n} x_{ik}y_i
\end{array}$$

The above systems of equations are known as least square normal equations. The solution for these normal equations will give the predicted regression coefficients $\widehat{\beta_0}, \widehat{\beta_1} \ldots, \widehat{\beta_k}$. With the predicted regression coefficients, the response variable $\widehat{y_i}$ can be predicted. Once the regression coefficients terms are estimated, they are tested for their means (t-test) to check if the terms are statistically significant.

2.2.3 Analysis of Variance (ANOVA)

Analysis of variance is a statistical method to test for the variability between data by checking the homogeneity of their means. In regression, ANOVA is performed to test the level of variability within the regression model, and form a hypothesis based on level of

significance. The null hypothesis is that the fit of the intercept-only model (mean model) and the predicted model are equal, and the alternate hypothesis is the predictive power of intercept-only model is significantly less than the predicted model. The intercept-model is also known as constant mean model, uses the intercept or mean to predict the points. Table 2-3 shows a general ANOVA table which is obtained on a regression analysis along with method of calculation which are summarized below.

Table 2-3 ANOVA Table

Source of variation	DoF	SS	MSS	F-Value	P-Value
Regression	k-1	$RSS = \sum_{i=0}^{n} (\hat{y}_i - \overline{y})^2$	$MSR = \frac{RSS}{k-1}$	$F = \frac{MSR}{MSE}$	$F(k-1, n-k)$
Error	n-k	ESS=TSS-RSS	$MSE = \frac{ESS}{n-k}$		
Total	n-1	$TSS = \sum_{i=0}^{n} (y_i - \overline{y})^2$			

The first column in table is the degree of freedom (DoF) which represents the number of free variable in test static that can be varied. The number of degrees of freedom for regressor (k) is k-1, for the error term it is n-k where n is number of samples, while the total degree of freedom is sum of regressor and error terms DoF.

The Total Sum of Squares (TSS) is summation of squares of difference between each individual measured response variable (y_i) and its mean, while Regression Sum of Squares (RSS) is summation of squares of difference between each individual predicted response ($\hat{y}_i$) variable and its mean. Sum of Square for error term is the difference between TSS and RSS.

The Mean Sum of square (MSS) is ratio of Sum of Square (SS) of each variation to degree of freedom. The F- Value is calculated as ratio of variance between the treatments. The critical p-value for variance is obtained from the F-table at the desired level of significance based on the calculated F-value and the critical table value, if calculated F is less than the critical

value, we accept the null hypothesis and conclude that there is no significant difference between.

The final summary of regression model is estimated based on the data from ANOVA. A typical model summary table of regression is given below.

Table 2-4 R-Model Summary Table

Std. Error	R-sq	R-sq(adj)
$\sqrt{MSE}$	$R-Squared = \frac{RSS}{TSS}$	$R-Squared(Adj.) = 1-(1-R^2)\frac{n-1}{n-k-1}$

The R-Squared value of a model explains how much linear variability in response variable is explained by the predicted model. The higher the R-squared value, the greater is the variability captured by the response variable, while lower the R-squared it is vice versa. Based on number of predictors present in the model, the R-Squared value is adjusted to give a new modified R- value (R-sq(adj)).

Chapter 3. Parameter Selection and Experimental Procedure

Chapter 3 exclusively discusses the parameters selected for Design of Experiment (DoE), materials, consumables, experimental procedure and setup used in this study. To measure the bead geometry in GMAW, a number of experiments were performed in the bead on plate condition by varying welding parameters such as wire feed rate, voltage, travel speed along with a different composition of shielding gas.

3.1 Materials and Consumables

Welding was performed using two ER70-S-6 wires with 0.045 in (1.14mm) and 0.035 in (0.90mm) diameters as electrode (filler metal) in conjunction with an AISI 1020 base plate for this study. AISI 1020 steel plates were used as the base plate, because of its similarity in carbon content (having low carbon i.e. same as that of filler wire) and match in tensile strength (being comparable to that of filler wire, thereby preventing any strength mismatch). ER70S-6 welding wire is classified under clause as AWS 5.18 [14] as solid plain carbon steel wire. AWS designation for this wire is given as:

ER	Filler metal is in form of Electrode/Rod
70	Fillet metal wire has a minimum tensile strength of 70,000 psi (482.6 MPa)
S	Filler metal is a solid wire (not cored)
6	Chemical composition of the filler metal

ER70S-6 is one of the most commonly used wires and has a high silicon content in it which acts as a deoxidizer, thereby not requiring much cleaning of samples. Typical application of this wire includes sheet metal applications, automotive repair, structural steels, and pressure vessels [24]. The nominal chemical composition of the welding wire as per the manufacturer's specification is given in Table 3-1.

Table 3-1 Chemical composition of welding wire (As per manufacturer specification) [24]

Element (wt %)	C	Mn	Si	S	P	Cu	Ni	Cr	Mo	V
Welding Wire	0.06-0.15	1.40-1.85	0.80-1.15	0.035 max	0.025 max	0.50 max	0.15 max	0.15 max	0.15 max	0.03 max

The AISI 1020 base plates is a mild carbon steel, and these were sandblasted prior to welding to remove mill scale. The 1020 steel plates were obtained in two different thickness values, 6.35mm and 12.7 mm respectively. Low heat-input welds were performed using 6.35mm ($\frac{1}{4}\ in$) thickness plates, while for welding higher heat input parameters in order to prevent the burn through obtained from excessive penetration in cases with thinner plate, a plate with thickness of 12.7mm ($\frac{1}{2}\ in$) was used. The nominal chemical composition of base plate is given in Table 3-2.

Table 3-2 Chemical composition of base metal (As per manufacturer specification)

Element (wt %)	C	Mn	Si	S	P
Base Metal	0.18-0.23	0.30-0.60	-	0.050 max	0.040 max

3.2 Welding System

Welding was performed on the carbon steel base metal in the bead on plate condition in direct current electropositive (DCEP) mode. A Lincoln Electric R500 series was used as power source and all the welds were automated and performed using FANUC® Arcmate i120c. FANUC R3-J controller was used for controlling the movements of the robot, and a simple linear travel weld program was used to perform the welds and a pendent to train and guide the robot through the weld points. The gas flow rate was kept constant at 35cfh ($1\ \frac{m^3}{hr}$) during welding for all the three gasses and the welds were to a length of 100mm for each runs. A Data Acquisition System (DAQ) from National instrument® was used to record the

electrical signals for current and voltage during each experimental run. Figure 17 shows the experimental setup.

Figure 17 Welding System (a) FANUC R3J Controller; (b) Lincoln Electric™ R500 Power Supply; (c) Bead on Plate Setup; (d) FANUC Arcmate i120c automatic welder robot; (e) Gas Cylinders with flow meter

3.3 Selection of Parameters for Design of Experiments (DoE)

In this investigation, four main parameters were varied: wire feed speed, voltage, travel speed and gas type, and each response variable i.e. weld bead width, penetration, reinforcement height, penetration area, and reinforcement area were the response variables modeled separately using sets of input factors, with the technique of DoE determining the experimental tests.

A 3^3 full factorial design was used to identify main and interaction effect of different input variables on bead characteristics for each of three different gas types. Identifying and selecting the parameter range for DoE involved performing a number of initial trial experiments, and the parameters were selected based on the weldability, arc-stability and appearance/quality (visual inspection) of bead. For example, a wire feed rate of more than 600 ipm, with 30V at a travel speed less than 14ipm, the energy available at the torch will be less than the wire feed rate, causing excess wire sticking to the weld pool. The factors coded level (-1) represents the lowest parameter range with which a bead can be produced with a 10% variation added to it, and the factors coded (+1) represents the higher parameters limits with which a proper bead can be produced with a -10% correction added to it upper limit.

Table 3-3 Experimental Parameters for weld tests with 0.045 in diameter (1.14mm) ER 70S-6 Wire

Parameter	Low (-1)	Intermediate (0)	High (+1)	# of levels
Wire feed Speed (ipm)	200	390	580	3
Travel Speed (ipm)	20	25	30	3
Voltage (V)	20	25	30	3
Gas type	100% Ar	85% Ar-15% CO_2	100% CO_2	3

[Notice that ipm units are most common in welding procedure documentation, and thus these are used for the majority of graphs in the present work, where travel speeds of 20 to 30 ipm equate to 0.508 to 0.762 m/min, and wire feed speeds of 200 to 580 ipm equate to 5.08 to 14.732 m/min].

There was one major limitation with the parameters listed in Table 3-3. The above factorial DoE covered entire range of possible parameters for wire feed speed and voltage, but the range of travel speed in the DoE could be further extend beyond that limit. For example, when a wire feed speed and voltage value between lower-intermediate level is used,

the range of travel speed can be further lowered beyond its lower limit (-1) and vice versa at the intermediate-high level, the range of travel speed can be increased beyond the (+1) limit.

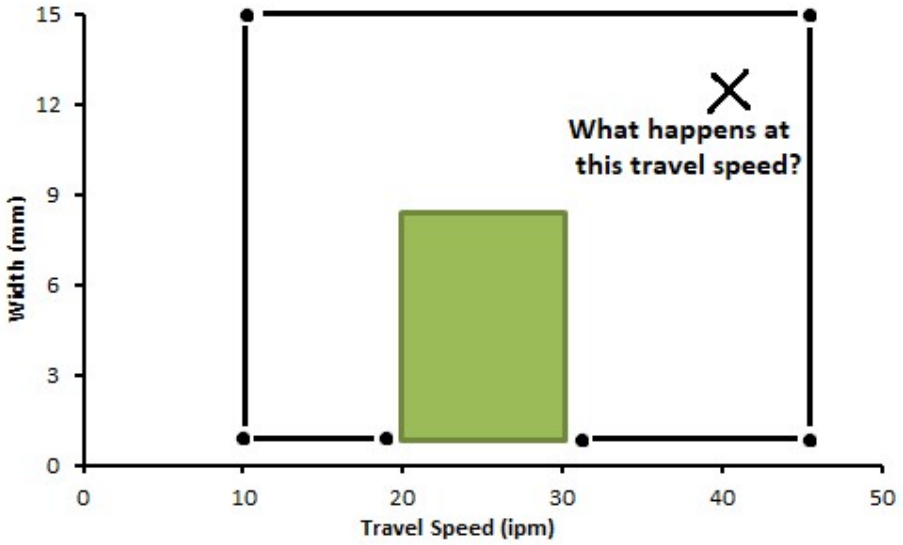

Figure 18 Estimating the effect of travel speed variation beyond the limit (-1) and (+1)

To capture this effect an additional factorial design was used and preferred over Central Composite Design (CCD) with star points circumscribed, which is an another alternative methodology to capture this effect. However, the limitation using CCD model is the numbers of additional points are 2k (where k is number of independent variables), which would result in performing only 6 additional experiments and would still not be able to sufficiently describe the effect of travel speed beyond the limits.

Therefore a 2^3 factorial design with parameters given in Table 3-4 below was used to identify effects of parameter of lower (decreased travel) speed at lower-Intermediate level wire feed speed and voltage range. While parameters given in Table 3-5 were used to estimate the effect of higher (increased) travel speeds at upper intermediate-high levels.

The low-intermediate factor for wire feed and voltage were taken as two intermediate points between the factors (-1) and (0) i.e. (-0.67) and (-0.33). While the intermediate-high factor were taken as intermediate points between the factors (0) and (+1) i.e. (+0.33) and

(+0.67) respectively. Overall 121 weld beads were made in total for the 0.045 in wire to develop statistical model for prediction.

Table 3-4 Weld Parameters for low-intermediate Wire Feed speed, Voltage range (0.045 in/1.14mm wire)

Parameter	Factor 1	Factor 2	No. of level
Wire feed Speed (ipm)	264 (-0.67)	326 (-0.33)	2
Voltage (V)	21.6 (-0.67)	23.4 (-0.33)	2
Travel Speed (ipm)	12	16	2

Table 3-5 Weld Parameters for intermediate-high wire Feed speed, and voltage range (0.045 in/1.14mm wire)

Parameter	Variable 1	Variable 2	No. of level
Wire feed Speed (ipm)	454 (+0.33)	516 (+0.67)	2
Voltage (V)	26.6 (+0.33)	28.4 (+0.67)	2
Travel Speed (ipm)	37	44	2

Similar steps were followed for ER 70S-6 wire with a diameter of 0.035 in (0.90mm). The ER 70S-6 wire of 0.045 in diameter is 1.6 times greater in area compared to 0.035 in wire. To identify main and interaction effect of different input variables on bead characteristics for each of three different gas types, a 3^3 full factorial design shown in Table 3-6 was used and to capture effects of variation in travel speed at low-intermediate and intermediate-range of wire feed speed and voltage, based on a 2^3 factorial design shown in

Table 3-7 and Table 3-8.

Table 3-6 Experimental Parameters for ER 70S-6 Wire with 0.035 in diameter (0.90mm)

Parameter	Low (-1)	Intermediate (0)	High (+1)	Levels
Wire feed Speed (ipm)	250	425	600	3

Travel Speed (ipm)	16	23	30	3
Voltage (V)	20	25	30	3
Gas type	100% Ar	85% Ar-15% CO_2	100% CO_2	3

Table 3-7Weld Parameters for low-intermediate Wire Feed speed, Voltage range (0.035 in/0.9mm wire)

Parameter	Variable 1	Variable 2	Levels
Wire feed Speed (ipm)	308 (-0.67)	367 (-0.33)	2
Voltage (V)	21.6 (-0.67)	23.4 (-0.33)	2
Travel Speed (ipm)	10	13	2

Table 3-8 Weld parameters for intermediate-high wire Feed speed, and voltage range (0.035 in/0.9mm wire)

Parameter	Variable 1	Variable 2	Levels
Wire feed Speed (ipm)	484 (+0.33)	542 (+0.67)	2
Voltage (V)	26.6 (+0.33)	28.4 (+0.67)	2
Travel Speed (ipm)	37	44	2

3.4 Weld bead geometry Measurement

Figure 19 shows an outline sketch of a weld bead with five main bead geometries, namely width (W), penetration (P), reinforcement height (R), penetration area (PA) and reinforcement area (RA) which are measured in this study. Here the width represents the spread of weld pool over base metal surface, penetration represents the extent to which weld pool has penetrated into the base metal, penetration area represents total area penetrated by the deposited metal into base metal, while reinforcement height is total height of deposited metal from base metal to peak of reinforcement, and reinforcement area is measured as total area of the deposited metal above the surface of base metal.

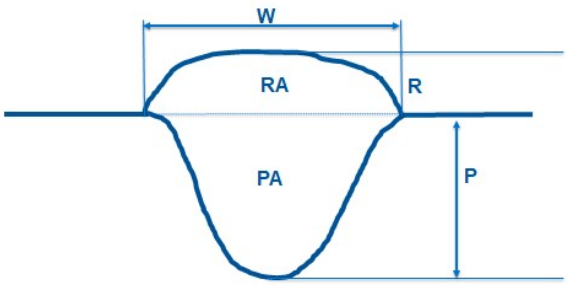

Figure 19 Outline of weld bead geometry denoting key dimensions measured here.

The plate and resultant beads were prepared for imaging and measurements by sandblasting it after welding to get their clear image, and Adobe Photoshop® CS3 software was used to measure the bead width precisely. An image of the top surface of each weld was taken, and an area of the bead was selected, excluding the end sections, using the software quick selection tool. The length of selected bead area was measured using the ruler tool and the average width of the weld bead was then calculated as ratio of the area to the length of the selected section, using a minimum length of at least 50 mm in each weld. Figure 20 shows the steps followed in measuring width of the bead.

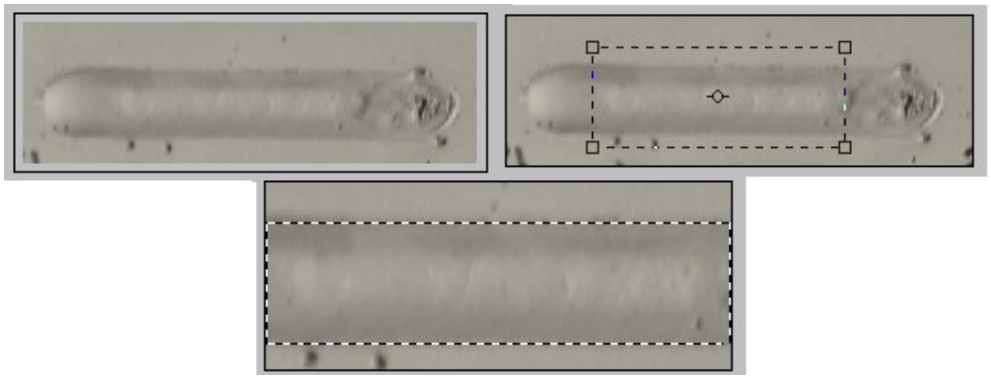

Figure 20 Measurement of Bead Width using Adobe Photoshop® CS3

To measure the depth of penetration, reinforcement height, penetration area and reinforcement area, two cross sections of the welds were cut one at approximately one-third of distance from start of weld bead and one at the mid-length. The cut-samples were mounted in epoxy and grinded up to 1200 grit size. The samples were then etched using Nital and the

macro-images of the cross section was imaged using stereo microscope as shown in Figure 21. Penetration, reinforcement height and their respective areas were calculated for each cross sections using Adobe Photoshop® software using the ruler and quick selection tool.

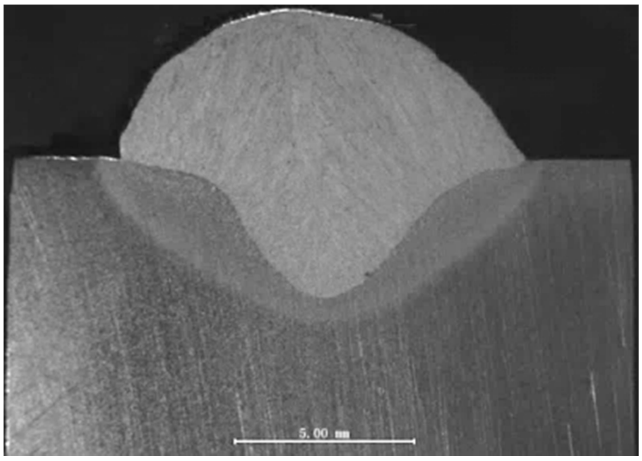

Figure 21 Optical micrograph of a cross-section of a weld bead

3.5 Statistical Model

In this investigation the weld bead width, penetration, reinforcement height, penetration area and reinforcement area were the response variables modeled. In order to capture the relationships between the response variables and factor inputs, each factor was tested at different levels. Furthermore, to determine if any interactions exist between input variables, a full factorial DOE was used. The models that underlie the factorial design are of the form:

$$\boldsymbol{W = \beta_0 + \beta_1 S + \beta_2 V + \beta_3 T + \beta_4 S^2 + \beta_5 V^2 + \beta_6 T^2 + \beta_7 SV + \beta_8 ST + \beta_9 VT + \varepsilon} \quad \textit{Equation (8)}$$

$$\boldsymbol{P = \beta_0 + \beta_1 S + \beta_2 V + \beta_3 T + \beta_4 S^2 + \beta_5 V^2 + \beta_6 T^2 + \beta_7 SV + \beta_8 ST + \beta_9 VT + \varepsilon} \quad \textit{Equation (9)}$$

$$\boldsymbol{R = \beta_0 + \beta_1 S + \beta_2 V + \beta_3 T + \beta_4 S^2 + \beta_5 V^2 + \beta_6 T^2 + \beta_7 SV + \beta_8 ST + \beta_9 VT + \varepsilon} \quad \textit{Equation (10)}$$

$$\boldsymbol{PA = \beta_0 + \beta_1 S + \beta_2 V + \beta_3 T + \beta_4 S^2 + \beta_5 V^2 + \beta_6 T^2 + \beta_7 SV + \beta_8 ST + \beta_9 VT + \varepsilon} \quad \textit{Equation (11)}$$

$$\boldsymbol{RA = \beta_0 + \beta_1 S + \beta_2 V + \beta_3 T + \beta_4 S^2 + \beta_5 V^2 + \beta_6 T^2 + \beta_7 SV + \beta_8 ST + \beta_9 VT + \varepsilon} \quad \textit{Equation (12)}$$

where W, P, R, PA and RA are the weld bead width, penetration, reinforcement height, penetration area and reinforcement area respectively, V is the arc voltage, T is the travel

speed, S is the wire feed speed, β_i are the model parameter to be estimated, and ε is the random error variable. Interactions among main effects are indicated by the model terms with factor products, and possible non-linear dependencies are indicated by squared model terms. *Equation (8)* to *Equation (12*) represent five separate width, depth, reinforcement models, penetration area and reinforcement area one for each shielding gas type; and the model coefficients β_i are determined by the appropriate selection. The maximum order for each of the polynomial terms was taken two i.e. second order. Though the higher complexity order provides a better fit, an order for the polynomial terms was taken as two to eliminate the over fitting of data.

To prevent over-fitting the data, the full models were reduced after determining the statistically significant model parameters using an analysis of variance (ANOVA). The insignificant covariate terms were determined from ANNOVA table and based on the p-values the terms were removed. The models were re-run again to find if there were other insignificant terms, and the process was followed until all the insignificant terms were eliminated and the terms in model had statistically significant p-values. Some of the main covariate terms that are theoretically important or were significant based on prior studies were kept in the model even though they were insignificant. Statistical analyses were performed using the Minitab and R programming language version 3.4.3 in RStudio [25]. Two sets of data for each experimental condition were taken so as to obtain an independent estimate of the error, and the test order was randomized to avoid any potential bias and lurking variables.

Chapter 4. Results & Discussion

The measurements of the resultant welds for all experimental trails are evaluated here, including the bead width, penetration, reinforcement height, penetration and reinforcement area along with the model predictions overlaid on the data. Magnitudes of each welding parameter on measured geometry and their interaction effects are also discussed based on the corresponding ANOVA results which are summarized in Appendix C.

4.1 Results of bead on plate welds

This section primarily discusses the experimental results of bead-on-plate welding for all the bead geometry for two different diameter wires along with their multivariate regression fits. Additional useful data from experiments, ANOVA analysis tables, linear regression models and coefficients for DoE, and macro images for each weld beads are given in Appendix A, B and C respectively.

4.1.1 Weld Width

In general, bead width increased progressively with voltage level between 20 and 25 V for all the gas types, and decreased or leveled off at higher voltages depending on voltage, thereby achieving a plateau at intermediate voltage for most points. As the travel speed is increased, the amount of weld metal deposited per unit length is decreased while reducing the time allowed for wetting on the plate surface, resulting in a reduction in weld width for all the gases. From Figure 22, it can be seen that for 100% Argon and 85% Argon-15% CO_2 mixed gas, increasing voltage appeared to have a diminishing effect on the bead-width at lower voltages, and the concavity of model changes as voltage is increased. Conversely, in 100%

CO_2 the relationship between input-voltage and bead-width appeared to be almost linear for most cases. At low-intermediate coded factors and the width increased with voltage similar to trend observed between 20 and 25 V in Figure 22 and at intermediate-high coded factors showing a decreasing trend similar to observation seen at 30ipm in Figure 22. The trends observed at lower-intermediate and intermediate-high factors are given in Appendix D.

The resulting width model for 0.045 in wire with 100% Argon gas consisted, an interaction of voltage with wire feed speed and travel speed, 85% Argon-15% CO_2 model had a second-order polynomial in wire feed speed, voltage, travel speed and interaction of wire feed speed with voltage and travel speed, and 100% CO_2 model had second-order polynomial in wire feed speed and voltage.

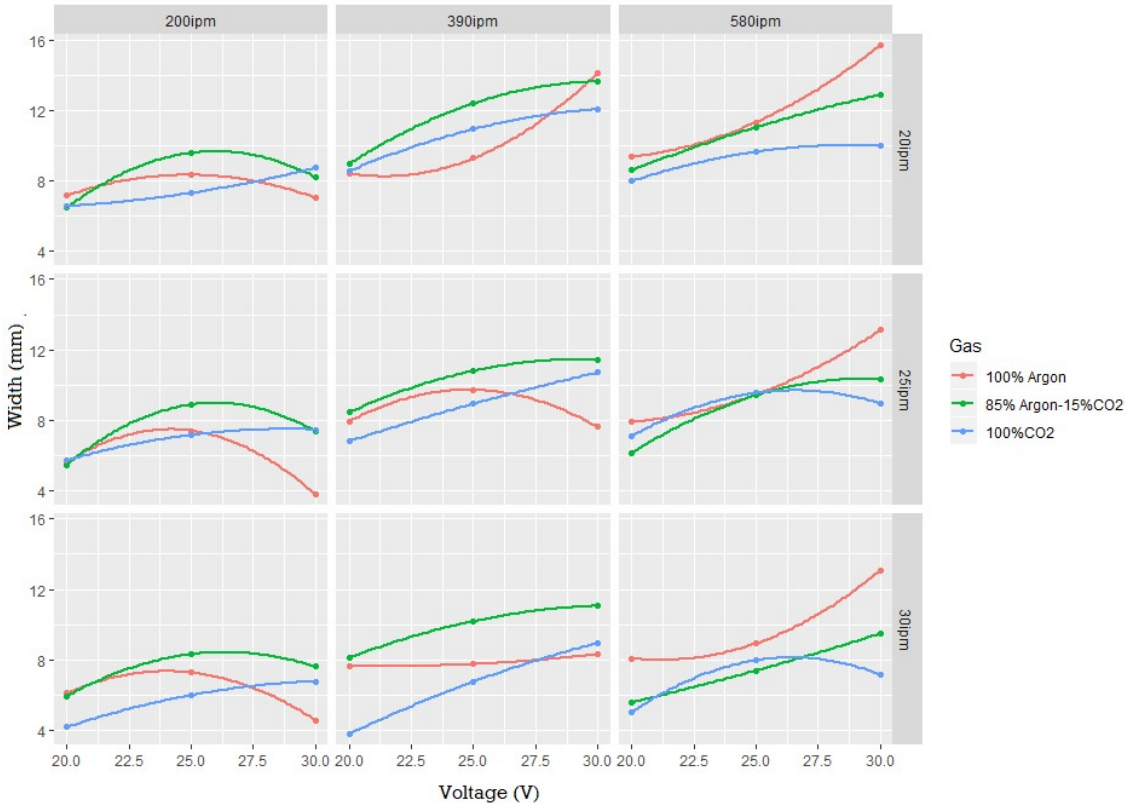

Figure 22 Weld width as a function of wire feed speed for 0.045 in wire (Each grid plots the width versus wire feed speed, with raw data for different Voltage and Travel Speed for each gas, and the model predictive equation for that quadrant represented).

The width voltage relationship at varying wire feed and travel speed levels for welds produced with 0.035 in diameter wire is given in Appendix D. The width increased between 20 and 25 V along for all the wire feed speed and between intermediate-high travel speed and voltage levels, the width-voltage relationship approached a limiting value range, a trend similar to one observed with 0.045 in. The statistical model for bead width with 0.035 in wire had wire feed speed, voltage, travel speed, an interaction of voltage with travel speed and a second order polynomial for travel speed for all the gasses. For welds produced using 100% Argon the model had an additional second order polynomial term for voltage and an interaction term between wire fee speed and voltage, while using 100% CO_2 had an additional second order term for wire feed speed. The welds made using 85% Argon-15% CO_2 resulted in a model which had second order polynomial terms for all the input three variable i.e. V^2, W^2, TS^2 and also an interaction between them i.e. *W*V, W*TS, V*TS*.

4.1.2 Weld Penetration (Depth)

The penetration for welds increased when the wire feed speed was increased, which is due to the relationship between wire feed speed and welding current for constant voltage welding machines. The concavity of the penetration model as a function of wire feed speed appears to be governed by the gas type, see Figure 23. From the trends observed in Figure 23 with pure argon, the penetration rapidly increased with wire feed speed, and was concave up for most voltage and travel speed range except for low travel speed and high voltage level, whereas with 100% CO_2 and mixed gas concavity of the penetration-wire feed speed relationship changed with increase in voltage. Figure 24 shows the relationship penetration-wire feed speed relation at low-intermediate and intermediate-high coded factors. It can be noted that depth of penetration increases progressively with wire feed speed similar to the trend observed in Figure 23.

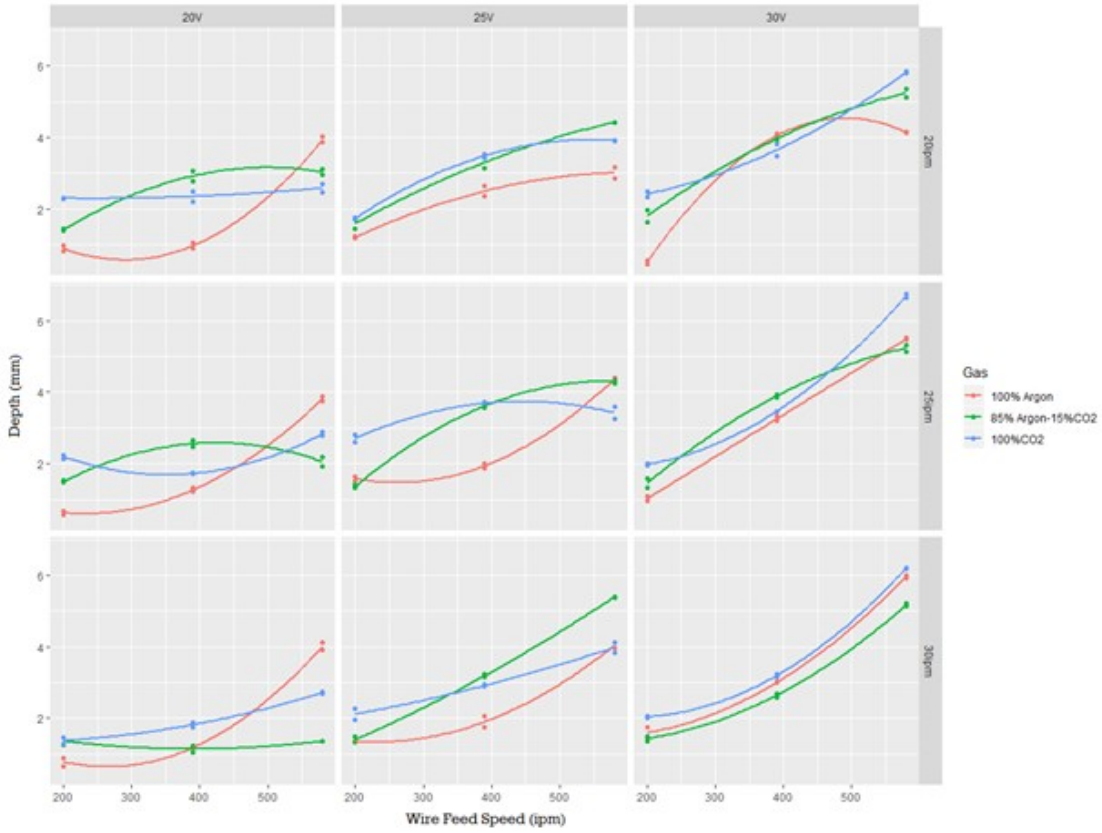

Figure 23 Weld penetration as a function of wire feed speed for 0.045 in wire (Each plot in the grid relates the width versus wire feed speed, with raw data for different voltage and travel Speed for each gas, along with the predictive model equation for that quadrant).

Statistically, there are several variables (wire feed speed, voltage, travel speed, second order polynomial of wire feed speed, the interaction between wire feed speed and voltage, as well as the wire feed speed and travel speed) were significant in predicting the penetration for 100% Argon gas. The 85% Argon-15% CO_2 gas had a model similar to 100% Argon with an additional second order polynomial term for voltage. The resulting model for 100% CO_2 consisted of wire feed speed, voltage, travel speed, second order polynomial of wire feed speed and travel speed, along with an interaction between wire-feed speed and voltage.

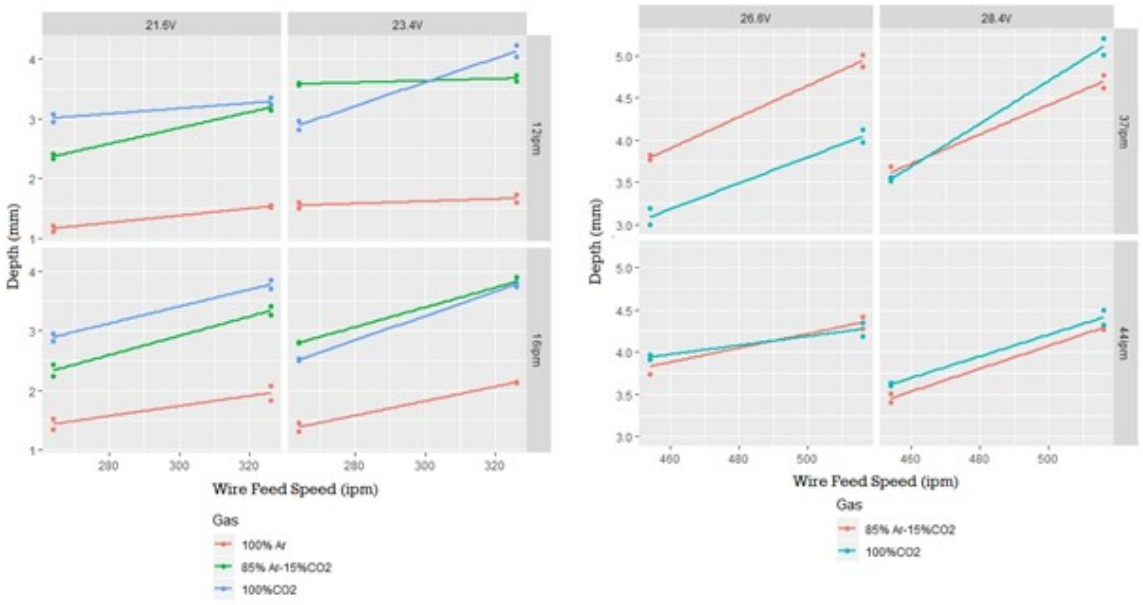

Figure 24 Weld penetration as a function of wire feed speed for 0.045 in wire (Each grid plots the width versus wire feed speed, with raw data from extended DoE for different Voltage and Travel Speed for each gas, and the model predictive equation for that quadrant represented)

The depth- wire feed speed relationship at varying voltage and travel speed levels for 0.035 in diameter wire is given in Appendix D. With increase in voltage from left to right and increase in travel speed from up to down, we can see the increase in depth across each plot, which shows that the depth of penetration increased with voltage and travel speed for all the wire feed speeds. With higher wire feed speed, the depth decreased/levelled at lower level voltage that can be explained due to transfer mode occurring at low voltage. The statistical model for bead depth had wire feed speed, voltage, travel speed, an interaction of wire feed speed with voltage for all the gasses. The model for 100% Argon welds had an additional second order polynomial term for wire feed speed and an interaction term between voltage and travel speed, while 100% CO_2 had an additional second order term for travel speed and an interaction between wire feed speed and voltage. The 85% Argon-15% CO_2 model had second order polynomial terms for all the input three variable i.e. V^2, W^2, TS^2 and an interaction between voltage and travel speed.

4.1.3 Reinforcement Height

The reinforcement height generally increased with wire feed speed as expected based on the mass conservation of wire material. The reinforcement height slightly decreased as the travel speed increased, as expected based on a reduced deposition rate per unit length due to faster travel rate of torch. Figure 25 shows the weld reinforcement height as function of wire feed speed for different voltage and travel speed range. Reinforcement height decreased with increases in voltage, or increases in travel speed. The concavity of the models also changed with voltage, and unlike penetration, the concavities of the trend lines in Figure 25 were comparable for each parameter for most bead measurements at 20 and 25V.

From the ANOVA analysis, the statistical model indicates an interaction of voltage with wire feed and travel speed as significant term for all the gas types. The model for 100% Argon had an additional second order polynomial including the wire feed speed term, while the 100% CO_2 gas had a second order polynomial of wire feed speed and voltage along with an interaction of voltage with wire feed and travel speed. The model for 85% Argon-15% CO_2 gas had no additional terms.

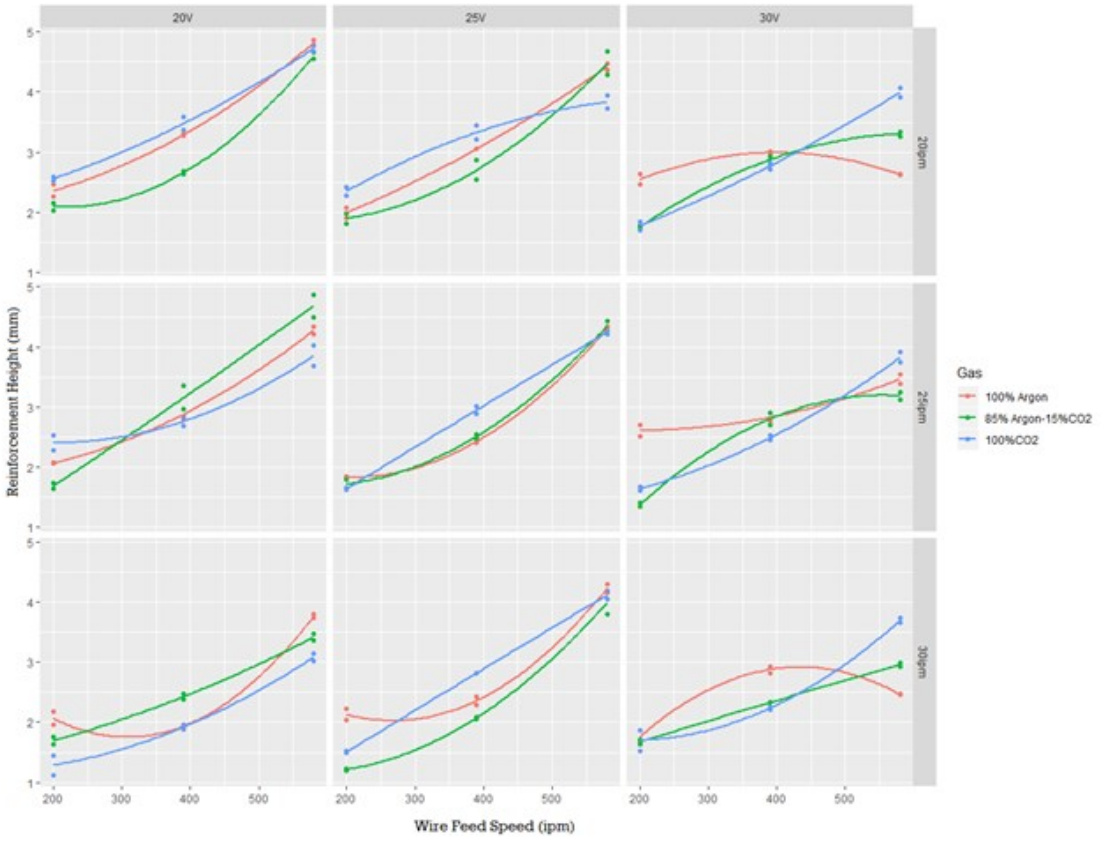

Figure 25 Weld reinforcement height as a function of wire feed speed for 0.045 in wire (Each grid plots the width versus wire feed speed, with raw data for different Voltage and Travel Speed for each gas, and the model predictive equation for that quadrant represented)

For the case of welds produced using the 0.035 in diameter wire, the reinforcement height-wire feed speed relationships for different voltage and travel speed are shown in Appendix D. A similar trend is observed to that produced using 0.045 in wire, i.e. with an increase in wire feed the reinforcement height increased at all levels, and with increase in voltage and travel speed, reinforcement height of weld decreased. The resulting statistical model for reinforcement for 100% CO_2 gas includes wire feed speed, voltage, travel speed for all the gasses without additional terms. However, the model for 85% Argon-15% CO_2 and 100% Argon model had a second order polynomial for voltage term. The 85% Argon-15% CO_2 gas model also had an additional interaction term between wire feed speed and voltage ($W*V$) and a second order polynomial term for travel speed.

4.1.4 Reinforcement Area

As expected based on the conservation of material, the reinforcement area i.e. area of filler metal deposited, increased with increasing wire feed speed and decreased with travel speed. Figure 26 shows the relationship between reinforcement area as function of wire feed speed for different voltage and travel speed range for 0.045 in diameter wire. The concavity of the model was linear for the gas types and increased progressively with feed rate.

Statistically, in addition to wire feed speed, voltage, and travel speed, the model for all the gasses had a second order polynomial term for travel speed and an interaction between wire feed speed and travel speed. The models for welds produced with 100% Argon and 100% CO_2 gases had no additional interaction terms, while the model for 85% Argon-15% CO_2 gas had an additional second order polynomial for wire feed.

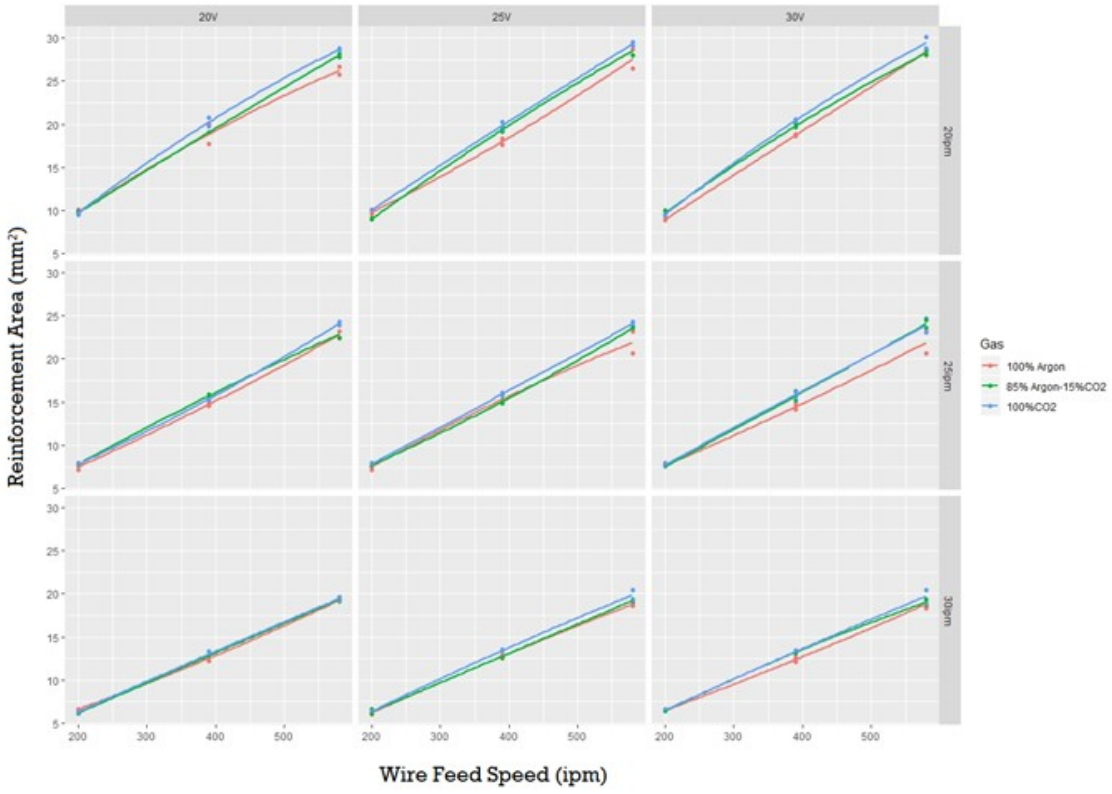

Figure 26 Weld reinforcement area as a function of wire feed speed for 0.045 in wire (Each grid plots the width versus wire feed speed, with raw data for different Voltage and Travel Speed for each gas, and the model predictive equation for that quadrant represented)

For 0.035 in diameter wire, the reinforcement area of the weld increased with wire feed speed and decreased with increase in travel speed, similar to trend observed with 0.045 in wire. The statistical model for reinforcement area had wire feed speed, voltage, travel speed, second order polynomial of wire feed speed and the interaction between wire feed speed and travel speed as well as significant terms for each of the gases. In addition to the foresaid terms, the model for welds using 100% Argon and 100% CO_2 gas had an interaction between wire feed speed and voltage (*W*V*) term and the 85% Argon-15% CO_2 gas had an additional second order polynomial term for wire feed speed.

4.1.5 Penetration Area

The penetration area for welds is the extent to which weld metal has penetrated into the base metal. From Figure 27 the penetration area of the weld increased when the wire feed speed increased; due to higher welding current at increased wire feed speeds. The concavity of the penetration model as a function of wire feed speed is governed by the gas type. From Figure 27 which shows the relationships for 100% argon gas, the penetration area increased with wire feed speed for all the speed levels, whereas with 100% CO_2 gas the concavity (fit) changed with voltage levels. At low-intermediate and intermediate-high coded factors Table 3-4 and Table 3-5, the penetration-wire feed speed relationship increased with wire feed speed following a pattern similar to that observed in Figure 27.

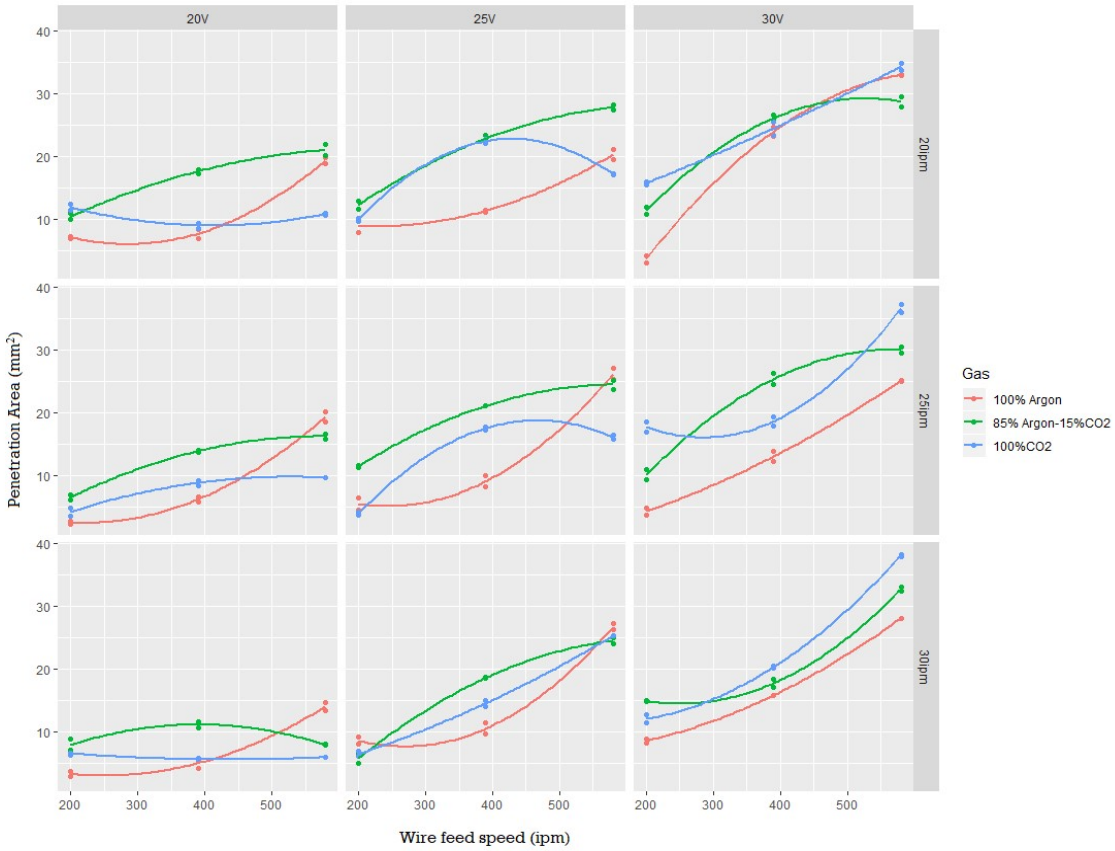

Figure 27 Weld penetration area as a function of wire feed speed for 0.045 in wire (Each grid plots the width versus wire feed speed, with raw data for different Voltage and Travel Speed for each gas, and the model predictive equation for that quadrant represented)

Statistically in addition to wire feed speed, voltage, travel speed, all the gas models had an interaction effect between wire feed speed and voltage. For 100% argon gas, model had an additional second order polynomial term for wire feed and travel speed. While the model for 100% CO_2 welds had an interaction term between wire feed speed and travel speed. For welds produced with 85% Argon-15% CO_2 gas, an additional second order polynomial is needed for wire feed speed, travel speed and voltage.

The penetration area vs. wire feed speed relationship for all gases with 0.035 in diameter wire is given in Appendix D. The penetration area of weld increased with wire feed speed for all welds, and with increase in voltage from left to right the area of penetration increased slightly. Also when travel speed was increased the size of penetrated area was reduced

drastically due to low heat input per unit area from faster torch travel. Statistical models for all the three gases had a common wire feed speed, voltage, travel speed, an interaction between wire feed speed and voltage (*W*V*). The models for 100% argon and for 100% CO_2 gas had no additional terms, while that for 85% argon-15% CO_2 had an additional second order polynomial for wire feed speed and travel speed, and an interaction term between wire feed speed and travel speed (*W*TS*).

4.1.6 Welding Current

The wire current during welding is directly proportional to the rate at which wire is fed. As wire feed rates through the torch increase, a higher current is required to melt the wire, and this can be seen from trends in model fits for the 0.045 in wire and 0.035 in wire. Figure 28 shows the concavity of current-wire feed speed relationship coded for different voltage and travel speed for various types of gases, and is found to be linear for all cases and progressively increased with feed rate.

In addition to wire feed speed, voltage, travel speed the statistical model for all the gasses had a second order polynomial term for travel speed and an interaction between wire feed speed and travel speed. The 100% argon and 100% CO_2 gases had the above aforementioned terms with no additional interaction terms, while 85% argon-15% CO_2 gas model had an additional second order polynomial for wire feed.

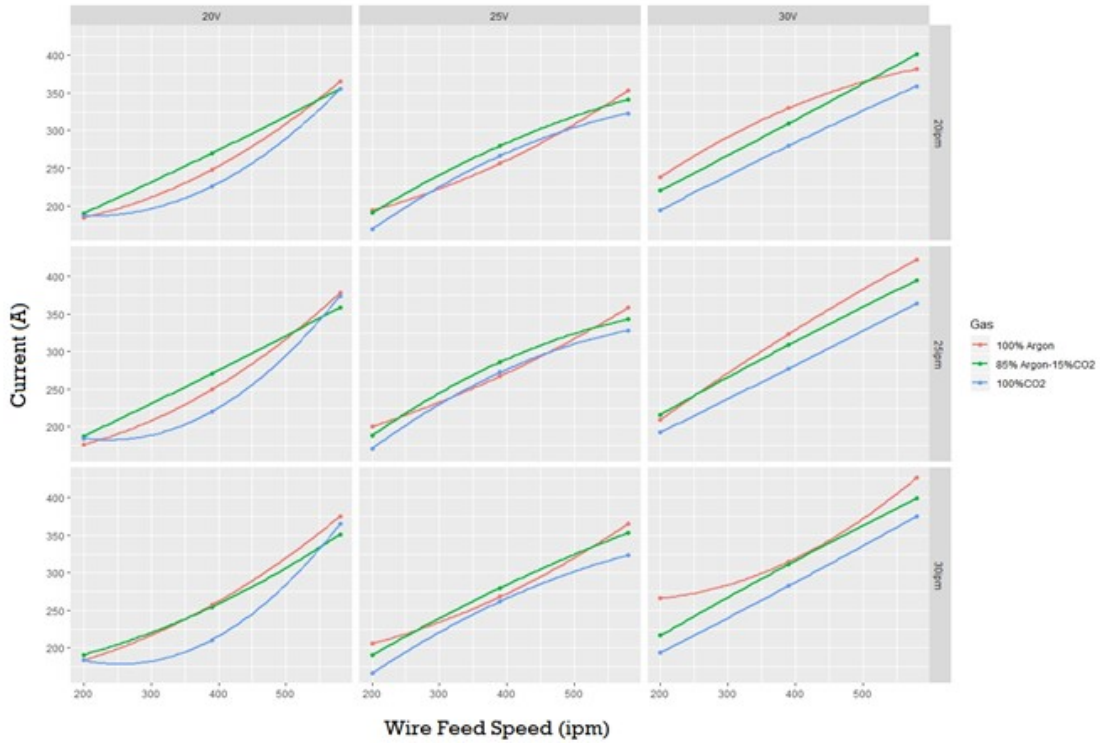

Figure 28 Welding current as a function of wire feed speed for 0.045 in wire (Each grid plots the width versus wire feed speed, with raw data for different Voltage and Travel Speed for each gas, and the model predictive equation for that quadrant represented)

For welds produced with 0.035 in diameter wire, the statistical model had wire feed speed, voltage, travel speed, second order polynomial of wire feed speed for each gas. The model for 100% argon gas had second order polynomial of voltage and an interaction terms for wire feed speed with voltage and travel speed. The results with 85% argon-15% CO_2 gas are described by a model with second order polynomial for travel speed and an interaction terms for voltage with travel speed, and the model for 100% CO_2 had interaction terms for wire feed speed with voltage and a second order polynomial term for travel speed (TS^2).

4.1.7 Statistical Analysis – Final Model

Six separate equations—one for each gas type, due to the qualitative nature of this factor—are given for current, width, penetration, reinforcement height, penetration area and reinforcement area for each wire in Table 4-1 and Table 4-2. The models have been reduced from their full forms in *Equation (8)* to *Equation (12)* by including only factors determined to be significant from the ANOVA, and the model coefficients are minimally correlated least-squares estimates [9]. The intercepts of these equations represent the main effect of changing gas type.

For a given model, the factor coefficients which change with gas type reflect the interaction between the given factor and gas type. The predicted weld bead width, penetration, reinforcement height, penetration area and reinforcement area for a given gas type are found by substituting the coded factor levels (i.e. -1, -0.67, -0.33, 0, 0.33, 0.67, 1) into the corresponding models.

Table 4-1 Statistical models for weld bead width, penetration, reinforcement height, reinforcement area, penetration area and welding current for each gas type, using only significant parameters from the ANOVA for 0.045 in wire

Gas	Model	Equation	Standard Error
100% Argon	Current (A)	I = 548 + 0.183*WFS - 39.75*V + 0.908*TS + 0.000352*WFS^2 + 0.901*V^2	±12.61
	Penetration (mm)	P = 2.40 - 0.01320*WFS + 0.0122*V - 0.0802*TS + 0.000011*WFS^2 + 0.000285*WFS*V + 0.000236*WFS*TS	±0.53
	Reinforcement Height (mm)	R = 4.61 + 0.01051*WFS - 0.0491*V - 0.2364*TS+ 0.000006*WFS^2 - 0.000423*WFS*V+ 0.00709*V*TS	±0.39
	Width (mm)	W = 3.16 - 0.03332*WFS + 0.251*V + 0.534*TS + 0.001785*WFS*V - 0.0295*V*TS	±1.22
	Penetration Area (mm^2)	PA = 36.32 + 0.04058*WFS - 0.021*V - 2.389*TS - 0.000003*WFS^2 + 0.03629*TS^2 + 0.000061*WFS*V	±1.19
	Reinforcement Area (mm^2)	RA = 28.94 + 0.07676*WFS - 0.0033*V - 2.366*TS + 0.04704*TS^2 - 0.001485*WFS*TS	±0.74
85% Argon +15% CO2	Current (A)	I = 429.9 + 0.4486*WFS - 28.16*V - 1.599*TS - 0.0001*WFS^2 + 0.606*V^2 + 0.0290*TS^2 + 0.00423*WFS*V	±7.05
	Penetration (mm)	P = -11.01 - 0.01145*WFS + 1.228*V - 0.1047*TS - 0.00001*WFS^2 - 0.02819*V^2 + 0.000882*WFS*V + 0.000165*WFS*TS	±0.47
	Reinforcement Height (mm)	R = 2.53 + 0.01177*WFS - 0.0386*V - 0.1168*TS - 0.000235*WFS*V + 0.00292*V*TS	±0.30
	Width (mm)	W =-26.35 + 0.04829*WFS + 2.385*V - 0.2546*TS - 0.000061*WFS^2 - 0.04664*V^2 + 0.00452*TS^2 + 0.000640*WFS*V - 0.000540*WFS*TS	±0.60
	Penetration Area (mm^2)	PA = -57.4 - 0.0272*WFS + 5.34*V+ 0.140*TS - 0.000042*WFS^2 - 0.1139*V^2	±3.19
	Reinforcement Area (mm^2)	RA = 15.76 + 0.08757*WFS + 0.0126*V- 1.2825*TS - 0.000012*WFS^2 + 0.02207*TS^2- 0.001467*WFS*TS	±0.97
100% CO2	Current (A)	I = 40+ 0.4432* WFS +2.153*V-0.052*TS	±16.28
	Penetration (mm)	P = 9.77 - 0.02489*WFS - 0.1841*V- 0.1891*TS + 0.000009*WFS^2 + 0.002714*TS^2	±0.54
	Reinforcement Height (mm)	R = 7.36 - 0.00931*WFS + 0.086*V- 0.3151*TS + 0.000012*WFS^2 - 0.00888*V^2	±0.39
	Width (mm)	Width = -19.65 + 0.03187*WFS + 1.857*V- 0.1982*TS - 0.000035*WFS^2 - 0.0314*V^2	±0.71
	Penetration Area (mm^2)	PA = 35.5 - 0.1256*WFS - 0.139*V - 1.092*TS + 0.004547*WFS*V + 0.001616*WFS*TS	±4.32
	Reinforcement Area (mm^2)	RA = 15.61 + 0.08151*WFS + 0.0141*V- 1.2080*TS + 0.02137*TS^2 - 0.001543*WFS*TS	±0.87

Table 4-2 Statistical models for weld bead width, penetration, reinforcement height, reinforcement area, penetration area and welding current for each gas type, using only significant parameters from the ANOVA for 0.035 in wire

Gas	Model	Equation	Standard Error
100% Argon	Current (A)	I =438.3 + 0.232*WFS - 33.30*V - 1.457*TS - 0.000350*W^2 + 0.714*V^2+ 0.00912*W*V + 0.00337*W*TS	±7.97
	Penetration (mm)	P=-1.385 + 0.002212*WFS + 0.1108*V - 0.03049*TS + 0.000000*W^2 + 0.000002*W*V- 0.000336*V*TS	±0.35
	Reinforcement Height (mm)	R = 4.204 + 0.003635*WFS - 0.0547*V - 0.07479*TS - 0.000118*V^2	±0.39
	Width (mm)	W = -5.69 - 0.02185*WFS + 1.359*V- 0.274*TS - 0.0282*V^2 + 0.00890*TS^2+ 0.001203*W*V - 0.01092*V*TS	±0.80
	Penetration Area (mm^2)	PA = 1.23 + 0.01020*WFS+ 0.3001*V- 0.2928*TS - 0.000025*W*V	±2.76
	Reinforcement Area (mm^2)	RA = 14.16 + 0.02547*WFS + 0.0399*V- 0.5899*TS - 0.00053*TS^2 - 0.000111*W*V + 0.000066*W*TS	±1.78
85% Argon +15% CO2	Current (A)	I = 78.1 + 0.4496*WFS - 0.09*V - 5.674*TS - 0.000222*W^2 + 0.0528*TS^2+ 0.1087*V*TS	±6.06
	Penetration (mm)	P =-0.28 - 0.00123*WFS + 0.216*V- 0.1034*TS - 0.000003*W^2 - 0.00771*V^2 + 0.000538*TS^2 + 0.000356*W*V + 0.00192*V*TS	±0.23
	Reinforcement Height (mm)	R = 6.52 + 0.00657*WFS - 0.289*V- 0.1462*TS + 0.00585*V^2 + 0.001943*TS^2- 0.000136*W*V	±0.21
	Width (mm)	W = -8.17 + 0.01221*WFS + 1.045*V - 0.1179*TS - 0.000015*W^2 - 0.01312*V^2 + 0.00870*TS^2 + 0.000558*W*V - 0.000336*W*TS - 0.01396*V*TS	±0.46
	Penetration Area (mm^2)	PA = 25.17 - 0.0451*WFS - 0.626*V - 0.599*TS + 0.000039*W^2 + 0.01467*TS^2 + 0.002449*W*V - 0.000985*W*TS	±1.57
	Reinforcement Area (mm^2)	RA =8.18 + 0.06678*WFS + 0.0429*V - 0.9482*TS - 0.000022*W^2 + 0.01718*TS^2 - 0.000968*W*TS	±1.04
100% CO2	Current (A)	I=32.5 + 0.369*WFS+ 0.31*V - 2.216*TS - 0.000267*W^2 + 0.0452*TS^2+ 0.00468*W*V	±7.07
	Penetration (mm)	P=3.75 - 0.00506*WFS - 0.0618*V - 0.1185*TS + 0.001711*TS^2+ 0.000329*W*V	±0.42
	Reinforcement Height (mm)	R = 3.381 + 0.004071*WFS- 0.0697*V- 0.03842*TS	±0.46
	Width (mm)	W =-5.28 + 0.01978*WFS + 0.622*V - 0.203*TS - 0.000018*W^2+ 0.00617*TS^2 - 0.01167*V*TS	±0.69
	Penetration Area (mm^2)	PA =11.53 - 0.0496*WFS - 0.219*V- 0.2713*TS + 0.002866*W*V	±2.06
	Reinforcement Area (mm^2)	RA = 5.80 + 0.07288*WFS+ 0.2270*V- 1.0372*TS + 0.02113*TS^2 - 0.000552*W*V	±0.91

The ability of a statistical model to describe a data set is usually characterized by the coefficient of determination (R^2), where a high R^2 indicates that the model accounts for a high degree of variability in the data. From Table 4-3 and Table 4-4, for both the wires all six

models have high R^2 values indicating the excellent ability of the model to describe the variability of data considering the wide range of factors selected. However, one weakness of R^2 value is that it monotonically increases with the number of terms in a given model. To avoid this issue, an R^2 adjusted for the number of model parameters (R^2_{adj}) was used, which are also reported in Table 4-3 and Table 4-4. The R^2_{adj} for all models are comparable to the original R^2 value, indicating that the reduced models still describe the data reasonably well without including unnecessary model terms.

A further regression analysis statistic to determine the suitability of the model is the predicted R^2 (R^2_{pred}). The R^2_{pred} is calculated by removing a single measured observation from the existing data set, re-calculating the regression model coefficients, evaluating how closely the model predicts the removed observation, and repeating this procedure for all data in the set [9]. Again, the R^2_{pred} values are comparable to the other R^2 values with values ranging from 69.63% to 98.65% for 0.045 in wire and 57.62% - 96% for 0.035 in wire, demonstrating that the models in Table 4-1 and Table 4-2 are reasonably good in describing the data without overfitting by including excessive model terms.

Table 4-3 Multiple goodness of fit metrics for each response model (0.045 in wire)

Gas	Variable	Regression Statistic		
		R^2	R^2_{adj}	R^2_{pred}
100% Ar	Current	97.68%	97.29%	96.48%
	Width	79.30%	75.73%	69.74%
	Penetration	87.59%	86.41%	83.98%
	Reinforcement Height	79.54%	77.59%	73.57%
	Penetration Area	97.16%	96.89%	96.38%
	Reinforcement Area	98.89%	98.80%	98.65%
85% Ar/ 15% CO_2	Current	99.05%	98.86%	98.54%
	Width	94.24%	92.88%	90.80%
	Penetration	87.75%	86.65%	85.35%
	Reinforcement Height	88.48%	87.76%	86.70%
	Penetration Area	78.23%	76.27%	73.58%
	Reinforcement Area	98.03%	97.89%	97.66%
100% CO_2	Current	94.06%	93.60%	92.71%
	Width	86.97%	85.21%	82.13%
	Penetration	81.65%	80.26%	78.70%
	Reinforcement Height	82.90%	81.36%	79.05%
	Penetration Area	74.86%	73.29%	69.63%
	Reinforcement Area	98.43%	98.33%	98.16%

Table 4-4 Multiple goodness of fit metrics for each response model (0.035 in wire)

Gas	Variable	Regression Statistic		
		R^2	R^2_{adj}	R^2_{pred}
100% Ar	Current	97.26%	96.54%	95.28%
	Width	86.44%	82.92%	78.81%
	Penetration	70.06%	67.21%	61.61%
	Reinforcement Height	77.77%	76.41%	74.19%
	Penetration Area	43.61%	40.14%	33.61%
	Reinforcement Area	88.81%	87.75%	86.40%
85% Ar/ 15% CO_2	Current	97.71%	97.33%	96.86%
	Width	95.13%	93.80%	92.04%
	Penetration	89.65%	88.57%	86.86%
	Reinforcement Height	89.30%	88.49%	87.65%
	Penetration Area	87.70%	86.59%	85.41%
	Reinforcement Area	96.04%	95.74%	95.31%
100% CO_2	Current	96.98%	96.48%	96.11%
	Width	89.28%	87.50%	85.23%
	Penetration	62.43%	60.08%	57.62%
	Reinforcement Height	64.58%	63.29%	61.60%
	Penetration Area	83.87%	83.08%	82.16%
	Reinforcement Area	97.55%	97.37%	97.19%

4.2 Discussion

This section discusses the trends observed from the experimental results of welds as in bead on plate condition for each of weld bead geometry in Section 4.1 and also discusses the main and interaction effects for each statistically significant variable in the model.

4.2.1 Current

The current passing during the welding process is directly related to wire feed speed. In the CV mode the internal circuitry of the welding equipment tries to select an appropriate current required to melt the wire depending on voltage-current characteristics established by the power supply characteristics. From Figure 28, the concavity of the current vs. wire feed speed relation was linear for all the gas types. When wire feed rate was increased from -1 to +1, the current value increased for the welds due to higher current requirement to melt the wire. This resulted in a positive coefficient for the wire speed term for all the gases. At lower and intermediate voltages, the type of gas greatly influenced the current required.

Since 100% CO_2 gas has higher thermal conductivity compared to 100% Ar and 85% Argon-15% CO_2 gas, it required less current for the same wire feed speed. Increasing the voltage from level -1 to 0 did not produce a significant increase in current for each of the gas types at the same levels of wire feed and travel speed. However, when voltage was increased from 0 to +1, an increase in current was observed for all the gasses. This resulted in a negative coefficient for the voltage term for the 100% Ar and 85% Argon-15% CO_2 gas welds, with both 0.045 in and 0.035 in wire. Meanwhile the second order polynomial term for voltage had a positive coefficient indicating the increasing rate in current during weld at higher voltage levels. In contrast, welds using 100% CO_2 gas had a positive voltage term for current, indicating an increase in current with voltage levels.

The interaction effect of variables on current during welding varied based on the type of gas for both 0.045 in and 0.035 in wires. From the model for 0.045 in wire in Table 4-1, only 85%Ar-15%CO_2 gas had a term for wire feed speed interaction with voltage, whereas the results for 0.035 in wire suggest interaction effects for all the three gasses. The welds produced using both 100% Ar and 100% CO_2 gasses had a wire feed rate interaction with voltage, while 100% Ar had an additional interaction for wire feed speed on travel speed.

The results observed using 85%Ar-15%CO_2 gas indicate an interaction of voltage on travel speeds, with the effects of these interactions on current shown in Figure 29. The interaction effect of wire feed speed on voltage had a positive coefficient for all the gasses, showing that with an increase in feed rate and voltage, the welding current increases. Welds produced using 0.035 in wire and 100% Ar gas had a positive coefficient for interaction between wire feed speed and travel speed. For both interactions, the wire feed term has a positive coefficient with a greater degree of control on the effect, and negates the negative coefficient of voltage at lower levels and travel speed at higher levels. This can be seen from Figure 29 (*a, c, d*) where with an increase in feed rate across the range of voltage and travel speed, the value of current increases progressively.

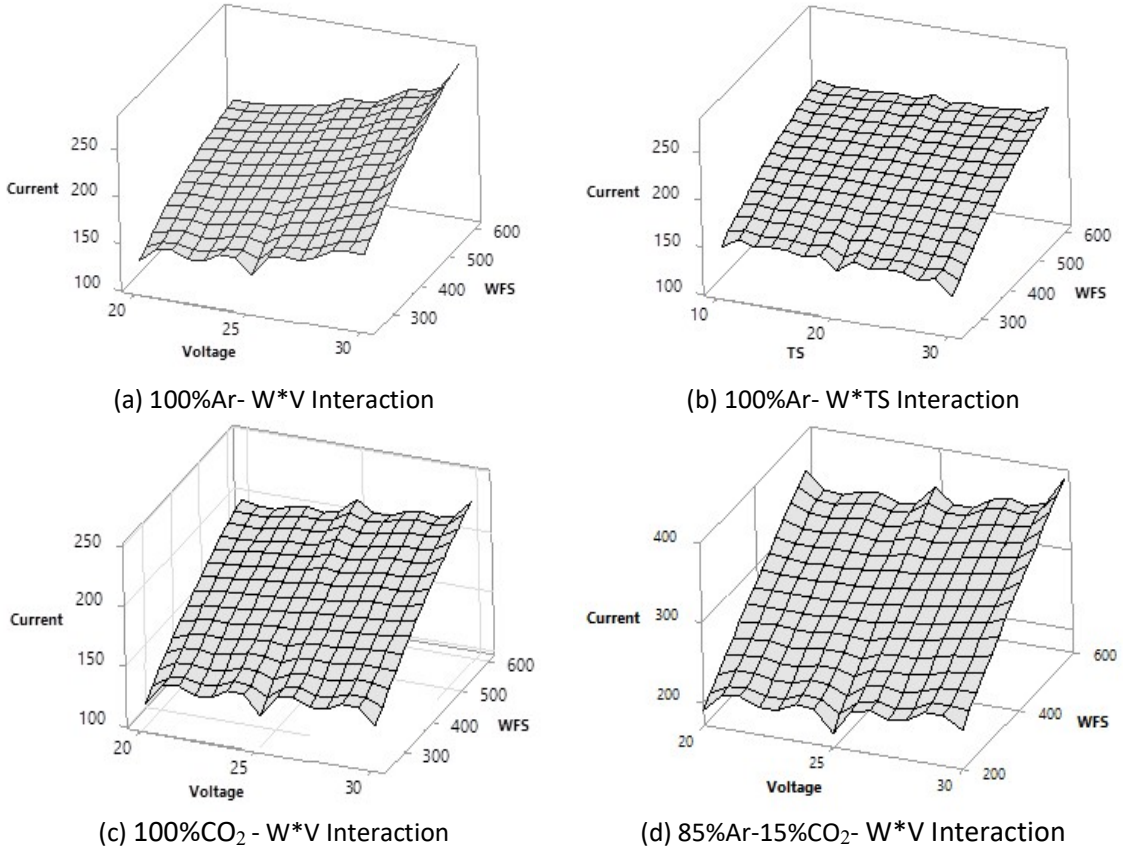

(a) 100%Ar- W*V Interaction

(b) 100%Ar- W*TS Interaction

(c) 100%CO_2 - W*V Interaction

(d) 85%Ar-15%CO_2- W*V Interaction

Figure 29 Interaction effects of input variable on welding current (a, b, c) 0.035 in wire; (d) 0.045 in wire

4.2.2 Bead Width

Weld-bead width depends on the wetting of the molten pool across the base metal, and the area of the base metal under the moving arc cone. These factors were influenced by a number of parameters, such as arc voltage, gas type, travel speed and arc-temperature. From model fits for the width model, the width-voltage relationship was concave down and linear at all travel speeds and wire speeds for 85% Ar-15% CO_2 and 100% CO_2 gasses, except at higher wire feeds speed when using 100% Ar gas which had a concave up/linear trend regardless of travel speed. The resulting width model for all the three gasses include the voltage, wire feed and travel speed and interaction terms. When voltage was increased from -1 to +1 (20 to 30V) there was an increase in bead width for the welds due to an increase in

the size of the arc cone. A higher voltage is usually associated with a wider arc cone, as the driving forces for conventional current increases, increasing the arc plasma velocity and deflecting it radially outward, causing the arc cone to widen, resulting in a higher bead width [45]. This produced a positive coefficient for the voltage term for all the gases, while the second order polynomial term for voltage had negative coefficient implying that at higher voltages the width is increasing at a decreasing rate.

With increasing travel speed from -1 to +1, a decrease in bead width was observed for all the gas types (except for the 100% Ar model with 0.045 in diameter wire), thereby giving the travel speed term a negative coefficient. At low travel speed, there is more heat input and the torch travels relatively slow resulting in more metal deposited causing an increase in width and vice versa at higher speeds. When wire feed speed was increased from -1 to +1, the bead width increased for the welds due to an increase in metal deposition, causing the weld pool to spread due to better wetting. This resulted in a positive coefficient for the wire feed term, while the second order polynomial term for wire feed speed had a negative coefficient indicating a reduction or decreasing rate in width of weld at higher wire feed rates with an exception to the 100% Ar model with 0.045 in diameter wire, which had a positive coefficient that was close to zero, which may suggest a slight difference in the wetting behaviour with gas type.

The interaction effect for bead width varied depending on gas type for both 0.045 in and 0.035 in wire. From Table 4-1 it can be noted that when using 0.045 in wire both 100% Ar and 85%Ar-15% CO_2 gasses had wire feed rate interactions with voltage and an additional separate effect of voltage on travel speed for 100% Ar, along with an interaction effect of wire feed on travel speed for 85%Ar-15%CO_2. These effects are shown in the Figure 30 which shows a 3D wireframe plot outlining the trends of the interaction.

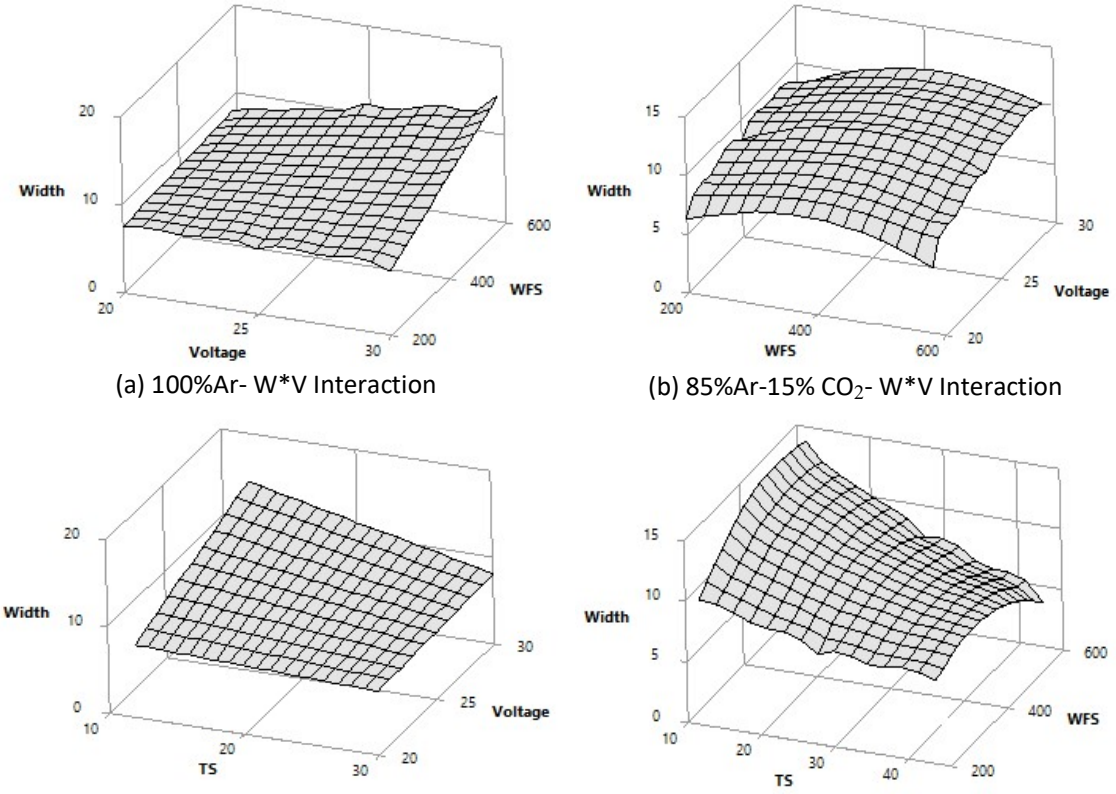

(a) 100%Ar- W*V Interaction

(b) 85%Ar-15% CO_2- W*V Interaction

(c) 100%Ar- V*TS Interaction

(d) 85%Ar-15%CO_2- W*TS Interaction

Figure 30 Interaction Effect of input variable on bead Width for 0.045 in diameter wire

The interaction effect of wire feed speed on voltage had positive coefficient for both the gasses showing that width increases with increasing voltage and feed rate (and both having positive coefficient as discussed earlier). The interaction effect of feed rate with travel speed for 100%Ar had a negative coefficient indicating that width progressively decreases when travel speed is increased, which is due to the travel speed having a negative coefficient, thereby having a greater effect than wire feed speed. Another interaction which was observed is interaction between voltage and travel speed which also had a negative coefficient when using 85%Ar-15%CO_2 gas, again indicating the greater negative effect of increased travel speed on width compared to the positive effect of voltage. Hence even though when size of arc cone is increased, the size of width decreases due to a faster torch travel speed. Previous work done by Murugan and Parmar [26] evaluating SAW with voltage levels between 24 to

32 (V) and travel speeds 0.43 to 0.75 (m/min) showed a similar trend the interaction effect between voltage and travel speed on width.

Therefore, as voltage and wire feed is increased, a positive coefficient leads to a wider bead at higher levels of voltage and feed rate, while with interaction of travel speed with wire feed and voltage has a negative coefficient. One finds that a wider bead is obtained at lower travel speed and higher voltage or feed rate, and vice versa.

From Table 4-2, for welds produced using 0.035 in wire all the three gases 100%Ar, 85%Ar-15%CO_2 and 100%CO_2 had interaction effects. The interaction effect of voltage on travel speed was common between all the three, in which 100% Ar gas had an additional interaction effect of feed rate and voltage, while 85%Ar-15%CO_2 had all the three interaction effects *(W*V, W*TS, V*TS).*

The interaction effect of voltage on travel speed had negative coefficient for all the three gasses, showing that width decreases even with increasing voltage due to increased travel speed which as a negative coefficient as explained earlier. The interaction effect of wire feed speed and voltage on bead width has a positive coefficient for both 100%Ar and 85%Ar-15%CO_2, as both voltage and feed rate has positive coefficient resulting in increased width of bead at higher feed and voltage. Another interaction effect in 85%Ar-15%CO_2 was interaction between feed rate and travel speed. This had a negative effect because of the negative coefficient of travel speed compared to feed rate i.e. as less metal is deposited at higher travel speed of torch, thereby giving narrow bead compared to one obtained at lower travel speed. The trends observed with interaction among variable closely correlates with previous work done in SAW which indicated similar signs for interaction coefficients for *W*V, W*TS, V*TS* [26, 29, 46].

One of the interesting observations was reduction in width of the weld with increase in voltage. At high voltage (30V), width decreased for welds at lower and intermediate wire

feed rates. To find the reason for this a high-dynamic range video camera by Xiris^{TM} was used in order to capture the image of arc cone which is shown in Figure 31. It can be seen that with increase in travel speed the arc length decreases altering the width of arc cone which causes the decrease in bead width due to smaller weld pool size.

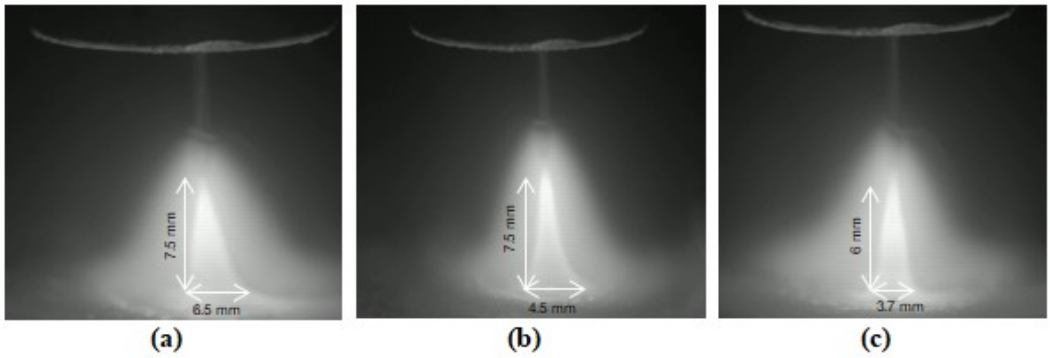

Figure 31 High dynamic range images of arc cone with 100% argon gas at higher voltage (30V) with varying travel speeds (a)-20ipm; (b)-25ipm; (c)-30ipm

4.2.3 Bead Penetration

In terms of weld penetration, the Lorentz force plays an important role in carrying the heat from the arc, and causes a deeper penetration by pushing the liquid droplet downward in the pool, and displacing it behind the arc to melt new plate material below the arc. Hence, the applied current is the most important parameter in determining the penetration of weld, as at higher current density the magnitude of the Lorentz force is high which makes the penetration deeper along with several other factors such as buoyancy forces, Marangoni convection, and plasma jet shear on the pool surface [40, 41].

From Figure 23 for the penetration model, concavity of penetration-wire feed speed relationship changed for all the three gas type with voltage and travel speed. The final penetration model for 0.045 in and 0.035 in for all the three gases had wire feed speed, voltage, travel speed, with an interaction between wire feed speed and voltage and second

order polynomial term for wire feed speed (except for 0.035 in, 100% CO_2) as common significant terms. When the wire feed speed was increased from -1 to +1 there was an increase in bead penetration which is largely correlated to the increase in the arc current and related forces i.e. higher arc pressures, giving a positive coefficient for all the three gases while the second order term had positive coefficient for 100% Ar and 100% CO_2 gas whereas the 85% Argon-15% CO_2 gas had a negative coefficient for this second order term. One of the pretexts to this variation is obvious in Figure 32 which shows the penetration profile for different gases with varying wire speed and travel speed. It can be seen that welds made with 100% Ar welds had a finger-like penetration while CO_2 had a bell shaped one. This distinct finger-like penetration obtained with argon welds produces further penetration giving a positive coefficient for argon welds. As travel speed is increased from 10ipm to 44ipm, the torch moves faster and the heat input applied per unit length of weld is low at higher speed as less time is spent by the torch at a point. This gives the travel speed a negative coefficient, indicating that a higher travel speed gives a shallower penetration and vice versa for lower speeds.

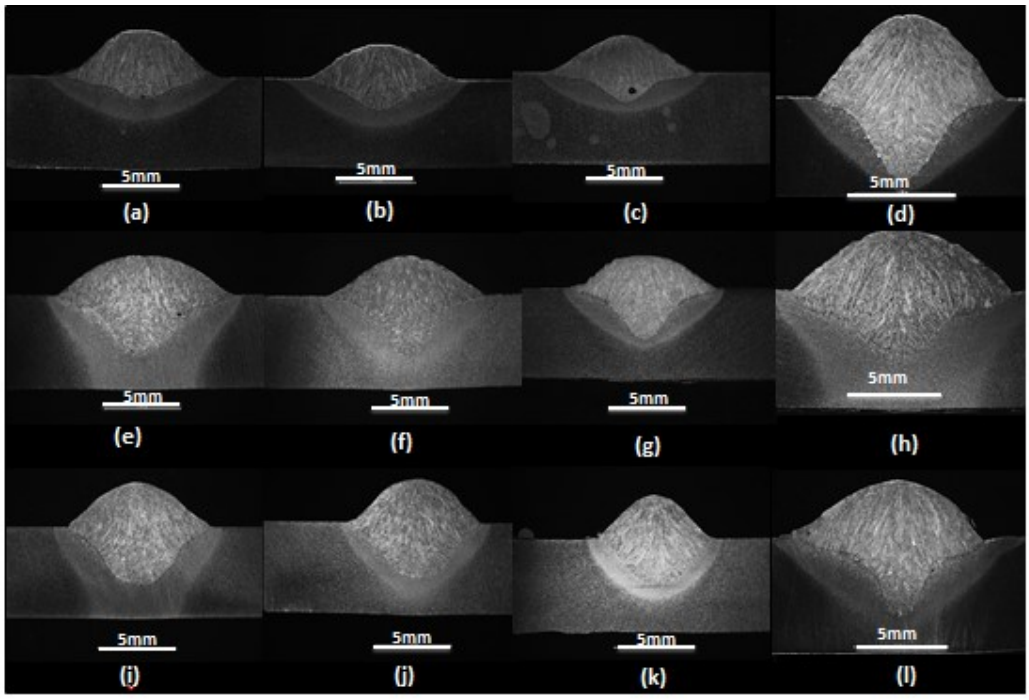

Figure 32. Bead penetration profile with varying shielding gas at WFS:390ipm, V:25V; (a,b,c)-100%Ar with TS:20ipm,25ipm,30ipm;(e,f,g)-85%Ar/15% CO_2 with TS:20ipm,25ipm,30ipm; (i,j,k)-100% CO_2 with TS:20ipm,25ipm,30ipm.;(d,h,l) WFS:580ipm,V:25V,85%Ar-15%CO2 with TS:20ipm,25ipm,30ipm

From Table 4-1 and Table 4-2 the interaction effect for penetration (depth) varied depending on gas type for both the 0.045 in and 0.035 in wire. For 0.045 in wire all the gasses had an interaction between wire feed speed and voltage, while 100% Ar and 85%Ar-15% CO_2 gasses had additional wire feed rate interaction with travel speed. These effects are represented by a 3D wireframe plot shown in Figure 33.

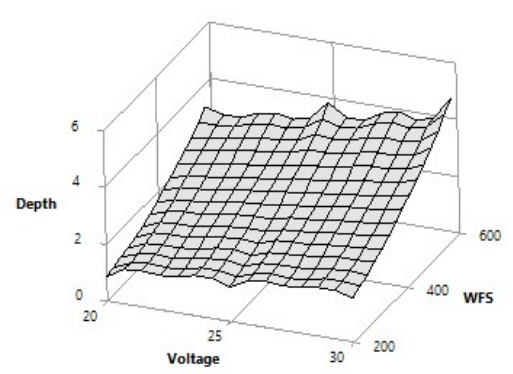

(a) 100%Ar- W*V Interaction

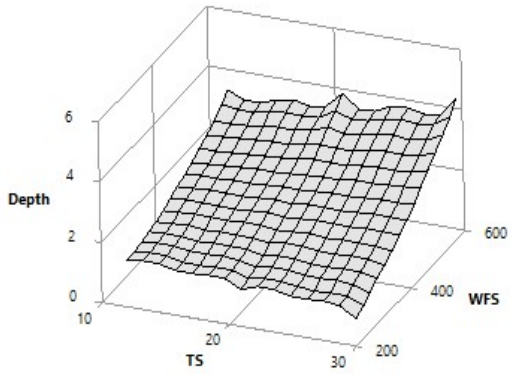

(b) 100%Ar- W*TS Interaction

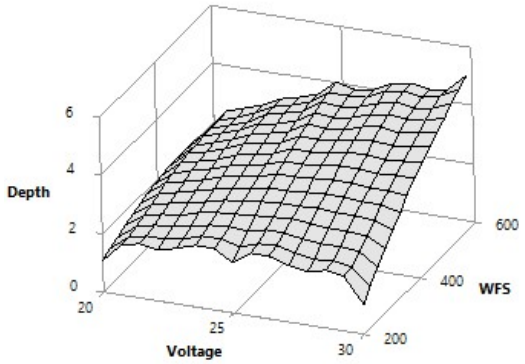

(c) 85%Ar-15%CO_2- W*V Interaction

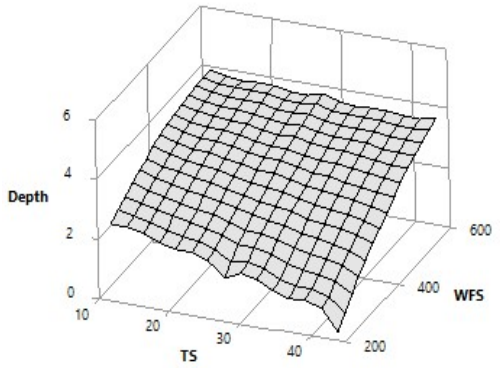

(d) 85%Ar-15%CO_2- W*TS Interaction

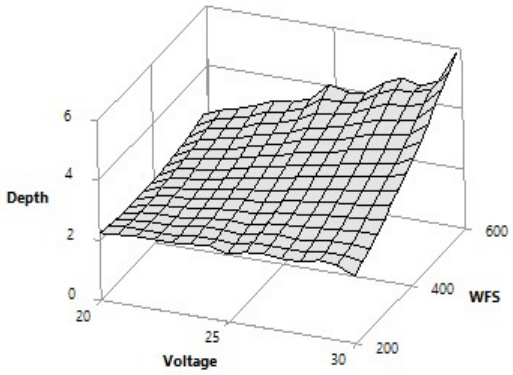

(e) 100%CO_2- W*V Interaction

Figure 33 Interaction Effect of variables on bead penetration for 0.045 in diameter wire

The interaction effect of wire feed speed on voltage had a positive coefficient for all the gasses showing that depth of penetration increased with increasing wire feed rate and voltage as both have positive coefficient. The interaction effect of feed rate with travel speed for 100% Ar and 85%Ar-15%CO_2 also had a positive coefficient, indicating that depth progressively increases, even when travel speed is increased, which is due to wire feed speed

having positive coefficient, thereby having a greater effect on penetration even when travel speed is high. Therefore, when wire feed is increased due to its positive coefficient in interaction term, a deeper bead is obtained at higher levels of feed rate, while at lower feed rates shallow penetration is obtained.

Similarly from Table 4-2 for 0.035 in wire all the three gases had interaction effects, namely the interaction of wire feed speed with voltage. The interaction effect of wire feed speed on voltage had positive coefficient for all the three gasses, which has already been discussed in this section (i.e. wire feed rate and voltage have positive coefficient, showing that penetration increases with increase in feed rate and voltage).

Also it should be noted that all the experiments were performed at room temperature with no pre-heating given to the plate. If pre-heated, the cooling rate for the weld and plate would be slower, resulting in a higher penetration and dilution ratio of weld metal.

4.2.4 Reinforcement Height

The filler wire fed during the welding process is melted at the end of the wire tip, and transferred through the arc plasma when it is deposited onto the weld base metal. The vertical height of this deposited metal is referred to as reinforcement height of weld bead. In general, when feed rate is increased the amount of filler metal deposited into the pool increases, producing higher weld reinforcement, and when travel speed is increased the amount of metal deposited over a unit length of weld bead is less reduced, thereby causing a reduction in height of weld reinforcement. Another important parameter which influences the reinforcement is voltage and gas type. When voltage is increased the size of arc cone increases, producing a better wetting of deposited filler with base metal thereby reducing the height of reinforcement. Similarly, a higher conductive gas produces a higher arc temperature promoting the circulation and spread of deposited metal. This is shown in

Figure 34, which shows relationship between reinforcement height and width with arc cone. With increase in voltage the arc cone spread increases the width causing a dip in reinforcement height and vice versa at lower arc cone size.

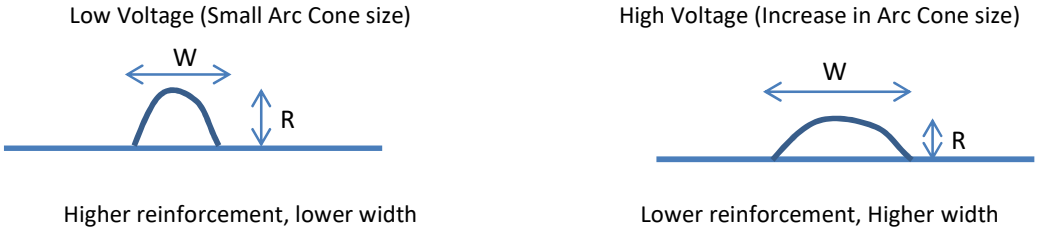

Figure 34 Arc Cone relationship with width and reinforcement height

The reinforcement model fits for both the wire diameters, showed that the concavity of the reinforcement-wire speed relation was linear for most levels of voltage and travel speed. As the melted wire is deposited as reinforcement, it was obvious that as wire feed speed increased from -1 to +1, the statistical model had positive coefficient for wire feed speed for all gases except for 100% CO_2. For the case of 100% CO_2 gas with 0.045 in diameter wire, a negative coefficient for the wire feed term is observed at lower levels, and this had a positive coefficient for the second order polynomial term for wire feed, indicating increasing reinforcement at higher feed rates. The CO_2 gas is more thermally conductive, which contributes to the negative coefficient. When the travel speed is increased there is a decrease in the amount of wire deposited, and hence the model had negative coefficient for travel speed among all the gas types. With increases in voltage, the size of the arc cone increases, this leads to the voltage negative term.

From Table 4-1 and Table 4-2, the interaction effect for reinforcement height varied depending on gas type for both 0.045 in and 0.035 in wire. For the 0.045 in wire, all the gasses had interaction of voltage with wire feed speed and travel speed. The interaction effect of wire feed speed on voltage had negative coefficient for 100%Ar and 85%Ar-15% CO_2, showing that reinforcement decreases with increasing voltage due to increased arc cone size.

The higher voltage negates the effect of higher feed rate, thereby giving the term a negative coefficient. This effect is shown by a 3D wireframe plot shown in Figure 35. It can be seen that a combination of lower voltage and higher feed rate gives the highest weld reinforcement height and vice versa at higher voltage levels.

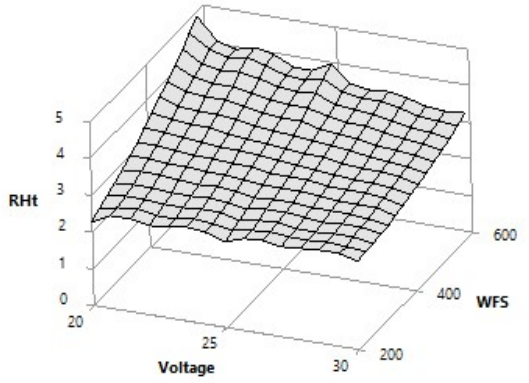

(a) 100%Ar- W*V Interaction

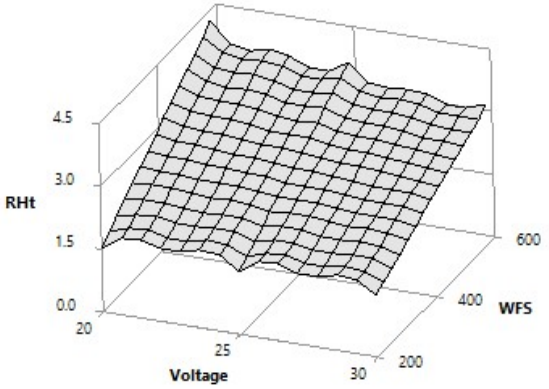

(b) 85%Ar-15%CO_2- W*V Interaction

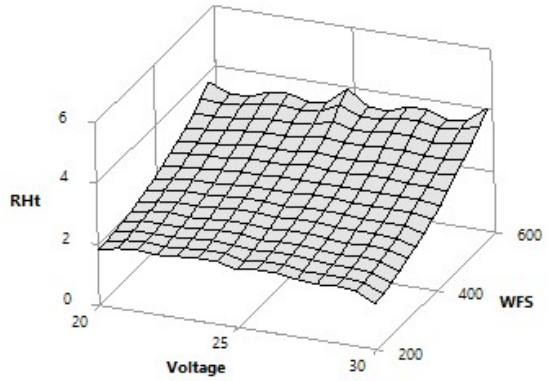

(c) 100%CO_2- W*V Interaction

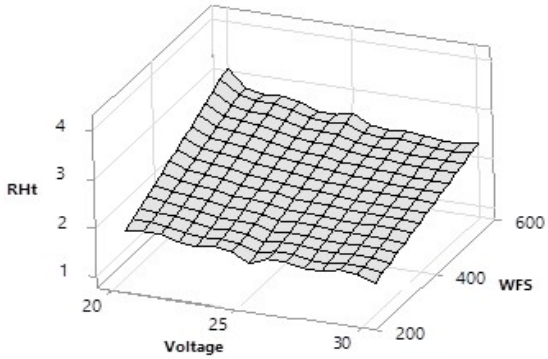

(d) 85%Ar-15%CO_2- W*V Interaction

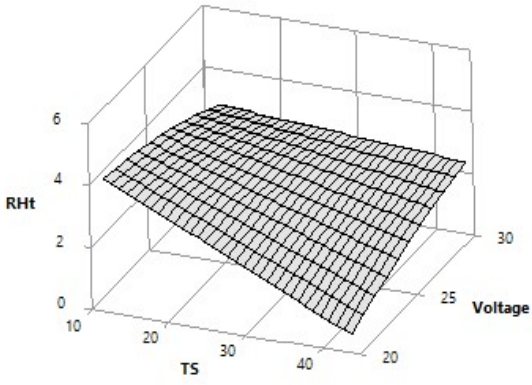

(e)100%CO_2- V*TS Interaction

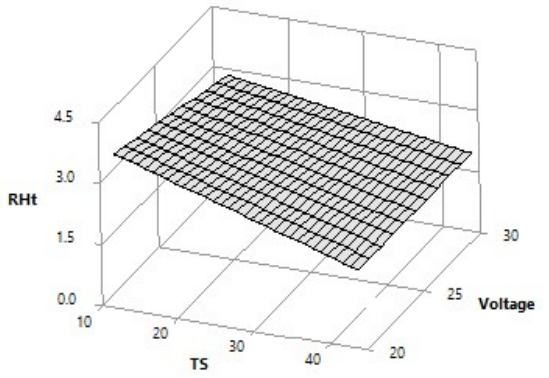

(f) 85%Ar-15%CO_2- V*TS Interaction

Figure 35 Interaction effects of input variable on Reinforcement Height (a, b, c, e, f) 0.045 in wire; (d) 0.035 in wire

Figure 35 shows the control plot with the interaction effect of voltage and travel speed on reinforcement height. There is a small increase in the reinforcement at lower voltage and travel speed levels compared to high levels. Even though this term was statistically significant there appears to be no physical significance for this term.

4.2.5 Reinforcement Area

Reinforcement area is the area of filler metal deposited onto the substrate which remains above the surface after the welding process. During welding a portion of filler metal is lost as evaporated fumes, spatter and other losses, and the remaining metal which is deposited after these losses is the actual reinforcement material. Similar to reinforcement height, one of the most important factors which influences the reinforcement area is wire feed speed, since this directly contributes to the material making up the reinforcement area. Voltage influences the losses during the process; contributed by spatter at lower voltage and metal lost to fumes at higher voltage. The losses are further discussed in section 4.2.8 where deposition efficiency is calculated as actual reinforcement area deposited after losses.

From the reinforcement area trends for 0.045 in and 0.35in wire diameters, the concavity of reinforcement area-wire speed relationship was linear for all levels of voltage and travel speed with all the gasses. When wire feed is increased from -1 to +1 the reinforcement area increased rapidly as more metal is being deposited giving the term positive coefficient. When travel speed was increased from 10 to 40ipm, there was a decrease in reinforcement area due to the faster travel of the torch, resulting in a negative coefficient for the travel speed term.

For the welds produced with 0.045 in and 0.035 in wires, all the gasses had an interaction of wire feed speed on travel speed for reinforcement area. When using 0.035 in wire with 100% Ar and 100% CO_2 gases, an additional interaction effect is noted between wire feed

speed and voltage. A 3D wireframe surface plot outlining the trends of interaction is shown in Figure 36.

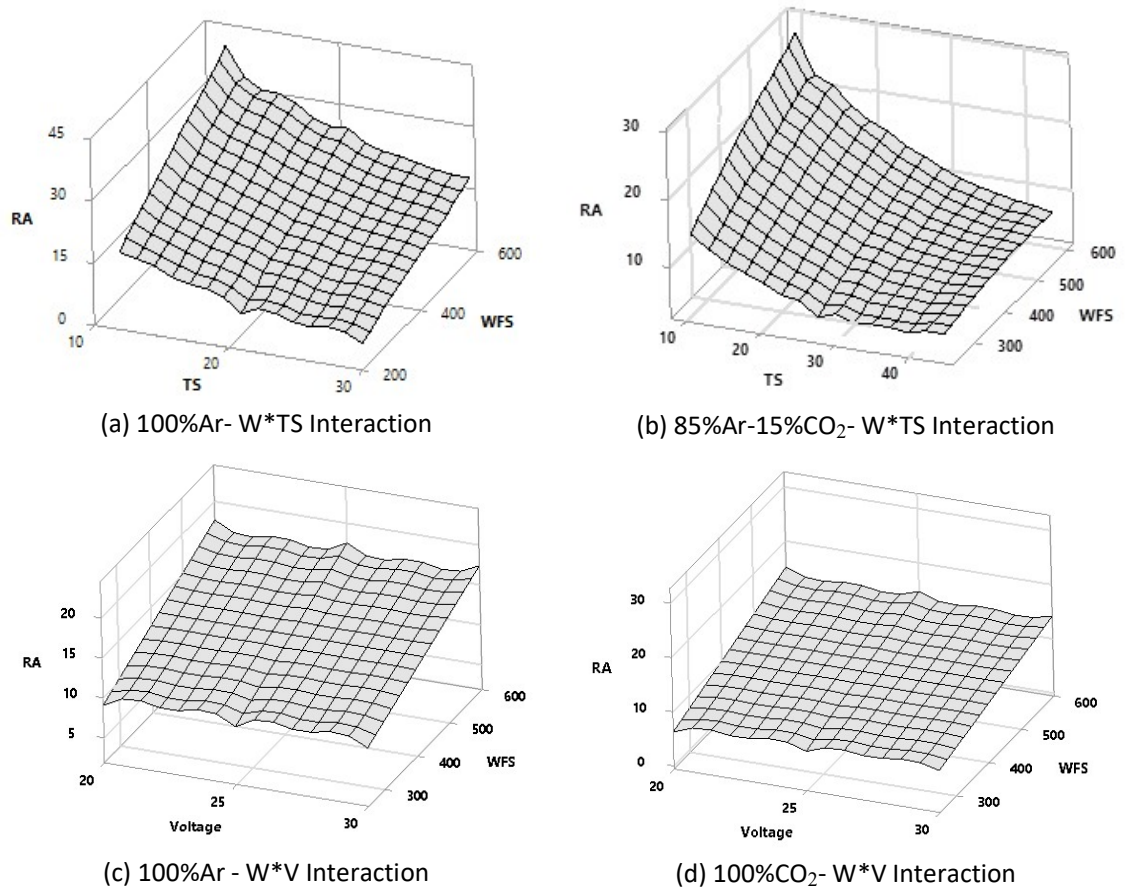

(a) 100%Ar- W*TS Interaction

(b) 85%Ar-15%CO_2- W*TS Interaction

(c) 100%Ar - W*V Interaction

(d) 100%CO_2- W*V Interaction

Figure 36 Interaction effects of input variable on Reinforcement Area (a) 0.045 in wire; (b, c, d) 0.035 in wire

From Figure 36 (a, b) it can be seen that for the interaction between wire feed speed and travel speed, a higher reinforcement area is obtained at lower travel speed and higher wire feed rate, and the reinforcement area decreases as travel speed is increased and feed rate is decreased. Likewise Figure 36 (c, d) shows an interaction between wire feed speed and voltage. The interaction had a negative coefficient, which explains for the drop in reinforcement area at higher voltage levels.

4.2.6 Penetration Area

Penetration area represents the area underneath the substrate which has been heated by the arc plasma from the moving torch. Parameters affecting the penetration area are comparable to depth of penetration as mentioned in (section 4.1.2) with applied current and Lorentz force playing an important role in transferring the heat from arc to the liquid droplet and into the pool, causing deeper penetration. From Figure 27 when wire feed speed was increased the current associated also increases thereby creating a higher penetration area on the substrate. The applied voltage decides the transfer mode and arc pressure exerted onto the weld pool, whereas the travel speed controls the amount of hear supplied to the substrate. At lower speed more heat is applied and vice versa at higher speed. This gives the travel speed term a negative coefficient for all the gasses with both wire diameters, describing an increasing penetration at slower torch speed, except for 85%Ar-15 CO_2 mixed gas with 0.045 in diameters which had positive coefficient for travel speed term and a negative coefficient for polynomial term of travel speed, explaining an increasing penetration at lower speeds.

The interaction effect for bead penetration area varied based on gas type for both 0.045 in and 0.035 in wire. From Table 4-1 and Table 4-2 all the gas types had an interaction effect between wire feed speed and voltage, and an additional interaction effect was present between wire feed speed and travel speed for 85% Argon-15% CO_2 gas with 0.035 in and 100%CO_2 with the 0.045 in diameter wire. These interaction effects are shown in Figure 37 by the 3D wireframe surface plot outlining the trends of the interaction. Figure 37 *(a, c)* shows the interaction between wire feed and voltage, and it can be noted that penetration area increases continuously with feed rate and voltage. A high penetration area is obtained at combinations of high feed rate and voltage levels, and the area decreases with reduction in voltage and feed rate. At higher feed-voltage level combinations, the high arc pressure exerted onto the weld pool combined with the spray transfer mode promotes higher

penetration, compared to short circuit occurring at lower voltage and feed rates. Figure 37 *(b, d)* shows the interaction effect of wire feed speed on travel speed. At lower travel speed when the torch moves slowly, the heat input applied per unit area is high. This higher heat input applied to substrate at low-travel speed and high feed rate promotes a higher penetration area. This effect decreases when travel speed is increased, hence the negative coefficient for the term describing the greater influence of travel speed in the term.

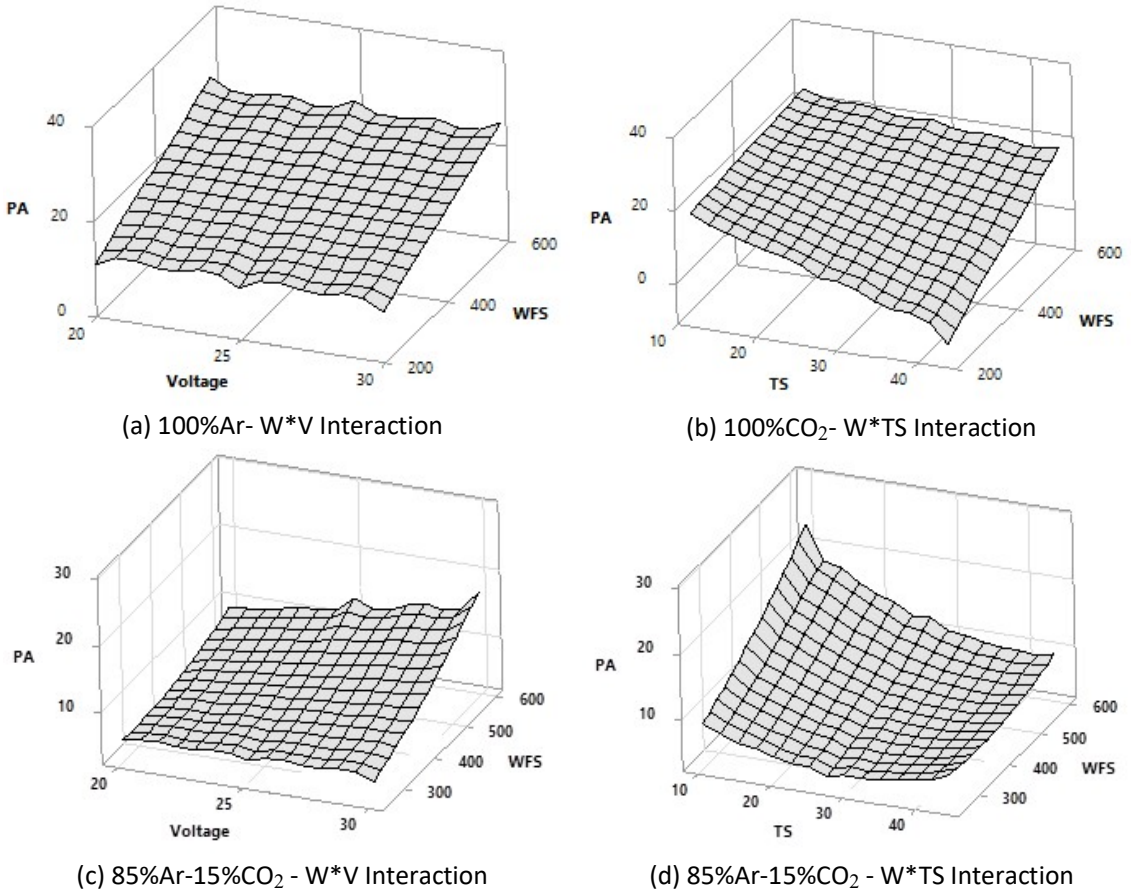

(a) 100%Ar- W*V Interaction

(b) 100%CO_2- W*TS Interaction

(c) 85%Ar-15%CO_2 - W*V Interaction

(d) 85%Ar-15%CO_2 - W*TS Interaction

Figure 37 Interaction effects of input variable on penetration area (a, b) 0.045 in wire; (c, d) 0.035 in wire

4.2.7 Dilution Ratio

Figure 38 and Figure 39 shows the dilution ratio of welds obtained with 0.035 in and 0.045 in diameter wires. Dilution is referred as the ratio of penetrated weld metal area to the total area of the weld. A higher dilution can be preferred for thicker substrates/joints to ensure

more complete bonding between the plates, while for thinner sections a lower dilution is preferred to reduce the HAZ degradation and chance of burn-through. Dilution of weld varies based on the process variables selected during welding i.e. current, voltage, travel speed and gas type. From Figure 38 and Figure 39 it can be seen that dilution ratio of welds varies across the range of heat input, with more scatter around the lower heat input range.

Two important factors controlling the dilution ratio are power input and travel speed. When current and voltage (power input) during welding were increased, the arc pressure increases as discussed in previous sections producing deeper penetration, thereby creating a higher dilution of weld. Likewise, when travel speed is reduced, the heat input applied is higher producing a higher dilution and vice versa at higher speeds. Therefore, a combination of high power input- low travel speed gives highest dilution and low power input-high travel speed gives lowest dilution. Another important factor effecting dilution is gas type, with 100% CO_2 gas and 85% Argon-15% CO_2 gas having higher thermal conductivity producing a hotter arc relative to 100% Ar, thereby generating a higher dilution of weld which can be seem from the trends in the figure for both the wire diameters.

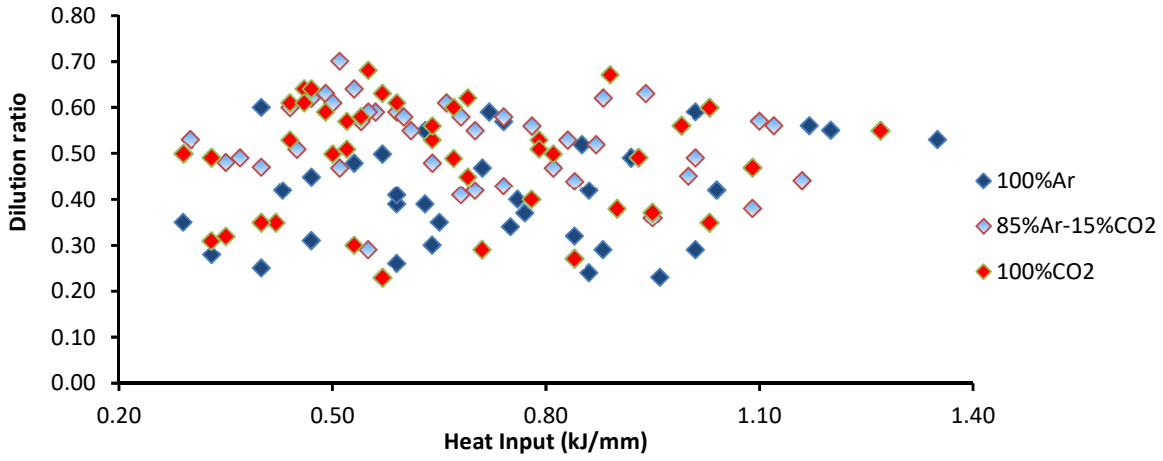

Figure 38 Dilution ratio for 0.045 in diameter wire

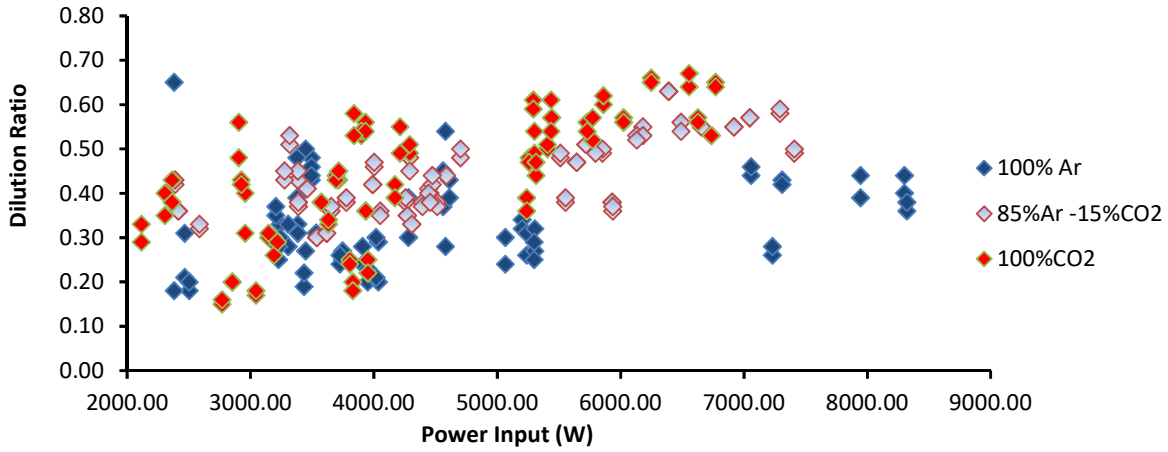

Figure 39 Dilution ratio for 0.035 in diameter wire

4.2.8 Deposition Efficiency

Deposition efficiency refers to the ratio between the area of wire deposited onto the substrate (reinforcement area) to total area of wire consumed during the process (based on the wire feed volume divided by the length of the weld). In GMAW, several percent of the melted wire may be lost as flumes during the process depending on parameters selected. This typically depends on the wire transfer mode and molten droplet temperature, which is related to weld heat or power input.

Figure 40 and Figure 41 shows the deposition efficiency for beads obtained with 0.035 in and 0.045 in diameter wires respectively. Deposition efficiency during welding varied for beads depending on power input and type of gas used for the process. For low heat input parameters, there was more variation in deposition efficiency when compared to ones with a higher heat input range. Low heat input can be grouped as parameters with high travel speeds, whereas high heat input are parameters low travel speed rate and high power. At lower heat input the mode of metal transfer is predominantly short-circuit, which produces a considerable amount of spatter during the welding process resulting in lower deposition efficiency. For the CO_2 and 85% Argon-15% CO_2 shielding gasses, the higher thermal conductivity produces a hotter arc, resulting in more metal lost to evaporated fumes

compared to pure argon, which can be noted by fitting an average line to the data. This indicates that the average deposition efficiency with 0.035 in wire was 90.1% with welds made using 100% Ar, 85%Ar-15% CO_2, 100% CO_2 having an efficiency of 90.1%, 92% and 88.1% respectively. In comparison, welds made using 0.045 in diameter wire had an average overall deposition efficiency of 94.2% and individual efficiency of 93.4%, 94.2% and 95.1% for 100% Ar, 85%Ar-15% CO_2, 100% CO_2 shielding gasses respectively.

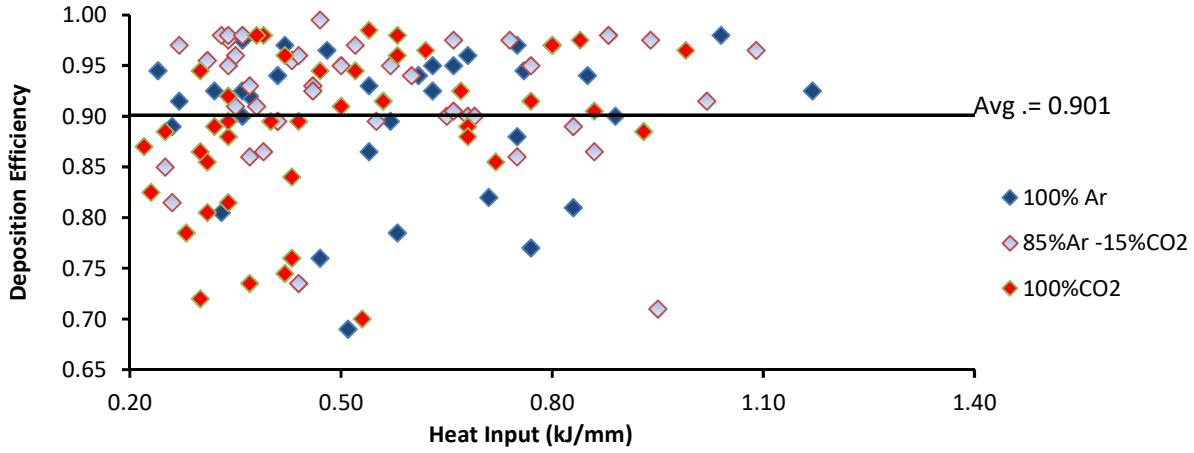

Figure 40 Deposition Efficiency for 0.035 in diameter wire

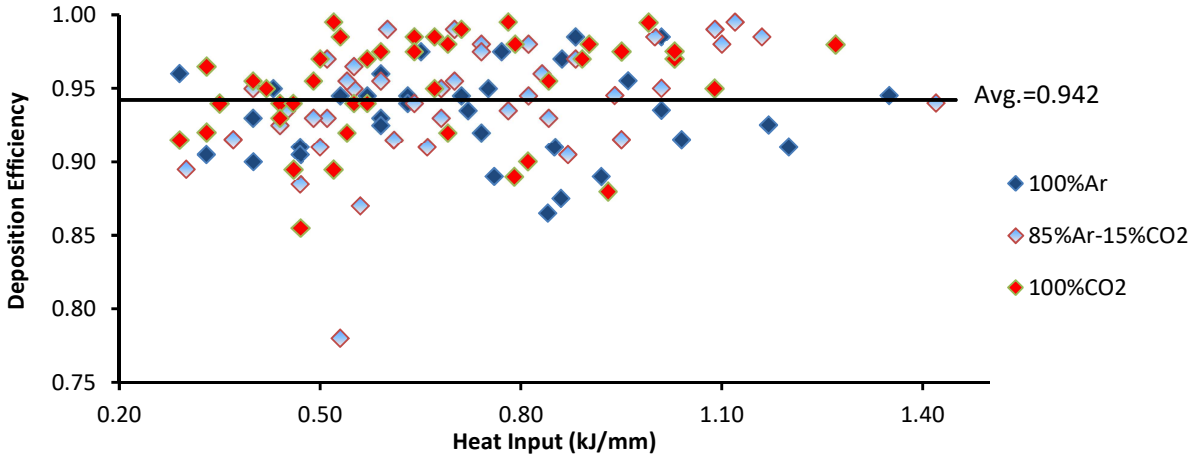

Figure 41 Deposition Efficiency for 0.045 in diameter wire

4.2.9 Statistical Model

The models overlaid on the weld bead data in Table 4-1 and Table 4-2, as well as the large R^2 values in Table 4-3 and Table 4-4, demonstrate that the models explain the variability in data accurately. However, the adequacy of the model can be investigated more rigorously. One standard appraisal of model adequacy is the analysis of model residuals, where a residual is the difference between the measured value and model predicted value.

Inherent in the models in *Equation (8) to Equation (12)* the assumption is that the errors are random, independent, and uniformly distributed with a mean of zero and constant variance. As the model residuals are estimates of the error, the distribution of the model residuals should have the same properties as the true error. Equivalently, the residuals can be standardized by taking the ratio of the model residual with its standard deviation, where the standardized residuals are expected to be distributed normally around zero, with a unit variance. By plotting the standardized residuals against a number of variables, each of these assumptions can be checked systematically.

Each model's standardized residuals are plotted against test order as shown in Figure 42, to check if there is any obvious pattern in the residuals with order and whether they are fairly evenly distributed about zero, suggesting the independence assumption is satisfactory. From Figure 42 it can be seen that all reinforcement residuals have a magnitude of approximately 1 mm or less, indicating there are no outliers. Nevertheless, the models have shown that they do not appear to be dependent on the test-order affirming that they are independent.

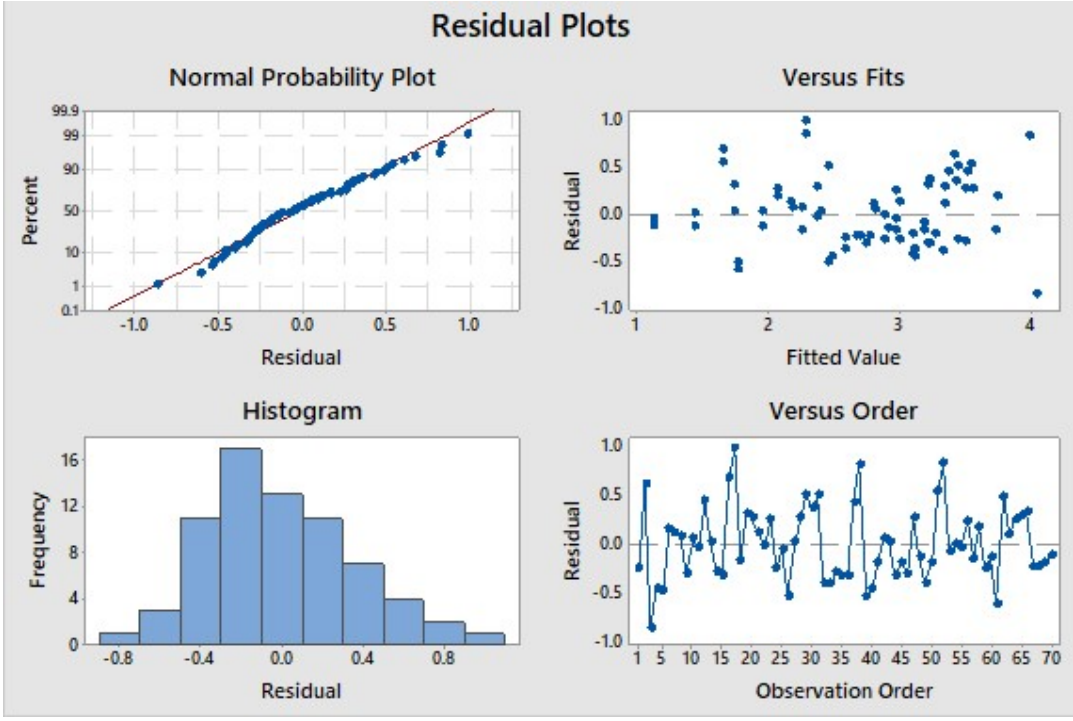

Figure 42: Q-Q plot, model standardized residuals plotted as a function of predicted values, residual histogram and standardized residuals as a function of test order for Reinforcement Height of 100%Ar (0.035 in wire)

Likewise, standardized residuals as a function of test order should be checked for patterns. If no pattern are observed as in Figure 42 when the residuals were plotted against their corresponding model predicted value, it indicates that the form of the models used were suitable.

The normality assumption can be checked by plotting the standardized residuals against a normally distributed data set, as in the quantile-quantile (QQ). If the residuals are normally distributed with mean zero and unit variance, they should fall along a straight line when plotted against the quantiles of a normal distribution with mean zero and unit variance. From Figure 42 the residuals fall along a straight line reasonably well overall, although there is some deviation from the trend with the largest magnitude residuals. However, this deviation typically occurs as the tail end of the distribution is approached. The histogram bar charts show the residuals and their frequency and a bell curve specifies the uniform distribution of the data. Figure 42 shows a bell curve distribution of data, confirming that the residuals are

uniformly distributed over the sample space. Overall, inspection of the residuals should be checked for all the models to confirm it does not raise any concerns; and whether the assumptions about model errors are satisfied, and if the models are adequate in describing the data.

For the model in Figure 42 the inspection of the residuals does not raise any concerns; the assumptions about model errors are satisfied, and therefore the models are adequate in describing the data. The residual plots for each model from regression were checked for their residuals and were found to be satisfactory, with no specific pattern or peculiar observations.

4.2.10 Test for variance in data (F Test)

In this study a total of 121 welds were produced for each wire diameter and two cross-sections were cut within the welds to measure different bead geometries such as depth, reinforcement height, reinforcement area, and penetration area. From the table in Appendix E it can be noted that for the same parameters, the measured values for each geometry within the cross sections of same bead slightly vary. Thus, to test for variation in collected data, the F-statistics test was performed which compares the variances of samples to an estimate if variances are same or different. The procedure and results of the test are discussed below in this section as follows.

a) Test for variance in experimental data within the cross sections of weld bead

As with every statistical hypothesis testing there was two hypothesis set-up for this test. The null-hypothesis in this testing is that variances of the cross sections are the same and the alternate hypothesis is that the variance is different. The F-value for each of the bead geometries was calculated as the ratio of the larger variance to smaller variance. The calculated value of F is compared with critical (table) F_c value at significance level of 5% to estimate the hypotheses. The full test results of this F-Test are given in Appendix E. It was

found that calculated $F < F_c$ (i.e. critical value of F is greater than calculated value), so we can accept the null hypothesis and infer that there is not any variation between the data obtained from cross sections.

b) Test for variance in predicted data between different wire diameter

For this study, welds produced with ER 70S-6 wires with two different diameters (0.035 in and 0.045 in) were evaluated. The 0.045 in wire is 1.63 times larger in size by cross-sectional area when compared to the 0.035 in wire. To know whether the regression models for each geometry and data obtained by these two wires vary significantly or not, the F-test was done on the values predicted by the regression models of each wire. If the variances between the wires are same, regression models for other wire diameters can be derived based on present experimental/predicted data for each geometry.

The same values for voltage, travel speed were inputted into the models for both of the wire diameters and wire feed speed was multiplied by a factor of 1.63 to the feed rate of 0.045 in wire, to get the equivalent wire feed speed for 0.035 in wire. An F-Test was performed on each of the bead geometry between two wires types for each gas at a 0.05 (5%) significance level and it was found that calculated $F > F_c$ (i.e. calculated value of F is greater than critical value) for most of the bead geometries, implying that there is not a significant variation between the predicted data obtained between two different wires.

4.3 Model Validation

While the models given in Table 4-1 and Table 4-2 describes the data reasonably well, the true utility of a model is not in the ability to describe an existing data set, but the ability to predict future response. To validate the statistical model obtained for different each of the weld geometry, a number of experimental tests were conducted. Experiments were

performed for different weld configurations with the results obtained from each of the tests discussed in this section.

4.3.1 Parameter

This section lists the parameters used in model validation for testing the statistical model in the three welding/joint positions, from the basic bead on plate, to fillet, and V-groove joints. The basis for choosing fillet and V-groove geometry is, it's one of the most commonly used configuration used in construction and pipeline joint designs. The schematic diagram of these weld configuration are shown in Figure 43.

a) Fillet Weld b) V-Groove-with root

Figure 43 Weld joint geometry configuration

4.3.1.1 Bead on plate

For validating the statistical model for each bead geometries obtained based on experimental results conducted as in bead on plate, and a number of tests were performed as bead on plate welds for different gas types. A total of 24 welds were performed with eight for each gas. The parameters for test were taken as intermediate levels (factors -0.75,-0.50,-0.25, +0.25, +0.50, +0.75). The parameters used for tests were same for all the gases and are given in Table 4-5.

Table 4-5 Parameter for model validation- bead on plate test

Test#	Wire Feed Speed (ipm)	Voltage (V)	Travel Speed (ipm)
1	247.5	20	16
2	295.0	21	20
3	342.5	23	24
4	437.5	25	28
5	485.0	27	32
6	532.5	30	36
7	485.0	25	24
8	532.5	27	28

4.3.1.2 Fillet Weld

Fillet tests were done by placing plate perpendicular to each other. A total of 8 tests were done for fillet joint condition, five with 0.045 in wire and 3 using 0.035 in diameter wire. Plates with thickness values of 1/4 and 1/8 inch were used for this test. The parameters used for fillet weld test is given in the Table 4-6 and Table 4-7.

Table 4-6 Parameter for fillet test (0.045 in wire)

#	WFS	V	TS	Gas	Thickness
Fillet 1	350	23	20	100%CO_2	1/4in (6.35mm)
Fillet 2	475	25	25	100%CO_2	1/8in (3.175mm)
Fillet 3	325	24	23	85%Ar-15%CO_2	1/4in (6.35mm)
Fillet 4	450	26	20	85%Ar-15%CO_2	1/8in (3.175mm)
Fillet 5	435	28	26	100%Ar	1/8in (3.175mm)

Table 4-7 Parameter for fillet test (0.035 in wire)

#	WFS	V	TS	Gas	Thickness
Fillet 1	400	24	23	85%Ar-15%CO_2	1/8in (3.175mm)
Fillet 2	400	24	23	100%CO_2	1/8in (3.175mm)
Fillet 3	500	30	20	100%Ar	1/8in (3.175mm)

4.3.1.3 V-Groove

A total of five experimental tests were conducted on V-groove with a 45° groove angle. V-groove were made on a plate with ½ in (12.7 mm) thickness, and a multi-pass weld was performed on V-groove using both 0.035 in and 0.045 in with different shielding gases. The parameters used for root, fill and cap passes are listed in the Table 4-8 which was obtained from prior studies [47] with some modification.

Table 4-8 Parameter for V-groove test (0.035 in wire)

#	Wire Diameter (Gas Type)	#Pass	WFS (ipm)	V (V)	TS (ipm)
A	0.045 in ER70 S-6 (100% Ar)	Root	380	23	24
		Fill (1)	400	26	17
		Fill (2)	425	28	20
		Cap	490	30	22
B	0.045 in ER70 S-6 (85% Ar-15 %CO_2)	Root	375	23	24
		Fill (1)	520	29	16
		Fill (2)	520	29	16
		Cap	400	31	22
C	0.045 in ER70 S-6 (100%CO_2)	Root	390	23	23
		Fill	475	27	19
		Cap	490	30	15
D	0.035 in ER70 S-6 (85% Ar-15 %CO_2)	Root	350	25	28
		Fill (1)	425	26	15
		Fill (2)	500	27	19
		Cap	610	29	20
E	0.035 in ER70 S-6 (100%CO_2)	Root	380	25	22
		Fill (1)	440	26	18
		Fill (2)	580	28	16
		Fill (3)	500	26	20
		Cap	600	31	30

4.3.2 Model Prediction- Results and Discussion

The results of measured and predicted values of bead geometries for bead on plate, is given in Appendix F and for fillet and V-groove welds in Table 4-10 and

Table 4-11. The comparison of weld bead measurements and model predictions for each model from bead on plate tests are summarized in Figure 44, in which the predicted values are plotted against the measured value. The points closer to the line presents better fit, while the points far from the linear line represent poor fit of the model for measured data. If the data points are on left side of the line, it indicates that the predicted value is higher than the measured value. From the plots it can be seen that results of bead geometry measured from experiment and the predicted value falls close to the 1:1 line, showing a rather good fit and the predictive power of the regression model. Since the model prediction intervals were

created using a relatively high significance level of 95%, only 5% of measurements are expected to fall outside the interval.

Overall, out of 24 points, there were 3 points outside the prediction interval for current, depth and reinforcement height models, whereas width and reinforcement height had four points outside the interval, which is reasonable considering the inherently high variability of those geometries. In comparison, penetration area had no points outside the predicted interval due to higher standard error because of their complicated varying nature, even though there were more points scattered beyond the 1:1 line. The Table 4-9 shows the list of parameters with points outside the prediction interval.

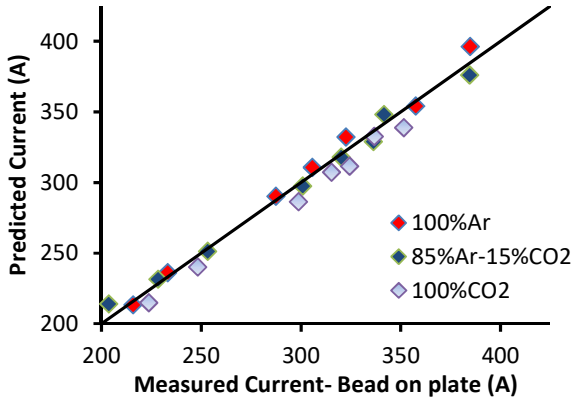

(a) Current

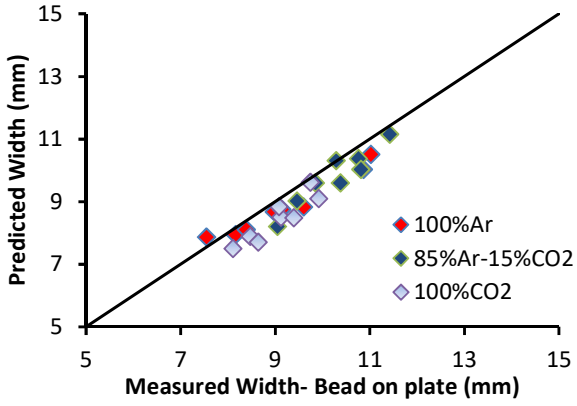

(b)Width

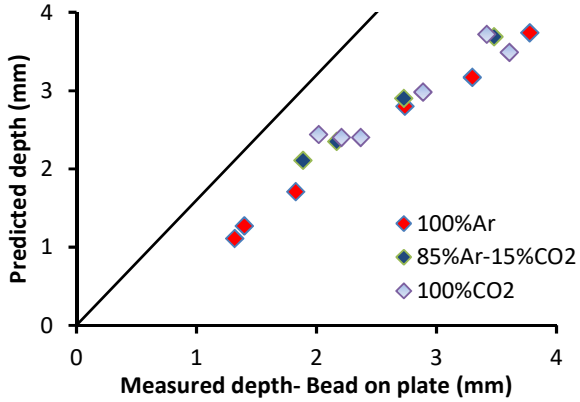

(c) Penetration

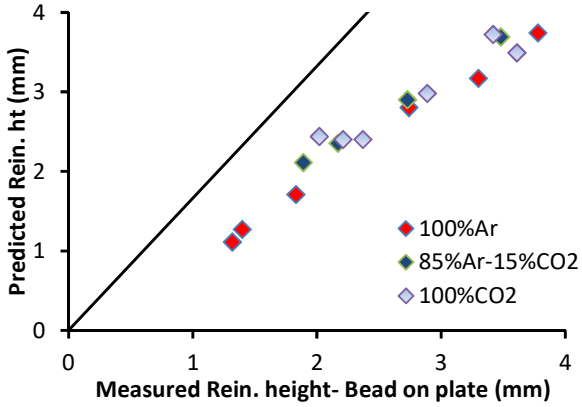

(d) Reinforcement Height

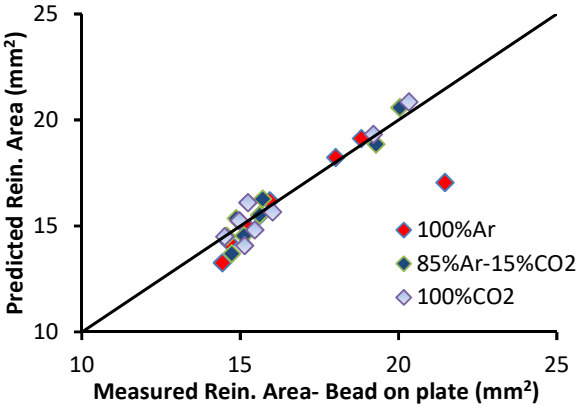

(e)Reinforcement Area

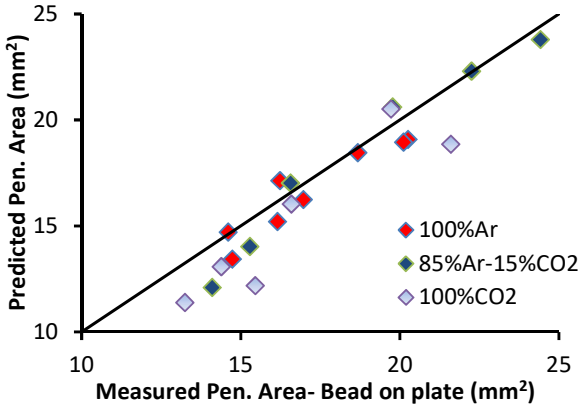

(f)Penetration Area

Figure 44 Fit- between predicted and measured value 0.045 in wire

Table 4-9 Parameters with points outside the prediction interval (in bold)

Trial #	Gas Type	Width (mm)		Depth (mm)		Reinforcement Height(mm)		Reinforcement Area (mm^2)	
		Measu-red	Predict-ed	Measu red	Predicted	Meas-ured	Predicte d	Meas-ured	Predict ed
1	100% Ar	8.39	8.11 ±1.22	1.83	1.71±0.53	2.98	2.69±0. 39	**14.44**	13.26± 0.74
6	100% Ar	9.60	8.83±1. 22	4.67	5.05±0.53	**3.13**	2.82±0. 39	**21.47**	17.04± 0.74
8	100% Ar	11.02	10.51± 1.22	**3.62**	4.19±0.53	3.36	3.24±0. 39	18.02	18.22± 0.74
5	85%Ar-15%CO_2	**10.38**	9.60±0. 60	3.88	4.21±0.47	2.92	2.90±0. 30	15.11	14.54± 0.97
6	85%Ar-15%CO_2	**9.05**	8.21±0. 60	**4.18**	4.73±0.47	2.74	2.83±0. 30	14.73	13.68± 0.97
8	85%Ar-15%CO_2	**10.81**	10.03± 0.60	4.42	4.59±0.47	3.08	3.31±0. 30	19.29	18.85± 0.97
5	100%CO_2	**8.64**	7.71±0. 71	**4.15**	5.08±0.54	**3.00**	3.57±0. 39	**15.14**	14.07± 0.87
6	100%CO_2	9.74	9.62±0. 71	3.61	3.49±0.54	**2.99**	3.54±0. 39	20.33	20.85± 0.87
8	100%CO_2	9.92	9.10±0. 71	4.07	4.27±0.54	**3.24**	3.75±0. 39	19.21	19.32± 0.87

Most of the parameters lying outside the interval correspond to high power input conditions. For weld bead width, the values predicted by the model were less than the measured value for the points. This can be explained by the plateau of the fit achieved in between the 25 to 30V range across the travel speeds, causing the model to slightly under-predict, and this is also the same case for the reinforcement height model which has a similar trend. For the bead depth, the model has a concave up fit (exponential) at high wire feed-voltage-travel speed rates causing an over-estimation of the predicted values indicating the increase is at a slower pace than expected. Another consideration is that weld depth is considering the penetration profile of a deep column-like protrusion (*i.e.* finger like penetration) of the weld, as was observed earlier with argon and 85% Argon-15% CO_2 gas, which is expected to have some effect when measuring the depth. For reinforcement area though the model had almost linear fit, the values were moderately under-predicted at higher feed and travel speed rate. Among the test data, one of the points which had a higher

measured reinforcement value compared to the predicted one was trial #6. Also it was found that the area for measured reinforcement was higher than the actual theoretical reinforcement area for the weld. Even though the reinforcement area model was fairly linear, one of the reasons for the point being outlier is because of the travel speed which was used to perform the welding was around 36ipm. This higher travel speed is likely to begin experiencing oscillations in the weld pool, causing variation in reinforcement area of weld along the cross section. Another possible reason could be with 100%Ar gas the range of travel speed in DoE was 10-30ipm, and the point made using 36ipm could experience different arc dynamics, thereby causing the model to under-estimate the prediction of reinforcement area.

For fillet and V-groove welds, only two geometric dimensions namely reinforcement area and penetration area were measured for each welds. Figure 45 shows a cross section macro image of a weld made on the V-groove with a backing (V-groove #3), with the root, fill and cap pass shown separately.

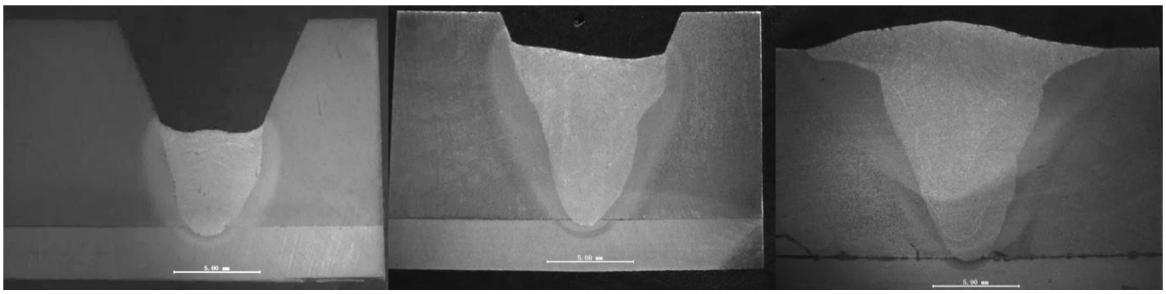

a) Root Pass b) Fill Pass c) Cap Pass

Figure 45 Cross section macro image of V-Groove #3

Table 4-10 Fillet Weld-Measured and Predicted Values

Wire	#Fillet	Reinforcement Area (mm^2)		Penetration Area (mm^2)	
		Measured	Predicted	Measured	Predicted
ER 70S-6 (0.045 in)	Fillet 1	17.62	16.83±0.87	15.60	14.42±2.06
	Fillet 2	18.74	17.93±0.87	19.78	18.25±2.06
	Fillet 3	14.21	14.47±0.97	23.10	18.01±1.57
	Fillet 4	22.52	23.04±0.97	26.22	24.73±1.57
	Fillet 5	15.95	15.73±0.74	17.49	15.23±2.76
ER 70S-6 (0.035 in)	Fillet 1	10.78	10.78±1.04	7.31	6.78±1.57
	Fillet 2	9.98	10.06±0.91	9.21	7.71±2.06
	Fillet 3	14.71	15.08±1.78	11.84	9.1±2.76

Table 4-11 V-Groove weld-Measured and Predicted Values

#Groove	#Pass	Reinforcement Area (mm^2)		Penetration Area (mm^2)	
		Measured	Predicted	Measured	Predicted
A	1-Root	14.53	14.8±0.74	5.02	14.92±1.19
	2-Fill (1)	23.83	22.80±0.74	12.32	22.04±1.19
	3-Fill (2)	21.78	20.34±0.74	23.73	19.9±1.19
	4-Cap	21.54	21.16±0.74	18.01	20.76±1.19
B	5-Root	15.85	15.93±0.97	8.94	15.93±3.19
	6-Fill (1)	23.12	23.16±0.97	14.31	23.16±3.19
	7-Fill (2)	30.08	31.34±0.97	16.7	31.34±3.19
	8-Cap	16.34	18.82±0.97	14.58	18.82±3.19
C	9-Root	17.45	17.4±0.87	10.97	13.49±4.32
	10-Fill	25.56	25.54±0.87	17.78	24.24±4.32
	11-Cap	33.53	31.32±0.87	31.32	32.12±4.32
D	12-Root	7.76	7.36±1.04	1.22	5.02±1.57
	13-Fill (1)	16.6	17.17±1.04	12.18	11.87±1.57
	14-Fill (2)	14.42	16.22±1.04	13.93	13.09±1.57
	15-Cap	18.65	18.07±1.04	16.72	19.21±1.57
E	16-Root	8.18	10.10±0.91	3.12	8.47±2.06
	17-Fill (1)	14.97	14.99±0.91	9.23	11.92±2.06
	18-Fill (2)	22.92	21.80±0.91	10.47	18.83±2.06
	19-Fill (3)	14.51	15.23±0.91	15.52	12.87±2.06
	20-Cap	11.59	10.01±0.91	11.33	20.15±2.06

Table 4-10 shows the measured and predicted values for fillet welds. It was observed that reinforcement area for the fillet weld was same as the case of bead on plate welds, since this only considers the melted wire deposited onto the substrate. However, for penetration area, an increase in area was observed for almost all the fillet welds. In the case of bead on plate conditions, the only penetration is from the top of the substrate, but with fillet welds

there is additional penetration on sides of the substrate held at an angle, leading to a higher penetration rate in the substrate for fillet joints.

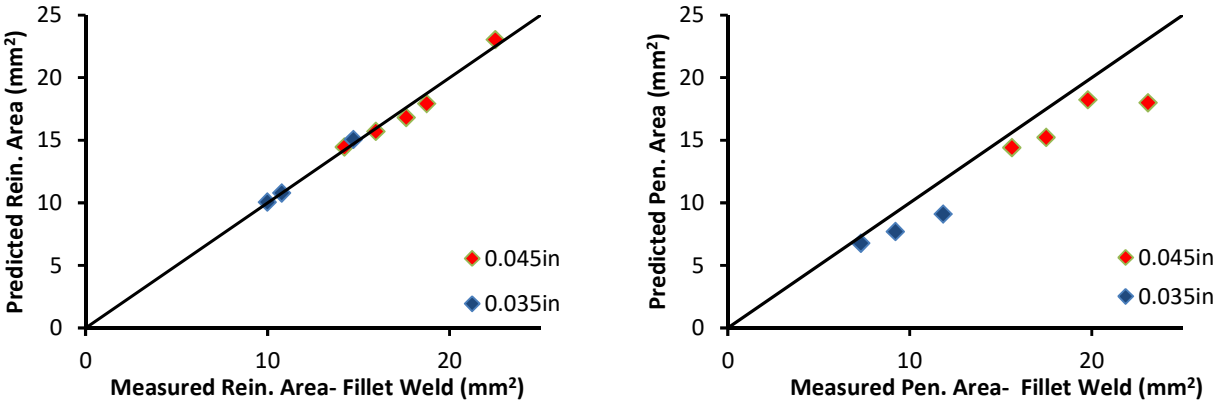

(a)Reinforcement area (b) Penetration area

Figure 46 Fit- between predicted and measured value- Fillet Weld

The comparison of measured weld bead dimension and model predictions for reinforcement and penetration area is shown in Figure 46, with predicted values plotted against the measured value from the bead on plate test. Here the points closer to line signify a good fit between predicted and measured value. It can be seen from the plots for the reinforcement area that almost all the points were on line, indicating an excellent fit, whereas for penetration area the points were at right side of the line indicating a highvalue for penetrated area. Only one value of penetration was outside the prediction interval, and all the reinforcement measurements were within predicted interval. The high value measured for penetrated area can be explained by the increased area of fillet coming under the contact with moving arc.

Table 4-11 shows the measured and predicted values for various weld passes with a 45° V-groove. Comparing the predicted and measured values, the penetration area for a different pass i.e. the area of the substrate penetrated, varied by a greater extent for most of the weld passes. For a V-groove the penetration area represents area penetrated into the side

walls of groove and back plate in case of groove with plate-backing, and penetration through deposited metal in case of multiple-pass welds.

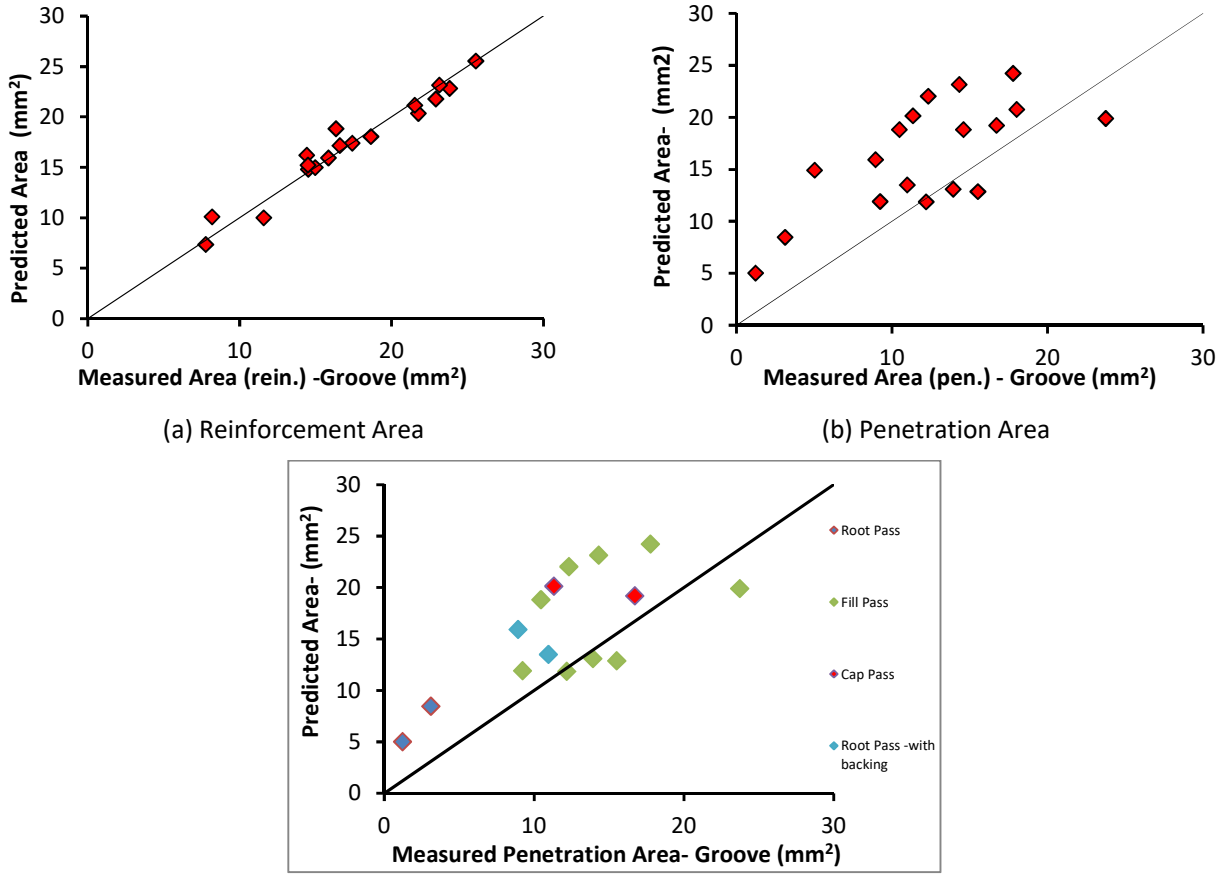

(a) Reinforcement Area

(b) Penetration Area

(c) Penetration Area – Classified according to passes

Figure 47 Fit- between predicted and measured value- V-groove Weld

The Figure 47 shows a plot between predicted and measured values for passes performed on V-Groove. From left plot it can be seen that for reinforcement area most of the data points for welds were along the line showing a good fit between the predicted and measured value. Whereas for the penetration area most of the data points were above the 1:1 line indicating a higher predicted value for penetration area versus the measured value. The rationale behind this lower penetration in this multi-pass welding is the increase in cooling rate with high thickness of work sample [48]. Thickness and area of the work sample effect the heat conduction and essentially the cooling rate. With higher cooling rate, the heat retained on the sample is less, because of this a thicker work piece acts as heat sink causing to

cool the weld down more quickly [16, 49]. This causes the V-groove welds with a ½ inch (12.7 mm) plate thickness to act as better heat sink, which in turn produces lesser penetration area in weld compared to a bead on plate weld.

Chapter 5. Conclusion and Future work

5.1 Conclusion

A factorial experimental design was used to study the effect of process parameters on bead geometry in Gas Metal Arc Welding, and statistical models were developed based on the experimental work. The following conclusions were reached:

- The statistical models are developed in this work and can be applied to predict the bead geometry and to select the required parameters to achieve specific bead geometry. The models can be developed into a calculator, which can also further be used to develop procedure plan for multi-pass welding and fillet welds.
- From experimental data it was shown to be determined that the welding travel speeds predominantly had negative effect on most of the bead geometry while wire feed speed had a positive effect and voltage a mixed- positive/negative effect on bead geometry.
- Voltage was the dominant factor in weld width and was seen to be greatly correlated with reinforcement height, with a decreasing influence on width rate at values 25-30V and lower travel speed being compensated by higher reinforcement.
- It was observed that penetration, reinforcement height and area for penetration and reinforcement increased with wire feed speed and voltage, while higher travel speed had negative effect altering the concavity of model fits along with shielding gas type.
- Overall the models predicted new experimental data fairly well. This is particularly interesting; given the rather large range of wire feed speeds, voltage and travel speed used in the experiment respectively (from 200 to 580ipm, 20 to 30 V and 10 to 44ipm). Validation tests done in bead on plate condition showed good prediction capabilities of the regression model with only 3 points outside the prediction interval

for current, depth and reinforcement height models, while width and reinforcement height had four points outside the interval out of 24 points, which is reasonable considering the range of parameters and inherently high variability of the geometries. Comparatively the average relative error (%) between predicted and measured values were 2.42%, 5.77, 7.66%, 6.97%, 3.92%, 7.63% for current, width, penetration, reinforcement height, reinforcement area and penetration area.

- The validation tests done on V-groove joint showed over prediction for penetration area by the model due to the effect of thickness, while fillet condition had only out of 8 trial points was outside the prediction interval. Therefore one of the effects of using thicker plate is that it will be expected to cool down faster due to a larger cross section, producing lower penetration and width with thicker plates and vice versa from thinner plates.
- Even though the measurements of bead geometry varied within the cross sections of the bead, results of F-tests showed that there was no statistically significant difference between the data measured from experimental results at 5% significance level. And similarly comparing the variation between the different diameters, it was found that there was a significant difference between predicted from models of 0.045 in and 0.035 in wire diameters.

5.2 Future Work

5.2.1 Refined experimental database

The scope for future possible work that can be extended to the current work being performed in this study include:

- Performing experiments on different wire types and material to derive statistical models for some of the most commonly used welding wires types and diameters. One may also conduct additional experiments using a calorimeter to determine the thermal efficiency.
- Analyzing the effect of different transfer modes on the bead geometry, to study the effect of variability in bead width, depth and penetration area at high arc power inputs (at globular and spray transfer mode).
- Perform mechanical testing on welds to provide a methodology to predict/estimate the mechanical properties of welds based on the experimental welds made so far.
- A sensitivity analysis can be further performed on statistical model to measure the uncertainty in output of the bead geometry by varying set of dependent variable at a time (i.e. keeping a set of inputs constant and varying one at a time), to know how sensitive is the output for a slight variation in the input variable.
- Perform statistical regression analysis on penetration area measured from V-grove welds and provide a correction factor to account for the effect of faster cooling rate on penetration area due to the thickness of the groove.
- Perform additional tests on different joint geometries to further validate the statistical models developed.

5.2.2 Welding app

The statistical model developed from this study was developed into a welding app with help of a student from Systems Design Engineering at University of Waterloo with the funding from Canadian Welding Bureau. A preview beta version of this welding app is shown in Figure 48. The welding app allows for user to enter the input parameters and provides prediction for different features of weld bead such as the dimensions of geometry for various weld joint geometry, number of passes required in case of multi-pass welding and cost analysis for the process. The statistical model for different wire types can be added to this app, and develop this as an open source tool where researchers/engineers/welders can add weld data to provide the welding community a predictive methodology to estimate the bead geometry and other interesting features of welds such as mechanical characteristics.

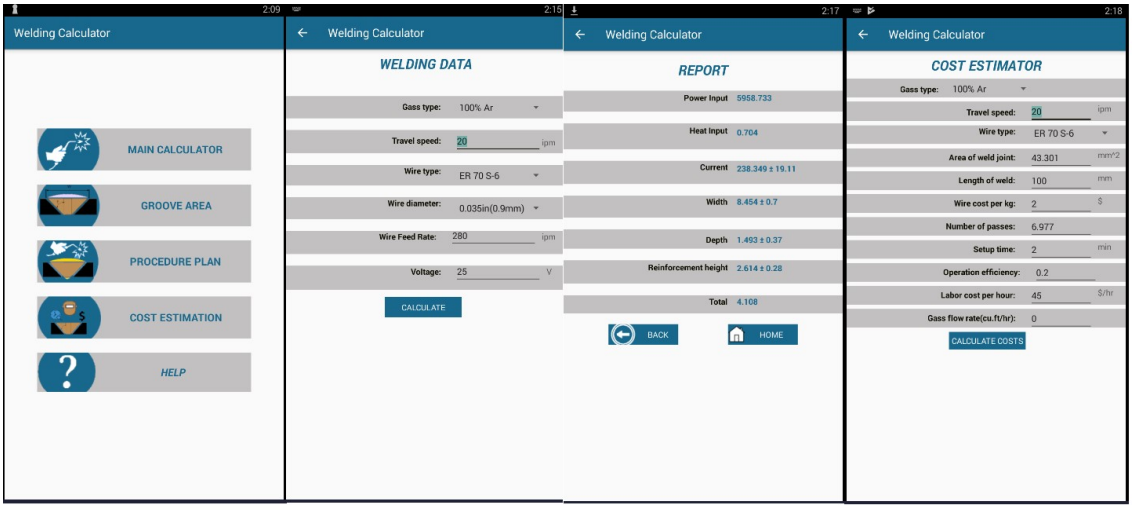

Figure 48 CWB Welding App- Beta Version Preview

Reference

[1]. Welding and the World of Metals, Miller Electric, April 2018.

[2]. Welding Process Handbook, Wood Head Publishing Ltd, 2003

[3]. Welding Consumables Market by Type (Stick Electrodes, Solid Wires, Flux Cored Wires, and SAW Wires & Fluxes), End-user Industry (Aerospace & Defense, Automotive & Transportation, Construction, Energy, Heavy Machinery, Shipbuilding, and Process & Others), Welding Technique (Arc Welding, Resistance Welding, Oxy-fuel Welding, Laser-beam Welding, and Others) - Global Opportunity Analysis and Industry Forecast, 2017-2023

[4]. Google Play Store: Lincoln electric Parameters Guide app
https://play.google.com/store/apps/details?id=com.lincolnelectric.parametersguide&hl=en
[5]. Google Play Store: Miller Weld Setting Calculator app
https://play.google.com/store/apps/details?id=com.lincolnelectric.parametersguide&hl=en

[6]. Google Play Store: Fronius Weld Wizard app
https://play.google.com/store/apps/details?id=com.lincolnelectric.parametersguide&hl=en

[7]. Quantitative and Qualitative analysis of 10 mm steel plate welding with 135, 136, 138 methods in PB position delivered during the Seminar on Steel Construction, Lincoln Electric Poland, 24-26th of November 2010 by Waldemar Radomski, Academy of Mining and Metallurgy, Cracow, Poland.

[8]. Fahrmeir L., Kneib T., Lang S. and Marx B., Regression - Models, Methods and Applications, 2nd edition. Springer; 2009.

[9]. Montgomery D.C., Design and analysis of experiments, 8th ed., Wiley NJ, 2012.

[10]. Geroge, C., Statistical design, Springer,2008

[11]. Angela D., Daniel V. and Danel D., Design and Analysis of Experiemnts 2nd edition, Springer, 2017

[12]. Paul B., Robert M. and Giovana B.C., Experimental Design with application in Management, Engineering and the Sciences, Springer 2018

[13]. AWS User's Guide to Filler Metals 2nd Edition, American Welding Society, 2010

[14]. Specification for Carbon Steel Electrodes and Rods for Gas Shielded Arc Welding (AWS A5.18/A5.18M:2005), American Welding Society, 2005

[15]. Cavazzuti M., Optimization Methods: From Theory to Design scientific and Technological Aspects in Mechanics, Springer 2013

[16]. Kou, S., Welding Metallurgy Second Edition, John Wiley & Sons Inc, 2003.

[17]. Jenney, C. and A. O'Brien, AWS Welding Handbook Volume 2, Second Edition. 2011.

[18]. Weman, K., Welding Processes Handbook 2nd Edition, Woodhead Publishing Ltd, 2003.

[19].Variables that Affect Weld Penetration, Lincoln Electric (https://www.lincolnelectric.com/en-gb/support/process-and-theory/Pages/variables-weld-penetration.aspx)

[20]. Norrish, J., Advanced welding processes, Woodhead Publishing Ltd, 2006.

[21]. Yupeng Z., The Effect of Shielding Gas Composition on Weld Bead Geometry during Short-circuit GMA Welding of Inconel625 Alloy, August 2016.

[22]. Lancaster, J.F., The Physics of Welding 2nd Edition, International Institute of Welding, 1986.

[23]. R.A. Ribeiro, The cold wire gas metal arc welding (CW-GMAW) process: Description and Applications, 2018.

[24].Lincoln Electric L-56 super arc welding wire(ER70S-6)(https://www.lincolnelectric.com/assets/g lobal/products/consumable_miggmawwires-superarc-superarcl-56/c4105.pdf)

[25]. R Core Team, "R: A Language and Environment for Statistical Computing", 2017.

[26]. Murugan N. and Parmar R.S., Effects of MIG process parameters on the geometry of the bead in the automatic surfacing of stainless steel., Journal of Materials Processing Technology 41 381-398 (1994)

[27]. Khanna, P. and Maheshwari, S., Effect of Welding Parameters on Weld Bead Characteristics during MIG Welding of Stainless Steel 409M., Journal of production engineering Vol.19 (2) (2016)

[28]. Aghakhani M., Mehrdad E., and Hayati E., Parametric Optimization of Gas Metal Arc Welding Process by Taguchi Method on Weld Dilution, International Journal of Modeling and Optimization Vol. 1, No. 3, 216 August 2011

[29]. Gunaraj V. and Murugan N., Prediction and optimization of weld bead volume for the submerged arc process—part 1., Welding journal, 78, 286s-294s (2000).

[30]. Datta S., Bandyopadhyay A. and Pal P. K., Grey-based Taguchi method for optimization of bead geometry in submerged arc bead-on-plate welding, The International Journal of Advanced Manufacturing Technology, 39(11-12), 1136-1143 (2008).

[31]. Tarng Y. S. and Yang W. H., Optimisation of the weld bead geometry in gas tungsten arc welding by the Taguchi method, The International Journal of advanced manufacturing technology14 (8), 549-554, 1998.

[32]. Gunaraj V. and Murugan N., Application of response surface methodology for predicting weld bead quality in submerged arc welding of pipes, Journal of Materials Processing Technology, 88(1-3), 266-275 (1999).

[33]. Nagesh D. S. and Datta G. L., Prediction of weld bead geometry and penetration in shielded metal-arc welding using artificial neural networks, Journal of Materials Processing Technology, 123(2), 303-312 (2002).

[34]. Kanti K. M. and Rao P. S., Prediction of bead geometry in pulsed GMA welding using back propagation neural network, Journal of Materials Processing technology, 200(1-3), 300-305 (2008).

[35]. Millermetric Calculator, Miller Electric™

[36]. Natarajan R. and Seppo A. K., Fluid Dynamics of a Stationary Weld Pool, Metallurgical Transactions A, Volume 21, Issue 1, pp 45–57, January 1990.

[37]. Fan H., Tsai H.L. and Na S.J., Heat transfer and fluid flow in a partially or fully penetrated weld pool in gas tungsten arc welding, International Journal of Heat and Mass Transfer 44(2): p. 417-428, 2001.

[38]. Hu J., Guo H., and Tsai H.L., Weld pool dynamics and the formation of ripples in 3D gas metal arc welding, International Journal of Heat and Mass Transfer 51 2537–2552, 2008.

[39]. Kou S. and Wang Y., Weld pool convection and its effect, Weld Journal 65(3): p. 63s-70s, 1986.

[40]. Kou S. and Sun D., Fluid flow and weld penetration in stationary arc welds, Metallurgical Transactions A16 (2): p. 203-213, 1985.

[41]. Hondros E.D., McLean M., Mills K. C., Keene B. J., Brooks R. F., and Shirali A., Marangoni effects in welding, Philosophical Transactions-Royal Society of London Series A Mathematical Physical and Engineering Sciences: p. 911-926, 1998.

[42]. Tsai M. C. and Kou S., Weld pool Convection and Expansion due to density variations, Numerical Heat Transfer, Part A: Applications, 17:1, 73-89 (1990) DOI:10.1080/10407789008944733

[43]. Eisazadeh H., Haines D. J. and Torabizadeh M., Effects of gravity on mechanical properties of GTA welded joints, Journal of Materials Processing Technology 214 1136–1142 (2014)

[44]. http://www.fronius.com/cps/rde/xchg/SID-06AD9288-4664C7E5/fronius international /hs.xsl/79_17490_ENG_HTML.htm#.VwLIOU8rJhE

[45]. Tsai M. C. and Kou S., Electromagnetic Force Induced Convection in Weld Pools with a Free Surface, Welding Research Supplement 241-246s, 1990.

[46]. Murugan N.and Gunaraj V., Prediction and control of weld bead geometry and shape relationships in submerged arc welding of pipes Journal of Materials Processing Technology 168 pg:478–487, 2005.

[47]. Nazmul H., Yuquan D. and Adrian P.G., Temper-treatment development to decompose detrimental martensite–austenite and its effect on linepipe welds, Materials science and Technology Vol. 33, NO. 16 pg: 1978–1992, 2017

[48]. Kihara, H., Suzuki, H. and Tamura, H., Researches on Weldable High-Strength Steels, 60th Anniversary Series,Vol. 1, Society of Naval Architects of Japan, Tokyo, 1957.

[49]. Inagaki, M. and Sekiguchi, H., Trans. Nat. Res. Inst. Metals, Tokyo, Japan, 2(2): 102 (1960).

[50]. Marcia L.H. and Allan H.H., Thermal Conductivity of Gases, CRC Handbook of Chemistry and Physics, June 06, 2011

Appendix A: Experimental Data-Results

Wire Type: ER70 S-6

Wire Diameter: Manufacturer label (0.9mm; 0.035 in), Measured (0.9mm)

Gas: 100%CO_2

						Cross Section 1						Cross Section 2					
	WFS (ipm)	Voltage (V)	TS (ipm)	Current (I)	Width (mm)	Depth (mm)	Rein-forcement ht (mm)	Rein-forcement area (mm^2)	Penetrated area (mm^2)	Depo-sition. Eff.	Dilution ratio	Depth (mm)	Rein-forcement ht (mm)	Rein-forcement area (mm^2)	Penetrated area (mm^2)	Depo-sition. Eff.	Dilution ratio
1	250	20	16	115.20	6.78	1.35	2.71	8.91	4.71	0.90	0.35	1.3	2.66	8.50	5.71	0.86	0.40
2	425	20	16	159.52	7.08	1.77	3.54	16.1	7.04	0.95	0.30	1.83	3.65	15.83	5.51	0.94	0.26
3	600	20	16	197.56	7.34	1.88	3.64	23.03	7.64	0.97	0.25	1.9	3.91	22.65	6.21	0.95	0.22
4	250	25	16	118.20	8.02	1.32	1.81	8.73	5.78	0.88	0.40	1.23	1.71	9.00	3.97	0.91	0.31
5	425	25	16	166.83	10.43	2.21	2.89	16.34	11.85	0.97	0.42	2.08	3.12	16.27	10.30	0.96	0.39
6	600	25	16	209.58	9.35	2.36	3.56	21.62	13.62	0.91	0.39	2.56	3.36	21.85	12.41	0.92	0.36
7	250	30	16	129.96	9.36	1.35	1.75	9.65	11.07	0.97	0.53	2.01	1.84	9.79	11.32	0.99	0.54
8	425	30	16	180.22	11.35	2.34	2.56	16.33	16.49	0.97	0.50	2.14	2.45	16.38	16.75	0.97	0.51
9	600	30	16	224.55	12.07	3.09	2.87	22.9	25.98	0.96	0.53	3.27	3.07	23.17	25.66	0.97	0.53
10	250	20	23	105.76	4.18	1.11	2.36	6.04	2.52	0.87	0.29	0.91	2.16	5.98	2.88	0.87	0.33
11	425	20	23	157.36	4.83	1.38	3.14	10.34	4.46	0.88	0.30	1.16	2.94	10.60	4.76	0.90	0.31
12	600	20	23	190.22	5.46	1.61	3.74	16.16	5.45	0.97	0.25	1.64	3.93	16.36	5.25	0.99	0.24
13	250	25	23	116.21	6.17	1.24	1.83	4.35	5.46	0.63	0.56	1.15	1.16	5.61	5.20	0.81	0.48
14	425	25	23	168.51	8.16	1.57	1.79	7.86	9.61	0.67	0.55	1.98	1.68	9.96	9.51	0.85	0.49
15	600	25	23	210.35	9.08	2.54	3.03	16.21	15.06	0.98	0.48	2.76	3.05	16.49	14.78	0.99	0.47
16	250	30	23	131.06	7.54	1.51	1.79	5.83	7.42	0.84	0.56	1.5	1.3	6.58	7.67	0.95	0.54
17	425	30	23	181.42	8.58	2.17	2.32	10.52	13.74	0.90	0.57	2.01	2.21	10.93	14.56	0.93	0.57

18	600	30	23	220.93	8.4	3.07	2.74	14.58	19.4	0.88	0.57	3.07	2.7	14.85	19.20	0.90	0.56
19	250	20	30	118.15	4.23	1.09	1.86	3.32	2.55	0.63	0.43	0.94	1.11	3.70	2.29	0.70	0.38
20	425	20	30	160.85	4.68	1.37	2.45	8.11	3.27	0.90	0.29	1.23	2.84	7.84	3.17	0.87	0.29
21	600	20	30	191.49	4.11	1.11	3.25	10.97	2.72	0.86	0.20	0.88	3.09	11.04	2.44	0.87	0.18
22	250	25	30	116.94	4.97	0.95	1.26	4.08	3.13	0.77	0.43	0.78	1.26	4.65	3.38	0.88	0.42
23	425	25	30	171.63	5.69	1.62	1.95	8.35	7.88	0.93	0.49	1.53	2.18	8.21	8.70	0.91	0.51
24	600	25	30	212.57	5.33	2.28	2.78	12.26	9.65	0.96	0.44	2.32	2.83	12.21	10.65	0.96	0.47
25	250	30	30	127.96	5.87	1.19	1.71	5.14	7.06	0.97	0.58	1.33	1.53	4.87	5.53	0.92	0.53
26	425	30	30	181.23	7.07	1.59	1.96	7.05	10.82	0.78	0.61	1.84	1.63	8.11	9.39	0.90	0.54
27	600	30	30	225.65	8.32	2.56	2.41	8.51	16.09	0.67	0.65	2.41	2.14	9.25	16.32	0.73	0.64
28	308	21.6	10	140.90	7.44	3.44	0.57	16.75	3.49	0.86	0.17	3.67	0.63	16.55	3.63	0.85	0.18
29	367	21.6	10	168.18	8.92	2.24	3.29	21.26	10.69	0.91	0.33	2.13	3.39	21.00	10.74	0.90	0.34
30	308	23.4	10	152.74	10.01	2.03	2.32	19.17	11.63	0.98	0.38	2.19	2.72	19.07	11.90	0.97	0.38
31	367	23.4	10	168.11	10.38	1.96	3.43	20.84	11.51	0.89	0.36	2.01	3.27	20.56	11.45	0.88	0.36
32	308	21.6	13	128.22	6.48	0.42	3	13.61	2.31	0.90	0.15	0.72	3.07	13.86	2.57	0.92	0.16
33	367	21.6	13	171.01	8.39	2.49	3.28	16.24	12.62	0.90	0.44	2.46	3.14	17.06	12.82	0.95	0.43
34	308	23.4	13	121.83	7.62	0.81	2.88	13.73	3.42	0.91	0.20	0.96	2.64	14.73	3.68	0.98	0.20
35	367	23.4	13	158.78	9.2	2.58	3.26	16.58	12.27	0.92	0.43	2.39	3.12	15.05	12.37	0.84	0.45
36	484	26.6	37	199.30	6.64	2.07	1.84	8.13	7.71	0.98	0.49	1.84	2.04	6.70	7.99	0.81	0.54
37	542	26.6	37	217.02	6.08	2.12	2.31	7.75	8.42	0.83	0.52	1.98	2.16	5.94	8.01	0.64	0.57
38	484	28.4	37	212.13	6.49	2.1	2.5	8.06	10.57	0.97	0.57	2.31	2.39	8.21	10.30	0.99	0.56
39	542	28.4	37	230.85	7.13	2.76	2.4	7.55	13.53	0.81	0.64	2.84	2.14	6.34	13.15	0.68	0.67
40	484	26.6	44	199.01	6.21	1.47	1.66	5.17	7.99	0.74	0.61	1.59	1.86	5.82	8.26	0.83	0.59
41	542	26.6	44	215.37	6.04	2.21	2.31	6.18	7.74	0.79	0.56	2.04	2.04	6.44	7.67	0.82	0.54
42	484	28.4	44	206.41	6.03	2.33	1.75	6.14	9.23	0.88	0.60	2.16	1.94	5.82	9.46	0.83	0.62
43	542	28.4	44	220.02	6.18	2.39	1.73	6.21	12.32	0.79	0.66	2.42	1.83	6.57	12.46	0.84	0.65

Gas: 85%Ar -15%CO_2

						Cross Section 1						Cross Section 2					
	WFS (ipm)	Voltage (V)	TS (ipm)	Current (I)	Width (mm)	Depth (mm)	Rein-forcement ht (mm)	Rein-forcement area (mm^2)	Penetrated area (mm^2)	Depo-sition. Eff.	Dilution ratio	Depth (mm)	Rein-forcement ht (mm)	Rein-forcement area (mm^2)	Penetrated area (mm^2)	Depo-sition. Eff.	Dilution ratio
1	250	20	16	129.29	6.64	1.26	2.28	9.14	4.38	0.92	0.32	1.08	2.39	8.94	4.44	0.90	0.33
2	425	20	16	176.829	7.08	1.79	3.03	16.52	7.05	0.98	0.30	1.83	2.99	16.27	6.87	0.96	0.30
3	600	20	16	219.67	8.74	2.01	3.71	21.02	12.94	0.88	0.38	2.63	3.47	21.87	12.79	0.92	0.37
4	250	25	16	135.33	8.19	1.17	1.92	9.57	7.23	0.96	0.43	1.54	2.01	9.38	7.54	0.94	0.45
5	425	25	16	183.56	9.45	2.41	2.61	14.99	11.76	0.89	0.44	2.04	2.46	15.34	11.87	0.91	0.44
6	600	25	16	225.71	11.43	3.07	2.83	21.35	18.61	0.90	0.47	3.18	3.01	20.97	18.88	0.88	0.47
7	250	30	16	148.10	9.37	0.95	1.67	9.16	6.25	0.92	0.41	0.71	1.59	8.80	5.90	0.89	0.40
8	425	30	16	197.71	12.13	2.14	2.48	16.46	10.07	0.97	0.38	1.71	2.09	16.75	10.24	0.99	0.38
9	600	30	16	246.98	13.72	2.97	2.82	22.81	22.31	0.96	0.49	3.56	2.76	23.01	22.63	0.97	0.50
10	250	20	23	120.73	5.39	0.84	1.72	6.06	3.37	0.88	0.36	1.03	1.54	5.70	3.19	0.82	0.36
11	425	20	23	169.35	6.59	1.56	2.65	11.63	6.83	0.99	0.37	2.49	1.43	10.90	6.82	0.93	0.38
12	600	20	23	214.52	6.85	2.08	3.21	11.62	10.73	0.70	0.48	1.92	3.14	12.78	10.39	0.77	0.45
13	250	25	23	131.02	7.55	1.02	1.26	6.84	5.09	0.99	0.43	1.13	1.45	6.62	5.38	0.96	0.45
14	425	25	23	180.44	8.54	1.94	2.19	10.89	6.67	0.93	0.38	1.61	1.63	10.87	6.42	0.93	0.37
15	600	25	23	222.18	8.67	2.76	2.34	15.96	9.95	0.96	0.38	2.63	2.45	15.62	10.04	0.94	0.39
16	250	30	23	148.51	8.41	0.91	1.46	6.37	4.22	0.92	0.40	0.77	1.44	6.45	3.99	0.93	0.38
17	425	30	23	195.16	10.02	2.11	1.91	11.13	10.56	0.95	0.49	1.81	1.73	10.96	10.77	0.93	0.50
18	600	30	23	243.10	10.81	3.19	2.24	14.31	20.1	0.86	0.58	3.12	2.08	14.22	20.37	0.86	0.59
19	250	20	30	119.37	6.03	0.79	1.42	4.95	3.59	0.93	0.42	0.72	1.4	4.63	3.52	0.87	0.43
20	425	20	30	172.87	6.79	1.61	2.08	8.55	6.01	0.95	0.41	1.41	2.09	8.91	6.24	0.99	0.41
21	600	20	30	213.54	6.14	1.64	2.96	11.94	6.41	0.94	0.35	1.9	2.75	12.24	6.55	0.96	0.35

22	250	25	30	132.67	6.99	0.84	1.19	4.48	4.6	0.85	0.51	0.95	1.11	4.12	4.65	0.78	0.53
23	425	25	30	188.13	7.36	1.75	1.88	8.58	7.78	0.95	0.48	1.68	1.79	8.18	8.05	0.91	0.50
24	600	25	30	220.45	7.96	2.54	1.95	12.268	11.432	0.96	0.48	2.61	2.34	12.04	11.37	0.95	0.49
25	250	30	30	149.12	6.62	0.53	1.22	4.79	3.53	0.90	0.42	0.47	1.2	4.85	3.79	0.92	0.44
26	425	30	30	197.91	8.92	1.64	1.92	9.81	5.6	1.09	0.36	1.26	1.44	9.99	5.80	1.11	0.37
27	600	30	30	234.97	8.88	2.56	2.06	11.35	15.24	0.89	0.57	2.61	2.01	11.48	15.50	0.90	0.57
28	308	21.6	10	169.17	10.09	1.84	3.03	17.03	9.72	0.87	0.36	1.86	3.06	16.93	9.82	0.86	0.37
29	367	21.6	10	185.28	11.08	2.42	2.83	16.57	14.25	0.71	0.46	2.28	2.71	16.66	14.53	0.71	0.47
30	308	23.4	10	170.57	10.93	1.81	3.1	19.01	13.93	0.97	0.42	1.93	3.12	19.10	13.68	0.98	0.42
31	367	23.4	10	184.05	12.06	2.07	3.22	21.17	10.61	0.91	0.33	1.9	3.21	21.39	10.72	0.92	0.33
32	308	21.6	13	167.51	9.13	1.93	2.52	14.61	6.46	0.97	0.31	1.78	2.47	14.82	6.73	0.98	0.31
33	367	21.6	13	187.61	9.75	2.23	2.58	17.47	9.74	0.97	0.36	2.11	2.72	17.54	9.39	0.98	0.35
34	308	23.4	13	161.40	9.86	1.48	2.19	13.67	8.48	0.91	0.38	1.68	2.24	13.34	8.65	0.89	0.39
35	367	23.4	13	181.91	11.06	2.02	2.47	17.11	10.48	0.95	0.38	2.23	2.56	17.12	10.80	0.95	0.39
36	484	26.6	37	217.96	7.44	2.03	1.44	7.24	7.33	0.87	0.50	1.99	1.53	7.10	6.93	0.85	0.49
37	542	26.6	37	232.35	7.84	2.42	2.09	7.92	9.65	0.85	0.55	2.36	2.15	8.20	9.29	0.88	0.53
38	484	28.4	37	228.55	8.19	2.41	1.59	7.33	9.3	0.88	0.56	2.31	1.54	7.61	9.07	0.91	0.54
39	542	28.4	37	243.63	8.02	2.28	1.97	9.05	11.04	0.97	0.55	2.51	1.93	8.85	10.90	0.95	0.55
40	484	26.6	44	214.99	7.69	1.72	1.68	6.74	6.92	0.96	0.51	1.66	1.53	6.63	6.99	0.95	0.51
41	542	26.6	44	230.48	7.79	1.94	1.68	7.67	8.52	0.98	0.53	2.16	1.73	7.70	8.18	0.98	0.52
42	484	28.4	44	224.97	7.56	2.44	1.54	6.91	11.83	0.99	0.63	2.57	1.61	6.76	11.62	0.97	0.63
43	542	28.4	44	234.39	7.62	2.37	1.87	7.59	9.45	0.97	0.55	2.28	2.06	7.72	9.68	0.99	0.55

Gas: 100%Ar

	WFS (ipm)	Voltage (V)	TS (ipm)	Current (I)	Width (mm)	Cross Section 1						Cross Section 2					
						Depth (mm)	Rein-forcement ht (mm)	Rein-forcement area (mm^2)	Penetrated area (mm^2)	Depo-sition. Eff.	Dilution ratio	Depth (mm)	Rein-forcement ht (mm)	Rein-forcement area (mm^2)	Penetrated area (mm^2)	Depo-sition. Eff.	Dilution ratio
1	250	20	16	125.15	4.47	0.89	2.52	8.75	1.95	0.88	0.18	0.95	2.41	9.57	2.33	0.96	0.20
2	425	20	16	161.34	5.35	1.26	4.02	15.83	5.22	0.94	0.25	1.18	3.8	16.83	6.57	0.99	0.28
3	600	20	16	197.39	6.89	0.85	3.18	19.47	4.87	0.82	0.20	0.88	4.82	17.94	5.51	0.75	0.23
4	250	25	16	137.39	5.48	0.62	2.01	6.59	1.51	0.66	0.19	0.65	1.91	7.16	2.04	0.72	0.22
5	425	25	16	171.23	7.87	1.53	2.63	16.55	7.22	0.98	0.30	1.26	2.64	14.74	9.38	0.87	0.39
6	600	25	16	208.08	7.51	1.91	3.91	17.63	9.06	0.74	0.34	1.68	3.54	19.08	9.07	0.80	0.32
7	250	30	16	168.89	5.74	1.59	2.28	8.33	2.7	0.84	0.24	1.15	2.23	9.12	3.82	0.92	0.30
8	425	30	16	235.27	8.07	2.69	2.89	16.43	12.98	0.97	0.44	2.54	2.84	16.68	14.36	0.99	0.46
9	600	30	16	264.90	11.62	2.51	3.14	21.84	13.99	0.92	0.39	3.25	3.18	22.1	17.34	0.93	0.44
10	250	20	23	119.01	3.97	0.85	2.31	6.48	1.47	0.94	0.18	0.62	2.06	6.59	12.11	0.95	0.65
11	425	20	23	161.99	5.09	0.91	2.85	9.48	4.65	0.81	0.33	0.76	2.59	9.45	4.08	0.80	0.30
12	600	20	23	201.80	4.28	0.93	3.96	16.53	4.08	1.00	0.20	1.04	3.76	14.52	5.89	0.88	0.29
13	250	25	23	139.67	4.21	1.26	1.97	6.32	5.81	0.91	0.48	1.31	1.81	6.18	5.25	0.89	0.46
14	425	25	23	182.47	7.26	1.72	2.31	9.71	5.76	0.83	0.37	1.89	2.19	8.11	6.57	0.69	0.45
15	600	25	23	209.60	6.99	2.12	2.89	15.51	5.4	0.94	0.26	1.19	3.01	15.27	6.88	0.92	0.31
16	250	30	23	176.82	4.67	1.22	2.32	6.14	2.27	0.89	0.27	1.28	2.18	5.82	2.71	0.84	0.32
17	425	30	23	243.68	5.96	2.08	3.27	11.34	8.5	0.97	0.43	2.09	3.11	11.38	8.24	0.97	0.42
18	600	30	23	276.76	9.73	2.92	2.74	16.11	10.56	0.97	0.40	2.96	2.9	15.17	11.94	0.91	0.44
19	250	20	30	123.34	3.84	0.89	2.03	4.72	1.23	0.89	0.21	0.65	1.73	4.87	2.21	0.92	0.31
20	425	20	30	165.19	4.77	1.07	2.63	8.29	3.21	0.92	0.28	0.7	2.32	7.71	3.76	0.86	0.33
21	600	20	30	200.90	4.41	0.93	3.12	12.52	3.23	0.98	0.21	1.04	3.2	11.07	4.78	0.87	0.30

22	250	25	30	137.82	4.45	0.56	1.41	5.03	1.82	0.95	0.27	0.47	1.28	4.64	4.57	0.88	0.50
23	425	25	30	184.52	6.48	1.64	2.32	8.79	5.71	0.98	0.39	1.61	2.23	8.75	6.47	0.97	0.43
24	600	25	30	212.04	7.11	1.44	2.45	12.55	4.25	0.99	0.25	1.28	2.41	12.02	4.85	0.95	0.29
25	250	30	30	152.66	3.54	0.89	1.06	4.81	1.88	0.91	0.28	0.81	0.98	4.96	5.88	0.94	0.54
26	425	30	30	241.06	4.88	1.73	1.23	7.83	2.78	0.87	0.26	1.86	1.15	8.29	3.19	0.92	0.28
27	600	30	30	277.41	8.39	2.54	2.41	12.22	6.92	0.96	0.36	2.39	2.94	11.9	7.28	0.94	0.38
28	308	21.6	10	148.33	6.53	1.27	3.61	18.77	10	0.96	0.35	1.13	3.44	18.14	10.74	0.93	0.37
29	367	21.6	10	163.51	6.88	1.50	4.06	18.7	8.34	0.80	0.31	1.38	3.82	19.19	8.7	0.82	0.31
30	308	23.4	10	144.56	8.04	1.39	3.59	19.51	9.45	1.00	0.33	1.34	3.52	18.32	8.26	0.94	0.31
31	367	23.4	10	160.13	9.05	1.80	3.94	20.48	6.7	0.88	0.25	1.63	3.77	21.51	7.94	0.92	0.27
32	308	21.6	13	156.25	7.21	1.58	2.72	14.93	9.4	0.99	0.39	1.46	2.86	13.41	12.55	0.89	0.48
33	367	21.6	13	172.43	8.25	1.44	2.92	17.13	5.51	0.95	0.24	1.58	3.04	17.36	6.07	0.97	0.26
34	308	23.4	13	149.24	7.89	1.42	2.72	14.48	11.01	0.96	0.43	1.44	2.77	14.18	11.21	0.94	0.44
35	367	23.4	13	166.97	8.87	1.65	2.89	14.15	4.44	0.79	0.24	1.77	3.06	15.18	5.79	0.85	0.28

Wire Type: ER70 S-6

Wire Diameter: Manufacturer label (1.14mm; 0.045 in), Measured (1.15mm)

Gas: $100\%CO_2$

						Cross Section 1						Cross Section 2					
	WFS (ipm)	Voltage (V)	TS (ipm)	Current (I)	Width (mm)	Depth (mm)	Rein-forcement ht (mm)	Rein-forcement area (mm^2)	Penetrated area (mm^2)	Depo-sition. Eff.	Dilution ratio	Depth (mm)	Rein-forcement ht (mm)	Rein-forcement area (mm^2)	Penetrated area (mm^2)	Depo-sition. Eff.	Dilution ratio
1	200	20	20	186.33	6.54	2.31	2.53	9.99	11.45	0.96	0.53	2.29	2.59	9.50	12.36	0.92	0.57
2	390	20	20	225.80	8.55	2.21	3.37	20.13	8.59	0.99	0.30	2.49	3.58	19.74	9.42	0.98	0.32
3	580	20	20	354.89	7.97	2.46	4.77	28.77	10.67	0.96	0.27	2.71	4.68	28.57	11.03	0.95	0.28
4	200	25	20	168.63	7.29	1.77	2.28	10.15	10.23	0.98	0.50	1.71	2.42	10.01	9.68	0.96	0.49
5	390	25	20	266.39	10.92	3.44	3.22	20.23	22.73	1.00	0.53	3.54	3.44	19.48	22.16	0.96	0.53
6	580	25	20	322.84	9.62	3.91	3.72	29.54	17.08	0.98	0.37	3.92	3.94	29.09	17.25	0.97	0.37
7	200	30	20	194.34	8.72	2.34	1.84	9.64	16.00	0.93	0.62	2.50	1.71	9.47	15.54	0.91	0.62
8	390	30	20	279.73	12.04	3.49	2.71	20.22	25.51	1.00	0.56	3.82	2.83	20.08	23.49	0.99	0.54
9	580	30	20	359.08	9.95	5.79	4.07	28.83	34.92	0.96	0.55	5.86	3.92	30.08	33.75	1.00	0.53
10	200	20	25	184.55	5.72	2.14	2.28	7.73	3.61	0.93	0.32	2.25	2.53	7.91	4.90	0.95	0.38
11	390	20	25	220.41	6.81	1.71	2.69	15.25	8.39	0.94	0.35	1.73	2.84	15.51	9.24	0.96	0.37
12	580	20	25	374.46	7.1	2.79	3.69	23.90	9.66	0.99	0.29	2.88	4.02	23.88	9.59	0.99	0.29
13	200	25	25	170.94	7.15	2.61	1.63	7.96	4.21	0.96	0.35	2.82	1.66	7.85	3.64	0.95	0.32
14	390	25	25	272.49	8.93	3.73	2.89	16.06	17.78	0.99	0.53	3.64	3.02	15.82	17.32	0.98	0.52
15	580	25	25	328.12	9.53	3.26	4.22	23.91	15.80	0.99	0.40	3.59	4.27	24.07	16.39	1.00	0.41
16	200	30	25	192.60	7.45	2.01	1.61	7.94	16.90	0.96	0.68	1.94	1.68	7.60	18.63	0.92	0.71

17	390	30	25	277.48	10.7	3.47	2.45	15.62	17.92	0.96	0.53	3.47	2.53	16.17	19.36	1.00	0.54
18	580	30	25	363.66	8.96	6.63	3.91	23.70	36.03	0.98	0.60	6.75	3.74	23.14	37.36	0.96	0.62
19	200	20	30	183.52	4.18	1.29	1.12	6.41	6.33	0.93	0.50	1.45	1.45	6.26	6.67	0.90	0.52
20	390	20	30	210.83	3.79	1.76	1.88	12.70	5.72	0.94	0.31	1.88	1.96	13.30	5.44	0.99	0.29
21	580	20	30	364.93	5.02	2.7	3.15	19.25	5.87	0.96	0.23	2.73	3.02	19.66	5.95	0.98	0.23
22	200	25	30	166.25	5.98	1.96	1.49	6.38	6.03	0.92	0.49	2.27	1.52	6.40	6.91	0.92	0.52
23	390	25	30	261.96	6.76	2.89	2.82	13.36	14.09	0.99	0.51	2.94	2.82	13.51	15.00	1.00	0.53
24	580	25	30	323.37	7.96	3.84	4.19	19.88	25.39	0.99	0.56	4.13	4.04	19.25	25.26	0.96	0.57
25	200	30	30	193.66	6.76	2.06	1.53	6.39	11.40	0.92	0.64	2.02	1.87	6.65	12.66	0.96	0.66
26	390	30	30	282.57	8.95	3.15	2.21	13.19	20.12	0.98	0.60	3.24	2.26	13.42	20.48	0.99	0.60
27	580	30	30	375.27	7.16	6.21	3.74	18.95	37.90	0.94	0.67	6.19	3.65	20.00	38.33	1.00	0.66
28	264	21.6	12	210.75	9.47	2.94	3.59	22.23	13.68	0.97	0.38	3.08	3.62	22.69	13.32	0.99	0.37
29	326	21.6	12	242.05	10.03	3.22	4.04	27.71	14.68	0.98	0.35	3.35	4.18	27.41	15.80	0.97	0.37
30	264	23.4	12	202.60	10.68	2.82	3.26	19.89	19.40	0.87	0.49	2.97	3.50	20.28	19.71	0.89	0.49
31	326	23.4	12	235.93	10.61	4.04	3.79	26.49	23.40	0.94	0.47	4.23	3.73	27.11	22.18	0.96	0.45
32	264	21.6	16	211.12	8.77	2.96	2.82	15.88	14.99	0.93	0.49	2.83	2.93	16.69	14.12	0.97	0.46
33	326	21.6	16	248.94	9.42	3.85	3.21	19.05	19.58	0.90	0.51	3.70	3.21	18.59	19.40	0.88	0.51
34	264	23.4	16	198.67	9.62	2.5	2.68	16.81	13.60	0.98	0.45	2.53	2.55	16.79	13.19	0.98	0.44
35	326	23.4	16	234.52	9.18	3.82	3.14	19.33	19.67	0.91	0.50	3.74	3.01	18.88	19.58	0.89	0.51
36	454	26.6	37	303.52	7.07	3.19	2.34	11.53	15.07	0.91	0.57	3.00	2.37	11.25	15.04	0.88	0.57
37	516	26.6	37	320.89	8.26	3.97	3.74	13.04	17.92	0.90	0.58	4.12	3.96	13.61	19.31	0.94	0.59
38	454	28.4	37	311.82	7.22	3.52	2.34	12.24	20.85	0.96	0.63	3.56	2.40	11.67	19.90	0.92	0.63
39	516	28.4	37	324.86	8.14	5.2	2.97	14.09	21.99	0.97	0.61	5.01	3.12	14.18	21.90	0.98	0.61
40	454	26.6	44	307.47	6.16	3.97	2.76	9.69	15.28	0.90	0.61	3.91	2.78	10.32	16.35	0.96	0.61
41	516	26.6	44	325.25	6.2	4.19	2.72	11.07	17.18	0.91	0.61	4.35	2.57	10.71	17.87	0.88	0.63
42	454	28.4	44	306.01	6.61	3.6	2.24	9.37	16.88	0.87	0.64	3.64	2.20	8.99	17.22	0.84	0.66
43	516	28.4	44	319.73	6.46	4.5	2.66	11.65	16.97	0.96	0.59	4.32	2.51	11.52	17.66	0.95	0.61

Gas: 85%Ar -15%CO_2

	WFS (ipm)	Voltage (V)	TS (ipm)	Current (I)	Width (mm)	Cross Section 1						Cross Section 2					
						Depth (mm)	Rein-forcement ht (mm)	Rein-forcement area (mm^2)	Penetrated area (mm^2)	Depo-sition. Eff.	Dilution ratio	Depth (mm)	Rein-forcement ht (mm)	Rein-forcement area (mm^2)	Penetrated area (mm^2)	Depo-sition. Eff.	Dilution ratio
1	200	20	20	189.93	6.46	1.44	2.03	9.58	9.96	0.92	0.51	1.39	2.15	9.86	10.93	0.95	0.53
2	390	20	20	269.79	8.95	2.79	2.68	19.03	17.35	0.94	0.48	3.06	2.64	19.08	17.98	0.94	0.49
3	580	20	20	355.72	8.59	3.11	4.55	28.23	21.88	0.94	0.44	2.96	4.66	27.82	20.15	0.92	0.42
4	200	25	20	190.27	9.57	1.45	1.81	9.01	12.99	0.87	0.59	1.74	1.99	9.06	11.65	0.87	0.56
5	390	25	20	279.77	12.39	3.15	2.54	19.63	22.41	0.97	0.53	3.47	2.87	19.15	23.38	0.95	0.55
6	580	25	20	341.31	11.03	4.42	4.28	29.06	27.43	0.97	0.49	4.43	4.67	27.99	28.24	0.93	0.50
7	200	30	20	220.19	8.19	1.64	1.78	9.38	11.94	0.90	0.56	1.97	1.73	10.04	10.87	0.97	0.52
8	390	30	20	309.45	13.61	4.01	2.81	20.02	26.6	0.99	0.57	3.93	2.94	19.60	25.64	0.97	0.57
9	580	30	20	401.59	12.87	5.12	3.34	28.46	28	0.95	0.50	5.37	3.26	28.05	29.54	0.93	0.51
10	200	20	25	187.85	5.47	1.53	1.73	7.65	6.94	0.92	0.48	1.47	1.65	7.94	6.18	0.96	0.44
11	390	20	25	270.64	8.45	2.46	2.96	15.61	13.75	0.96	0.47	2.65	3.35	15.84	14.04	0.98	0.47
12	580	20	25	359.05	6.14	1.93	4.5	23.21	15.86	0.96	0.41	2.18	4.87	22.53	16.60	0.94	0.42
13	200	25	25	188.33	8.88	1.41	1.64	7.59	11.57	0.91	0.60	1.32	1.80	7.83	11.31	0.94	0.59
14	390	25	25	286.22	10.8	3.66	2.54	15.25	21.17	0.94	0.58	3.57	2.49	14.90	21.08	0.92	0.59
15	580	25	25	342.87	9.41	4.24	4.27	23.62	23.69	0.98	0.50	4.35	4.43	23.56	25.25	0.98	0.52
16	200	30	25	216.38	7.37	1.32	1.41	7.56	9.37	0.91	0.55	1.59	1.35	7.62	10.93	0.92	0.59
17	390	30	25	309.05	11.42	3.86	2.71	15.22	24.49	0.94	0.62	3.93	2.90	16.24	26.27	1.00	0.62
18	580	30	25	394.90	10.33	5.14	3.12	23.6	30.56	0.98	0.56	5.32	3.25	24.55	29.60	1.02	0.55
19	200	20	30	190.90	5.94	1.26	1.64	6.24	7	0.90	0.53	1.46	1.75	6.13	8.80	0.89	0.59
20	390	20	30	254.51	8.12	1.05	2.38	12.95	11.59	0.96	0.47	1.23	2.47	12.68	10.67	0.94	0.46
21	580	20	30	351.22	5.58	1.36	3.47	19.13	7.84	0.95	0.29	1.35	3.36	19.57	7.99	0.98	0.29

22	200	25	30	190.42	8.31	1.32	1.2	6.59	6.43	0.95	0.49	1.48	1.23	6.10	5.05	0.88	0.45
23	390	25	30	279.94	10.19	3.24	2.06	12.92	18.69	0.96	0.59	3.15	2.09	12.63	18.50	0.94	0.59
24	580	25	30	353.25	7.38	5.41	3.8	19.3	24.01	0.96	0.55	5.38	4.18	19.15	24.96	0.95	0.57
25	200	30	30	216.44	7.6	1.36	1.71	6.42	14.91	0.93	0.70	1.50	1.63	6.45	14.86	0.93	0.70
26	390	30	30	311.38	11.06	2.7	2.33	13.36	18.42	0.99	0.58	2.59	2.33	13.12	17.06	0.97	0.57
27	580	30	30	398.68	9.49	5.21	2.92	18.67	32.37	0.93	0.63	5.13	2.98	19.36	33.11	0.96	0.63
28	264	21.6	12	222.82	11.26	2.33	2.84	20.85	11.84	0.91	0.36	2.41	2.88	21.09	12.77	0.92	0.38
29	326	21.6	12	255.38	12.64	3.14	3.49	28.17	17.22	1.00	0.38	3.24	3.46	27.58	17.70	0.98	0.39
30	264	23.4	12	217.98	12.69	3.57	3.14	22.57	18.54	0.99	0.45	3.59	3.16	22.46	19.19	0.98	0.46
31	326	23.4	12	251.83	14.14	3.72	3.11	27.82	22.06	0.99	0.44	3.63	3.05	27.76	22.60	0.98	0.45
32	264	21.6	16	220.49	11.31	2.24	2.24	17.04	12.36	0.99	0.42	2.43	2.07	16.88	12.04	0.99	0.42
33	326	21.6	16	253.46	11.43	3.26	2.84	20.24	17.65	0.96	0.47	3.41	2.74	19.61	16.92	0.93	0.46
34	264	23.4	16	215.22	10.86	2.79	2.26	16.36	12.25	0.96	0.43	2.81	2.11	17.00	13.38	0.99	0.44
35	326	23.4	16	252.87	11.77	3.89	2.57	18.96	20.63	0.90	0.52	3.75	2.56	19.15	21.53	0.91	0.53
36	454	26.6	37	320.23	8.39	3.82	2.69	12.63	17.05	0.99	0.57	3.77	2.62	11.70	17.09	0.92	0.59
37	516	26.6	37	347.17	8.93	4.87	3.27	13.95	19.74	0.96	0.59	5.01	3.14	13.77	20.09	0.95	0.59
38	454	28.4	37	332.66	8.17	3.69	2.42	12.51	17.49	0.98	0.58	3.55	2.46	12.68	18.50	1.00	0.59
39	516	28.4	37	364.73	8.98	4.77	2.82	13.33	20.8	0.92	0.61	4.62	2.97	13.04	21.45	0.90	0.62
40	454	26.6	44	329.9	7.49	3.92	2.21	9.06	14.59	0.85	0.62	3.74	2.19	9.85	13.15	0.92	0.57
41	516	26.6	44	346.12	7.89	4.28	2.52	11.18	18.7	0.92	0.63	4.42	2.70	11.49	19.31	0.94	0.63
42	454	28.4	44	325.24	7.13	3.51	2.24	9.52	14.97	0.89	0.61	3.40	2.27	9.97	15.83	0.93	0.61
43	516	28.4	44	349.88	7.54	4.27	2.59	9.03	15.9	0.74	0.64	4.31	2.45	10.02	14.84	0.82	0.60

Gas: 100%Ar

	WFS (ipm)	Voltage (V)	TS (ipm)	Current (I)	Width (mm)	Cross Section 1						Cross Section 2					
						Depth (mm)	Rein-forcement ht (mm)	Rein-forcement area (mm^2)	Penetrated area (mm^2)	Depo-sition. Eff.	Dilution ratio	Depth (mm)	Rein-forcement ht (mm)	Rein-forcement area (mm^2)	Penetrated area (mm^2)	Depo-sition. Eff.	Dilution ratio
1	200	20	20	184.09	7.16	0.83	2.26	10.15	7.23	0.98	0.42	0.97	2.46	9.50	7.01	0.92	0.42
2	390	20	20	247.97	8.37	0.89	3.27	20.01	7.01	0.99	0.26	1.06	3.31	17.71	8.43	0.87	0.32
3	580	20	20	365.13	9.34	4.02	4.78	26.67	18.95	0.89	0.42	3.87	4.86	25.78	19.81	0.86	0.43
4	200	25	20	193.47	8.31	1.18	1.91	9.63	9.79	0.93	0.50	1.23	2.08	10.01	7.94	0.96	0.44
5	390	25	20	256.36	9.27	2.36	3.05	17.63	11.54	0.87	0.40	2.65	3.06	18.36	11.21	0.91	0.38
6	580	25	20	353.57	11.32	2.85	4.37	26.45	19.53	0.88	0.42	3.17	4.48	28.69	21.14	0.95	0.42
7	200	30	20	238.12	7.02	0.56	2.46	8.88	4.24	0.86	0.32	0.45	2.64	9.02	3.03	0.87	0.25
8	390	30	20	329.67	14.11	3.99	2.97	18.63	23.29	0.92	0.56	4.12	3.01	18.86	24.69	0.93	0.57
9	580	30	20	381.50	15.68	4.17	2.64	28.82	33.13	0.96	0.53	4.14	2.62	27.95	32.92	0.93	0.54
10	200	20	25	176.43	5.61	0.57	2.08	7.11	2.70	0.86	0.28	0.68	2.06	7.88	2.26	0.95	0.22
11	390	20	25	249.56	7.94	1.32	2.79	14.96	6.66	0.92	0.31	1.21	2.97	14.54	5.75	0.90	0.28
12	580	20	25	378.31	7.9	3.89	4.22	22.43	20.18	0.93	0.47	3.76	4.34	23.21	18.60	0.96	0.44
13	200	25	25	200.37	7.39	1.65	1.81	7.82	6.40	0.94	0.45	1.51	1.85	7.19	4.52	0.87	0.39
14	390	25	25	267.48	9.71	2.01	2.41	15.85	9.93	0.98	0.39	1.87	2.45	14.82	8.23	0.91	0.36
15	580	25	25	358.70	9.46	4.41	4.27	23.22	25.35	0.96	0.52	4.33	4.33	20.61	27.04	0.86	0.57
16	200	30	25	209.51	3.76	0.96	2.51	7.60	4.81	0.92	0.39	1.08	2.71	7.72	3.76	0.93	0.33
17	390	30	25	323.60	7.61	3.19	2.76	14.17	13.79	0.87	0.49	3.32	2.90	14.76	12.28	0.91	0.45
18	580	30	25	422.39	13.11	5.51	3.39	20.62	25.25	0.86	0.55	5.46	3.54	23.20	24.95	0.96	0.52
19	200	20	30	183.73	6.11	0.66	1.96	6.67	3.66	0.96	0.35	0.90	2.17	6.62	2.81	0.96	0.30
20	390	20	30	257.05	7.65	1.16	1.94	12.24	4.18	0.91	0.25	1.20	1.93	12.79	5.80	0.95	0.31
21	580	20	30	375.14	8.07	3.91	3.79	19.13	13.38	0.95	0.41	4.13	3.74	19.40	14.72	0.97	0.43

22	200	25	30	205.72	7.26	1.35	2.03	6.01	9.11	0.87	0.60	1.34	2.23	6.41	8.04	0.93	0.56
23	390	25	30	268.11	7.74	1.76	2.29	12.57	11.38	0.93	0.48	2.05	2.43	12.93	9.61	0.96	0.43
24	580	25	30	365.29	8.93	3.96	4.15	18.64	26.29	0.93	0.59	4.13	4.30	18.95	27.20	0.94	0.59
25	200	30	30	265.84	4.57	1.44	1.66	6.57	8.16	0.95	0.55	1.75	1.86	6.42	8.91	0.93	0.58
26	390	30	30	314.63	8.31	3.02	2.82	12.12	15.75	0.90	0.57	2.99	2.93	12.66	15.86	0.94	0.56
27	580	30	30	426.40	13.05	5.93	2.47	19.34	28.15	0.96	0.59	6.01	2.46	18.30	28.05	0.91	0.61
28	264	21.6	12	201.58	7.27	1.21	3.62	22.38	7.04	0.98	0.24	1.11	3.70	21.84	7.18	0.96	0.25
29	326	21.6	12	226.89	8.32	1.51	3.89	27.1	8.09	0.96	0.23	1.55	3.98	26.70	9.37	0.95	0.26
30	264	23.4	12	191.07	8.95	1.59	3.07	22.76	9.31	1.00	0.29	1.50	3.21	22.13	8.97	0.97	0.29
31	326	23.4	12	218.26	9.28	1.73	3.79	27.53	11.02	0.98	0.29	1.60	3.96	27.94	10.34	0.99	0.27
32	264	21.6	16	202.70	9.03	1.35	2.56	16.77	9.07	0.98	0.35	1.52	2.44	16.55	8.48	0.97	0.34
33	326	21.6	16	234.58	9.72	1.83	3.12	20.04	10.11	0.95	0.34	2.08	3.25	20.02	8.69	0.95	0.30
34	264	23.4	16	186.51	9.38	1.31	2.31	16.85	7.08	0.98	0.30	1.46	2.36	17.01	7.00	0.99	0.29
35	326	23.4	16	221.92	11.19	2.14	3.12	20.78	12.32	0.98	0.37	2.13	3.30	20.61	11.87	0.97	0.37

Appendix B: Weld Bead Profile (Macro-Image)

Wire Type: ER70 S-6
Wire Diameter: Manufacturer label (0.9mm; 0.035 in), Measured (0.9mm)

a) 100% Argon Gas

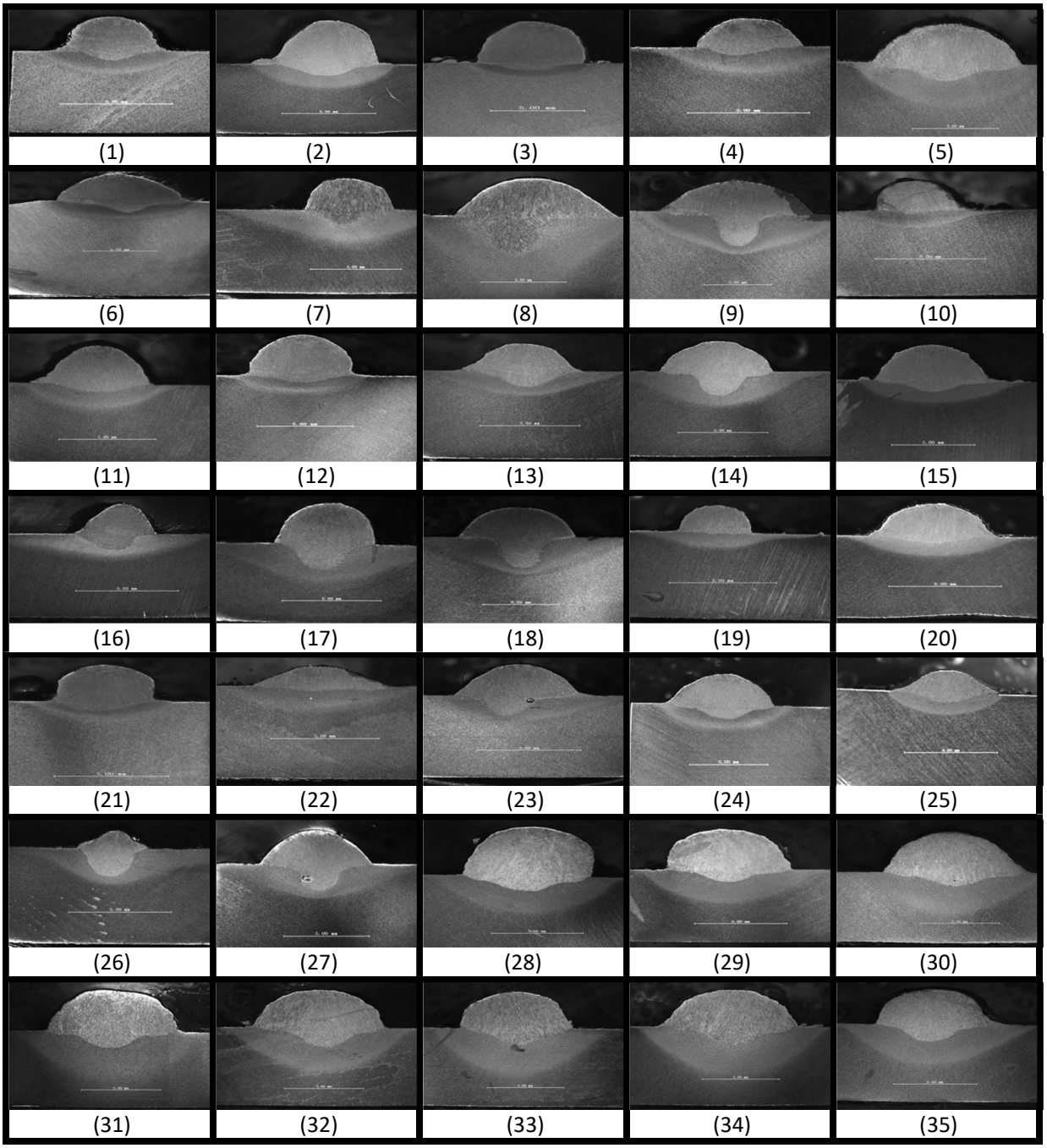

b) 85% Argon-15%CO_2 Gas

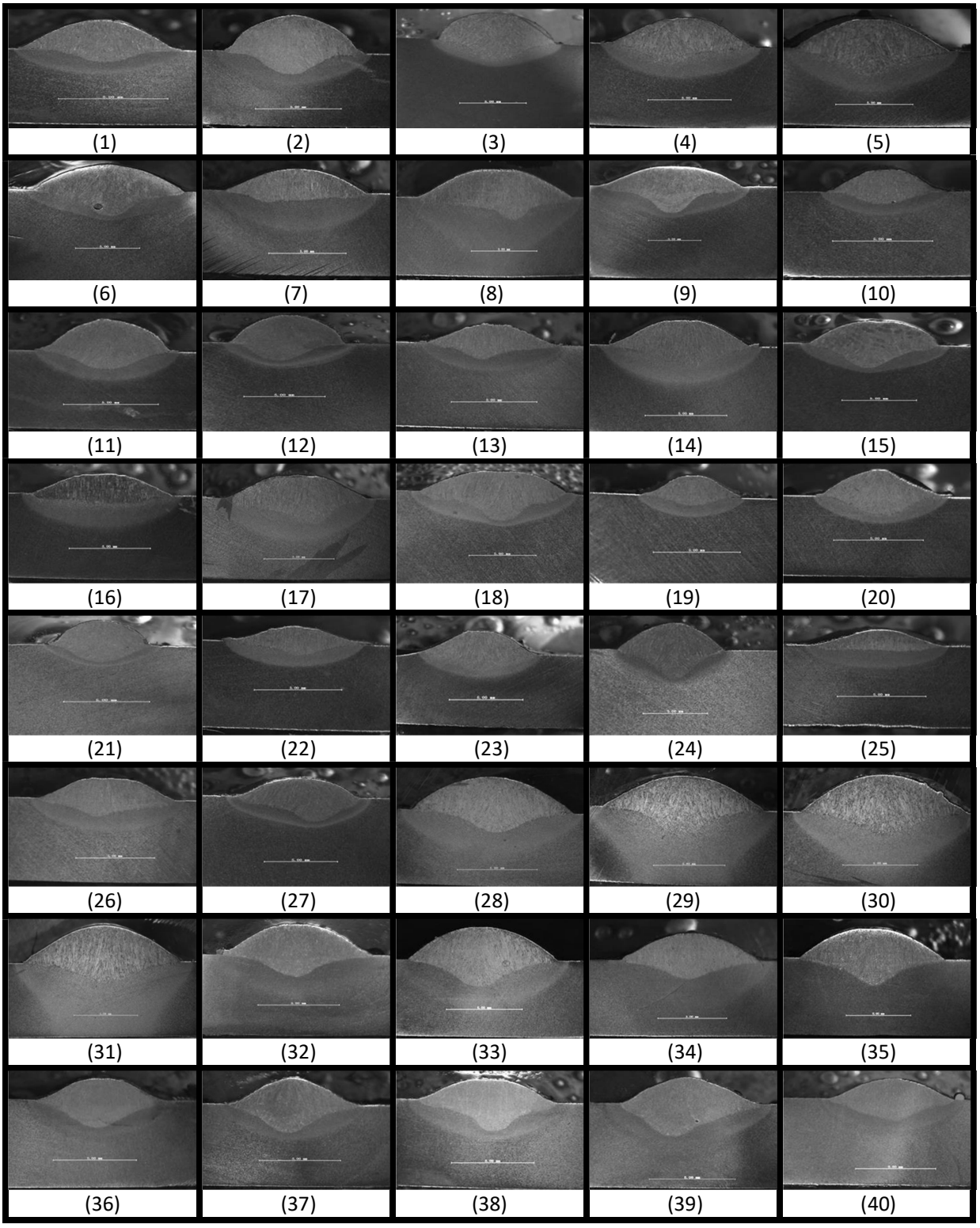

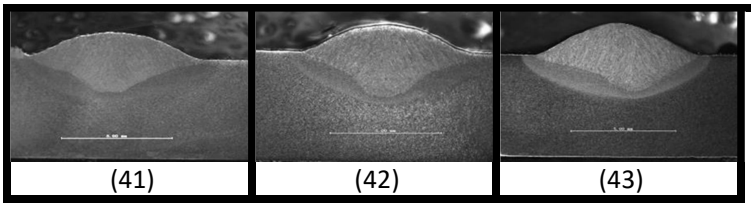

(41) (42) (43)

c) 100% CO_2 Gas

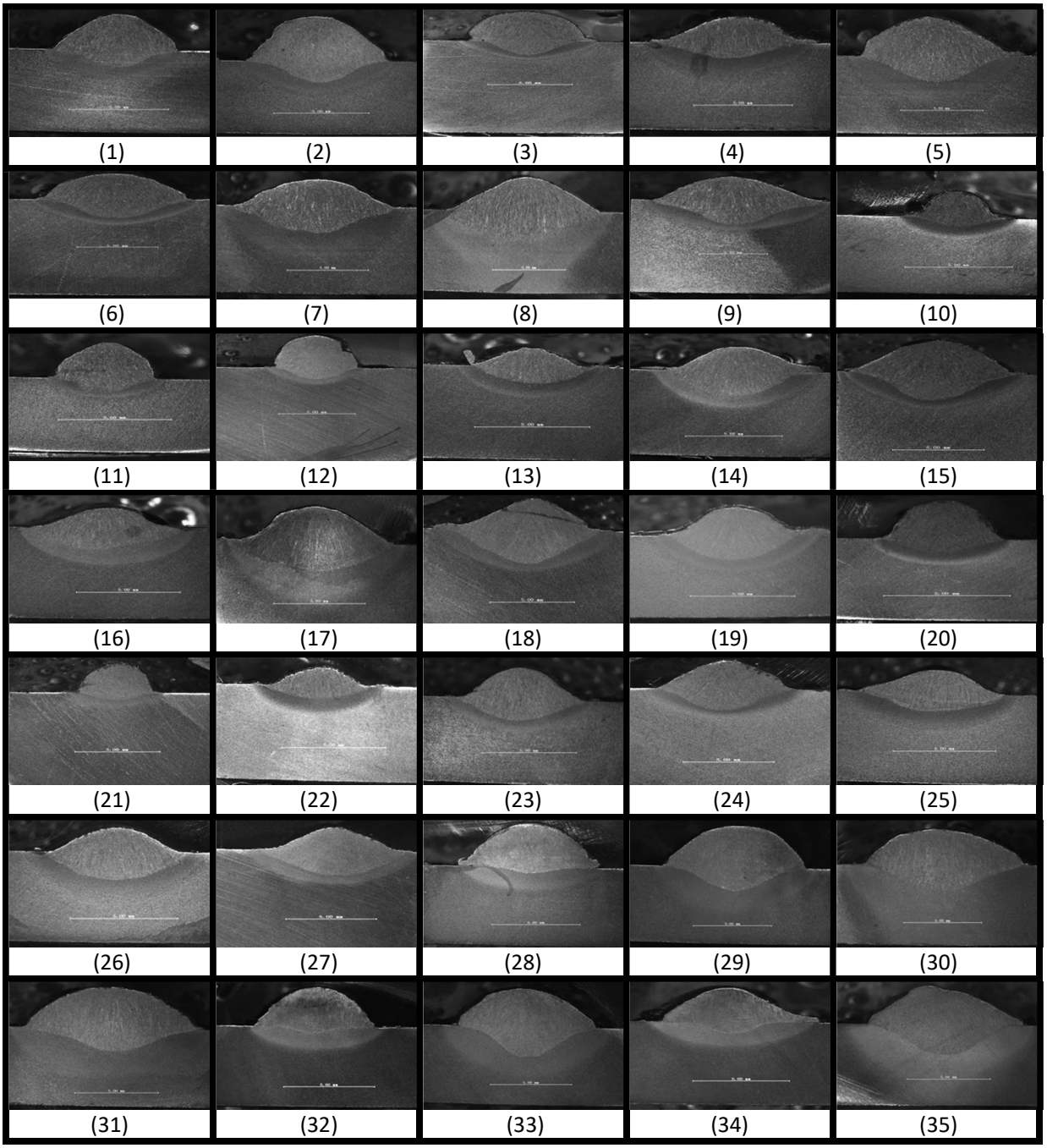

(1) (2) (3) (4) (5)

(6) (7) (8) (9) (10)

(11) (12) (13) (14) (15)

(16) (17) (18) (19) (20)

(21) (22) (23) (24) (25)

(26) (27) (28) (29) (30)

(31) (32) (33) (34) (35)

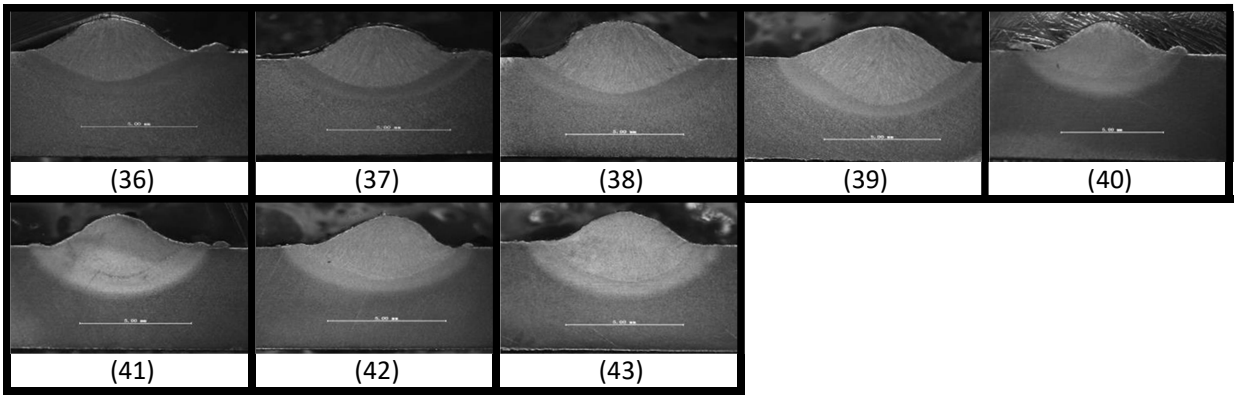

(36) (37) (38) (39) (40)

(41) (42) (43)

Wire Type: ER70 S-6
Wire Diameter: Manufacturer label (0.045 in), Measured (1.15mm)

a) 100% Argon Gas

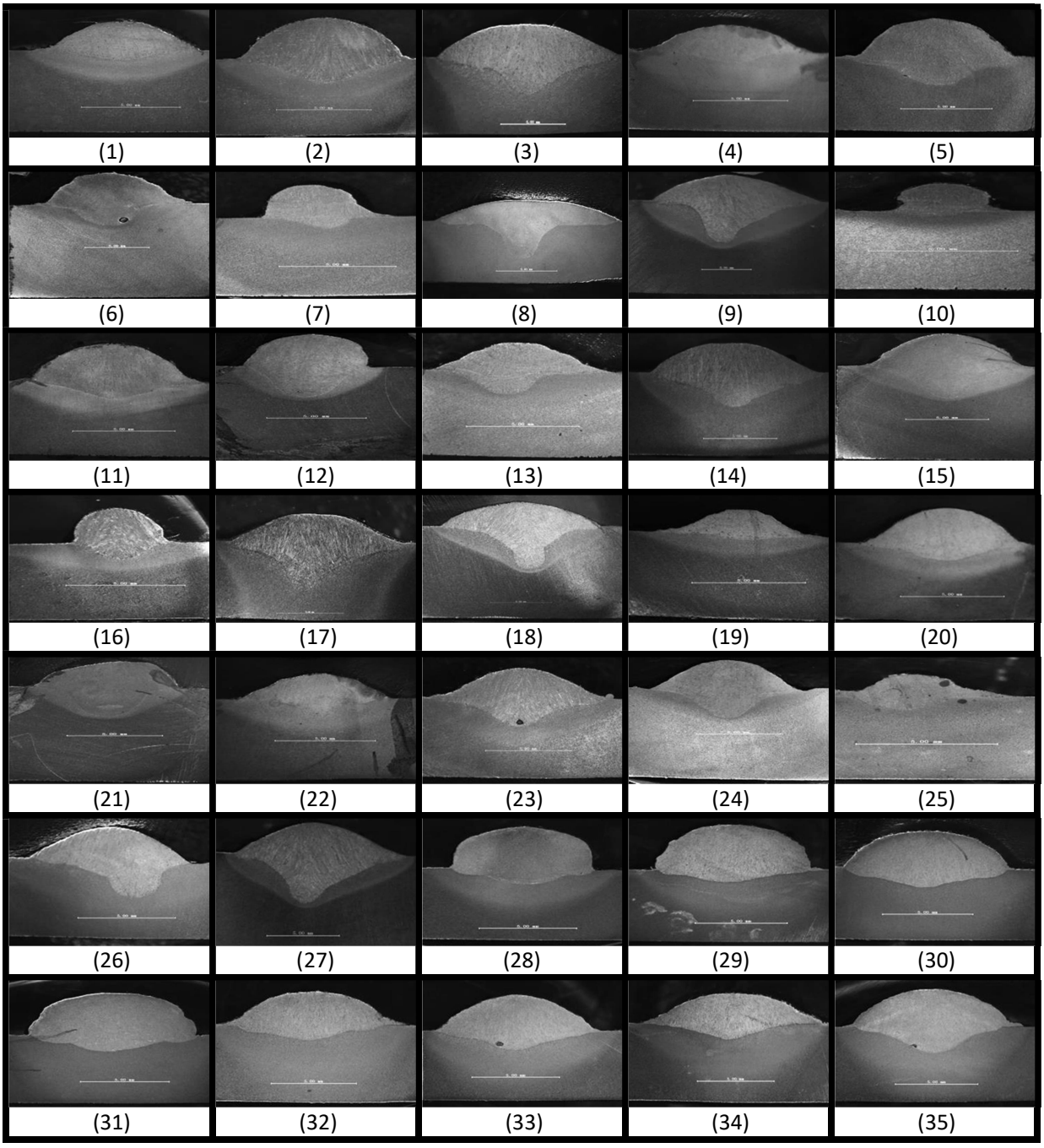

b) 85% Argon-15% CO_2 Gas

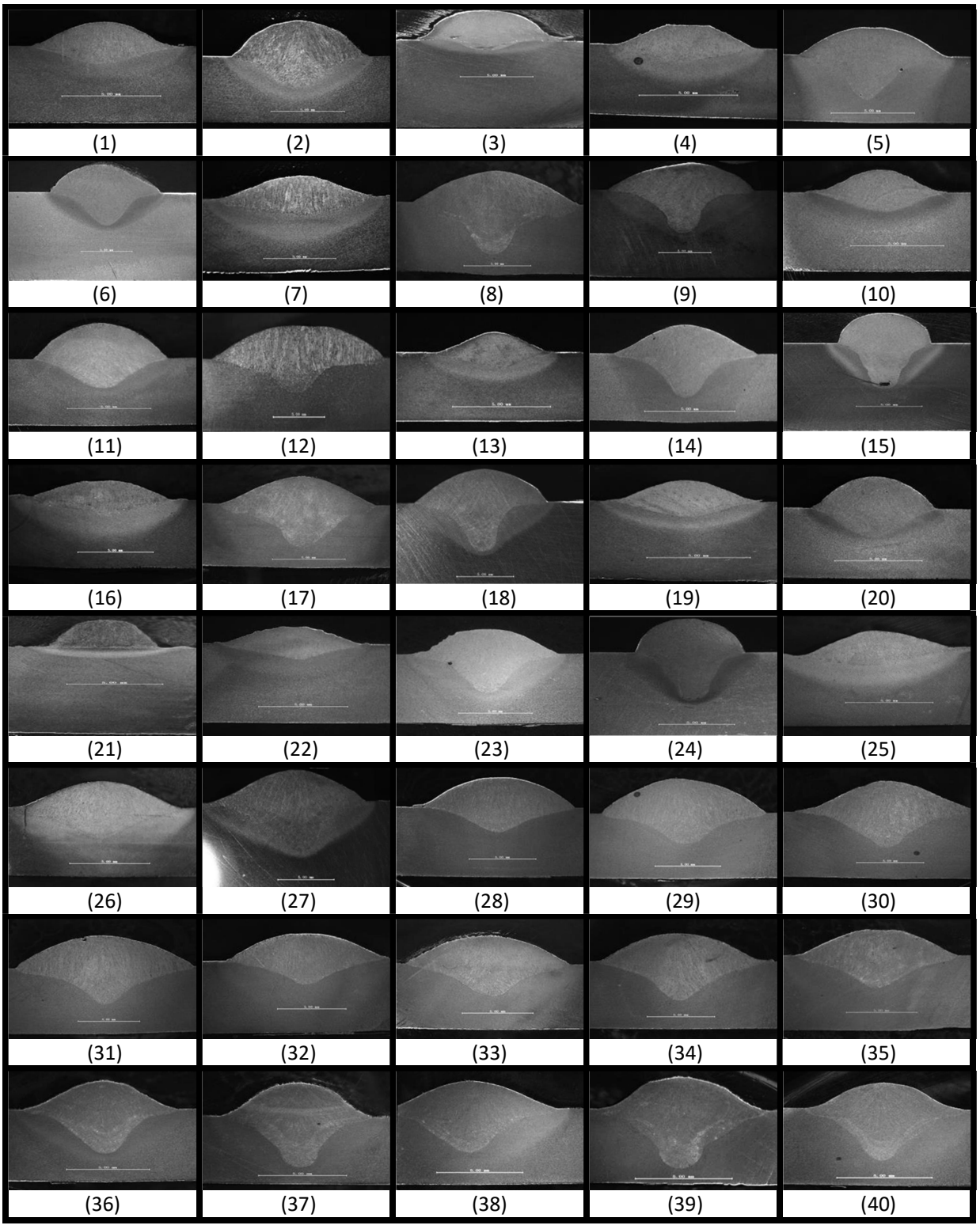

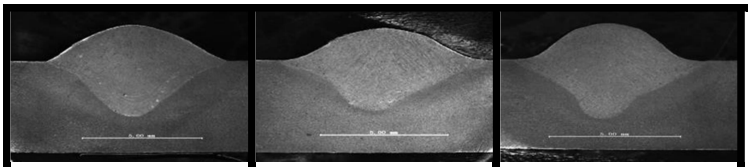

(41) (42) (43)

c) 100% CO_2 Gas

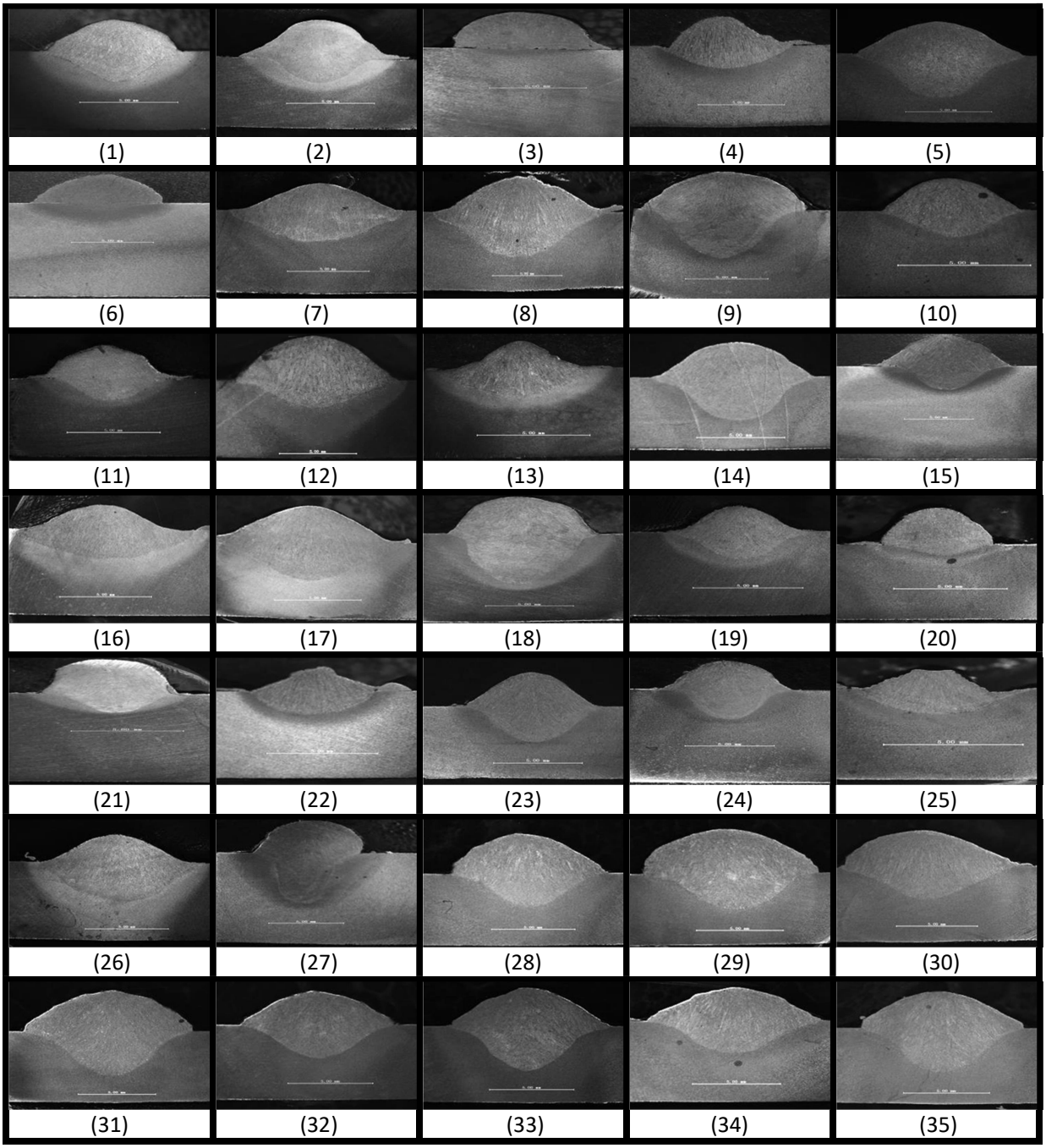

(1) (2) (3) (4) (5)

(6) (7) (8) (9) (10)

(11) (12) (13) (14) (15)

(16) (17) (18) (19) (20)

(21) (22) (23) (24) (25)

(26) (27) (28) (29) (30)

(31) (32) (33) (34) (35)

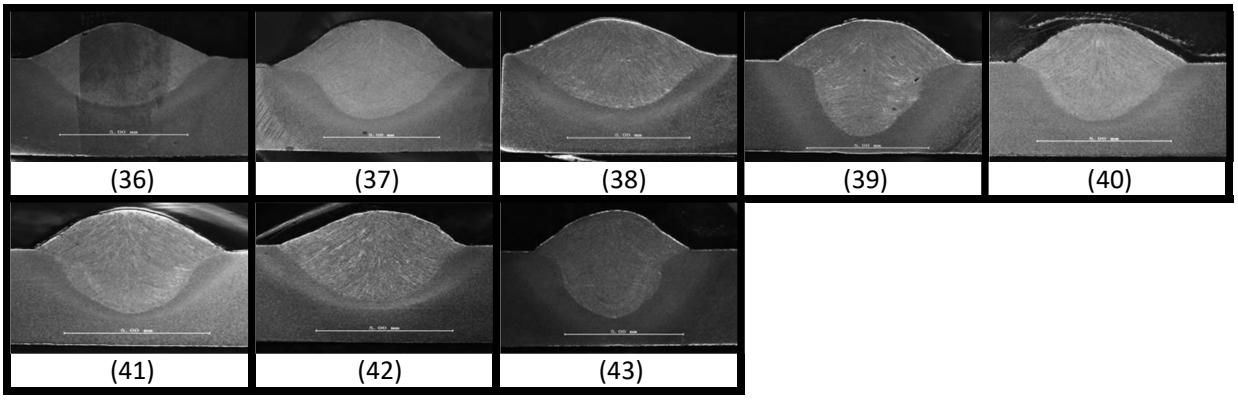

(36) (37) (38) (39) (40)

(41) (42) (43)

Appendix C: Statistical Analysis- ANNOVA & Regression Coefficient Table ER70S-6 wire (0.045 in)

Wire – ER 70 S 6 (0.045 in)

Gas Type: 100% Argon

Regression Analysis: Current

Analysis of Variance

Source	DF	Adj SS	Adj MS	F-Value	P-Value
Regression	5	194560	38912.0	244.73	0.000
WFS	1	459	458.5	2.88	0.100
V	1	2587	2586.7	16.27	0.000
TS	1	815	815.3	5.13	0.031
WFS^2	1	1060	1059.7	6.67	0.015
V^2	1	3342	3342.2	21.02	0.000
Error	29	4611	159.0		
Total	34	199171			

Model Summary

S	R-sq	R-sq(adj)	R-sq(pred)
12.6095	97.68%	97.29%	96.48%

Coefficients

Term	Coef	SE Coef	T-Value	P-Value	VIF
Constant	548	124	4.41	0.000	
WFS	0.183	0.108	1.70	0.100	52.19
V	-39.75	9.85	-4.03	0.000	302.33
TS	0.908	0.401	2.26	0.031	1.24
WFS^2	0.000352	0.000137	2.58	0.015	53.19
V^2	0.901	0.197	4.58	0.000	304.65

Regression Equation

Current = 548 + 0.183*WFS - 39.75*V + 0.908*TS + 0.000352*WFS^2 + 0.901*V^2

Regression Analysis: Bead Width

Analysis of Variance

Source	DF	Adj SS	Adj MS	F-Value	P-Value
Regression	5	164.645	32.9291	22.22	0.000
WFS	1	19.213	19.2129	12.97	0.001
V	1	0.863	0.8632	0.58	0.451
TS	1	5.003	5.0034	3.38	0.076
WFS*V	1	35.107	35.1074	23.69	0.000
V*TS	1	8.622	8.6220	5.82	0.022
Error	29	42.973	1.4818		
Total	34	207.619			

Model Summary

S	R-sq	R-sq(adj)	R-sq(pred)
1.21731	79.30%	75.73%	69.74%

Coefficients

Term	Coef	SE Coef	T-Value	P-Value	VIF
Constant	3.16	7.73	0.41	0.685	
WFS	-0.03332	0.00925	-3.60	0.001	41.21
V	0.251	0.329	0.76	0.451	36.11
TS	0.534	0.290	1.84	0.076	69.92
WFS*V	0.001785	0.000367	4.87	0.000	49.86
V*TS	-0.0295	0.0122	-2.41	0.022	119.24

Regression Equation

Bead Width = 3.16 - 0.03332*WFS + 0.251*V + 0.534*TS + 0.001785*WFS*V - 0.0295*V*TS

Regression Analysis: Bead Depth

Analysis of Variance

Source	DF	Adj SS	Adj MS	F-Value	P-Value
Regression	6	125.577	20.9296	74.14	0.000
WFS	1	2.017	2.0169	7.14	0.010
V	1	0.019	0.0189	0.07	0.797
TS	1	1.432	1.4321	5.07	0.028
WFS^2	1	2.079	2.0785	7.36	0.009
WFS*V	1	1.785	1.7850	6.32	0.014
WFS*TS	1	1.572	1.5722	5.57	0.021
Error	63	17.786	0.2823		
Total	69	143.363			

Model Summary

S	R-sq	R-sq(adj)	R-sq(pred)
0.531329	87.59%	86.41%	83.98%

Coefficients

Term	Coef	SE Coef	T-Value	P-Value	VIF
Constant	2.40	1.51	1.59	0.117	
WFS	-0.01320	0.00494	-2.67	0.010	123.20
V	0.0122	0.0470	0.26	0.797	7.76
TS	-0.0802	0.0356	-2.25	0.028	11.03
WFS^2	0.000011	0.000004	2.71	0.009	53.14
WFS*V	0.000285	0.000113	2.51	0.014	49.85
WFS*TS	0.000236	0.000100	2.36	0.021	48.61

Regression Equation

Bead Depth = 2.40 - 0.01320*WFS + 0.0122*V - 0.0802*TS + 0.000011*WFS^2 + 0.000285*WFS*V + 0.000236*WFS*TS

Regression Analysis: Reinforcement Height

Analysis of Variance

Source	DF	Adj SS	Adj MS	F-Value	P-Value
Regression	6	37.5116	6.25193	40.83	0.000
WFS	1	1.6890	1.68903	11.03	0.001
V	1	0.0656	0.06562	0.43	0.515
TS	1	1.9364	1.93639	12.65	0.001
WFS^2	1	0.5715	0.57149	3.73	0.058
WFS*V	1	3.9405	3.94048	25.73	0.000
V*TS	1	0.9878	0.98779	6.45	0.014
Error	63	9.6472	0.15313		
Total	69	47.1587			

Model Summary

S	R-sq	R-sq(adj)	R-sq(pred)
0.391318	79.54%	77.59%	73.57%

Coefficients

Term	Coef	SE Coef	T-Value	P-Value	VIF
Constant	4.61	1.86	2.48	0.016	
WFS	0.01051	0.00316	3.32	0.001	93.23
V	-0.0491	0.0750	-0.65	0.515	36.41
TS	-0.2364	0.0665	-3.56	0.001	70.95
WFS^2	0.000006	0.000003	1.93	0.058	53.46
WFS*V	-0.000423	0.000083	-5.07	0.000	49.87
V*TS	0.00709	0.00279	2.54	0.014	120.18

Regression Equation

Reinforcement Height = 4.61 + 0.01051*WFS - 0.0491*V - 0.2364*TS + 0.000006*WFS^2 - 0.000423*WFS*V + 0.00709*V*TS

Regression Analysis: Reinforcement Area

Analysis of Variance

Source	DF	Adj SS	Adj MS	F-Value	P-Value
Regression	5	3104.35	620.870	1136.15	0.000
WFS	1	229.33	229.334	419.67	0.000
V	1	0.01	0.010	0.02	0.891
TS	1	215.46	215.461	394.28	0.000
TS^2	1	144.27	144.266	264.00	0.000
WFS*TS	1	54.25	54.253	99.28	0.000
Error	64	34.97	0.546		
Total	69	3139.32			

Model Summary

S	R-sq	R-sq(adj)	R-sq(pred)
0.739234	98.89%	98.80%	98.65%

Coefficients

Term	Coef	SE Coef	T-Value	P-Value	VIF
Constant	28.94	1.46	19.80	0.000	
WFS	0.07676	0.00375	20.49	0.000	36.65
V	-0.0033	0.0243	-0.14	0.891	1.07
TS	-2.366	0.119	-19.86	0.000	63.85
TS^2	0.04704	0.00289	16.25	0.000	72.31
WFS*TS	-0.001485	0.000149	-9.96	0.000	55.68

Regression Equation

Reinforcement Area = 28.94 + 0.07676*WFS - 0.0033*V - 2.366*TS + 0.04704*TS^2 - 0.001485*WFS*TS

Regression Analysis: Penetration Area

Analysis of Variance

Source	DF	Adj SS	Adj MS	F-Value	P-Value
Regression	6	3050.30	508.383	359.77	0.000
WFS	1	25.10	25.103	17.76	0.000
V	1	0.05	0.055	0.04	0.845
TS	1	209.43	209.428	148.21	0.000
WFS^2	1	0.12	0.122	0.09	0.770
TS^2	1	95.56	95.560	67.63	0.000
WFS*V	1	0.08	0.081	0.06	0.812
Error	63	89.02	1.413		
Total	69	3139.32			

Model Summary

S	R-sq	R-sq(adj)	R-sq(pred)
1.18873	97.16%	96.89%	96.38%

Coefficients

Term	Coef	SE Coef	T-Value	P-Value	VIF
Constant	36.32	3.46	10.50	0.000	
WFS	0.04058	0.00963	4.21	0.000	93.55
V	-0.021	0.106	-0.20	0.845	7.82
TS	-2.389	0.196	-12.17	0.000	66.95
WFS^2	-0.000003	0.000009	-0.29	0.770	54.56
TS^2	0.03629	0.00441	8.22	0.000	64.97
WFS*V	0.000061	0.000253	0.24	0.812	49.97

Regression Equation

Penetration Area = 36.32 + 0.04058*WFS - 0.021 V - 2.389*TS - 0.000003*WFS^2 + 0.03629*TS^2 + 0.000061*WFS*V

Wire – ER 70 S 6 (0.045 in)

Gas Type: 85% Argon -15% Carbon di-Oxide

Regression Analysis: Current

Analysis of Variance

Source	DF	Adj SS	Adj MS	F-Value	P-Value
Regression	7	181105	25872.1	520.42	0.000
WFS	1	1591	1591.3	32.01	0.000
V	1	1332	1332.4	26.80	0.000
TS	1	219	219.4	4.41	0.043
WFS^2	1	184	184.2	3.71	0.062
V^2	1	1588	1588.1	31.94	0.000
TS^2	1	230	230.3	4.63	0.038
WFS*V	1	201	201.1	4.04	0.052
Error	35	1740	49.7		
Total	42	182845			

Model Summary

S	R-sq	R-sq(adj)	R-sq(pred)
7.05082	99.05%	98.86%	98.54%

Coefficients

Term	Coef	SE Coef	T-Value	P-Value	VIF
Constant	429.9	72.5	5.93	0.000	
WFS	0.4486	0.0793	5.66	0.000	102.37
V	-28.16	5.44	-5.18	0.000	335.02
TS	-1.599	0.761	-2.10	0.043	40.12
WFS^2	-0.000144	0.000075	-1.92	0.062	56.49
V^2	0.606	0.107	5.65	0.000	326.98
TS^2	0.0290	0.0135	2.15	0.038	40.36
WFS*V	0.00423	0.00211	2.01	0.052	60.39

Regression Equation

Current = 429.9 + 0.4486*WFS - 28.16*V - 1.599*TS - 0.000144*WFS^2 + 0.606*V^2
+ 0.0290*TS^2 + 0.00423*WFS*V

Regression Analysis: Bead Width

Analysis of Variance

Source	DF	Adj SS	Adj MS	F-Value	P-Value
Regression	8	198.810	24.8512	69.51	0.000
WFS	1	14.772	14.7720	41.32	0.000
V	1	9.517	9.5171	26.62	0.000
TS	1	5.395	5.3949	15.09	0.000
WFS^2	1	32.589	32.5891	91.16	0.000
V^2	1	9.339	9.3391	26.12	0.000
TS^2	1	3.326	3.3262	9.30	0.004
WFS*V	1	4.565	4.5645	12.77	0.001
WFS*TS	1	4.381	4.3813	12.26	0.001
Error	34	12.155	0.3575		
Total	42	210.965			

Model Summary

S	R-sq	R-sq(adj)	R-sq(pred)
0.597917	94.24%	92.88%	90.80%

Coefficients

Term	Coef	SE Coef	T-Value	P-Value	VIF
Constant	-26.35	6.26	-4.21	0.000	
WFS	0.04829	0.00751	6.43	0.000	127.82
V	2.385	0.462	5.16	0.000	336.42
TS	-0.2546	0.0655	-3.88	0.000	41.32
WFS^2	-0.000061	0.000006	-9.55	0.000	56.55
V^2	-0.04664	0.00912	-5.11	0.000	328.95
TS^2	0.00452	0.00148	3.05	0.004	67.81
WFS*V	0.000640	0.000179	3.57	0.001	60.75
WFS*TS	-0.000540	0.000154	-3.50	0.001	102.01

Regression Equation

Bead Width = -26.35 + 0.04829*WFS + 2.385*V- 0.2546*TS - 0.000061*WFS^2 - 0.04664*V^2
+ 0.00452*TS^2 + 0.000640*WFS*V - 0.000540*WFS*TS

Regression Analysis: Bead Depth

Analysis of Variance

Source	DF	Adj SS	Adj MS	F-Value	P-Value
Regression	7	123.978	17.7112	79.85	0.000
WFS	1	1.728	1.7284	7.79	0.007
V	1	5.214	5.2137	23.51	0.000
TS	1	3.085	3.0846	13.91	0.000
WFS^2	1	2.249	2.2489	10.14	0.002
V^2	1	7.089	7.0894	31.96	0.000
WFS*V	1	17.448	17.4479	78.66	0.000
WFS*TS	1	1.383	1.3830	6.24	0.015
Error	78	17.301	0.2218		
Total	85	141.280			

Model Summary

S	R-sq	R-sq(adj)	R-sq(pred)
0.470968	87.75%	86.65%	85.35%

Coefficients

Term	Coef	SE Coef	T-Value	P-Value	VIF
Constant	-11.01	3.42	-3.22	0.002	
WFS	-0.01145	0.00410	-2.79	0.007	122.91
V	1.228	0.253	4.85	0.000	325.71
TS	-0.1047	0.0281	-3.73	0.000	24.44
WFS^2	-0.000011	0.000003	-3.18	0.002	52.45
V^2	-0.02819	0.00499	-5.65	0.000	316.68
WFS*V	0.000882	0.000099	8.87	0.000	60.40
WFS*TS	0.000165	0.000066	2.50	0.015	60.71

Regression Equation

Bead Depth = -11.01 - 0.01145*WFS + 1.228*V - 0.1047*TS - 0.000011*WFS^2 - 0.02819*V^2 + 0.000882*WFS*V + 0.000165*WFS*TS

Regression Analysis: Reinforcement Height

Analysis of Variance

Source	DF	Adj SS	Adj MS	F-Value	P-Value
Regression	5	53.5919	10.7184	122.84	0.000
WFS	1	4.8477	4.8477	55.56	0.000
V	1	0.0772	0.0772	0.88	0.350
TS	1	0.8296	0.8296	9.51	0.003
WFS*V	1	1.2336	1.2336	14.14	0.000
V*TS	1	0.3447	0.3447	3.95	0.050
Error	80	6.9804	0.0873		
Total	85	60.5723			

Model Summary

S	R-sq	R-sq(adj)	R-sq(pred)
0.295390	88.48%	87.76%	86.70%

Coefficients

Term	Coef	SE Coef	T-Value	P-Value	VIF
Constant	2.53	1.02	2.46	0.016	
WFS	0.01177	0.00158	7.45	0.000	46.24
V	-0.0386	0.0410	-0.94	0.350	21.69
TS	-0.1168	0.0379	-3.08	0.003	113.11
WFS*V	-0.000235	0.000062	-3.76	0.000	60.43
V*TS	0.00292	0.00147	1.99	0.050	163.24

Regression Equation

Reinforcement Height = 2.53 + 0.01177*WFS - 0.0386*V - 0.1168*TS - 0.000235*WFS*V + 0.00292*V*TS

Regression Analysis: Reinforcement Area

Analysis of Variance

Source	DF	Adj SS	Adj MS	F-Value	P-Value
Regression	6	3710.47	618.412	656.88	0.000
WFS	1	142.11	142.110	150.95	0.000
V	1	0.15	0.153	0.16	0.688
TS	1	312.00	311.999	331.41	0.000
WFS^2	1	2.59	2.591	2.75	0.101
TS^2	1	165.88	165.877	176.19	0.000
WFS*TS	1	65.49	65.488	69.56	0.000
Error	79	74.37	0.941		
Total	85	3784.84			

Model Summary

S	R-sq	R-sq(adj)	R-sq(pred)
0.970279	98.03%	97.89%	97.66%

Coefficients

Term	Coef	SE Coef	T-Value	P-Value	VIF
Constant	15.76	1.90	8.29	0.000	
WFS	0.08757	0.00713	12.29	0.000	87.37
V	0.0126	0.0313	0.40	0.688	1.17
TS	-1.2825	0.0704	-18.20	0.000	36.27
WFS^2	-0.000012	0.000007	-1.66	0.101	56.31
TS^2	0.02207	0.00166	13.27	0.000	64.91
WFS*TS	-0.001467	0.000176	-8.34	0.000	100.81

Regression Equation

Reinforcement Area = 15.76 + 0.08757*WFS + 0.0126*V - 1.2825*TS - 0.000012*WFS^2 + 0.02207*TS^2 - 0.001467 WFS*TS

Regression Analysis: Penetration Area

Analysis of Variance

Source	DF	Adj SS	Adj MS	F-Value	P-Value
Regression	7	2854.62	407.803	40.03	0.000
WFS	1	11.72	11.717	1.15	0.287
V	1	95.90	95.905	9.41	0.003
TS	1	3.37	3.368	0.33	0.567
WFS^2	1	31.05	31.054	3.05	0.085
V^2	1	112.00	111.998	10.99	0.001
TS^2	1	52.67	52.674	5.17	0.026
WFS*V	1	291.19	291.186	28.59	0.000
Error	78	794.55	10.187		
Total	85	3649.17			

Model Summary

S	R-sq	R-sq(adj)	R-sq(pred)
3.19163	78.23%	76.27%	73.58%

Coefficients

Term	Coef	SE Coef	T-Value	P-Value	VIF
Constant	-57.4	23.2	-2.47	0.016	
WFS	-0.0272	0.0254	-1.07	0.287	102.37
V	5.34	1.74	3.07	0.003	335.02
TS	0.140	0.244	0.57	0.567	40.12
WFS^2	-0.000042	0.000024	-1.75	0.085	56.49
V^2	-0.1139	0.0343	-3.32	0.001	326.98
TS^2	-0.00981	0.00431	-2.27	0.026	40.36
WFS*V	0.003603	0.000674	5.35	0.000	60.39

Regression Equation

Penetration Area = -57.4 - 0.0272*WFS + 5.34*V + 0.140*TS - 0.000042*WFS^2 - 0.1139*V^2 - 0.00981*TS^2 + 0.003603*WFS*V

Wire – ER 70 S 6 (0.045 in)

Gas Type: 100% Carbon di-Oxide

Regression Analysis: Current

Analysis of Variance

Source	DF	Adj SS	Adj MS	F-Value	P-Value
Regression	3	167838	55946	205.91	0.000
WFS	1	135661	135661	499.31	0.000
Voltage	1	2228	2228	8.20	0.007
TS	1	7	7	0.03	0.872
Error	39	10596	272		
Total	42	178434			

Model Summary

S	R-sq	R-sq(adj)	R-sq(pred)
16.4833	94.06%	93.60%	92.71%

Coefficients

Term	Coef	SE Coef	T-Value	P-Value	VIF
Constant	40.0	18.0	2.22	0.032	
WFS	0.4432	0.0198	22.35	0.000	1.17
Voltage	2.153	0.752	2.86	0.007	1.17
TS	-0.052	0.324	-0.16	0.872	1.33

Regression Equation

Current Avg = 40.0 + 0.4432 WFS + 2.153 Voltage - 0.052 TS

Regression Analysis: Bead Width

Analysis of Variance

Source	DF	Adj SS	Adj MS	F-Value	P-Value
Regression	5	125.197	25.039	49.41	0.000
WFS	1	16.176	16.176	31.92	0.000
V	1	6.593	6.593	13.01	0.001
TS	1	101.119	101.119	199.52	0.000
WFS^2	1	12.524	12.524	24.71	0.000
V^2	1	4.730	4.730	9.33	0.004
Error	37	18.752	0.507		
Total	42	143.950			

Model Summary

S	R-sq	R-sq(adj)	R-sq(pred)
0.711913	86.97%	85.21%	82.13%

Coefficients

Term	Coef	SE Coef	T-Value	P-Value	VIF
Constant	-19.65	6.23	-3.16	0.003	
WFS	0.03187	0.00564	5.65	0.000	50.84
V	1.857	0.515	3.61	0.001	294.34
TS	-0.1982	0.0140	-14.13	0.000	1.34
WFS^2	-0.000035	0.000007	-4.97	0.000	50.44
V^2	-0.0314	0.0103	-3.05	0.004	293.57

Regression Equation

Width = -19.65 + 0.03187*WFS + 1.857*V - 0.1982*TS - 0.000035*WFS^2 - 0.0314*V^2

Regression Analysis: Depth

Analysis of Variance

Source	DF	Adj SS	Adj MS	F-Value	P-Value
Regression	6	101.806	16.9676	58.60	0.000
WFS	1	9.820	9.8204	33.92	0.000
V	1	4.344	4.3441	15.00	0.000
TS	1	6.748	6.7485	23.31	0.000
WFS^2	1	1.479	1.4786	5.11	0.027
TS^2	1	4.480	4.4802	15.47	0.000
WFS*V	1	19.305	19.3049	66.67	0.000
Error	79	22.875	0.2896		
Total	85	124.681			

Model Summary

S	R-sq	R-sq(adj)	R-sq(pred)
0.538105	81.65%	80.26%	78.70%

Coefficients

Term	Coef	SE Coef	T-Value	P-Value	VIF
Constant	9.77	1.38	7.10	0.000	
WFS	-0.02489	0.00427	-5.82	0.000	102.17
V	-0.1841	0.0475	-3.87	0.000	8.78
TS	-0.1891	0.0392	-4.83	0.000	36.47
WFS^2	0.000009	0.000004	2.26	0.027	56.27
TS^2	0.002714	0.000690	3.93	0.000	36.34
WFS*V	0.000928	0.000114	8.17	0.000	60.39

Regression Equation

Depth = 9.77 - 0.02489*WFS - 0.1841*V - 0.1891*TS + 0.000009*WFS^2 + 0.002714*TS^2 + 0.000928*WFS*V

Regression Analysis: Reinforcement Height

Analysis of Variance

Source	DF	Adj SS	Adj MS	F-Value	P-Value
Regression	7	58.3778	8.33968	54.01	0.000
WFS	1	1.3845	1.38445	8.97	0.004
V	1	0.0234	0.02335	0.15	0.698
TS	1	5.3988	5.39885	34.97	0.000
WFS^2	1	2.5167	2.51674	16.30	0.000
V^2	1	0.7367	0.73671	4.77	0.032
WFS*V	1	1.2493	1.24925	8.09	0.006
V*TS	1	3.5571	3.55706	23.04	0.000
Error	78	12.0430	0.15440		
Total	85	70.4208			

Model Summary

S	R-sq	R-sq(adj)	R-sq(pred)
0.392934	82.90%	81.36%	79.05%

Coefficients

Term	Coef	SE Coef	T-Value	P-Value	VIF
Constant	7.36	3.10	2.38	0.020	
WFS	-0.00931	0.00311	-2.99	0.004	101.40
V	0.086	0.220	0.39	0.698	353.57
TS	-0.3151	0.0533	-5.91	0.000	126.50
WFS^2	0.000012	0.000003	4.04	0.000	54.59
V^2	-0.00888	0.00407	-2.18	0.032	302.42
WFS*V	0.000236	0.000083	2.84	0.006	60.49
V*TS	0.00995	0.00207	4.80	0.000	183.78

Regression Equation

Reinforcement Height = 7.36 - 0.00931*WFS + 0.086*V - 0.3151*TS + 0.000012*WFS^2 - 0.00888*V^2
+ 0.000236*WFS*V + 0.00995*V*TS

Regression Analysis: Reinforcement Area

Analysis of Variance

Source	DF	Adj SS	Adj MS	F-Value	P-Value
Regression	5	3790.18	758.035	1000.28	0.000
WFS	1	312.36	312.360	412.18	0.000
V	1	0.19	0.192	0.25	0.616
TS	1	313.27	313.270	413.38	0.000
TS^2	1	169.62	169.624	223.83	0.000
WFS*TS	1	72.46	72.461	95.62	0.000
Error	80	60.63	0.758		
Total	85	3850.80			

Model Summary

S	R-sq	R-sq(adj)	R-sq(pred)
0.870530	98.43%	98.33%	98.16%

Coefficients

Term	Coef	SE Coef	T-Value	P-Value	VIF
Constant	15.61	1.29	12.09	0.000	
WFS	0.08151	0.00401	20.30	0.000	34.44
V	0.0141	0.0281	0.50	0.616	1.17
TS	-1.2080	0.0594	-20.33	0.000	32.05
TS^2	0.02137	0.00143	14.96	0.000	59.48
WFS*TS	-0.001543	0.000158	-9.78	0.000	100.74

Regression Equation

Reinforcement Area = 15.61 + 0.08151*WFS + 0.0141*V - 1.2080*TS + 0.02137*TS^2 - 0.001543*WFS*TS

Regression Analysis: Penetration Area

Analysis of Variance

Source	DF	Adj SS	Adj MS	F-Value	P-Value
Regression	5	4456.65	891.331	47.65	0.000
WFS	1	478.87	478.873	25.60	0.000
V	1	2.48	2.477	0.13	0.717
TS	1	373.25	373.247	19.95	0.000
WFS*V	1	464.26	464.258	24.82	0.000
WFS*TS	1	149.63	149.632	8.00	0.006
Error	80	1496.51	18.706		
Total	85	5953.17			

Model Summary

S	R-sq	R-sq(adj)	R-sq(pred)
4.32509	74.86%	73.29%	69.63%

Coefficients

Term	Coef	SE Coef	T-Value	P-Value	VIF
Constant	35.5	10.1	3.52	0.001	
WFS	-0.1256	0.0248	-5.06	0.000	53.34
V	-0.139	0.382	-0.36	0.717	8.77
TS	-1.092	0.244	-4.47	0.000	21.97
WFS*V	0.004547	0.000913	4.98	0.000	60.33
WFS*TS	0.001616	0.000571	2.83	0.006	53.51

Regression Equation

Penetration Area = 35.5 - 0.1256*WFS - 0.139*V - 1.092*TS + 0.004547*WFS*V + 0.001616*WFS*TS

Wire – ER 70 S 6 (0.035 in)

Gas Type: 100% Argon

Regression Analysis: Current

Analysis of Variance

Source	DF	Adj SS	Adj MS	F-Value	P-Value
Regression	7	60747.1	8678.16	136.66	0.000
WFS	1	255.5	255.53	4.02	0.055
V	1	1764.2	1764.17	27.78	0.000
TS	1	273.3	273.31	4.30	0.048
W^2	1	761.3	761.30	11.99	0.002
V^2	1	2110.3	2110.30	33.23	0.000
W*V	1	781.2	781.20	12.30	0.002
W*TS	1	245.5	245.54	3.87	0.060
Error	27	1714.5	63.50		
Total	34	62461.6			

Model Summary

S	R-sq	R-sq(adj)	R-sq(pred)
7.96867	97.26%	96.54%	95.28%

Coefficients

Term	Coef	SE Coef	T-Value	P-Value	VIF
Constant	438.3	85.5	5.12	0.000	
WFS	0.232	0.116	2.01	0.055	128.05
V	-33.30	6.32	-5.27	0.000	311.17
TS	-1.457	0.702	-2.07	0.048	13.33
W^2	-0.000350	0.000101	-3.46	0.002	72.78
V^2	0.714	0.124	5.76	0.000	302.80
W*V	0.00912	0.00260	3.51	0.002	52.84
W*TS	0.00337	0.00172	1.97	0.060	31.81

Regression Equation

Current = 438.3 + 0.232*WFS - 33.30*V - 1.457*TS - 0.000350*W^2 + 0.714*V^2
+ 0.00912*W*V + 0.00337*W*TS

Regression Analysis: Bead Width

Analysis of Variance

Source	DF	Adj SS	Adj MS	F-Value	P-Value
Regression	7	109.136	15.5909	24.58	0.000
WFS	1	6.991	6.9906	11.02	0.003
V	1	2.766	2.7662	4.36	0.046
TS	1	1.399	1.3994	2.21	0.149
V^2	1	3.211	3.2106	5.06	0.033
TS^2	1	3.573	3.5735	5.63	0.025
W*V	1	13.508	13.5080	21.30	0.000
V*TS	1	1.952	1.9524	3.08	0.091
Error	27	17.123	0.6342		
Total	34	126.260			

Model Summary

S	R-sq	R-sq(adj)	R-sq(pred)
0.796360	86.44%	82.92%	78.81%

Coefficients

Term	Coef	SE Coef	T-Value	P-Value	VIF
Constant	-5.69	8.99	-0.63	0.532	
WFS	-0.02185	0.00658	-3.32	0.003	41.36
V	1.359	0.651	2.09	0.046	330.73
TS	-0.274	0.185	-1.49	0.149	92.17
V^2	-0.0282	0.0125	-2.25	0.033	310.25
TS^2	0.00890	0.00375	2.37	0.025	66.86
W*V	0.001203	0.000261	4.62	0.000	53.12
V*TS	-0.01092	0.00622	-1.75	0.091	87.41

Regression Equation

Bead Width = -5.69 - 0.02185*WFS + 1.359*Voltage - 0.274*TS - 0.0282*V^2 + 0.00890*TS^2 + 0.001203*W*V - 0.01092*V*TS

Regression Analysis: Depth

Analysis of Variance

Source	DF	Adj SS	Adj MS	F-Value	P-Value
Regression	6	18.2739	3.04565	24.57	0.000
WFS	1	4.8595	4.85955	39.21	0.000
V	1	6.3955	6.39553	51.60	0.000
TS	1	2.8322	2.83217	22.85	0.000
W^2	1	0.0010	0.00101	0.01	0.928
W*V	1	0.0005	0.00050	0.00	0.950
V*TS	1	0.3520	0.35195	2.84	0.097
Error	63	7.8087	0.12395		
Total	69	26.0826			

Model Summary

S	R-sq	R-sq(adj)	R-sq(pred)
0.352062	70.06%	67.21%	61.61%

Coefficients

Term	Coef	SE Coef	T-Value	P-Value	VIF
Constant	-1.385	0.313	-4.42	0.000	
WFS	0.002212	0.000353	6.26	0.000	1.22
V	0.1108	0.0154	7.18	0.000	1.90
TS	-0.03049	0.00638	-4.78	0.000	1.13
W^2	0.000000	0.000001	0.09	0.928	10.08
W*V	0.000002	0.000037	0.06	0.950	11.77
V*TS	-0.000336	0.000199	-1.69	0.097	1.53

Regression Equation

Depth = -1.385 + 0.002212*WFS + 0.1108*V - 0.03049*TS + 0.000000*W^2 + 0.000002*W*V - 0.000336*V*TS

Regression Analysis: Reinforcement Height

Analysis of Variance

Source	DF	Adj SS	Adj MS	F-Value	P-Value
Regression	4	33.8012	8.4503	56.86	0.000
WFS	1	15.3476	15.3476	103.27	0.000
V	1	1.6756	1.6756	11.27	0.001
TS	1	17.8034	17.8034	119.79	0.000
V^2	1	0.0205	0.0205	0.14	0.711
Error	65	9.6601	0.1486		
Total	69	43.4613			

Model Summary

S	R-sq	R-sq(adj)	R-sq(pred)
0.385509	77.77%	76.41%	74.19%

Coefficients

Term	Coef	SE Coef	T-Value	P-Value	VIF
Constant	4.204	0.332	12.64	0.000	
WFS	0.003635	0.000358	10.16	0.000	1.04
V	-0.0547	0.0163	-3.36	0.001	1.77
TS	-0.07479	0.00683	-10.95	0.000	1.08
V^2	-0.000118	0.000316	-0.37	0.711	1.71

Regression Equation

Reinforcement Height = 4.204 + 0.003635*WFS - 0.0547*V - 0.07479*TS - 0.000118*V^2

Regression Analysis: Reinforcement Area

Analysis of Variance

Source	DF	Adj SS	Adj MS	F-Value	P-Value
Regression	6	1580.05	263.34	83.36	0.000
WFS	1	677.02	677.02	214.30	0.000
V	1	0.85	0.85	0.27	0.606
TS	1	1075.39	1075.39	340.40	0.000
TS^2	1	0.39	0.39	0.12	0.727
W*V	1	1.69	1.69	0.53	0.467
W*TS	1	0.44	0.44	0.14	0.710
Error	63	199.03	3.16		
Total	69	1779.08			

Model Summary

S	R-sq	R-sq(adj)	R-sq(pred)
1.77740	88.81%	87.75%	86.40%

Coefficients

Term	Coef	SE Coef	T-Value	P-Value	VIF
Constant	14.16	1.58	8.95	0.000	
WFS	0.02547	0.00174	14.64	0.000	1.16
V	0.0399	0.0771	0.52	0.606	1.86
TS	-0.5899	0.0320	-18.45	0.000	1.11
TS^2	-0.00053	0.00151	-0.35	0.727	10.83
W*V	-0.000111	0.000152	-0.73	0.467	7.65
W*TS	0.000066	0.000176	0.37	0.710	21.52

Regression Equation

Reinforcement Area = 14.16 + 0.02547*WFS + 0.0399*V - 0.5899*TS - 0.00053*TS^2 - 0.000111*W*V + 0.000066*W*TS

Regression Analysis: Penetration Area

Analysis of Variance

Source	DF	Adj SS	Adj MS	F-Value	P-Value
Regression	4	381.966	95.491	12.57	0.000
WFS	1	112.538	112.538	14.81	0.000
V	1	78.421	78.421	10.32	0.002
TS	1	273.052	273.052	35.93	0.000
W*V	1	0.559	0.559	0.07	0.787
Error	65	493.966	7.599		
Total	69	875.932			

Model Summary

S	R-sq	R-sq(adj)	R-sq(pred)
2.75671	43.61%	40.14%	33.61%

Coefficients

Term	Coef	SE Coef	T-Value	P-Value	VIF
Constant	1.23	2.36	0.52	0.605	
WFS	0.01020	0.00265	3.85	0.000	1.12
V	0.3001	0.0934	3.21	0.002	1.14
TS	-0.2928	0.0488	-5.99	0.000	1.08
W*V	-0.000025	0.000092	-0.27	0.787	1.18

Regression Equation

Penetration Area = 1.23 + 0.01020*WFS + 0.3001*V - 0.2928*TS - 0.000025*W*V

Wire – ER 70 S 6 (0.035 in)

Gas Type: 85% Argon- 15% Carbon di-Oxide

Regression Analysis: Current

Analysis of Variance

Source	DF	Adj SS	Adj MS	F-Value	P-Value
Regression	6	56246.3	9374.39	255.69	0.000
WFS	1	1769.7	1769.67	48.27	0.000
V	1	0.3	0.29	0.01	0.930
TS	1	1358.5	1358.47	37.05	0.000
W^2	1	317.9	317.90	8.67	0.006
TS^2	1	752.4	752.36	20.52	0.000
V*TS	1	227.4	227.36	6.20	0.018
Error	36	1319.9	36.66		
Total	42	57566.2			

Model Summary

S	R-sq	R-sq(adj)	R-sq(pred)
6.05500	97.71%	97.33%	96.86%

Coefficients

Term	Coef	SE Coef	T-Value	P-Value	VIF
Constant	78.1	27.8	2.80	0.008	
WFS	0.4496	0.0647	6.95	0.000	78.59
V	-0.09	1.04	-0.09	0.930	16.62
TS	-5.674	0.932	-6.09	0.000	105.51
W^2	-0.000222	0.000075	-2.94	0.006	78.26
TS^2	0.0528	0.0117	4.53	0.000	47.71
V*TS	0.1087	0.0437	2.49	0.018	205.25

Regression Equation

Current = 78.1 + 0.4496*WFS - 0.09*V - 5.674*TS - 0.000222*W^2 + 0.0528*TS^2 + 0.1087*V*TS

Regression Analysis: Bead Width

Analysis of Variance

Source	DF	Adj SS	Adj MS	F-Value	P-Value
Regression	9	138.203	15.3559	71.64	0.000
WFS	1	0.756	0.7562	3.53	0.069
V	1	1.768	1.7682	8.25	0.007
TS	1	0.548	0.5484	2.56	0.119
W^2	1	1.505	1.5047	7.02	0.012
V^2	1	0.741	0.7414	3.46	0.072
TS^2	1	14.934	14.9341	69.68	0.000
W*V	1	2.943	2.9429	13.73	0.001
W*TS	1	2.568	2.5682	11.98	0.002
V*TS	1	3.696	3.6958	17.24	0.000
Error	33	7.073	0.2143		
Total	42	145.276			

Model Summary

S	R-sq	R-sq(adj)	R-sq(pred)
0.462968	95.13%	93.80%	92.04%

Coefficients

Term	Coef	SE Coef	T-Value	P-Value	VIF
Constant	-8.17	5.08	-1.61	0.117	
WFS	0.01221	0.00650	1.88	0.069	135.59
V	1.045	0.364	2.87	0.007	347.43
TS	-0.1179	0.0737	-1.60	0.119	112.79
W^2	-0.000015	0.000006	-2.65	0.012	78.68
V^2	-0.01312	0.00705	-1.86	0.072	327.88
TS^2	0.00870	0.00104	8.35	0.000	65.12
W*V	0.000558	0.000151	3.71	0.001	65.28
W*TS	-0.000336	0.000097	-3.46	0.002	75.44
V*TS	-0.01396	0.00336	-4.15	0.000	208.26

Regression Equation

Bead Width = -8.17 + 0.01221*WFS + 1.045*V - 0.1179*TS - 0.000015*W^2 - 0.01312*V^2
+ 0.00870*TS^2 + 0.000558*W*V - 0.000336*W*TS - 0.01396*V*TS

Regression Analysis: Bead Depth

Analysis of Variance

Source	DF	Adj SS	Adj MS	F-Value	P-Value
Regression	8	33.6426	4.20532	83.36	0.000
WFS	1	0.0168	0.01680	0.33	0.566
V	1	0.1522	0.15217	3.02	0.086
TS	1	0.8644	0.86435	17.13	0.000
W^2	1	0.1422	0.14220	2.82	0.097
V^2	1	0.5150	0.51500	10.21	0.002
TS^2	1	0.1426	0.14257	2.83	0.097
W*V	1	2.3963	2.39634	47.50	0.000
V*TS	1	0.1407	0.14068	2.79	0.099
Error	77	3.8845	0.05045		
Total	85	37.5271			

Model Summary

S	R-sq	R-sq(adj)	R-sq(pred)
0.224606	89.65%	88.57%	86.86%

Coefficients

Term	Coef	SE Coef	T-Value	P-Value	VIF
Constant	-0.28	1.72	-0.16	0.872	
WFS	-0.00123	0.00214	-0.58	0.566	124.45
V	0.216	0.125	1.74	0.086	346.71
TS	-0.1034	0.0250	-4.14	0.000	110.07
W^2	-0.000003	0.000002	-1.68	0.097	78.63
V^2	-0.00771	0.00241	-3.20	0.002	325.83
TS^2	0.000538	0.000320	1.68	0.097	52.19
W*V	0.000356	0.000052	6.89	0.000	65.02
V*TS	0.00192	0.00115	1.67	0.099	206.62

Regression Equation

Bead Depth = -0.28 - 0.00123*WFS + 0.216*V - 0.1034*TS - 0.000003*W^2 - 0.00771*V^2
+ 0.000538*TS^2 + 0.000356*W*V + 0.00192*V*TS

Regression Analysis: Reinforcement Height

Analysis of Variance

Source	DF	Adj SS	Adj MS	F-Value	P-Value
Regression	6	29.2649	4.87748	109.90	0.000
WFS	1	1.2858	1.28584	28.97	0.000
V	1	0.2802	0.28021	6.31	0.014
TS	1	5.7122	5.71221	128.71	0.000
V^2	1	0.2985	0.29848	6.73	0.011
TS^2	1	2.9017	2.90168	65.38	0.000
W*V	1	0.3522	0.35217	7.93	0.006
Error	79	3.5062	0.04438		
Total	85	32.7710			

Model Summary

S	R-sq	R-sq(adj)	R-sq(pred)
0.210670	89.30%	88.49%	87.65%

Coefficients

Term	Coef	SE Coef	T-Value	P-Value	VIF
Constant	6.52	1.53	4.27	0.000	
WFS	0.00657	0.00122	5.38	0.000	46.15
V	-0.289	0.115	-2.51	0.014	335.83
TS	-0.1462	0.0129	-11.34	0.000	33.31
V^2	0.00585	0.00226	2.59	0.011	324.03
TS^2	0.001943	0.000240	8.09	0.000	33.44
W*V	-0.000136	0.000048	-2.82	0.006	64.65

Regression Equation

Reinforcement Height = 6.52 + 0.00657*WFS - 0.289*V - 0.1462*TS + 0.00585*V^2 + 0.001943*TS^2 - 0.000136*W*V

Regression Analysis: Reinforcement Area

Analysis of Variance

Source	DF	Adj SS	Adj MS	F-Value	P-Value
Regression	6	2086.08	347.680	319.27	0.000
WFS	1	66.08	66.083	60.68	0.000
V	1	1.79	1.785	1.64	0.204
TS	1	214.23	214.232	196.72	0.000
W^2	1	6.22	6.217	5.71	0.019
TS^2	1	153.18	153.184	140.67	0.000
W*TS	1	43.44	43.436	39.89	0.000
Error	79	86.03	1.089		
Total	85	2172.11			

Model Summary

S	R-sq	R-sq(adj)	R-sq(pred)
1.04355	96.04%	95.74%	95.31%

Coefficients

Term	Coef	SE Coef	T-Value	P-Value	VIF
Constant	8.18	2.27	3.61	0.001	
WFS	0.06678	0.00857	7.79	0.000	92.89
V	0.0429	0.0335	1.28	0.204	1.16
TS	-0.9482	0.0676	-14.03	0.000	37.37
W^2	-0.000022	0.000009	-2.39	0.019	77.83
TS^2	0.01718	0.00145	11.86	0.000	49.53
W*TS	-0.000968	0.000153	-6.32	0.000	74.05

Regression Equation

Reinforcement Area = 8.18 + 0.06678*WFS + 0.0429*V - 0.9482*TS - 0.000022*W^2 + 0.01718*TS^2 - 0.000968*W*TS

Regression Analysis: Penetration Area

Analysis of Variance

Source	DF	Adj SS	Adj MS	F-Value	P-Value
Regression	7	1371.93	195.990	79.43	0.000
WFS	1	20.65	20.646	8.37	0.005
V	1	37.34	37.341	15.13	0.000
TS	1	82.95	82.952	33.62	0.000
W^2	1	19.87	19.872	8.05	0.006
TS^2	1	110.63	110.629	44.83	0.000
W*V	1	113.77	113.769	46.11	0.000
W*TS	1	44.79	44.791	18.15	0.000
Error	78	192.47	2.468		
Total	85	1564.40			

Model Summary

S	R-sq	R-sq(adj)	R-sq(pred)
1.57084	87.70%	86.59%	85.41%

Coefficients

Term	Coef	SE Coef	T-Value	P-Value	VIF
Constant	25.17	4.92	5.12	0.000	
WFS	-0.0451	0.0156	-2.89	0.005	135.49
V	-0.626	0.161	-3.89	0.000	11.83
TS	-0.599	0.103	-5.80	0.000	38.50
W^2	0.000039	0.000014	2.84	0.006	77.84
TS^2	0.01467	0.00219	6.70	0.000	49.99
W*V	0.002449	0.000361	6.79	0.000	64.98
W*TS	-0.000985	0.000231	-4.26	0.000	74.41

Regression Equation

Penetration Area = 25.17 - 0.0451*WFS - 0.626*V - 0.599*TS + 0.000039*W^2 + 0.01467*TS^2 + 0.002449*W*V - 0.000985*W*TS

Wire – ER 70 S 6 (0.035 in)

Gas Type: 100% Carbon di-Oxide

Regression Analysis: Current

Analysis of Variance

Source	DF	Adj SS	Adj MS	F-Value	P-Value
Regression	6	57762.4	9627.07	192.63	0.000
WFS	1	753.5	753.54	15.08	0.000
V	1	4.6	4.62	0.09	0.763
TS	1	655.1	655.10	13.11	0.001
W^2	1	462.1	462.13	9.25	0.004
TS^2	1	781.8	781.81	15.64	0.000
W*V	1	209.0	208.99	4.18	0.048
Error	36	1799.2	49.98		
Total	42	59561.6			

Model Summary

S	R-sq	R-sq(adj)	R-sq(pred)
7.06942	96.98%	96.48%	96.11%

Coefficients

Term	Coef	SE Coef	T-Value	P-Value	VIF
Constant	32.5	30.3	1.07	0.291	
WFS	0.3687	0.0949	3.88	0.000	124.13
V	0.31	1.02	0.30	0.763	11.77
TS	-2.216	0.612	-3.62	0.001	33.39
W^2	-0.000267	0.000088	-3.04	0.004	77.83
TS^2	0.0452	0.0114	3.96	0.000	33.52
W*V	0.00468	0.00229	2.04	0.048	64.66

Regression Equation

Current = 32.5 + 0.3687*WFS + 0.31*V - 2.216*TS - 0.000267*W^2 + 0.0452*TS^2 + 0.00468*W*V

Regression Analysis: Bead Width

Analysis of Variance

Source	DF	Adj SS	Adj MS	F-Value	P-Value
Regression	6	143.170	23.8617	49.99	0.000
WFS	1	3.427	3.4271	7.18	0.011
V	1	13.086	13.0856	27.42	0.000
TS	1	1.734	1.7338	3.63	0.065
W^2	1	2.065	2.0649	4.33	0.045
TS^2	1	10.246	10.2460	21.47	0.000
V*TS	1	2.617	2.6171	5.48	0.025
Error	36	17.183	0.4773		
Total	42	160.353			

Model Summary

S	R-sq	R-sq(adj)	R-sq(pred)
0.690865	89.28%	87.50%	85.23%

Coefficients

Term	Coef	SE Coef	T-Value	P-Value	VIF
Constant	-5.28	3.18	-1.66	0.105	
WFS	0.01978	0.00738	2.68	0.011	78.59
V	0.622	0.119	5.24	0.000	16.62
TS	-0.203	0.106	-1.91	0.065	105.51
W^2	-0.000018	0.000009	-2.08	0.045	78.26
TS^2	0.00617	0.00133	4.63	0.000	47.71
V*TS	-0.01167	0.00498	-2.34	0.025	205.25

Regression Equation

Bead Width = -5.28 + 0.01978*WFS + 0.622*V - 0.203*TS - 0.000018*W^2
+ 0.00617*TS^2 - 0.01167*V*TS

Regression Analysis: Bead Depth

Analysis of Variance

Source	DF	Adj SS	Adj MS	F-Value	P-Value
Regression	5	23.8737	4.77474	26.58	0.000
WFS	1	0.7640	0.76397	4.25	0.042
V	1	0.3657	0.36573	2.04	0.157
TS	1	4.2044	4.20441	23.41	0.000
TS^2	1	2.5593	2.55930	14.25	0.000
W*V	1	2.0632	2.06319	11.49	0.001
Error	80	14.3693	0.17962		
Total	85	38.2430			

Model Summary

S	R-sq	R-sq(adj)	R-sq(pred)
0.423812	62.43%	60.08%	57.62%

Coefficients

Term	Coef	SE Coef	T-Value	P-Value	VIF
Constant	3.75	1.06	3.53	0.001	
WFS	-0.00506	0.00245	-2.06	0.042	46.15
V	-0.0618	0.0433	-1.43	0.157	11.76
TS	-0.1185	0.0245	-4.84	0.000	29.74
TS^2	0.001711	0.000453	3.77	0.000	29.42
W*V	0.000329	0.000097	3.39	0.001	64.65

Regression Equation

Bead Depth = 3.75 - 0.00506*WFS - 0.0618*V - 0.1185*TS + 0.001711*TS^2 + 0.000329*W*V

Regression Analysis: Reinforcement Height

Analysis of Variance

Source	DF	Adj SS	Adj MS	F-Value	P-Value
Regression	3	30.903	10.3009	49.84	0.000
WFS	1	19.672	19.6722	95.19	0.000
V	1	4.718	4.7184	22.83	0.000
TS	1	10.136	10.1361	49.04	0.000
Error	82	16.947	0.2067		
Total	85	47.850			

Model Summary

S	R-sq	R-sq(adj)	R-sq(pred)
0.454612	64.58%	63.29%	61.60%

Coefficients

Term	Coef	SE Coef	T-Value	P-Value	VIF
Constant	3.381	0.361	9.36	0.000	
WFS	0.004071	0.000417	9.76	0.000	1.16
V	-0.0697	0.0146	-4.78	0.000	1.16
TS	-0.03842	0.00549	-7.00	0.000	1.30

Regression Equation

Reinforcement Height = 3.381 + 0.004071*WFS - 0.0697*V - 0.03842*TS

Regression Analysis: Reinforcement Area

Analysis of Variance

Source	DF	Adj SS	Adj MS	F-Value	P-Value
Regression	6	2602.41	433.734	524.71	0.000
WFS	1	125.25	125.245	151.52	0.000
V	1	4.90	4.905	5.93	0.017
TS	1	273.85	273.853	331.29	0.000
TS^2	1	251.53	251.528	304.29	0.000
W*V	1	5.78	5.778	6.99	0.010
W*TS	1	83.36	83.360	100.84	0.000
Error	79	65.30	0.827		
Total	85	2667.71			

Model Summary

S	R-sq	R-sq(adj)	R-sq(pred)
0.909183	97.55%	97.37%	97.19%

Coefficients

Term	Coef	SE Coef	T-Value	P-Value	VIF
Constant	5.80	2.39	2.42	0.018	
WFS	0.07288	0.00592	12.31	0.000	58.37
V	0.2270	0.0932	2.44	0.017	11.82
TS	-1.0372	0.0570	-18.20	0.000	34.98
TS^2	0.02113	0.00121	17.44	0.000	45.65
W*V	-0.000552	0.000209	-2.64	0.010	64.97
W*TS	-0.001344	0.000134	-10.04	0.000	74.39

Regression Equation

Reinforcement Area = 5.80 + 0.07288*WFS + 0.2270*Voltage - 1.0372*TS + 0.02113*TS^2 - 0.000552*W*V- 0.001344*W*TS

Regression Analysis: Penetration Area

Analysis of Variance

Source	DF	Adj SS	Adj MS	F-Value	P-Value
Regression	4	1784.28	446.070	105.33	0.000
WFS	1	75.83	75.833	17.91	0.000
V	1	4.72	4.721	1.11	0.294
TS	1	504.66	504.661	119.16	0.000
W*V	1	161.89	161.885	38.22	0.000
Error	81	343.05	4.235		
Total	85	2127.33			

Model Summary

S	R-sq	R-sq(adj)	R-sq(pred)
2.05795	83.87%	83.08%	82.16%

Coefficients

Term	Coef	SE Coef	T-Value	P-Value	VIF
Constant	11.53	5.15	2.24	0.028	
WFS	-0.0496	0.0117	-4.23	0.000	44.64
V	-0.219	0.207	-1.06	0.294	11.40
TS	-0.2713	0.0248	-10.92	0.000	1.30
W*V	0.002866	0.000464	6.18	0.000	62.54

Regression Equation

Penetration Area = 11.53 - 0.0496*WFS - 0.219*Voltage - 0.2713*TS1 + 0.002866*W*V

Appendix D Model Fit (Linear)-Extended DoE

Weld width as a function of wire feed speed for 0.035 in wire (Each grid plots the width versus wire feed speed, with raw data for different Voltage and Travel Speed for each gas, and the model predictive equation for that quadrant represented)

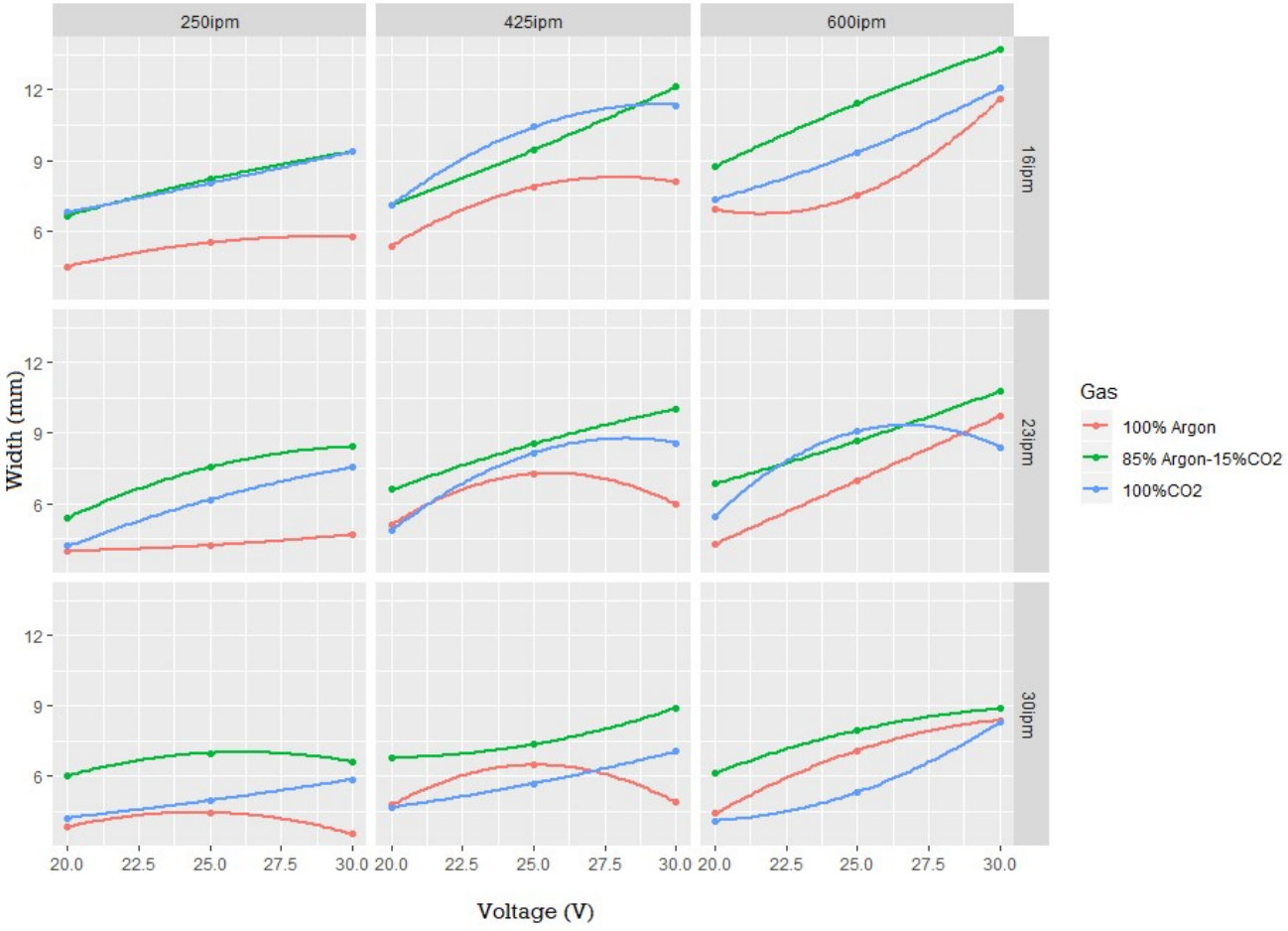

Weld penetration as a function of wire feed speed for 0.035 in wire (each grid plots the width versus wire feed speed, with raw data for different voltage and travel speed for each gas, and the predictive model equation for that quadrant)

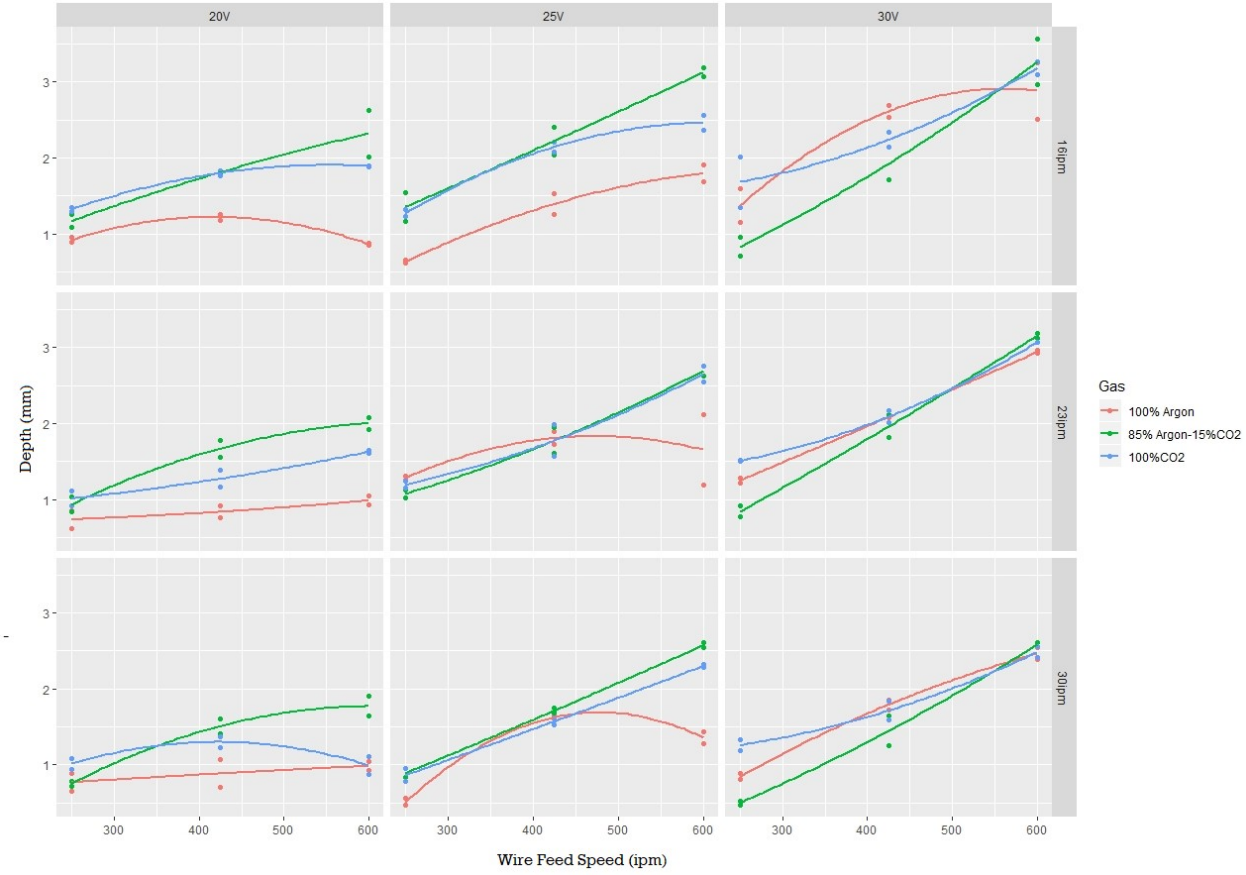

Weld reinforcement height as a function of wire feed speed for 0.035 in wire (Each grid plots the width versus wire feed speed, with raw data for different Voltage and Travel Speed for each gas, and the model predictive equation for that quadrant represented)

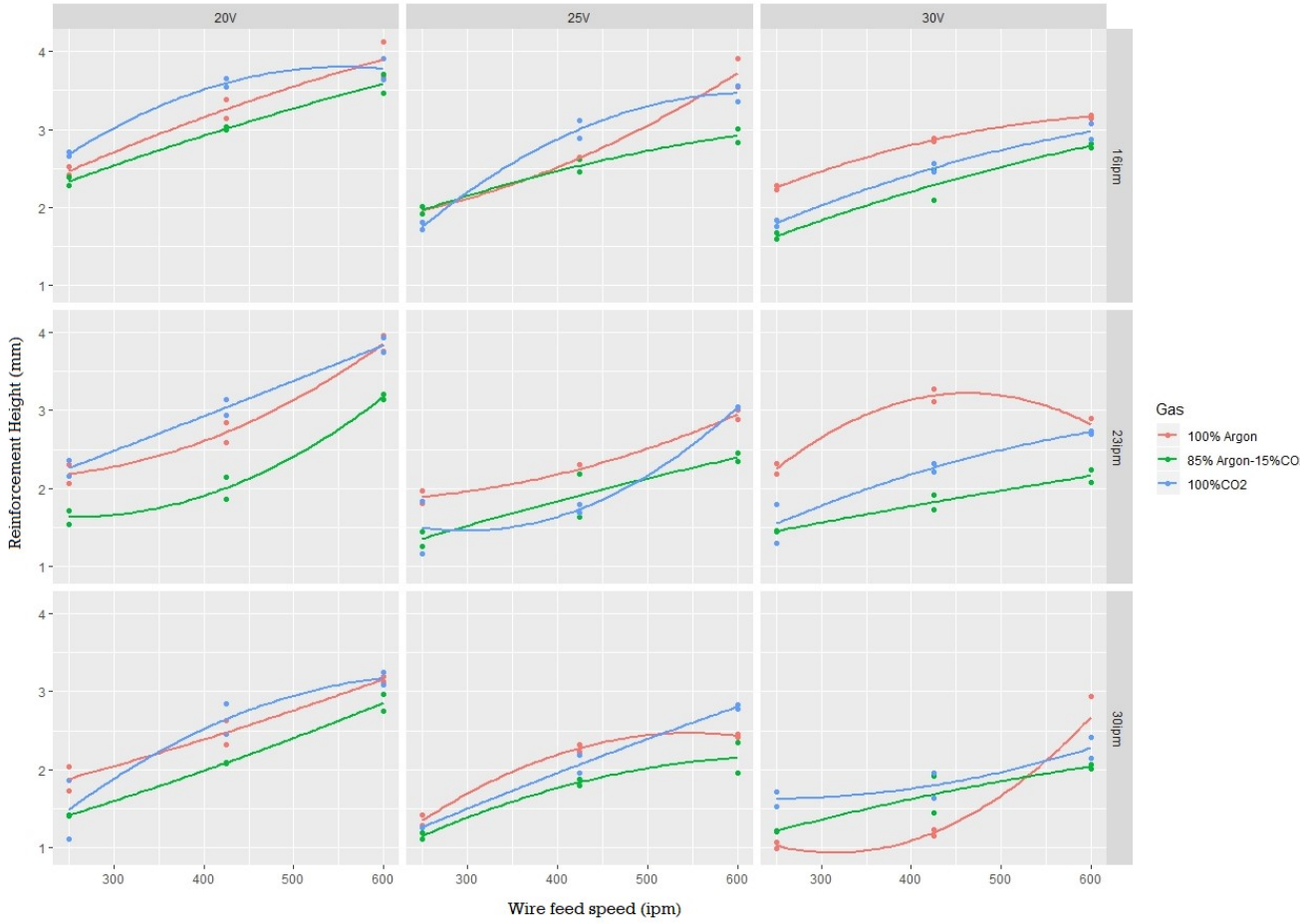

Weld reinforcement area as a function of wire feed speed for 0.035 in wire (Each grid plots the width versus wire feed speed, with raw data for different Voltage and Travel Speed for each gas, and the model predictive equation for that quadrant represented)

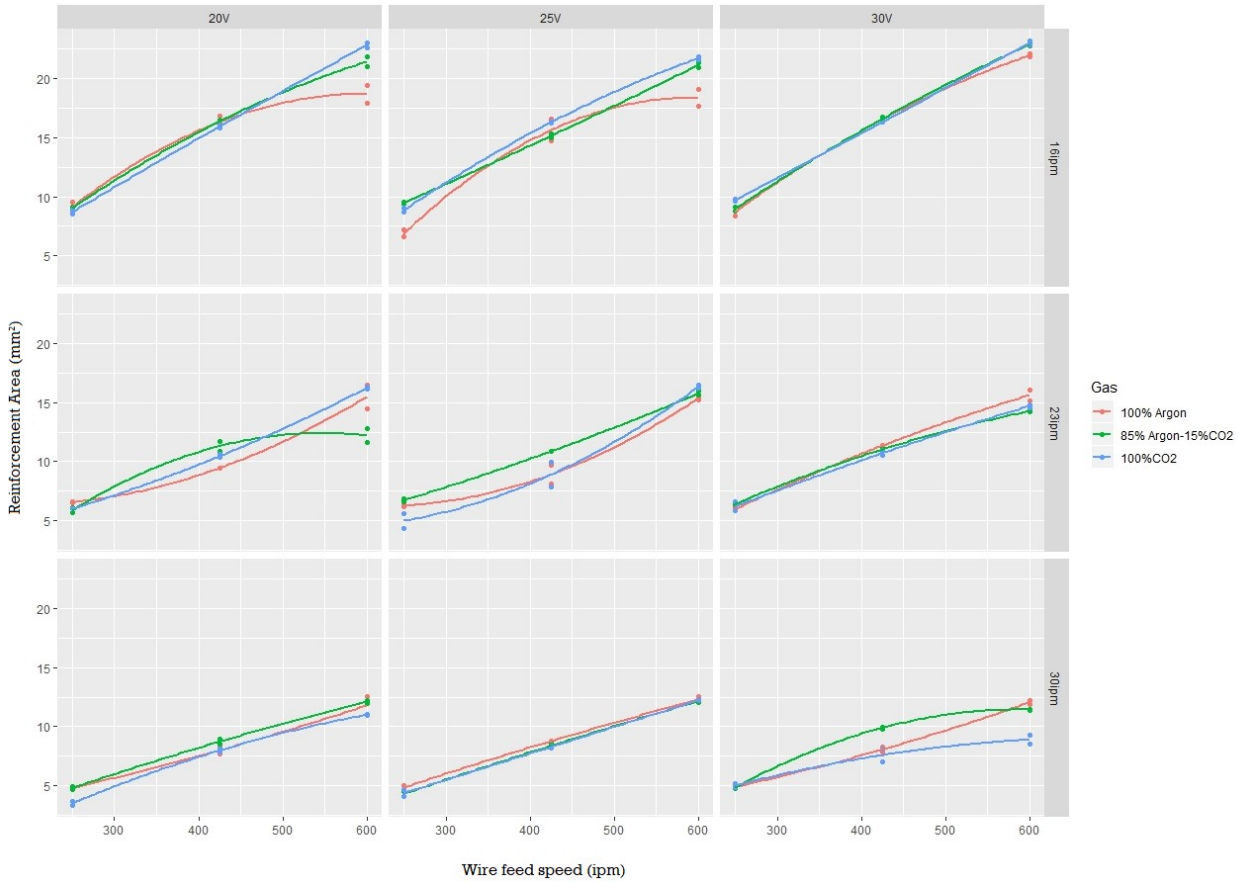

Weld penetration area as a function of wire feed speed for 0.035 in wire (Each grid plots the width versus wire feed speed, with raw data for different Voltage and Travel Speed for each gas, and the model predictive equation for that quadrant represented)

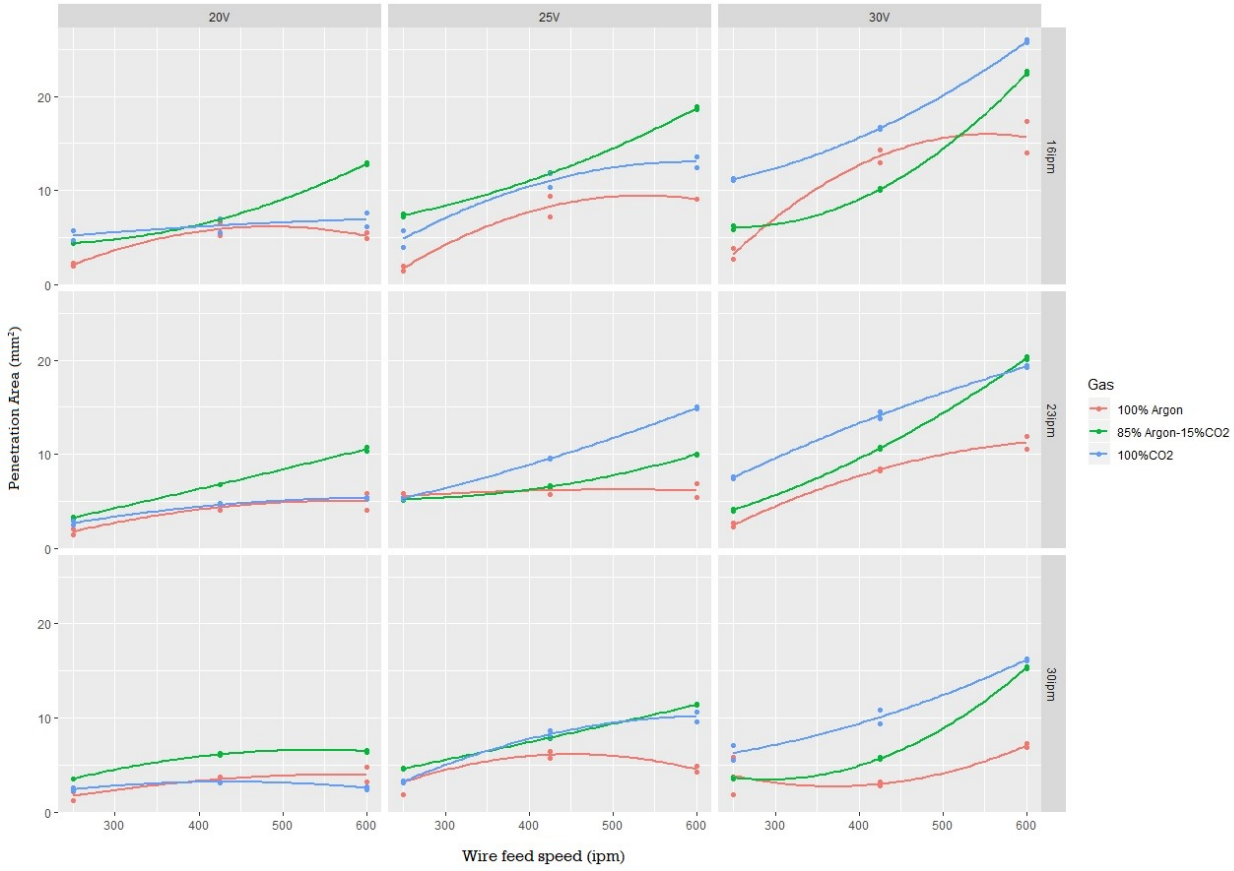

Welding current as a function of wire feed speed for 0.035 in wire (Each grid plots the width versus wire feed speed, with raw data for different Voltage and Travel Speed for each gas, and the model predictive equation for that quadrant represented)

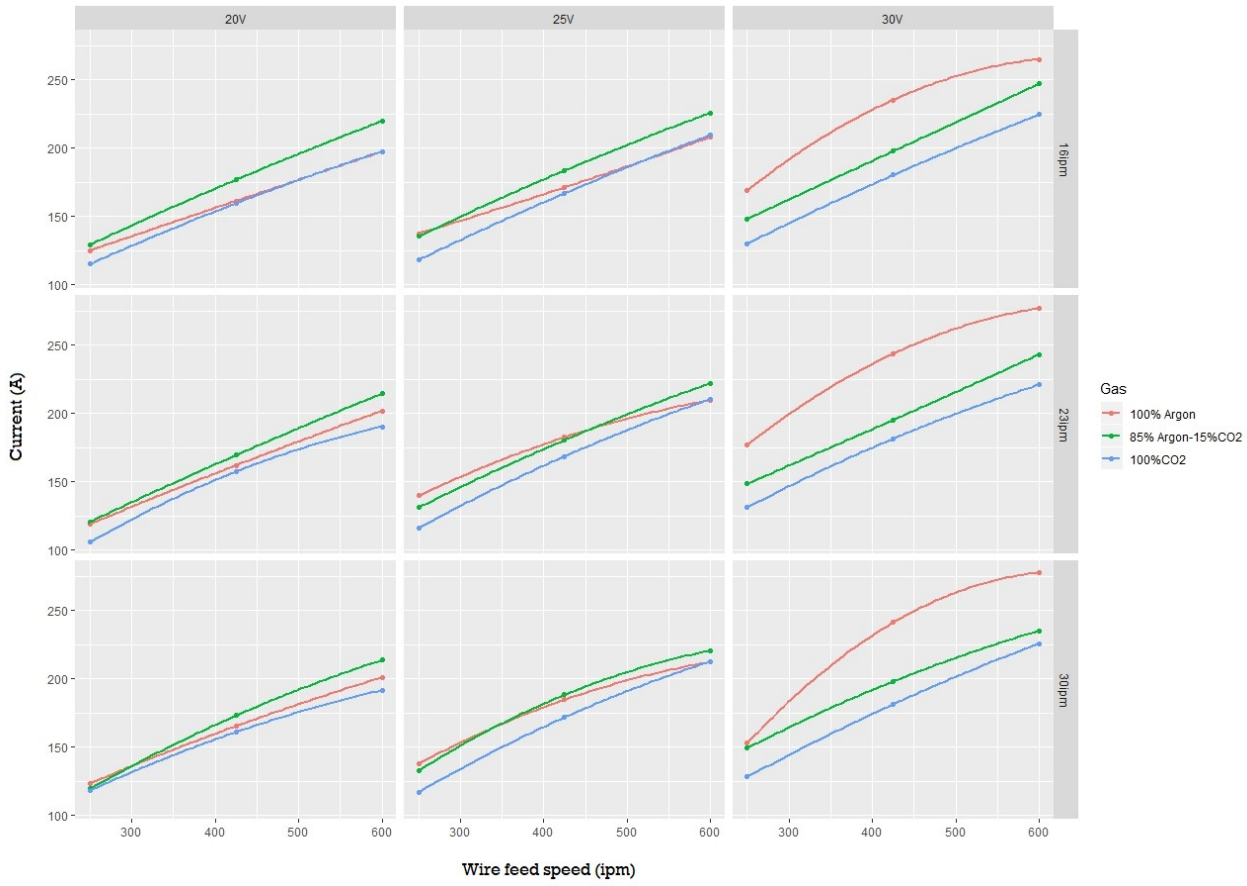

ER 70S-6 (0.035 in)

Model fit for low- intermediate wire feed speed and voltage range at lower travel speed rates

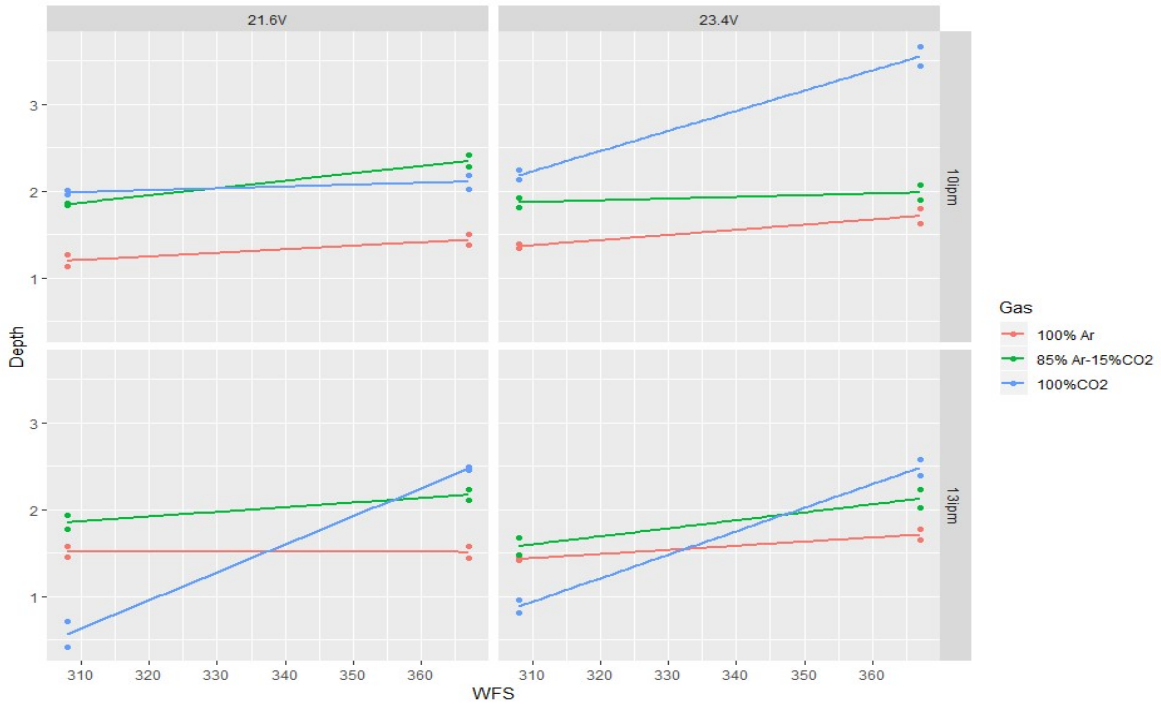

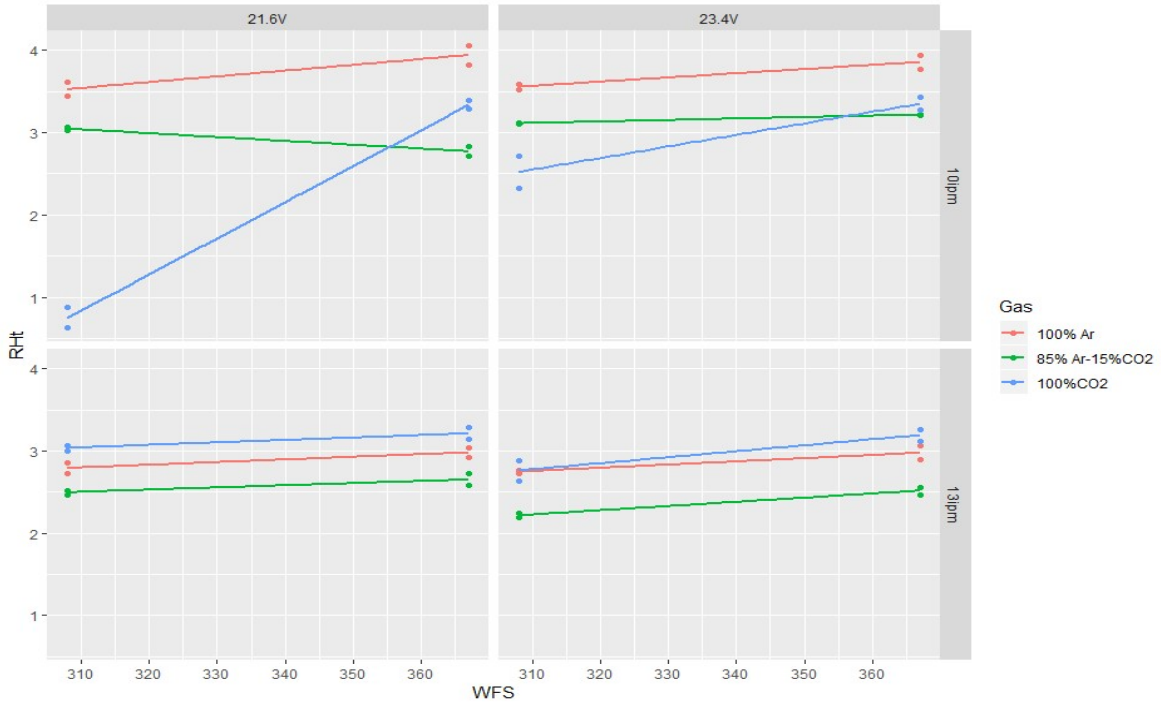

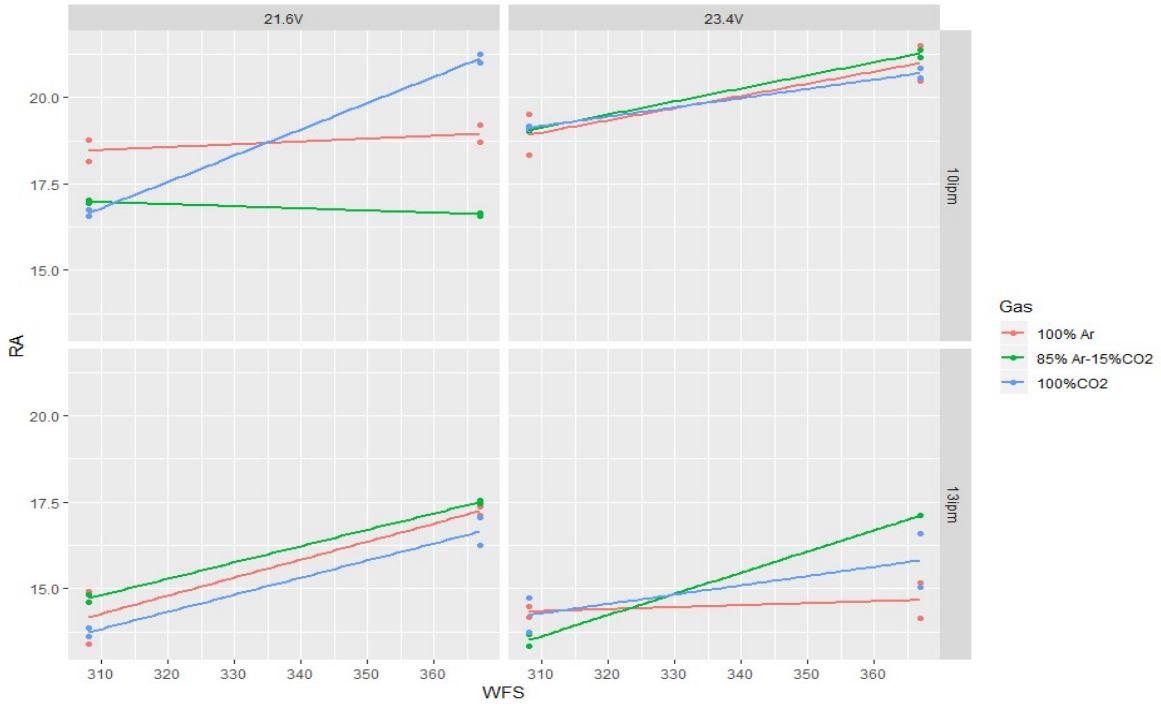
21.6V
23.4V
10ipm
13ipm
RA
20.0
17.5
15.0
310
320
330
340
350
360
WFS
Gas
100% Ar
85% Ar-15%CO2
100%CO2

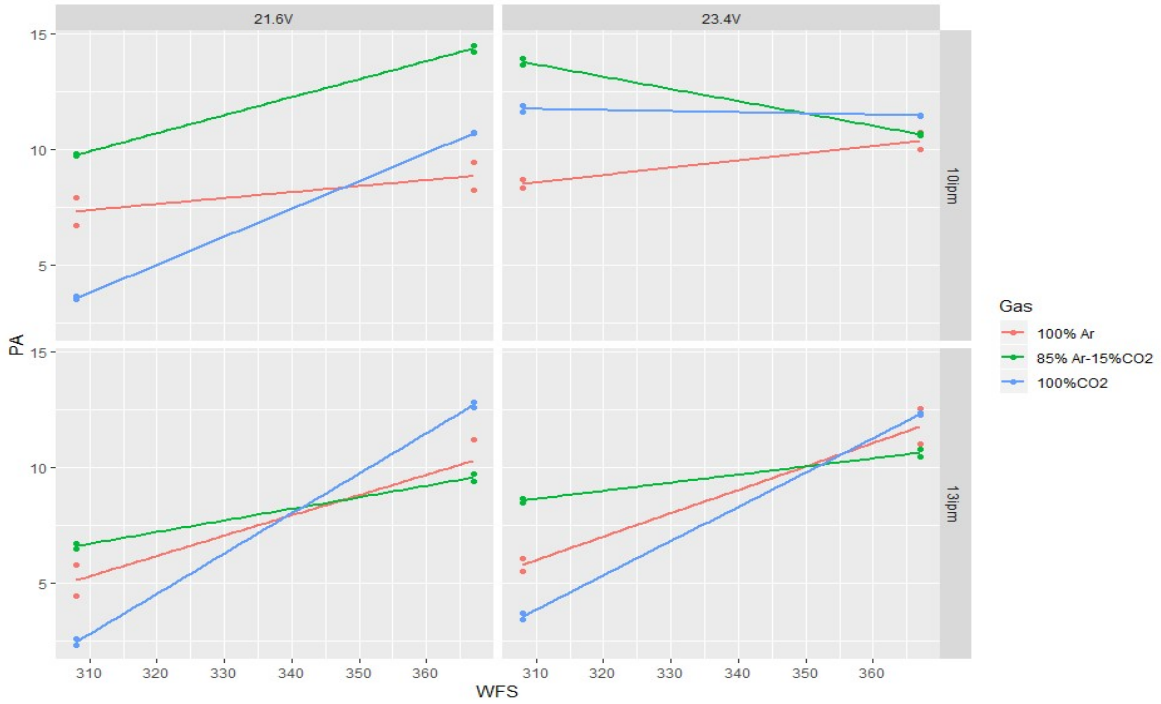
21.6V
23.4V
10ipm
13ipm
PA
15
10
5
310
320
330
340
350
360
WFS
Gas
100% Ar
85% Ar-15%CO2
100%CO2

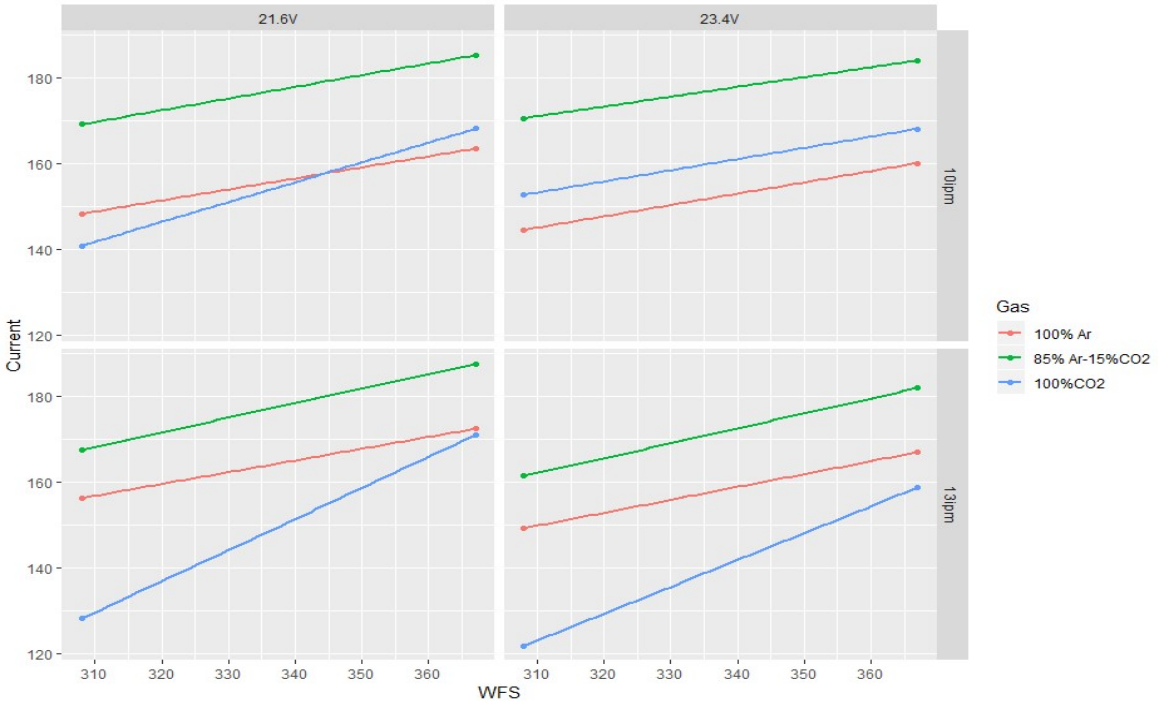
21.6V
23.4V
10ipm
13ipm
Current
WFS
180
160
140
120
310
320
330
340
350
360
Gas
100% Ar
85% Ar-15%CO2
100%CO2

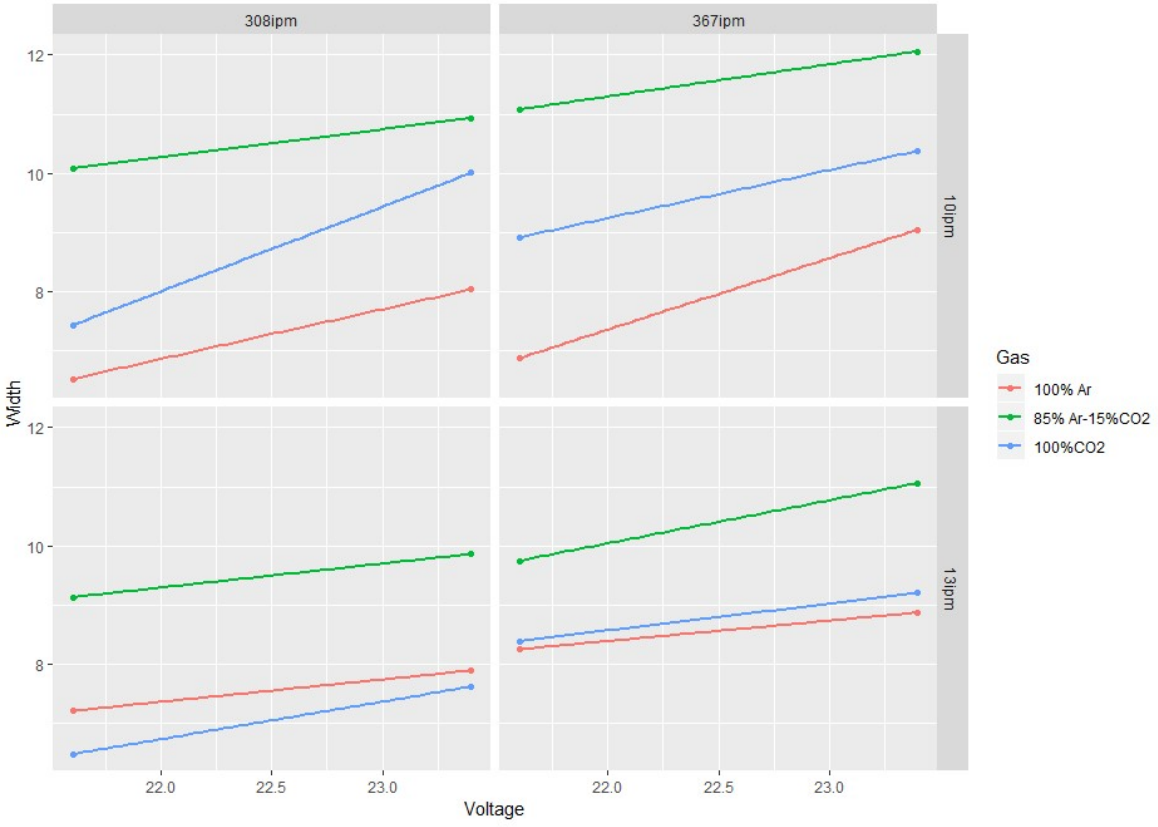
308ipm
367ipm
10ipm
13ipm
Width
Voltage
12
10
8
22.0
22.5
23.0
Gas
100% Ar
85% Ar-15%CO2
100%CO2

ER 70S-6 (0.035 in)

Model fit for intermediate-high wire Feed speed and voltage range at higher travel speed rates

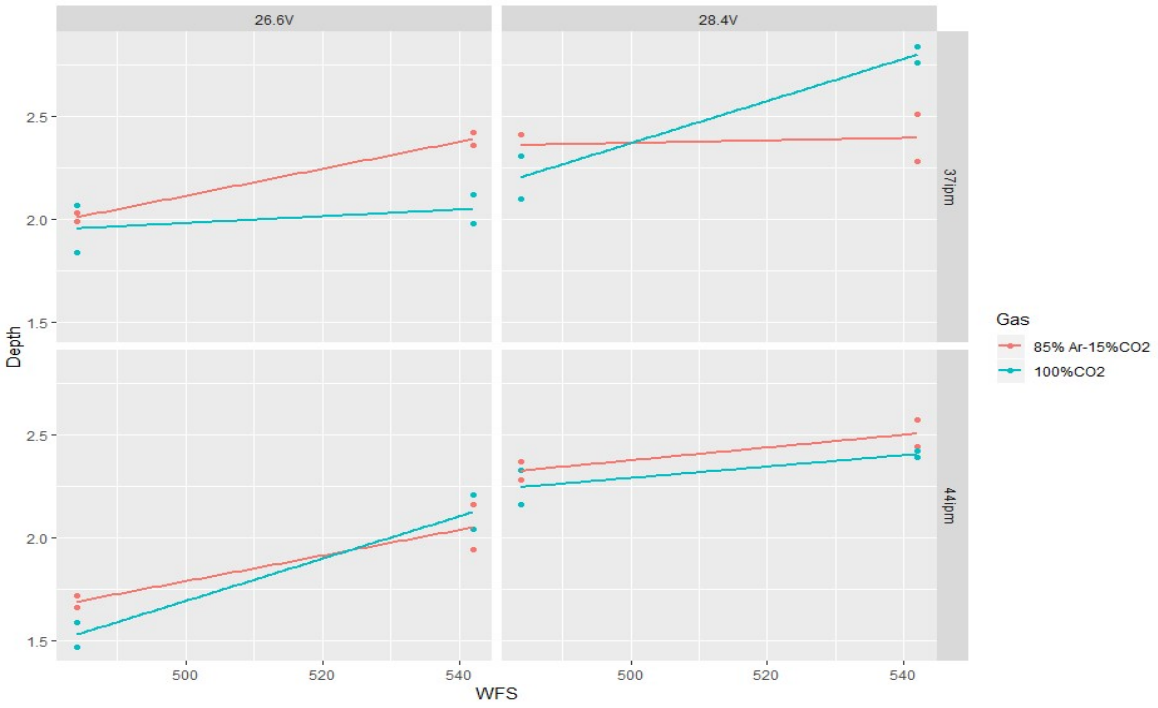

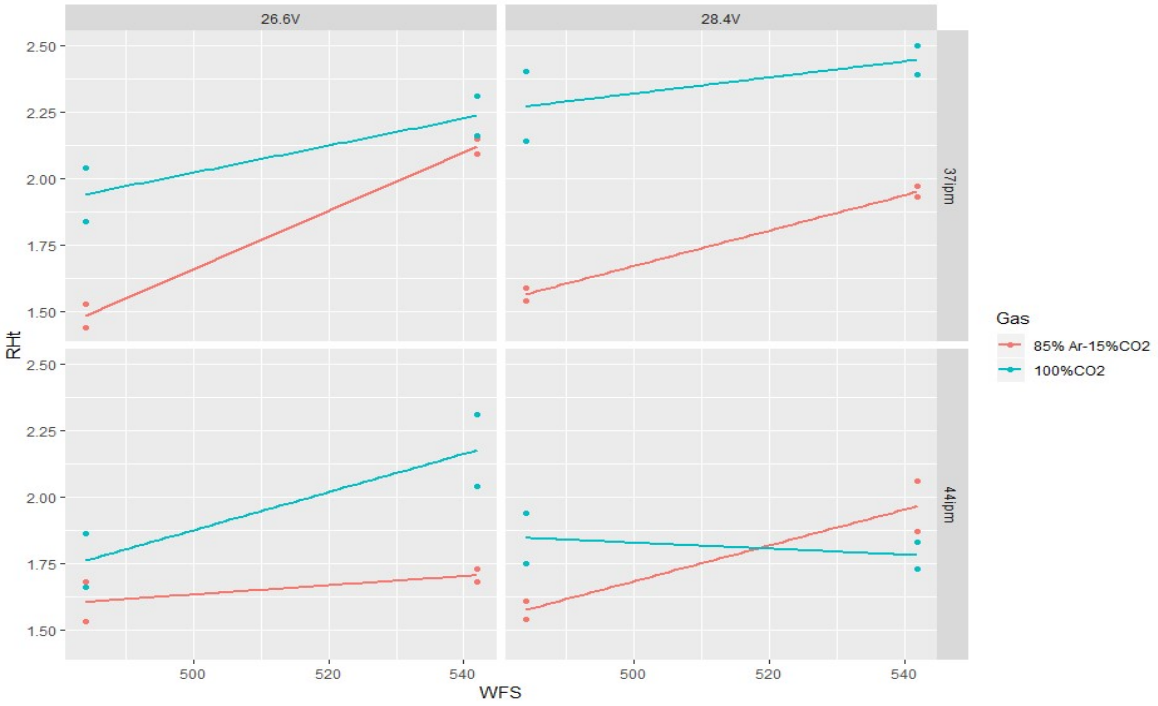

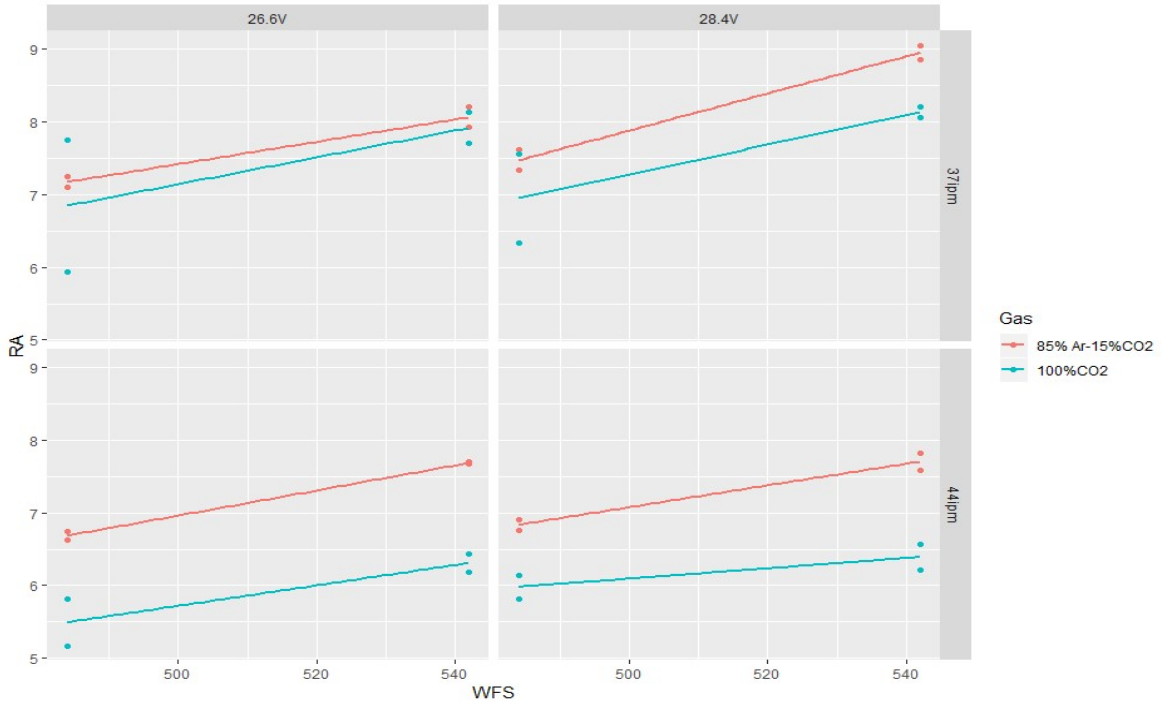
26.6V
28.4V
37lpm
44lpm
RA
WFS
Gas
85% Ar-15%CO2
100%CO2

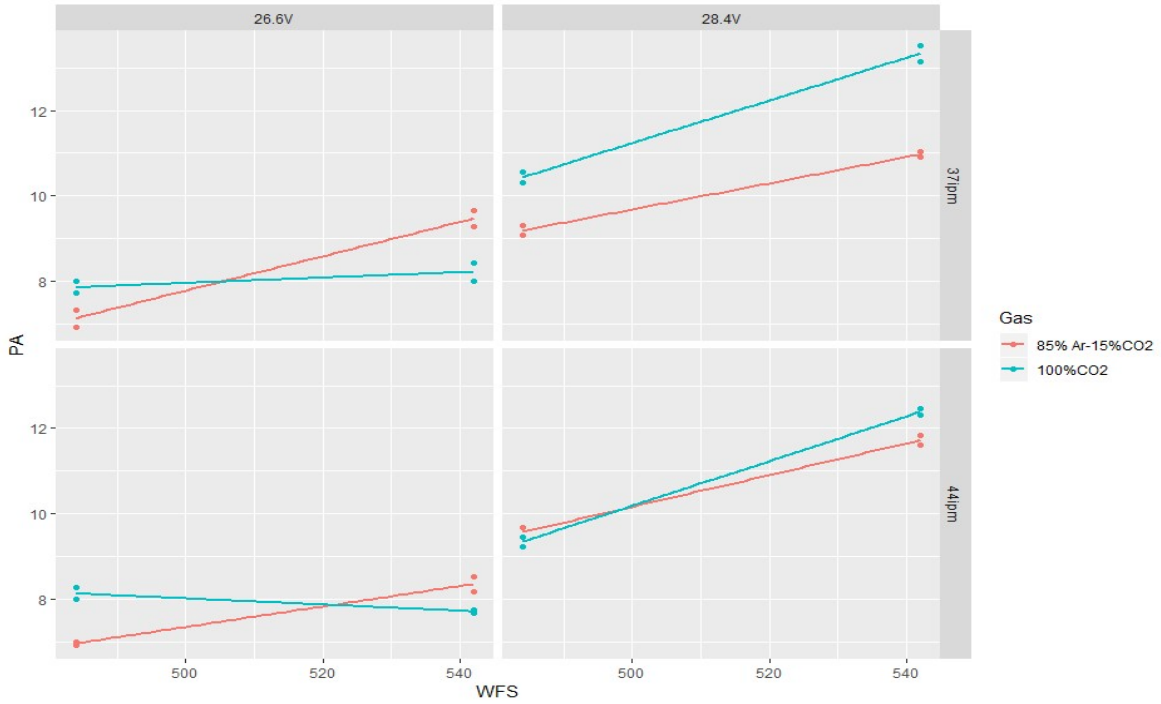
26.6V
28.4V
37lpm
44lpm
PA
WFS
Gas
85% Ar-15%CO2
100%CO2

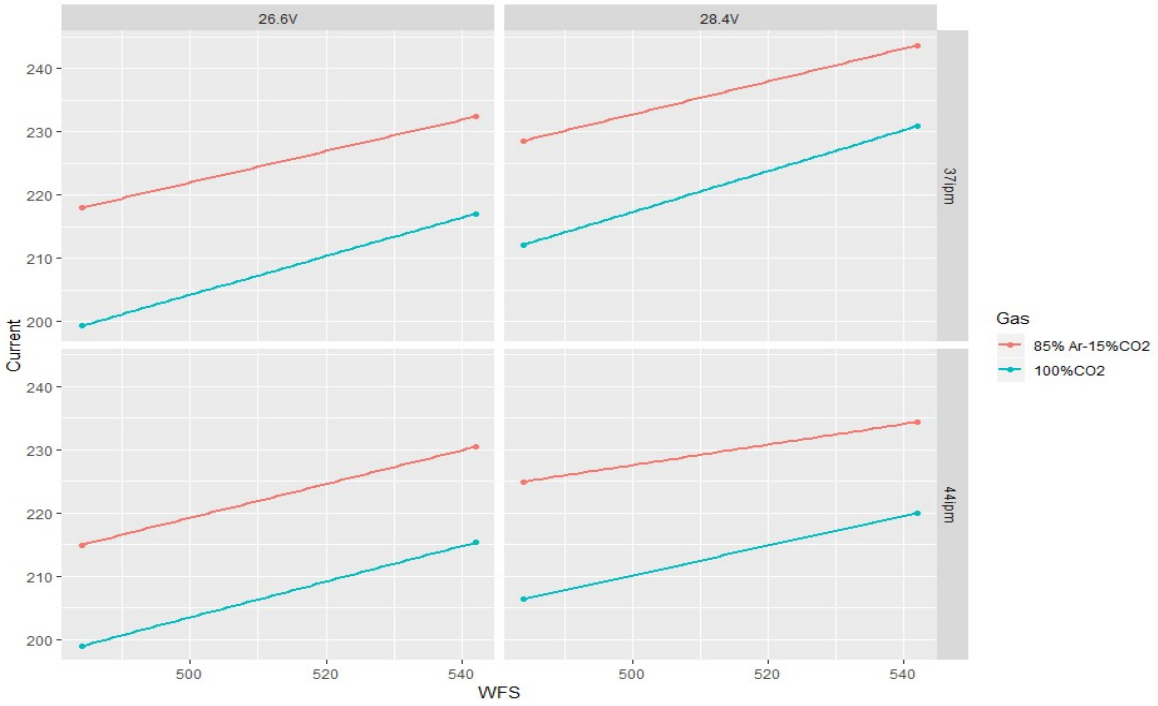
26.6V
28.4V
37ipm
44ipm
Current
WFS
240
230
220
210
200
500
520
540
Gas
85% Ar-15%CO2
100%CO2

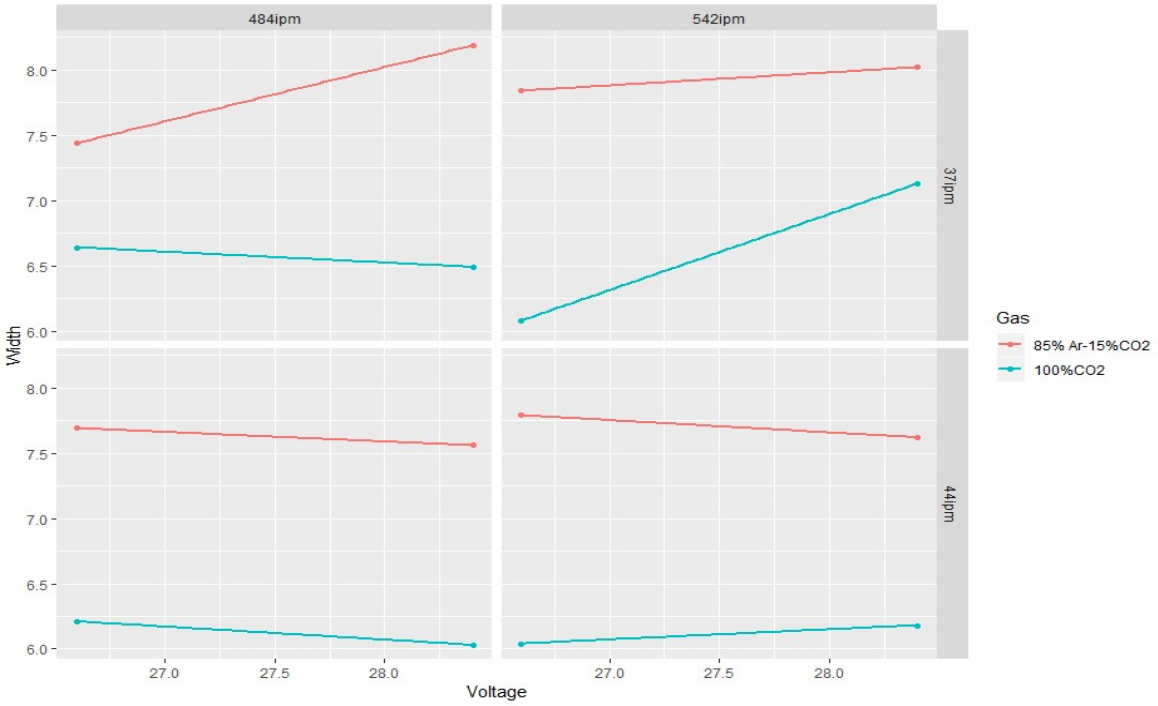
484ipm
542ipm
37ipm
44ipm
Width
Voltage
8.0
7.5
7.0
6.5
6.0
27.0
27.5
28.0
Gas
85% Ar-15%CO2
100%CO2

ER 70S-6 (0.045 in)

Model fit for low- intermediate wire feed speed and voltage range at lower travel speed rates

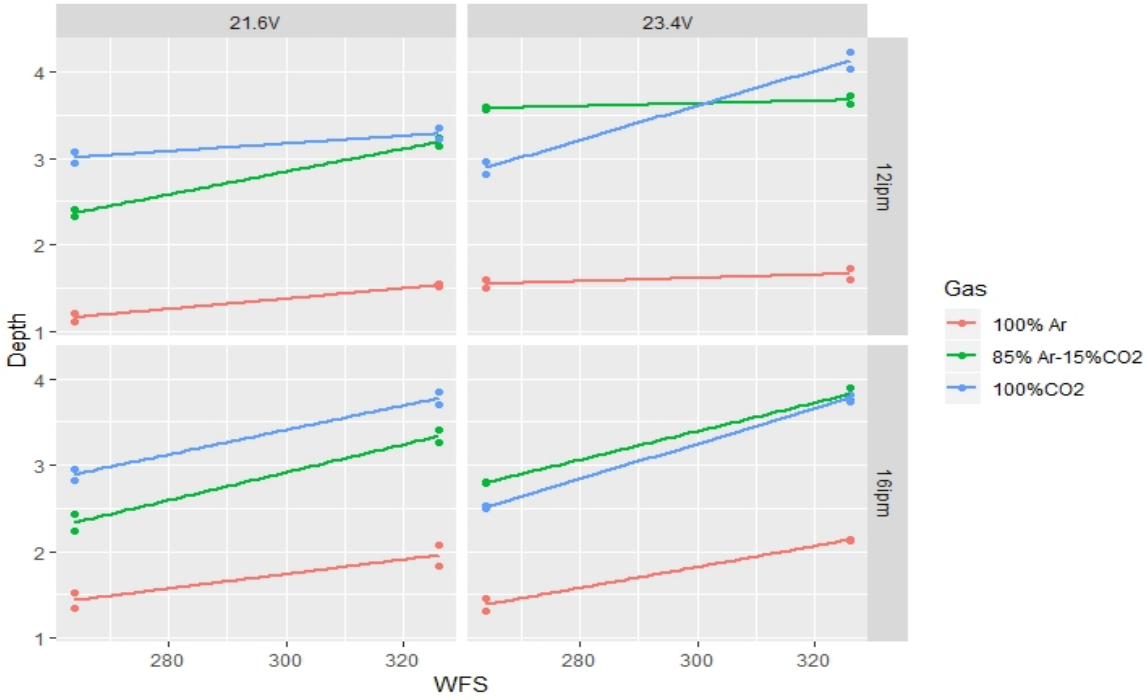

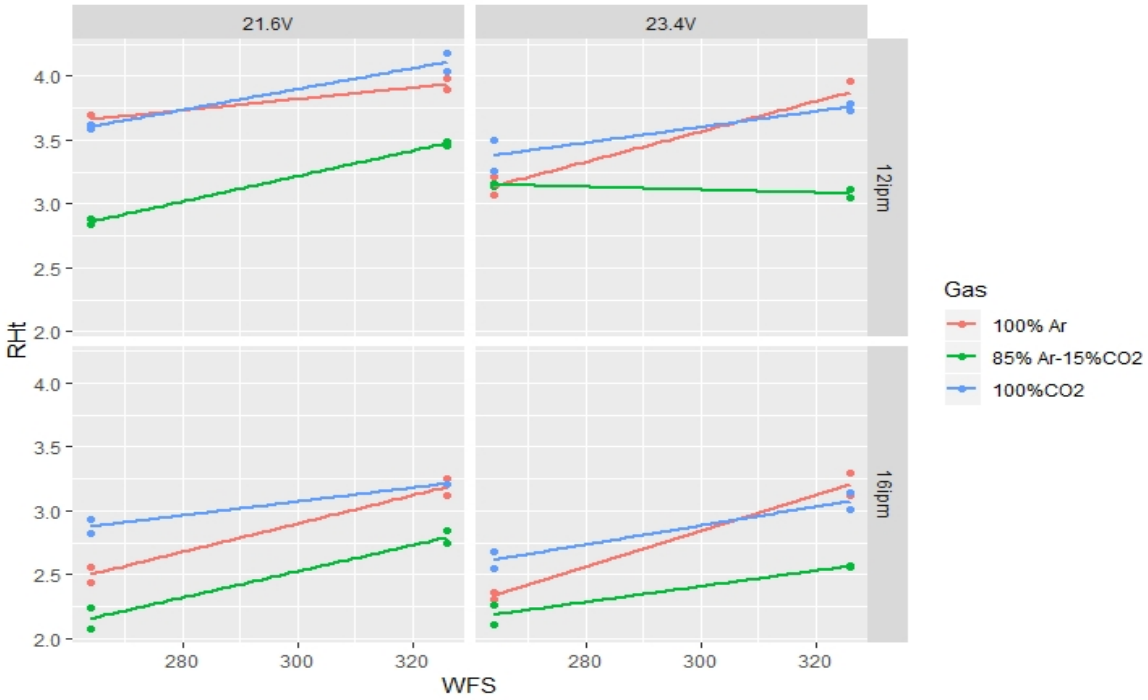

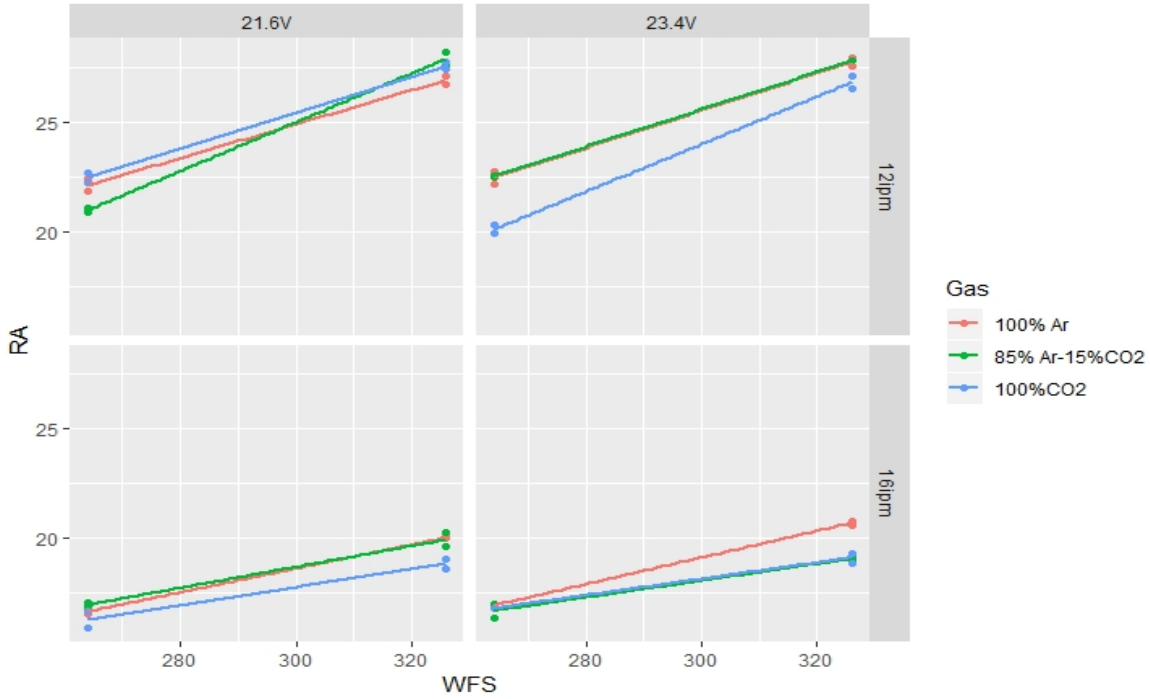
21.6V
23.4V
12ipm
16ipm
RA
25
20
280
300
320
WFS
Gas
100% Ar
85% Ar-15%CO2
100%CO2

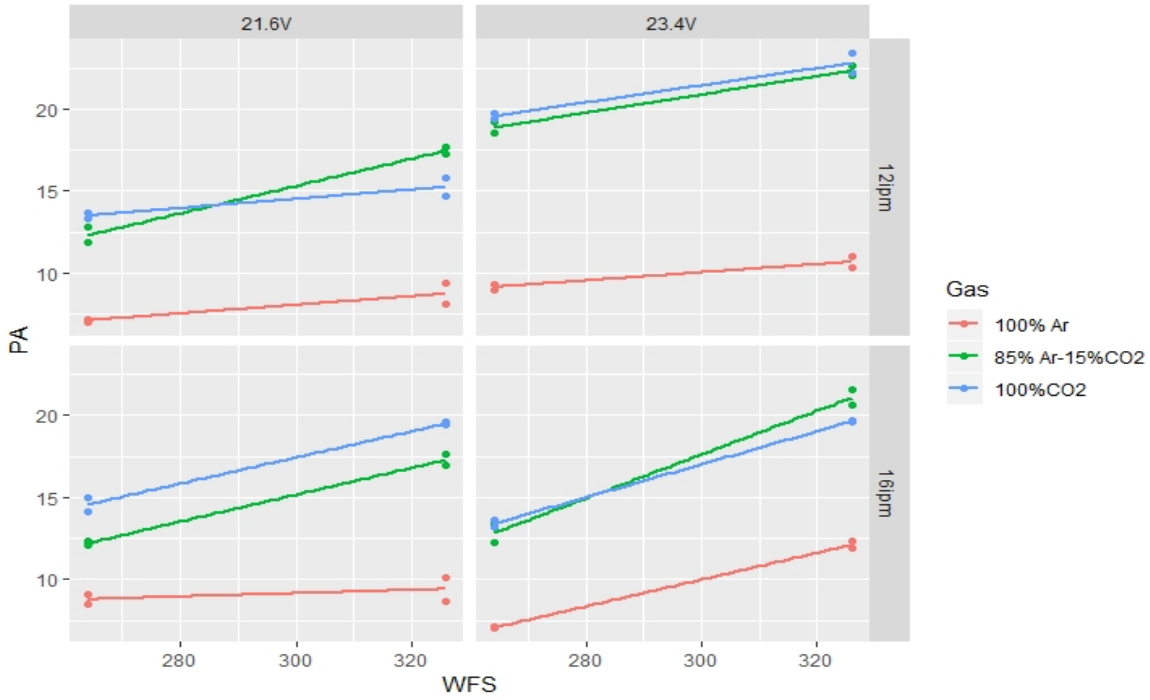
21.6V
23.4V
12ipm
16ipm
PA
20
15
10
280
300
320
WFS
Gas
100% Ar
85% Ar-15%CO2
100%CO2

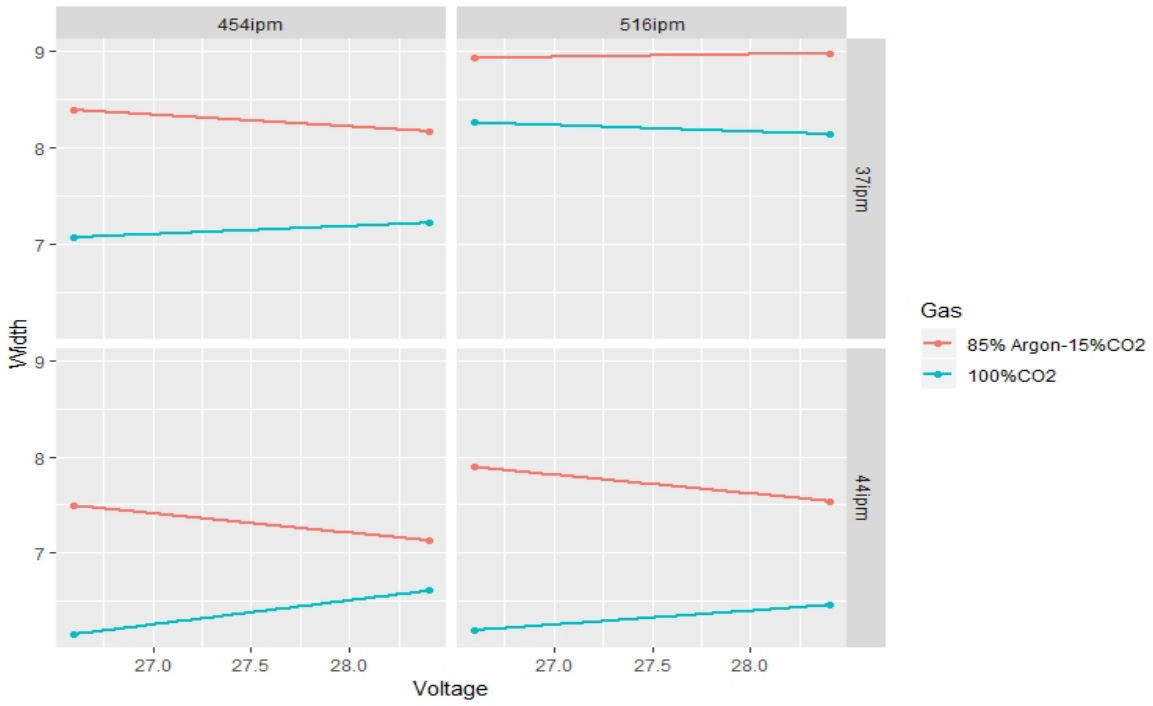
454ipm
516ipm
37ipm
44ipm
Width
9
8
7
27.0
27.5
28.0
Voltage
Gas
85% Argon-15%CO2
100%CO2

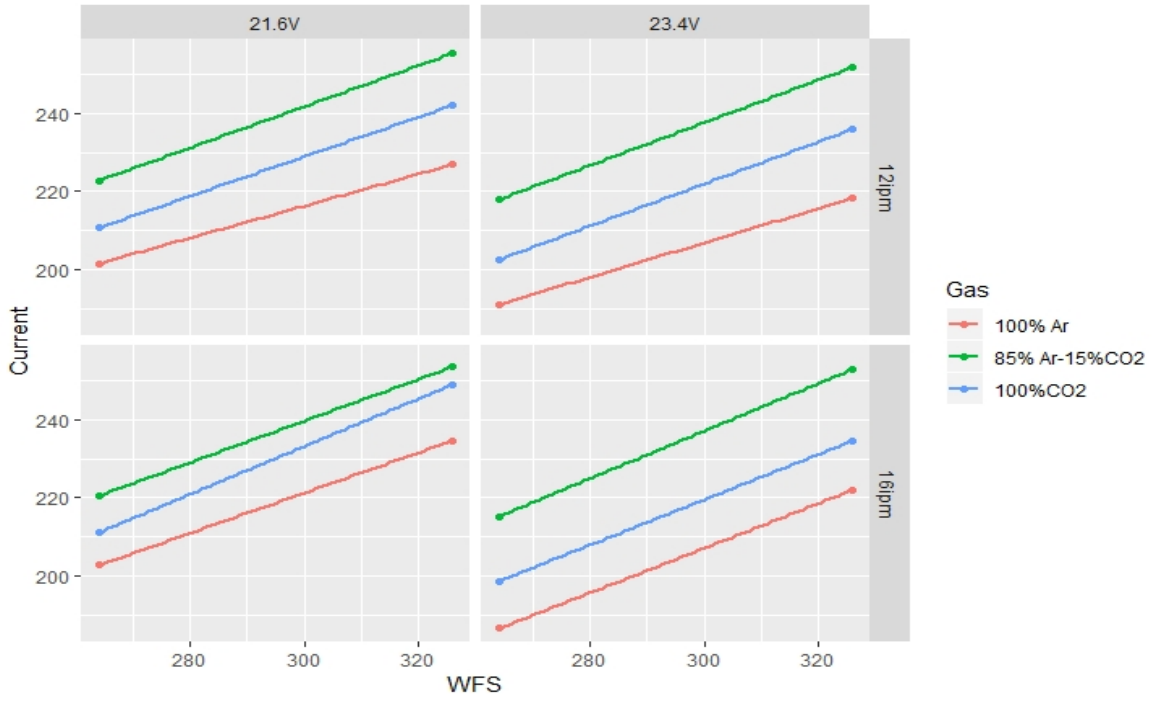
21.6V
23.4V
12ipm
16ipm
Current
240
220
200
280
300
320
WFS
Gas
100% Ar
85% Ar-15%CO2
100%CO2

ER 70S-6 (0.045 in)

Model fit for intermediate-high wire Feed speed and voltage range at higher travel speed rates

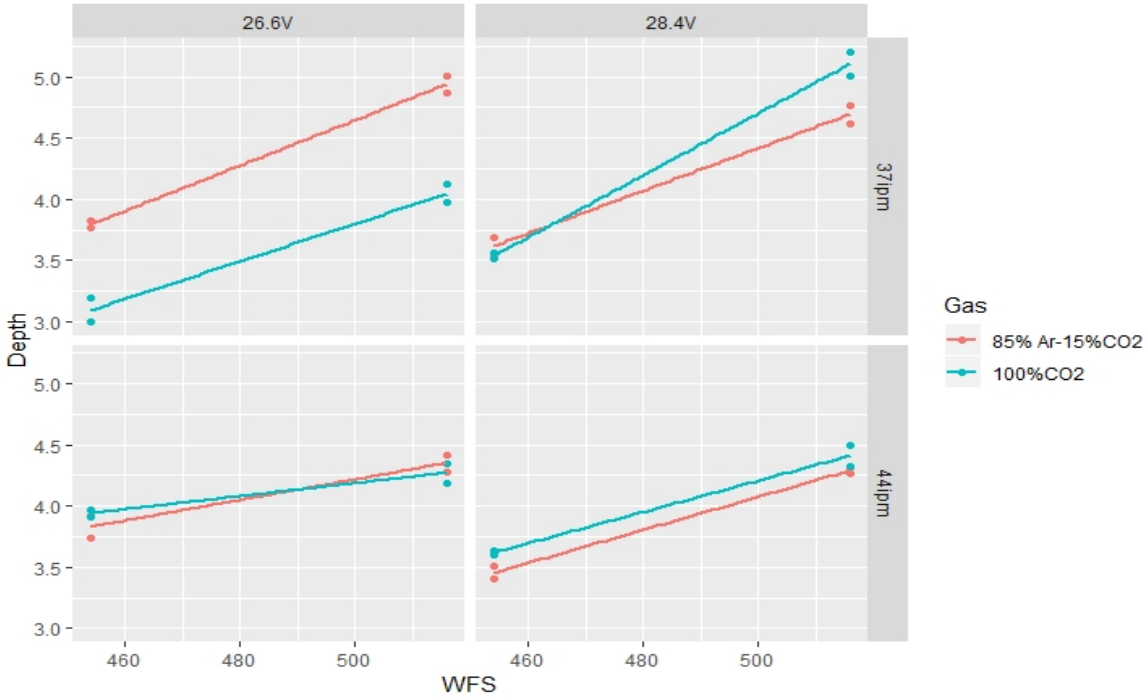

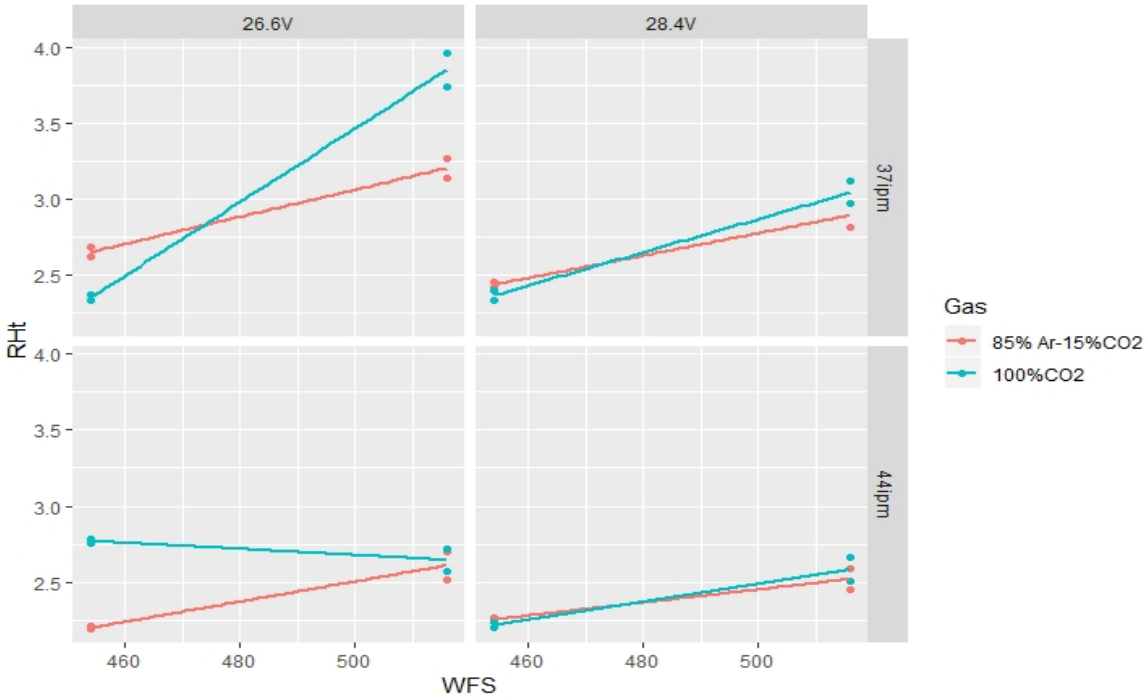

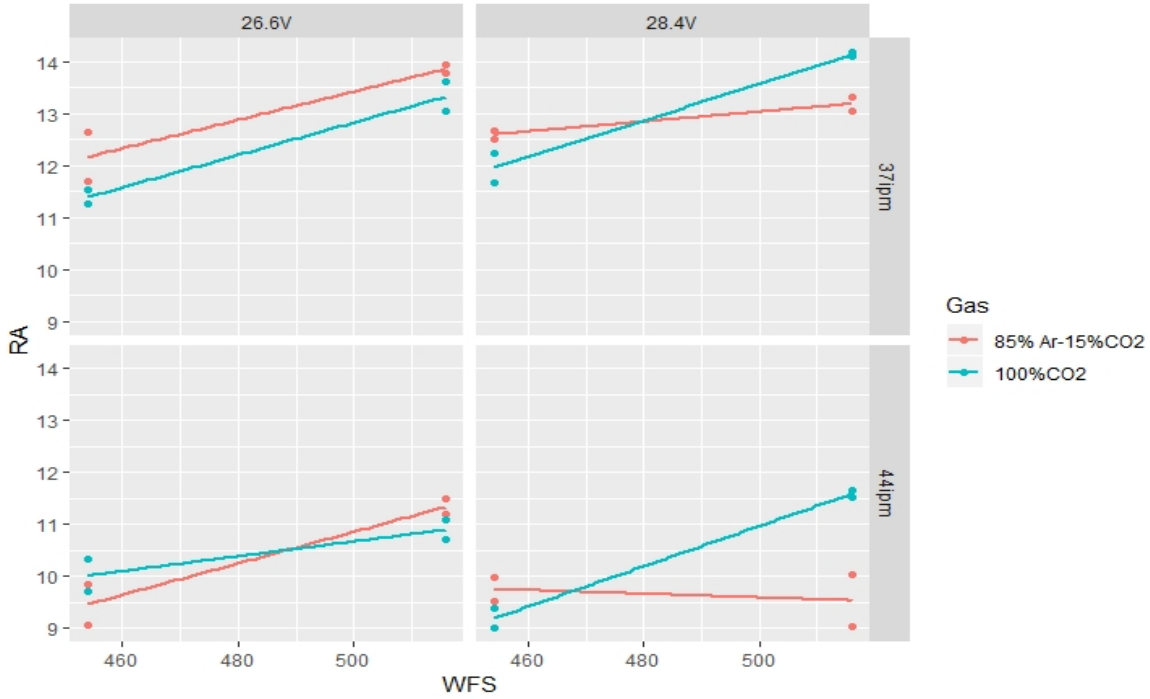
26.6V
28.4V
37lpm
44lpm
RA
WFS
460
480
500
9
10
11
12
13
14
Gas
85% Ar-15%CO2
100%CO2

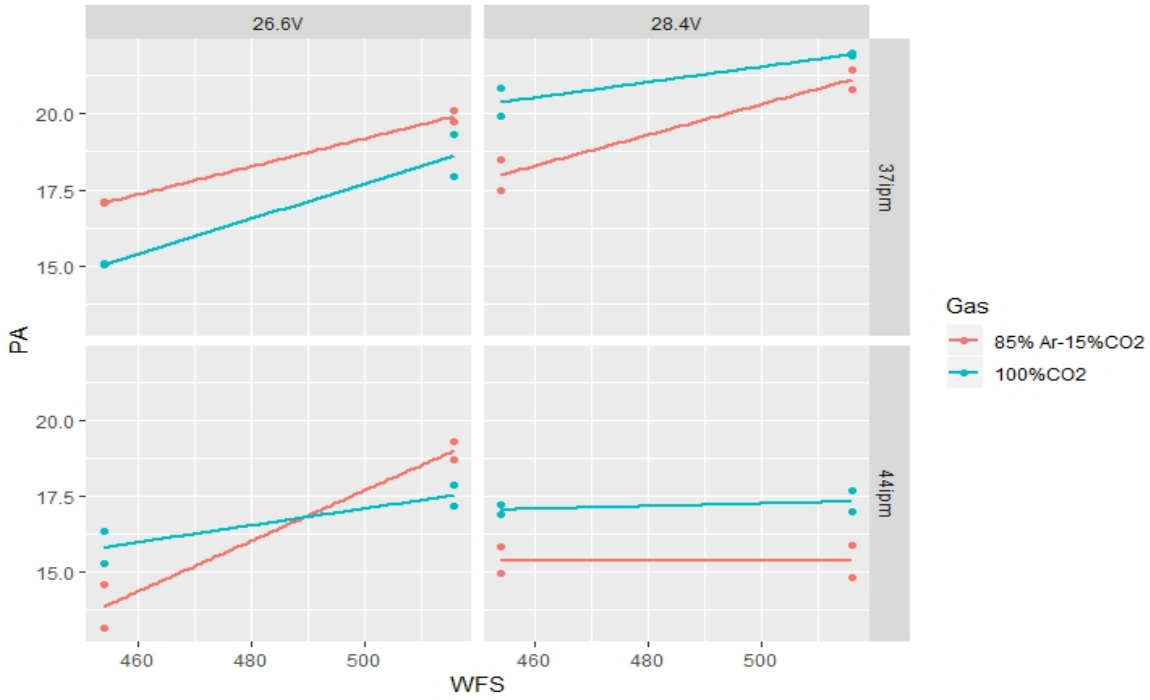
26.6V
28.4V
37lpm
44lpm
PA
WFS
460
480
500
15.0
17.5
20.0
Gas
85% Ar-15%CO2
100%CO2

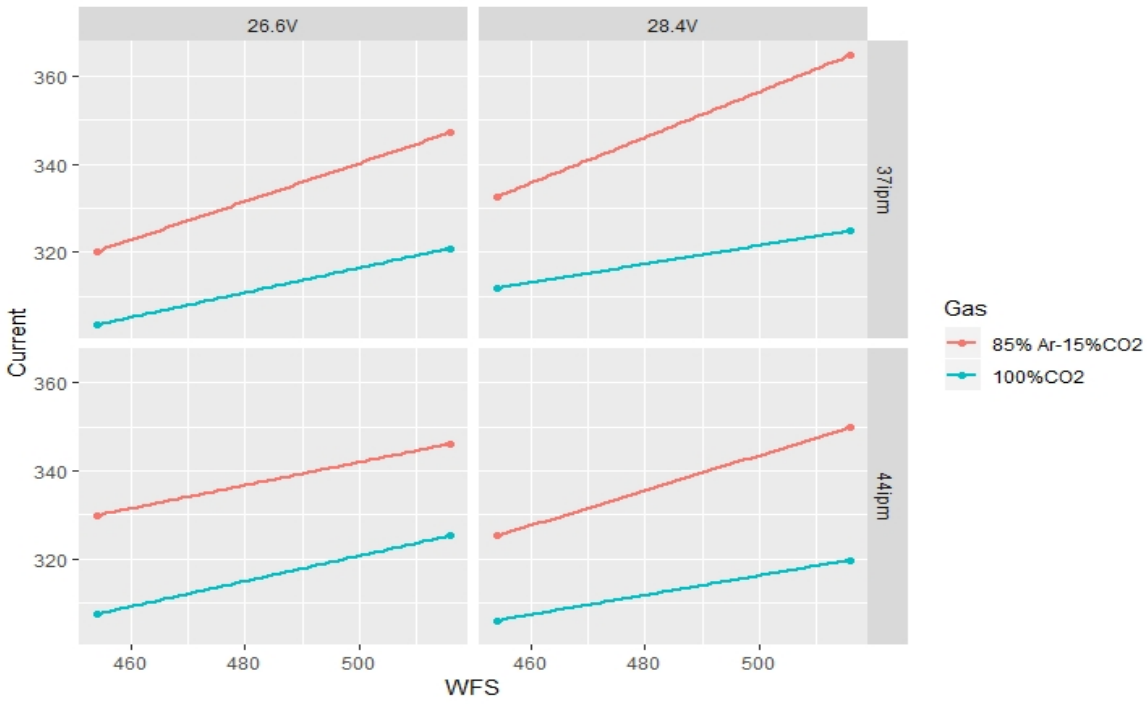
26.6V
28.4V
37lpm
44lpm
Current
WFS
360
340
320
460
480
500
Gas
85% Ar-15%CO2
100%CO2

Appendix E F-Test

a) Test for variance in experimental data from cross section within a weld bead

Test for variance in experimental data within cross section of Weld bead (0.045 in) – 100% Argon gas

a) F-Test Two-Sample for Variances (Depth)

	Depth Cross Section 1	*Depth Cross Section 2*
Mean	2.292	2.352286
Variance	2.121011	2.091277
Observations	35	35
df	34	34
F	1.014218	
P(F<=f) one-tail	0.483704	
F Critical one-tail	1.772066	

b) F-Test Two-Sample for Variances (Reinforcement Area)

	R.A Cross Section 1	*R.A Cross Section 2*
Mean	16.80429	16.77435
Variance	46.45227	45.88033
Observations	35	35
df	34	34
F	1.012466	
P(F<=f) one-tail	0.485699	
F Critical one-tail	1.772066	

c) F-Test Two-Sample for Variances (Reinforcement Height)

	R.Ht Cross Section 1	*R.Ht Cross Section 2*
Mean	2.929714	3.026286
Variance	0.691797	0.690424
Observations	35	35
df	34	34
F	1.001989	
P(F<=f) one-tail	0.497706	
F Critical one-tail	1.772066	

d) F-Test Two-Sample for Variances (Penetration Area)

	P.A Cross Section 2	*P.A Cross Section 1*
Mean	12.47057	12.68229
Variance	68.68949	62.40004
Observations	35	35
df	34	34
F	1.100792	
P(F<=f) one-tail	0.390556	
F Critical one-tail	1.772066	

Test for variance in experimental data within cross section of Weld bead (0.045 in) – 85% Argon+15%% CO_2 gas

a) F-Test Two-Sample for Variances (Depth)

	Depth Cross Section 1	*Depth Cross Section 2*
Mean	3.108372	3.164186
Variance	1.686462	1.585639
Observations	43	43
df	42	42
F	1.063585	
P(F<=f) one-tail	0.421307	
F Critical one-tail	1.670971	

b) F-Test Two-Sample for Variances (Reinforcement Area)

	R.A Cross Section 1	*R.A Cross Section 2*
Mean	16.05837	16.06744
Variance	46.11732	43.99795
Observations	43	43
df	42	42
F	1.04817	
P(F<=f) one-tail	0.439777	
F Critical one-tail	1.670971	

c) F-Test Two-Sample for Variances (Reinforcement Height)

	R.Ht Cross Section 2	*R.Ht Cross Section 1*
Mean	2.740698	2.685116
Variance	0.763602	0.651492
Observations	43	43
df	42	42
F	1.172081	
P(F<=f) one-tail	0.304609	
F Critical one-tail	1.670971	

d) F-Test Two-Sample for Variances (Penetration Area)

	P.A Cross Section 2	*P.A Cross Section 1*
Mean	17.60535	17.41884
Variance	44.12673	41.18605
Observations	43	43
df	42	42
F	1.0714	
P(F<=f) one-tail	0.412107	
F Critical one-tail	1.670971	

Test for variance in experimental data within cross section of Weld bead (0.045 in) – 100% CO_2 gas

a) F-Test Two-Sample for Variances (Depth)

	Depth Cross Section 1	*Depth Cross Section 2*
Mean	3.26093	3.327907
Variance	1.392023	1.347474
Observations	43	43
df	42	42
F	1.033061	
P(F<=f) one-tail	0.458279	
F Critical one-tail	1.670971	

b) F-Test Two-Sample for Variances (Reinforcement Area)

	R.A Cross Section 2	*R.A Cross Section 1*
Mean	16.23953	16.25349
Variance	45.91623	45.76941
Observations	43	43
df	42	42
F	1.003208	
P(F<=f) one-tail	0.495885	
F Critical one-tail	1.670971	

c) F-Test Two-Sample for Variances (Reinforcement Height)

	R.Ht Cross Section 1	*R.Ht Cross Section 2*
Mean	2.89093	2.944884
Variance	0.728832	0.690702
Observations	43	43
df	42	42
F	1.055206	
P(F<=f) one-tail	0.431294	
F Critical one-tail	1.670971	

d) F-Test Two-Sample for Variances (Penetration Area)

	P.A Cross Section 1	*P.A Cross Section 2*
Mean	16.31326	16.52
Variance	62.19877	60.07388
Observations	43	43
df	42	42
F	1.035371	
P(F<=f) one-tail	0.455426	
F Critical one-tail	1.670971	

Test for variance in experimental data within cross section of Weld bead (0.035 in) – 100% Argon gas

a) F-Test Two-Sample for Variances (Depth)

	Depth Cross Section 2	*Depth Cross Section 1*
Mean	1.406286	1.474286
Variance	0.419959	0.344796
Observations	35	35
df	34	34
F	1.217994	
P(F<=f) one-tail	0.284244	
F Critical one-tail	1.772066	

b) F-Test Two-Sample for Variances (Reinforcement Area)

	R.A Cross Section 1	*R.A Cross Section 2*
Mean	12.68429	12.49171
Variance	26.3273	25.97942
Observations	35	35
df	34	34
F	1.01339	
P(F<=f) one-tail	0.484646	
F Critical one-tail	1.772066	

c) F-Test Two-Sample for Variances (Reinforcement Height)

	R.Ht Cross Section 2	*R.Ht Cross Section 1*
Mean	2.728571	2.751714
Variance	0.697248	0.58075
Observations	35	35
df	34	34
F	1.200599	
P(F<=f) one-tail	0.298493	
F Critical one-tail	1.772066	

d) F-Test Two-Sample for Variances (Penetration Area)

	P.A Cross Section 2	*P.A Cross Section 1*
Mean	7.095429	5.825143
Variance	13.18685	11.7453
Observations	35	35
df	34	34
F	1.122734	
P(F<=f) one-tail	0.368831	
F Critical one-tail	1.772066	

Test for variance in experimental data within cross section of Weld bead (0.035 in) – 85% Argon+15%% CO_2 gas

a) F-Test Two-Sample for Variances (Depth)

	Depth Cross Section 2	*Depth Cross Section 1*
Mean	1.907209	1.895116
Variance	0.480459	0.412968
Observations	43	43
df	42	42
F	1.163427	
P(F<=f) one-tail	0.313004	
F Critical one-tail	1.670971	

b) F-Test Two-Sample for Variances (Reinforcement Area)

	R.A Cross Section 2	*R.A Cross Section 1*
Mean	11.84791	11.85437
Variance	26.31836	25.39848
Observations	43	43
df	42	42
F	1.036218	
P(F<=f) one-tail	0.454383	
F Critical one-tail	1.670971	

c) F-Test Two-Sample for Variances (Reinforcement Height)

	R.Ht Cross Section 2	*R.Ht Cross Section 1*
Mean	2.138605	2.204884
Variance	0.393469	0.384545
Observations	43	43
df	42	42
F	1.023209	
P(F<=f) one-tail	0.470544	
F Critical one-tail	1.670971	

d) F-Test Two-Sample for Variances (Penetration Area)

	P.A Cross Section 2	*P.A Cross Section 1*
Mean	9.32498	9.302837
Variance	18.86708	18.38024
Observations	43	43
df	42	42
F	1.026487	
P(F<=f) one-tail	0.466446	
F Critical one-tail	1.670971	

Test for variance in experimental data within cross section of Weld bead (0.045 in) – 100% CO_2 gas

a) F-Test Two-Sample for Variances (Depth)

	Depth Cross Section 2	*Depth Cross Section 1*
Mean	1.894651	1.884884
Variance	0.473006	0.437492
Observations	43	43
df	42	42
F	1.081177	
P(F<=f) one-tail	0.400761	
F Critical one-tail	1.670971	

b) F-Test Two-Sample for Variances (Reinforcement Area)

	R.A Cross Section 1	*R.A Cross Section 2*
Mean	11.55023	11.63721
Variance	32.16447	31.34852
Observations	43	43
df	42	42
F	1.026028	
P(F<=f) one-tail	0.467018	
F Critical one-tail	1.670971	

c) F-Test Two-Sample for Variances (Reinforcement Height)

	R.Ht Cross Section 2	*R.Ht Cross Section 1*
Mean	2.416047	2.470465
Variance	0.622058	0.515709
Observations	43	43
df	42	42
F	1.206218	
P(F<=f) one-tail	0.273091	
F Critical one-tail	1.670971	

d) F-Test Two-Sample for Variances (Penetration Area)

	P.A Cross Section 2	*P.A Cross Section 1*
Mean	9.069302	9.207442
Variance	25.38171	25.25918
Observations	43	43
df	42	42
F	1.004851	
P(F<=f) one-tail	0.493782	
F Critical one-tail	1.670971	

b) Test for variance in experimental data from cross section within a weld bead

Test for variance in predicted data with different diameter wire– 100% Argon gas

a) F-Test Two-Sample for Variances (Current)

	0.045 in	*0.035 in*
Mean	270.1139	203.3082
Variance	5708.334	1887.475
Observations	35	35
df	34	34
F	3.024323	
P(F<=f) one-tail	0.000883	
F Critical one-tail	1.772066	

b) F-Test Two-Sample for Variances (Width)

	0.035 in	*0.045 in*
Mean	7.488061	8.814299
Variance	7.632054	4.843888
Observations	35	35
df	34	34
F	1.575605	
P(F<=f) one-tail	0.09506	
F Critical one-tail	1.772066	

c) F-Test Two-Sample for Variances (Depth)

	0.045 in	*0.035 in*
Mean	2.323259	1.807246
Variance	1.81293	0.428969
Observations	70	70
df	69	69
F	4.226249	
P(F<=f) one-tail	4.91E-09	
F Critical one-tail	1.49	

d) F-Test Two-Sample for Variances (Reinforcement Area)

	0.045 in	*0.035 in*
Mean	16.79184	16.14895
Variance	44.98734	35.87658
Observations	70	70
df	69	69
F	1.253947	
P(F<=f) one-tail	0.174769	
F Critical one-tail	1.49	

e) F-Test Two-Sample for Variances (Reinforcement Height)

	0.035 in	*0.045 in*
Mean	3.296076	3.007241
Variance	0.826196	0.568568
Observations	70	70
df	69	69
F	1.453118	
P(F<=f) one-tail	0.061527	
F Critical one-tail	1.49	

f) F-Test Two-Sample for Variances (Penetration Area)

	0.045 in	*0.035 in*
Mean	16.7395	7.731994
Variance	43.95342	7.095677
Observations	70	70
df	69	69
F	6.194394	
P(F<=f) one-tail	6E-13	
F Critical one-tail	1.49	

Test for variance in predicted data with different diameter wire– 85% Argon gas+15%CO_2 gas

a) F-Test Two-Sample for Variances (Current)

	0.045 in	*0.035 in*
Mean	292.4269	225.2655
Variance	4933.152	1831.676
Observations	43	43
df	42	42
F	2.693245	
P(F<=f) one-tail	0.000875	
F Critical one-tail	1.670971	

b) F-Test Two-Sample for Variances (Width)

	0.035 in	*0.045 in*
Mean	7.974544	9.324047
Variance	5.055968	4.761308
Observations	43	43
df	42	42
F	1.061886	
P(F<=f) one-tail	0.423321	
F Critical one-tail	1.670971	

c) F-Test Two-Sample for Variances (Depth)

	0.045 in	*0.035 in*
Mean	3.239605	2.759469
Variance	1.607095	0.997814
Observations	86	86
df	85	85
F	1.610617	
P(F<=f) one-tail	0.014613	
F Critical one-tail	1.431643	

d) F-Test Two-Sample for Variances (Reinforcement Area)

	0.045 in	*0.035 in*
Mean	16.06921	13.4196
Variance	43.69631	31.17437
Observations	86	86
df	85	85
F	1.401674	
P(F<=f) one-tail	0.06077	
F Critical one-tail	1.431643	

e) F-Test Two-Sample for Variances (Reinforcement Height)

	0.045 in	*0.035 in*
Mean	2.747603	2.698523
Variance	0.629477	0.566245
Observations	86	86
df	85	85
F	1.11167	
P(F<=f) one-tail	0.313321	
F Critical one-tail	1.431643	

f) F-Test Two-Sample for Variances (Penetration Area)

	0.045 in	*0.035 in*
Mean	17.36568	13.4196
Variance	33.33479	31.17437
Observations	86	86
df	85	85
F	1.069301	
P(F<=f) one-tail	0.379063	
F Critical one-tail	1.431643	

Test for variance in predicted data with different diameter wire– 100% CO_2 gas

a) F-Test Two-Sample for Variances (Current)

	0.045 in	*0.035 in*
Mean	265.3295	205.1542
Variance	3996.329	1684.642
Observations	43	43
df	42	42
F	2.372213	
P(F<=f) one-tail	0.003061	
F Critical one-tail	1.670971	

b) F-Test Two-Sample for Variances (Width)

	0.035 in	*0.045 in*
Mean	6.355317	8.064816
Variance	3.967199	2.978382
Observations	43	43
df	42	42
F	1.331998	
P(F<=f) one-tail	0.178298	
F Critical one-tail	1.670971	

c) F-Test Two-Sample for Variances (Depth)

	0.045 in	*0.035 in*
Mean	3.271812	2.481744
Variance	1.185726	0.879
Observations	86	86
df	85	85
F	1.348949	
P(F<=f) one-tail	0.084841	
F Critical one-tail	1.431643	

d) F-Test Two-Sample for Variances (Reinforcement Area)

	0.035 in	*0.045 in*
Mean	3.233769	2.994167
Variance	0.765053	0.725725
Observations	86	86
df	85	85
F	1.054191	
P(F<=f) one-tail	0.404179	
F Critical one-tail	1.431643	

e) F-Test Two-Sample for Variances (Reinforcement Height)

	0.035 in	*0.045 in*
Mean	37.95019	16.24461
Variance	190.6492	44.57431
Observations	86	86
df	85	85
F	4.27711	
P(F<=f) one-tail	6.95E-11	
F Critical one-tail	1.431643	

f) F-Test Two-Sample for Variances (Penetration Area)

	0.035 in	*0.045 in*
Mean	13.47539	16.60238
Variance	60.46049	52.42936
Observations	86	86
df	85	85
F	1.15318	
P(F<=f) one-tail	0.2563	
F Critical one-tail	1.431643	

Appendix F Bead on Plate Validation Tests (0.045 in)

#	WFS (Ipm)	Voltage (V)	Travel Speed (ipm)	Gas	Current(A)		Width(mm)		Depth(mm)	
					Measured	Predicted	Measured	Predicted	Measured	Predicted
1	247.5	20	16	100% Ar	189.21	194.78±12.61	7.55	7.87±1.22	1.32	1.11±0.53
2	295	21	20	100% Ar	215.93	213.37±12.61	8.16	7.95±1.22	1.4	1.27±0.53
3	342.5	23	24	100% Ar	233.16	236.14±12.61	8.39	8.11±1.22	1.83	1.71±0.53
4	437.5	25	28	100% Ar	287.48	290.24±12.61	8.98	8.68±1.22	2.74	2.8±0.53
5	485	27	32	100% Ar	322.55	332.19±12.61	9.14	8.75±1.22	3.78	3.74±0.53
6	532.5	30	24	100% Ar	384.85	396.35±12.61	9.6	8.83±1.22	4.67	5.05±0.53
7	485	25	24	100% Ar	305.71	310.72±12.61	10.87	10.03±1.22	3.3	3.17±0.53
8	532.5	27	28	100% Ar	357.48	354.26±12.61	11.02	10.51±1.22	3.62	4.19±0.53
9	247.5	20	16	85% Ar + 15% CO2	203.72	214.09±7.05	9.46	9.02±0.6	1.89	2.11±0.47
10	295	21	20	85% Ar + 15% CO2	228.35	231.42±7.05	9.85	9.6±0.6	2.17	2.35±0.47
11	342.5	23	24	85% Ar + 15% CO2	**253.22**	251.2±7.05	**10.29**	10.31±0.6	**2.73**	2.9±0.47
12	437.5	25	28	85% Ar + 15% CO2	300.84	297.58±7.05	10.76	10.38±0.6	3.48	3.69±0.47
13	485	27	32	85% Ar + 15% CO2	336.3	328.97±7.05	10.38	9.6±0.6	3.88	4.21±0.47
14	532.5	30	36	85% Ar + 15% CO2	384.5	376.14±7.05	9.05	8.21±0.6	4.18	4.73±0.47
15	485	25	24	85% Ar + 15% CO2	320.16	317.97±7.05	11.42	11.16±0.6	4.13	4.03±0.47
16	532.5	27	28	85% Ar + 15% CO2	341.57	348.18±7.05	10.81	10.03±0.6	4.42	4.59±0.47
17	247.5	20	16	100%CO2	201.13	191.77±16.28	8.11	7.5±0.71	2.02	2.44±0.54
18	295	21	20	100%CO2	223.64	214.88±16.28	8.47	7.89±0.71	2.21	2.4±0.54
19	342.5	23	24	100%CO2	248.27	240.1±16.28	9.12	8.5±0.71	2.37	2.4±0.54
20	437.5	25	28	100%CO2	298.8	286.32±16.28	9.08	8.84±0.71	2.89	2.98±0.54
21	485	27	32	100%CO2	324.44	311.55±16.28	9.39	8.48±0.71	3.42	3.72±0.54

22	532.5	30	36	100%CO2	351.5	338.88±16.28	8.64	7.71±0.71	4.15	5.08±0.54
23	485	25	24	100%CO2	315.35	307.32±16.28	9.74	9.62±0.71	3.61	3.49±0.54
24	532.5	27	28	100%CO2	336.78	332.55±16.28	9.92	9.1±0.71	4.07	4.27±0.54

#	WFS (Ipm)	Voltage (V)	Travel Speed (ipm)	Gas	**Reinforcement Height (mm)**		**Reinforcement Area (mm^2)**		**Penetration Area (mm^2)**	
					Measured	Predicted	Measured	Predicted	Measured	Predicted
1	247.5	20	16	100% Ar	2.84	2.99±0.39	15.94	16.18±0.74	16.23	17.13±1.19
2	295	21	20	100% Ar	2.79	2.83±0.39	14.63	14.25±0.74	14.61	14.7±1.19
3	342.5	23	24	100% Ar	2.98	2.69±0.39	14.44	13.26±0.74	14.74	13.43±1.19
4	437.5	25	28	100% Ar	2.92	2.85±0.39	15.27	14.88±0.74	16.16	15.2±1.19
5	485	27	32	100% Ar	2.66	2.81±0.39	15.63	15.49±0.74	16.97	16.24±1.19
6	532.5	30	24	100% Ar	3.13	2.82±0.39	21.47	17.04±0.74	18.68	18.45±1.19
7	485	25	24	100% Ar	3.6	3.34±0.39	18.83	19.11±0.74	20.26	19.08±1.19
8	532.5	27	28	100% Ar	3.36	3.24±0.39	18.02	18.22±0.74	20.12	18.95±1.19
9	247.5	20	16	85% Ar + 15% CO2	2.48	2.57±0.30	15.71	16.27±0.97	14.11	12.1±3.19
10	295	21	20	85% Ar + 15% CO2	2.78	2.63±0.30	14.87	15.34±0.97	15.29	14.03±3.19
11	342.5	23	24	85% Ar + 15% CO2	2.81	2.63±0.30	14.58	14.51±0.97	16.56	17.02±3.19
12	437.5	25	28	85% Ar + 15% CO2	3.13	2.92±0.30	15.62	15.51±0.97	19.78	20.61±3.19
13	485	27	32	85% Ar + 15% CO2	2.92	2.9±0.30	15.11	14.54±0.97	22.25	22.29±3.19
14	532.5	30	36	85% Ar + 15% CO2	2.74	2.83±0.30	14.73	13.68±0.97	24.42	23.78±3.19
15	485	25	24	85% Ar + 15% CO2	3.19	3.37±0.30	20.04	20.58±0.97	25.08	23.24±3.19
16	532.5	27	28	85% Ar + 15% CO2	3.08	3.31±0.30	19.29	18.85±0.97	26.56	25.38±3.19
17	247.5	20	16	100%CO2	2.62	3.27±0.39	15.25	16.1±0.87	14.39	13.07±4.32
18	295	21	20	100%CO2	2.68	2.89±0.39	14.97	15.24±0.87	13.25	11.39±4.32

19	342.5	23	24	100%CO2	2.76	2.65±0.39	14.51	14.49±0.87	15.46	12.18±4.32
20	437.5	25	28	100%CO2	2.97	2.91±0.39	16.02	15.65±0.87	16.59	16.03±4.32
21	485	27	32	100%CO2	3.06	3.12±0.39	15.46	14.8±0.87	19.72	20.51±4.32
22	532.5	30	36	100%CO2	3	3.57±0.39	15.14	14.07±0.87	25.33	28.75±4.32
23	485	25	24	100%CO2	2.99	3.54±0.39	20.33	20.85±0.87	21.6	18.84±4.32
24	532.5	27	28	100%CO2	3.24	3.75±0.39	19.21	19.32±0.87	25.65	23.76±4.32